Imaging the mitochondrial permeability transition in single cells:

free radicals and calcium as determinants of cell fate

Derek William Niall Jacobson

Department of Physiology
University College London
Gower Street
London WC1E 6BT

Thesis submitted for PhD. in physiology

2000

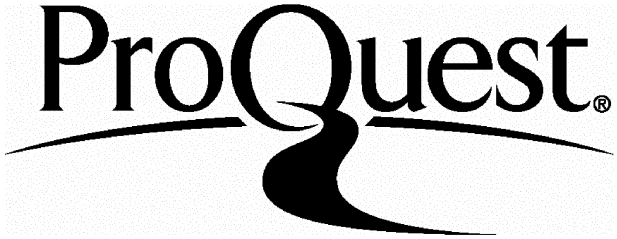

Abstract

The textbook interpretation of mitochondrial function has had to be revised in the light of recent discoveries establishing a central role for mitochondria in modulating cell signalling. In particular, the opening of the mitochondrial permeability transition pore (MPTP), a large conductance pore in the tightly impermeable inner mitochondrial membrane, may determine cell fate by inducing either necrotic or apoptotic cell death. I have developed an experimental protocol in which MPTP opening can be reliably induced in living cells. I have then used this as a model to study the relative roles of calcium and reactive oxygen species (ROS) in permeability transition and explored the consequences of these processes for cell fate.

The membrane-permeant, fluorescent dye, tetramethylrhodamine ethyl ester (TMRE), accumulates in mitochondria where its fluorescence signals changes in mitochondrial transmembrane potential ($\Delta\Psi_m$). Digital imaging of adult rat cortical astrocytes loaded with TMRE revealed spontaneous, transient depolarisations of individual mitochondria leading to a gradual and complete mitochondrial depolarisation in whole cells. Single mitochondria could depolarise and repolarise several times. Treatment of the cells with cyclosporin (an inhibitor of pore opening) significantly reduced the depolarisations suggesting that they were caused by MPTP opening and that TMRE could be used to signal MPTP in intact single cells. This model of MPTP opening was used to study the underlying mechanisms involved in MPTP opening.

Illumination of TMRE produces ROS. Attenuation of the excitation light intensity or treatment with free radical scavengers reduced the frequency of the depolarisations, confirming a role for ROS in this model of permeability transition.

Mitochondrial calcium loading is thought to be a prerequisite for permeability transition and I found that chelation of intracellular calcium or depletion of endoplasmic reticulum calcium stores inhibited the transient openings. Thus either free radical scavengers or chelation of calcium inhibited pore opening in this model, suggesting an interplay between ROS production and mitochondrial calcium loading in permeability transition, perhaps as a result of ROS-induced calcium release from intracellular stores.

The fate of cells that were illuminated with low intensity light, where MPTP was transient, was similar to non-illuminated controls, suggesting that opening of the pore does not inevitably lead to cell death. Those cells in which collapse of $\Delta\Psi_m$ was complete, however, died by a necrotic pathway.

Contents

List of abbreviations:

ANT	adenine nucleotide translocase
AM ester	acetoxy-methyl ester
ATP	adenosine triphosphate
BAPTA	1,2 bis(o-aminophenoxy)ethane-N,N,N',N'-tetraacetic acid
CCD	charge-coupled device
EBSS	Earle's balanced salt solution
$\Delta\psi_m$	mitochondrial membrane potential
FCCP	carbonyl cyanide p-trifluoromethoxyphenyl hydrazone
H_2DCFDA	6 carboxy-2',7'-dichlorodihydrofluorescein
IP_3	inositol 1,4,5 trisphosphate
MEM	minimal essential medium
ND	neutral density
MPT	mitochondrial permeability transition
PMT	photomultiplier tube
ROS	reactive oxygen species
TEMPO	2,2,6,6-tetramethyl-1-piperidine-N-oxyl
TMRE	tetramethylrhodamine ethyl ester
VDAC	voltage-dependent anion channel

Chapter 1: introduction

There has been an explosion in academic interest in mitochondria of late, a rekindling of curiosity that parallels that seen in the 1960s and 70s when Peter Mitchell and his colleagues were working to establish the chemiosmotic theory of oxidative phosphorylation. Oxidative phosphorylation underlies the majority of cellular energy transduction and thus mitochondria, the only site of this process, are central to eukaryotic cell life – indeed, mitochondrial oxidative phosphorylation makes oxygen essential for aerobic life. Current curiosity in the role of mitochondria in cell physiology centres less on this established function of the organelles and more on the realisation that mitochondria can participate in cellular signalling. It is now also clear that mitochondria are not only central to intracellular calcium signalling, the ubiquitous language of the intracellular milieu, but that they may also act as a functional 'switch', determining the fate of injured or superfluous cells. Thus, the revival in interest in mitochondria is largely due to the realisation that these organelles may also be central to eukaryotic cell death.

Chemiosmotic theory is largely regarded as 'solved' (Nicholls & Ferguson, 1992), however an appreciation of the mechanisms are essential to the burgeoning study of mitochondrial involvement in cell signalling. The production of adenosine triphosphate (ATP) remains the primary function of mitochondria and cessation of oxidative phosphorylation can be catastrophic for the cell. Moreover, the potential that is developed across the mitochondrial inner membrane, the driving force of ATP synthesis, also drives other aspects of mitochondrial physiology – ion exchange, protein uptake and volume regulation – all of which may influence how mitochondria modulate and respond to intracellular signals.

New information on two aspects of mitochondrial physiology have fuelled the recent interest. First, mitochondrial calcium uptake was once believed to be a pathophysiological phenomenon (Carafoli, 1987), however current evidence suggests that this is not the case. Mitochondria can, and do, take up calcium under physiological conditions and they can, and do, modulate calcium signals (for review, see Duchen 1999) . Second, the discovery that

cytochrome c translocation from the mitochondrial inter-membrane space may be a key part of the cascade of signals that dedicate a cell to an apoptotic death (Liu, Kim, Yang, Jemmerson & Wang, 1996). There is evidence that the opening of a large proteinaceous pore, the mitochondrial permeability transition pore, may underlie the release of cytochrome c (Kroemer, Dallaporta & Resche-Rigon, 1998; Bernardi, Scorrano, Colonna, Petronilli & Di Lisa, 1999; Crompton, 1999), however the exact mechanisms are still the subject of much investigation.

The data presented in this thesis demonstrate how microfluorimetry and digital imaging may be used to study detailed local events within single, living cells. These techniques have been used to reveal transient depolarisations of the mitochondrial membrane potential. It is shown that these depolarisations signal openings of the mitochondrial permeability transition pore. The data reveal an intimate interplay between local calcium signalling and nearby mitochondria, and the inter-relationship of pore opening and cell signalling events are analysed. Finally, the consequences of pore opening for cell fate is investigated.

Some of the concepts underlying mitochondrial physiology and its study are outlined below by way of a background for the thesis.

1.1 Chemiosmotic theory and oxidative phosphorylation

Mitochondria are bounded by two membranes, perhaps evidence of an invagination by an early ancestor of the eukaryotic cell, an invagination that engulfed an ancestor of today's purple bacteria (Margulis, 1975; Margulis, 1996). The organelles are probably descended from free-living prokaryotes that somehow evolved a symbiotic relationship with archaeic anaerobic organisms. The existence of a mitochondrial genome, and its similarity to bacterial genomic structure, lend support to the idea that mitochondria evolved separately until around 3 billion years ago, when they carried their ability to metabolise molecular oxygen with them to their symbiotic hosts.

The explosive release of energy that occurs when hydrogen is oxidised to water is unusable by the cell as most of this energy is released to the environment as heat. Instead, the mitochondrion has evolved a mechanism of harnessing the energy released from the same reaction by controlling the rate of the reaction, reducing it to small steps and storing the energy released.

Respiratory substrate, in the form of pyruvate and fatty acid, is taken up across the tightly impermeable mitochondrial inner membrane by carriers. Both substrates are metabolised to acetyl coenzyme A (acetyl CoA). Acetyl CoA enters the tricarboxylic acid cycle where a series of enzyme-catalysed steps produces carbon dioxide (CO_2) and electrons, which reduce nicotinamide adenine dinucleotide (NAD^+) to NADH. Additionally, a molecule of flavin adenine nucleotide (FAD^+) is reduced to $FADH_2$ with each turn of the cycle. Random collisions between the freely-diffusible NADH molecules and the membrane-bound enzymes of the respiratory chain result in the transfer of the electrons to the first enzyme, NADH dehydrogenase (Complex I). $FADH_2$ transfers its electrons directly to ubiquinone from the succinate dehydrogenase complex to which it is covalently bonded (Complex II). Electrons then pass along the electron transport chain, and as the redox potential of each electron acceptor is greater than its predecessor, the transfer is energetically favoured. The final complex in the chain, cytochrome oxidase (Complex IV), passes electrons to molecular oxygen.

The free energy released each time an electron is transferred between the carriers is proportional to the change in redox potentials between them, and this energy is utilised by Complexes I, III and IV to pump protons across the inner mitochondrial membrane. This coupling of proton pumping to electron transport is the basis of the chemiosmotic theory. The transfer of protons from the mitochondrial matrix to the cytosol generates a membrane potential of the order of 150 – 200 mV, negative on the inside of the inner mitochondrial membrane, as well as a pH gradient (0.5 – 1.0 pH units) from the cytosol to the mitochondrion. Protons travelling down the electrochemical gradient re-enter the mitochondrion and drive ATP synthase (Complex V) to phosphorylate ADP to ATP. The ATP

synthase is reversible, dissipation of the mitochondrial membrane potential and/or disruption of the ATP:ADP.P_i ratio may cause the enzyme to run in 'reverse', whereby it hydrolyses ATP in order to pump protons out of the mitochondrion. Hence intracellular ATP may be consumed rapidly if mitochondria are uncoupled, although the presence in some cells of a protein, IF1, which can inhibit the ATP synthase in reverse mode may limit ATP consumption (Rouslin & Broge, 1996). The mitochondrial membrane potential also drives mitochondrial calcium-uptake (below).

Figure 1.1 summarises the process outlined above. Chemiosmotic theory is reviewed and discussed in detail in Nicholls and Ferguson, 1992.

1.2 Mitochondria and cell signalling

Although primarily thought of as ATP-producing organelles, mitochondria also play a significant part in cell signalling. Mitochondria are well-placed to integrate disparate signals and react, either by modulating ATP production or by relaying integrated signals to other intracellular signalling pathways. For example, the necessity of mitochondrial RESPIRATORY SUBSTRATE and oxygen delivery has prompted suggestions that mitochondria may have a role in homeostatic regulation of these respiratory substrates (for review see Duchen, 1999). There is evidence in the pancreatic β-cell that mitochondria may control insulin secretion by way of an increase in ATP:ADP.P_i ratio, which in turn modulates the activity of a plasmalemmal potassium channel (the K_{ATP} channel). Closure of the channel by high ATP:ADP.P_i ratio leads to membrane depolarisation, calcium-influx and insulin secretion. Moreover, the glucose-sensing neurones of the hypothalamus, which seem to regulate the sensation of appetite, also express plasmalemmal K_{ATP} channels suggesting that neuronal excitability and appetite may, at least in part, be regulated by ATP:ADP.P_i ratio. Additionally, the mitochondrial membrane potential ($\Delta\psi_m$) in Type 1 cells of the carotid body (a specialised group of cells that respond to a drop in oxygen tension by stimulating an increase in respiration) responds to changes in PO_2 over a physiologically significant range (Duchen & Biscoe, 1992b; Duchen & Biscoe, 1992a); hypoxia-induced dissipation of $\Delta\psi_m$ in these cells was accompanied by a rise in intracellular calcium ($[Ca^{2+}]_i$) which was associated with transmitter release. Adrenal chromaffin cells

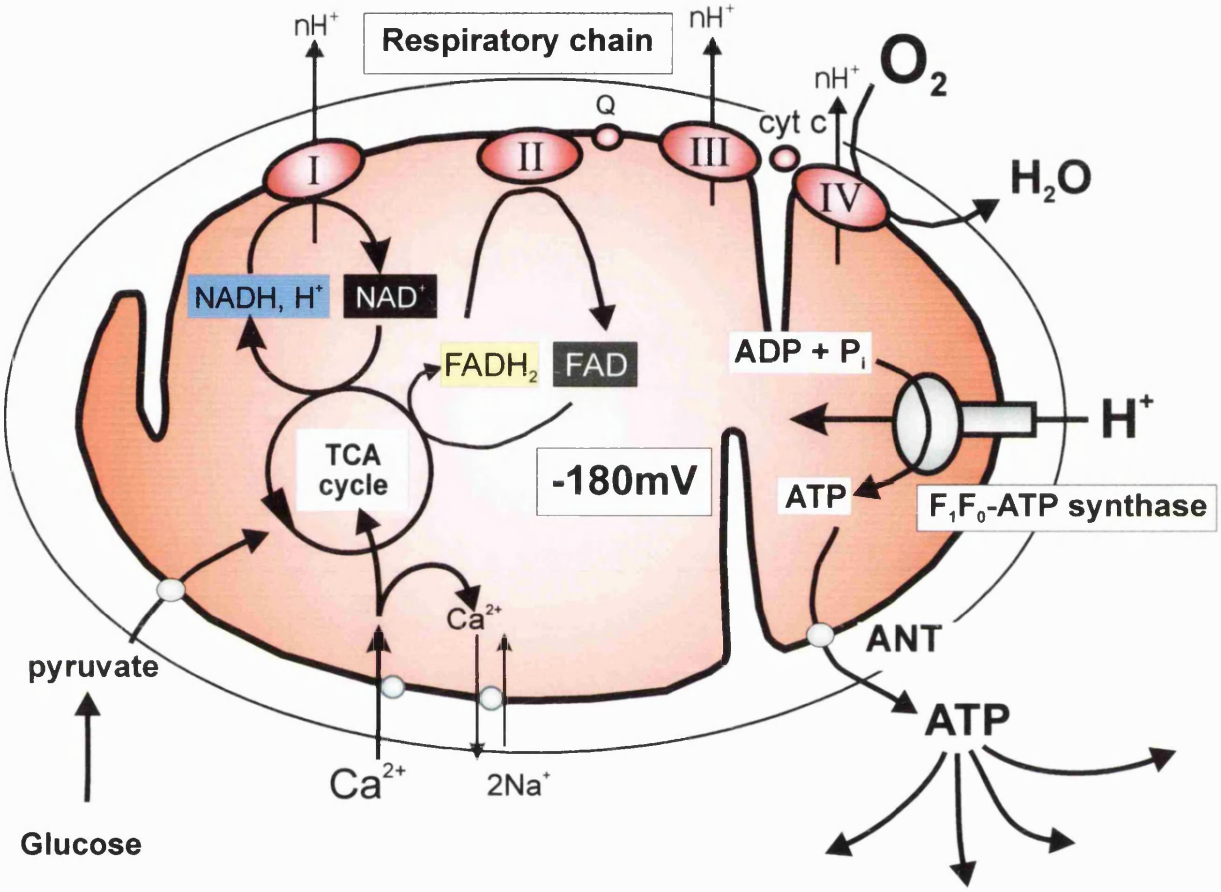

Figure 1.1: mitochondrial chemiosmotic coupling. Energy from foodstuffs is used to create an electrochemical proton gradient across the tightly impermeable inner mitochondrial membrane. Electrons, derived from the tricarboxylic acid (TCA) cycle are passed to the enzymes of the respiratory chain by NADH and $FADH_2$. The electrons are passed along the respiratory chain and the energy derived from this transport is utilised to pump protons out of the matrix. Thus a proton gradient is created, expressed largely as a membrane potential of ~180 mV. The membrane potential, in turn, drives the ATP synthase to phosphorylate ADP, as well as ion transport and mitochondrial protein uptake.

(which, in the new-born, respond to hypoxia by secreting catecholamines which in turn initiate respiration) can be induced to secrete catecholamines by inhibition of mitochondrial respiration (Mojet, Mills & Duchen, 1997). Thus, mitochondria, the ultimate consumers of both glucose and oxygen, may regulate their own supply of respiratory substrates by influencing the actions of whole physiological systems.

1.3 Mitochondria and calcium homeostasis

Mitochondria play a central role in intracellular calcium homeostasis. The presence of a calcium uniporter in the inner mitochondrial membrane facilitates electrophoretic uptake of cytosolic calcium ions, driven by the $\Delta\psi_m$. Although the molecular identity of the uniporter is unclear, it may correspond to that of a 20 pS Ca^{2+}-selective ion channel identified in mitoplast membranes (Zoratti & Szabó, 1994). Calcium may be buffered within the mitochondrial matrix, by inorganic phosphate and phospholipids, or transported out via a sodium/calcium exchanger (Gunter & Gunter, 1994; Babcock, Herrington, Goodwin, Park & Hille, 1997). A sodium-independent route of calcium efflux has also been proposed in some cells, (Puskin, Gunter, Gunter & Russell, 1976; Gunter & Gunter, 1994). The mitochondrial sodium balance is re-established by a sodium/proton antiporter. Thus the $\Delta\Psi_m$ and the ΔH^+_m generated by the electron transport chain, in addition to any mitochondrial / cytosolic calcium gradient, provide the driving forces necessary for mitochondrial calcium uptake and release. Net calcium uptake into mitochondria is therefore the balance between influx and efflux systems, and calcium accumulation by mitochondria occurs when uptake exceeds efflux (the 'set point' is exceeded). Mitochondrial $[Ca^{2+}]$ is thus the result of calcium cycling, which, in turn reflects the set point. Work in isolated mitochondria (Nicholls, 1978) has suggested that the set point for calcium accumulation is a $[Ca^{2+}]_{cyt}$ in excess of 300 nM, however in some cells it has been estimated as high as 1 μM (Nicholls & Budd, 2000). Once net uptake is initiated, the calcium buffering capacity of mitochondria is enormous, in excess of 100 mM Ca^{2+} can be accumulated while maintaining bioenergetic integrity (Nicholls & Scott, 1980). This has led to the characterisation of mitochondrial calcium uptake as 'low affinity, high capacity' which in turn has prompted the suggestion that mitochondria play little role in physiological intracellular calcium signalling and, until recently, the organelles were thought only to take up calcium in

conditions of severe calcium overload (Carafoli, 1987). Recent work, however, has established that mitochondria do indeed take up calcium in response to physiological stimuli. There is evidence that mitochondria may modulate intracellular calcium signalling by shaping calcium waves (Jouaville, Ichas, Holmuhamedov, Camacho & Lechleiter, 1995; Boitier, Rea & Duchen, 1999), mitochondrial Ca^{2+} uptake may be a decisive event in triggering cell death (Stout, Raphael, Kanterewicz, Klann & Reynolds, 1998; Szalai, Krishnamurthy & Hajnoczky, 1999), and calcium up-regulates three mitochondrial metabolic enzymes - pyruvate dehydrogenase, isocitrate dehydrogenase, and 2-oxoglutarate dehydrogenase (McCormack, Halestrap & Denton, 1990). Indeed, this last may have been the main evolutionary function of the mitochondrial Ca^{2+} uptake pathway. Work by Rizzuto and colleagues has revealed close apposition of mitochondria and intracellular calcium stores (endoplasmic reticulum, ER) in HeLa cells suggesting that the architecture of intracellular organelles may allow mitochondria to be exposed to microdomains of $[Ca^{2+}]$ that are high enough to initiate substantial calcium uptake under conditions of physiological calcium release. In addition, it is even possible that there are privileged routes of calcium movement that initiate mitochondrial calcium-loading directly from ER. In cortical oligodendrocytes, sites at which Ca^{2+} waves were amplified were identified as groups of mitochondria co-localised with IP_3 receptors (Simpson & Russell, 1996), prompting the suggestion that mitochondrial Ca^{2+} uptake may regulate Ca^{2+}-dependent release kinetics from the ER.

As the uptake of Ca^{2+} by mitochondria is electrogenic it is accompanied by a depolarisation of the $\Delta\Psi_m$ (Loew, Carrington, Tuft & Fay, 1994; Peuchen, Duchen & Clark, 1996b; Duchen, Leyssens & Crompton, 1998; Boitier *et al.*, 1999). The depolarisation is transient and reversible as accumulated Ca^{2+} up-regulates the actions of dehydrogenases that control the availability of substrates for the tricarboxylic acid cycle, increasing electron transport and hence proton translocation (McCormack *et al.*, 1990; McCormack & Denton, 1993; Denton *et al.*, 1996). In this way, the $\Delta\Psi_m$ is re-established, or even hyperpolarised (Robb-Gaspers *et al.*, 1998), and mitochondria may utilise local $[Ca^{2+}]$ as a mechanism to adjust oxidative phosphorylation to meet metabolic need. Additionally, there is evidence that raised $[Ca^{2+}]_{mit}$ may stimulate the activity of ATP synthase, independently of any Ca^{2+}-stimulated increase in

electron transfer, so that the rate of ADP phosphorylation increases together with that of proton pumping (Mildazien *et al.*, 1996).

The consequence of coupling oxidative phosphorylation to cytosolic [Ca^{2+}] signals is an increase in ATP synthesis in concert with an increase in Ca^{2+}-mediated cell activity. As Ca^{2+} signals may be associated with a huge range of cell processes, including muscle contraction, neurotransmitter release, synaptic plasticity, cell proliferation and cell death (Berridge, 1997), it makes sense that mitochondria are 'alerted' early to the increase in metabolic demand. For example, in paced cardiomyocytes, the steady-state $[Ca^{2+}]_{mit}$ reflected pacing frequency (Miyata *et al.*, 1991) and studies in hepatocytes have revealed that mitochondrial Ca^{2+}-sensitive dehydrogenases respond optimally to a high-frequency train of Ca^{2+} oscillations (Hajnóczky, Robb-Gaspers, Seitz & Thomas, 1995). In these cells, the mitochondrial response was greater to the train of oscillations when compared with a plateau of raised [Ca^{2+}], suggesting that mitochondria may integrate oscillatory $[Ca^{2+}]_{cyt}$ signals. Additionally, in the hepatocytes transmission of the [Ca^{2+}] oscillations to the mitochondria resulted in a sustained reduction of NAD^+ to NADH which out-lasted the [Ca^{2+}] signals, confirming a prolonged metabolic response to the [Ca^{2+}] oscillations.

Mitochondria may respond differently to [Ca^{2+}] changes originating from different sources. Rizzuto et al have shown, using the site-directed transfection of the [Ca^{2+}]-sensitive photoprotein, aequorin, targeted to the outer leaflet of the inner mitochondrial membrane, that mitochondria in HeLa cells are exquisitely responsive to Ca^{2+}-release from ER. The rapid mitochondrial Ca^{2+}-uptake seen in these cells on stimulation with histamine was ascribed to close apposition of the mitochondria to ER Ca^{2+}-release sites (Rizzuto *et al.*, 1998) and thus mitochondrial exposure to microdomains of high $[Ca^{2+}]_{cyt}$. However, in ECV304 cells, an endothelial cell line, the same group found that stimulation of Ca^{2+} influx from the extracellular space was more efficient at causing mitochondrial Ca^{2+}-loading than agonist-evoked Ca^{2+} release from internal stores (Lawrie, Rizzuto, Pozzan & Simpson, 1996). In these cells mitochondria are located near the plasmalemma, leading the authors to conclude that in any

given cell type, mitochondria may be localised to suit the metabolic demands of the cell in relation to their specialised actions.

1.4 The mitochondrial permeability transition

Despite the ability of mitochondria to take up and buffer huge quantities of Ca^{2+}, mitochondria Ca^{2+}- overload is still possible. Raised $[Ca^{2+}]_{mit}$, together with other sensitisers, may initiate a non-specific permeability of the inner mitochondrial membrane, the mitochondrial permeability transition (MPT). Hunter and Haworth demonstrated in isolated mitochondria that this increased permeability was due to the opening of a large pore (as opposed to more generalised membrane damage) by showing that there was a cut-off for solute admission at around 1500 Da (Haworth & Hunter, 1979; Hunter & Haworth, 1979b; Hunter & Haworth, 1979a). Electrophysiological studies in mitoplasts have identified a 'megachannel' with a maximum conductance of around 1.3 nS (Zoratti & Szabó, 1994). These studies revealed that the megachannel may have a number of sub-conductances and that the channel may flicker rapidly between a fully closed state and a sub-conductance state. Opening of the megachannel results in a rapid, complete dissipation of $\Delta\psi_m$, and equilibration of mitochondrial matrix solutes with those of the cytosol. ATP production ceases and reversal of the ATP synthase (to a proton-translocating ATPase) may accelerate the rate of intracellular ATP depletion. The loss of osmotic control conferred by the normally impermeable inner membrane results in mitochondrial swelling, and as the surface area of the inner membrane is far greater than the outer, mitochondria may swell until the outer membrane is disrupted (Bernardi *et al.*, 1999).

The molecular identity of the megachannel, or MPT pore, is still elusive however it is thought to involve proteins from the cytosol, from both mitochondrial membranes and from the mitochondrial matrix. Ligands of the adenine nucleotide translocase (ANT), which is located in the inner mitochondrial membrane, have been shown to modulate MPT pore opening, suggesting that the ANT is, at least, a component of the MPT pore (Halestrap, Kerr, Javadov & Woodfield, 1998). Additionally, both ADP and ATP may inhibit pore opening as binding of adenine nucleotides to the ANT alters the conformation of the carrier (Le Quoc and LeQuoc Arch Biochem Biophys 1989). The diameter of the MPT pore (2-3 nm) and that of the voltage-

dependent anion channel (VDAC) are similar and the VDAC displays conductances that are similar to sub-conductance states of the MPT pore (Zoratti & Szabò, 1995). The involvement of the VDAC was confirmed by experiments in which affinity matrix binding of the ANT from mitochondrial membranes extracted roughly equal amounts of VDAC, implying a 1:1 relationship of the two proteins (Crompton, Virji & Ward, 1998). Patch clamp experiments on proteoliposomes incorporating mitochondrial membrane contact sites derived from rat brain mitochondria show high conductances (Moran, Sandri, Panfili, Stühmer & Sorgato, 1990) suggesting that these sites may be the locus of pore formation *in vivo*. VDAC is located in the outer mitochondrial membrane, thus association of VDAC with ANT would explain pore openings at membrane contact sites. Inhibition of MPT by cyclosporin A was demonstrated by Crompton and co-workers (Crompton, Ellinger & Costi, 1988) and confirmed in numerous other studies (Halestrap & Davidson, 1990; Ichas, Jouaville, Sidash, Mazat & Holmuhamedov, 1994; Bernardi & Petronilli, 1996; Nieminen, Petrie, Lemasters & Selman, 1996; Bradham *et al.*, 1998; Dubinsky & Levi, 1998; Szalai *et al.*, 1999). Cyclosporin binds cyclophilins, ubiquitous enzymes capable of catalysing the interconversion of peptidyl-prolyl cis and trans isomers (PPIases) in proteins and peptides. The sensitivity of inhibition of MPT by cyclosporin and its analogues, together with the stoichiometry of the inhibition (Crompton *et al.*, 1998), have confirmed a role for a mitochondrial cyclophilin, Cyp D in the MPT pore.

1.4.1 The consequences of MPT

The consequences of MPT pore opening for cells can be catastrophic. As mentioned above, the rapid dissipation of the $\Delta\psi_m$ leads to ATP depletion as oxidative phosphorylation ceases and the ATP synthase may consume remaining intracellular ATP. ATP depletion will result in necrotic cell death (slowed only by the glycolytic capacity of the cell type) as plasmalemmal ATPases fail and Na^+/K^+ homeostasis ceases. Certainly, ATP depletion may occur in minutes in the presence of a mitochondrial uncoupler (Leyssens, Nowicky, Patterson, Crompton & Duchen, 1996). Recently, however, there has been accumulating evidence that MPT may be a trigger to apoptotic cell death, an ATP-requiring process characterised by activation of a family of intracellular cysteine proteases ('caspases'). Apoptosis is highly regulated ('programmed') and thought to be the means by which the body removes superfluous, aged

or damaged cells (Kroemer, Petit, Zamzami, Vayssière & Mignotte, 1995), and much work has centred on elucidating the signalling pathways that trigger the caspase activation. Mitochondrial involvement in apoptotic cell death was confirmed when Liu et al observed that caspase activation in a cell-free system required ATP and cytochrome c (Liu *et al.*, 1996). The release of cytochrome c activates a cytosolic caspase-recruiting protein, Apaf-1, which in turn stimulates the conversion of inactive procaspase 9 to an active form, triggering further caspase recruitment and apoptotic death. The possibility that opening of the MPT pore might be the trigger for the release of cytochrome c from the mitochondrial intermembrane space has been extensively investigated by a number of groups (for review see Kroemer, 1998), and MPT has been linked to apoptotic cell death in a number of models (Nieminen, Saylor, Tesfai, Herman & Lemasters, 1995; Nieminen *et al.*, 1996; Lemasters, Nieminen, Qian, Trost & Herman, 1997; Bossy-Wetzel, Newmeyer & Green, 1998; Szalai *et al.*, 1999). However there is also evidence that cytochrome c may be released via an MPT-independent pathway (Shimizu, Narita & Tsujimoto, 1999). The relevance of MPT to apoptotic cell death is further discussed in the Introduction to Chapter 8.

If MPT does release cytochrome c with consequent caspase activation, the ability of the MPT pore to flicker is intriguing. Sub-conductance states of the pore are reported (Moran *et al.*, 1990; Zoratti & Szabó, 1994) and certainly the pore closes completely on chelation of Ca^{2+} by EGTA (Crompton & Costi, 1988). In a 'lawn' of isolated mitochondria plated on a coverslip, individual mitochondria have been seen to undergo repeated depolarisations, followed by near-complete repolarisations, that were inhibited by cyclosporin A (Hüser, Rechenmacher & Blatter, 1998), again implying that pore opening is fully reversible. Some studies show that cytochrome c release may *precede* loss of $\Delta\psi_m$; ultraviolet light irradiation of CEM cells has been shown to induce cytochrome c translocation to the cytosol, followed by caspase activation (Bossy-Wetzel *et al.*, 1998) after 2 hours. However, in these experiments, dissipation of $\Delta\psi_m$ did not occur until 3 hours after the irradiation. Additionally, cytochrome c release in cells where the $\Delta\psi_m$ is maintained has been reported (Krohn, Wahlbrink & Prehn, 1999). The ability for the MPT pore to flicker, together with the requirement for maintained $[ATP]_i$ for apoptosis, have lead some authors to suggest that transient opening of the pore

may be sufficient to release enough cytochrome c to trigger apoptosis while $\Delta\psi_m$ is re-established on pore closure. Szalai et al have demonstrated caspase activation in HepG2 cells following a combination of apoptotic stimuli and IP_3-mediated calcium signals. In these cells, the $\Delta\psi_m$ recovered after delivery of the apoptotic stimuli, but cytochrome c was released and a significant increase in apoptosis ensued (Szalai *et al.*, 1999).

A more benign explanation for flickering MPT has been proposed by Ichas et al (Ichas, Jouaville & Mazat, 1997). In a preparation of isolated mitochondria plated onto a coverslip, these workers were able to create a propagating, cyclosporin-sensitive, $[Ca^{2+}]$ wave in response to a microdomain of raised $[Ca^{2+}]$ at one edge of the preparation. This observation led to the suggestion that MPT may therefore contribute to a form of Ca^{2+}-induced Ca^{2+} -release (CICR), whereby a low conductance state of the MPT pore allows Ca^{2+} efflux from the mitochondrion, consequent uptake by a neighbouring organelle, MPT in that organelle, and so on. The idea that MPT may function as a rapid-release pathway for Ca^{2+}_{mit} has been proposed before (Bernardi & Petronilli, 1996), however some dismiss this theory as the very antithesis of $[Ca^{2+}]_{mit}$ control by Ca^{2+} cycling (Crompton, 1999) and point out that if mitochondria exist primarily to synthesise ATP, then loss of tricarboxylic acid cycle intermediates on MPT is inconsistent with cell viability. Certainly, using the MPT as Ca^{2+}-release channel per se would appear to be living dangerously, for both the mitochondrion and the cell. In one study in intact rat livers perfused with cyclosporin A, Ca^{2+}-handling by mitochondria was found to be unaltered as compared with controls (Eriksson, Pollesello & Geimonen, 1999).

1.5 Mitochondria and production of reactive oxygen species

Many factors, in combination with mitochondrial Ca^{2+} overload, have been shown to induce MPT (for extensive review see Zoratti and Szabo, 1995). In particular, reactive oxygen species are potent promoters of pore opening. Highly reactive intermediates of the reduction of oxygen to water, such as singlet oxygen, superoxide, hydrogen peroxide and the hydroxyl radical, are referred to collectively as reactive oxygen species (ROS). As aerobic mitochondrial respiration entails the production of ROS, even under basal conditions, cells are

continually exposed to varying amounts of ROS. These highly reactive molecules have been implicated in a variety of cell pathologies ranging from peroxidation of lipid membranes, to oxidative DNA damage and activation of apoptotic cell death pathways. Unsurprisingly, plant and animal cells have evolved a range of enzymatic and other defences that act as antioxidants, metabolising the pro-oxidant ROS and providing protection against oxidative damage. However, the steady state of pro-oxidants and antioxidants may be disrupted and an imbalance in favour of oxidation has been called 'oxidative stress' (Sies & Cadenas, 1985).

Mitochondria are major sources of ROS (Beal, Howell & Bodis-Wollner, 1997). Molecular oxygen is fully reduced to water by Complex IV of the mitochondrial respiratory chain but a small proportion (~ 5%, Chance, Sies & Boveris, 1979) may undergo a single electron reduction at Complex III, generating the superoxide anion, $O_2^{\cdot-}$. The transfer of a single electron from reduced ubiquinone (UQH_2) to cytochrome c may leave a highly reactive ubisemiquinone which can transfer the remaining electron to O_2 (Nicholls & Budd, 2000). Additionally, there is evidence of ROS generation at Complex I (Herrero & Barja, 1997), although this complex appears to be a quantitatively less active $O_2^{\cdot-}$ producer than Complex III (Turrens & Boveris, 1980). Ca^{2+}-loading of mitochondria, in the presence of Pi, may increase the production of $O_2^{\cdot-}$ (Kowaltowski, Castilho, Grijalba, Bechara & Vercesi, 1996), however the underlying mechanism is unclear. A combination of mitochondrial Ca^{2+}-loading and mitochondrial oxidative stress is a potent sensitiser of MPT.

Investigations of the consequences of mitochondrially-derived oxidative stress have often utilised the addition of oxidising agents to isolated mitochondria. These experiments have established that as well as producing ROS, mitochondria may be susceptible to oxidative damage. The addition of pro-oxidant tert butylhydroperoxide to isolated mitochondria has been shown to inhibit respiration (Nishida *et al.*, 1987; Vlessis, 1990), induce MPT (Petit *et al.*, 1998) and cause lipid peroxidation of the inner mitochondrial membrane (Antunes, Salvador, Marinho, Alves & Pinto, 1996; Yagi, Shidoji, Komura, Kojima & Ohishi, 1998). However, exogenous addition of pro-oxidants may have limited physiological relevance as the highly reactive ROS may oxidise other cell components and/or be metabolised by

endogenous antioxidants outwith the mitochondrion. Moreover, the rapid interconversion of the ROS within a living cell means that the original oxidant molecule may not reach the mitochondrion.

1.6 Fluorescence measurement of mitochondrial potential

In isolated mitochondria, for many years the potential has been measured by following the distribution of lipophilic cations such as tetraphenyl phosphonium (TPP^+) using an electrode incorporating a semipermeable membrane. The same principle has been employed, using fluorescent lipophilic cations. The existence of a single, delocalised charge on the fluorescent compounds rhodamine-123 (Rh123), tetramethyl-rhodamine ethyl and methyl esters (TMRE and TMRM, respectively), 5,5',6,6'- tetrachloro-1,1',3,3'-tetraethylbenzamidazolocarbocyanine (JC-1) and $DiOC_6(3)$ and DASPMI permits these dyes to cross the cell membranes easily, where they partition into compartments in response to their electrochemical potential gradients. Most of these indicators partition between the perfusate and cytosol and then between the cytosolic and mitochondrial compartments in response to a series of potential differences.

1.6.1 Use of indicators in fluorescence 'quench and dequench' mode.

When this kind of work began, in the late 1980s, imaging technology was not generally accessible and so photomultiplier tubes were used to measure the averaged signal across a cell or cuvette of cells. Under these conditions, if a dye moves from the mitochondria to the cytosol in response to a mitochondrial depolarisation, it is quite possible to measure no change in signal at all. Several groups therefore adopted a strategy which may seem confusing: dyes were loaded into cells at relatively high concentrations (~10-20μM) for short periods - usually 10-15 minutes - followed by washing. At higher concentrations, many dyes undergo a phenomenon called autoquenching – fluorescence energy is transferred by collisions between monomeric dye molecules. The concentration of dye may also promote the formation of aggregates of dye molecules which may be non-fluorescent. This tends to occur following the potential dependent concentration of indicator into the mitochondria. Mitochondrial depolarisation promotes the redistribution of the dye into the cytosol where its

dilution relieves the quench and the net fluorescence signal increases. Thus, in this mode, mitochondrial depolarisation is associated with an increase in fluorescence. TMRM, TMRE and Rh123 have all been used in this mode by several groups.

1.6.2 Use of dyes as redistribution probes.

An alternative approach is to bathe cells continuously in a very low concentration of dye - in the range of 2-30nM to allow the probe to equilibrate. Concentrations up to 300nM have been used, but the higher the concentration the greater the chance of quench and non-specific binding, varying with the indicator. Under these conditions, the indicator will equilibrate between saline, cytosol and mitochondria. Mitochondrial depolarisation causes the redistribution of dye from mitochondria to cytosol and very little net change in signal over the whole cell, whilst depolarisation of the plasma membrane may cause loss of dye from the cytosol across the plasmamembrane. To use this technique well, high resolution microscopy, ideally confocal microscopy, is required, with digitisation to 12 or even 14 bits if it is to prove possible to resolve differences in cytosolic and mitochondrial signals which may reach a difference of several hundred-fold.

As an ion will partition across a polarised membrane according to the Nernst equation, one might expect a lipophilic dye bearing a charge to behave likewise, as long as the concentration is very low, with no quench and no non-specific binding.

Thus ion distribution may be described from:

$$V = -(RT/ZF) \ln (c_i/c_o)$$

where V is the equilibrium potential across the membrane, C_o and C_i are the outside and inside concentrations of the ion, respectively, R is the gas constant, T is the absolute temperature, F is Faraday's constant, z is the valence of the ion, and l is the logarithm to the base e. From the Nernst equation, the term c_i/c_o may be replaced by F_m/F_o, where F_m is the

The equilibrium potential (V) is measured in volts, absolute temperature (T) is measured in degrees Kelvin, the gas constant (R) is 2 cal mol^{-1} $^oK^{-1}$, and Faraday's constant (F) is 2.3×10^4 cal V^{-1}.

fluorescence over the mitochondrion and F_o is that over the mitochondrion-free cytosol adjacent to the organelle (the fluorescence ratio must be collected confocally to exclude fluorescence from out of focus regions of the cell), with the proviso that the fluorescence signal must be proportional to dye concentration.

In practice, however, most cationic dyes show significant binding to lipid membranes, and membrane binding can enhance the fluorescence of the probe. Thus, the distribution of the fluorescence signal may not be directly proportional to the local dye concentration and it is therefore very difficult to provide reliable calibrations for the signals from these dyes to quantify $\Delta\psi_m$. However, useful qualitative information on mitochondrial polarity is reflected by its distribution and thus valuable - and otherwise inaccessible - data may be obtained by digital imaging of dye-loaded cells.

Additionally, care must be taken to account for the series of electrochemical gradients in the living cell. There is a substantial potential difference across the plasma membrane, and dye will partition across it as it does across the inner mitochondrial membrane. Hence depolarisation of the plasmalemma will induce a redistribution of cytosolic dye into the extracellular space, magnifying the $[dyel]_{mit}/[dye]_{cyt}$ ratio. This then leads to re-equilibration of dye between mitochondrion and cytosol, affecting the fluorescence measured over single mitochondria. Some authors have suggested that depolarisation of the plasma membrane may account for some of the changes in $\Delta\psi_m$ reported in cells loaded with fluorescent potentiometric probes (Nicholls , 2000). Perhaps the most rigorous way to examine the effect of plasma membrane depolarisation is to record changes in signal while voltage-clamping the cell membrane potential. Using this approach, Duchen showed that a voltage step from -70mV to +60mV (the potential at which the Ca^{2+} current appears to reverse) caused no significant change in Rh 123 signal, while a step to 0mV caused a small but significant (~20%) increase in signal (Duchen, 1992). This latter response was shown to be due to the mitochondrial response to a rise in $[Ca^{2+}]_i$ and mitochondrial calcium uptake (which generates an inward current across the mitochondrial inner membrane and a transient depolarisation). In this laboratory, using Rh123 or TMRE in dequench mode or using TMRE at very low

concentrations, we see no significant change in signal simply with plasma membrane depolarisation, even if one might expect it on theoretical grounds.

1.6.3 Toxicity of fluorescent probes

Most indicators have direct toxic effects on mitochondrial function. Thus, carbocyanine dyes such as $DiOC_6(3)$ and JC-1 have long been known to inhibit Complex I (NADH dehydrogenase) and at concentrations of 40-100nM, concentrations often used in flow cytometric studies, $DiOC_6(3)$ inhibits mitochondrial respiration by ~90%, an inhibition equivalent to rotenone (Rottenberg & Wu, 1998). Rh123 inhibits the F_1F_0-ATPase at high concentrations (Emaus, Grunwald & Lemasters, 1986).

Photobleaching of fluorescent dyes, whereby light-induced oxidation of the fluorophore results in a gradual loss of signal, may occur if the intensity of illumination by the excitation light is too great. This is particularly relevant if dyes are loaded at low concentrations when low fluorescence signals may prompt an increase in excitation intensity. Limiting the duration of exposure by closing a shutter intermittently may reduce bleaching.

Light-induced oxidative damage can be equally problematic with mitochondrial probes loaded at high concentrations. Illumination of fluorophores may result in the production of reactive oxygen species, and the consequent oxidative stress can have wide-ranging effects, including induction of local calcium release, inhibition of the electron transport chain and induction of mitochondrial permeability transition. As with photobleaching, limiting the intensity of the excitation light by attenuating the excitation output or reducing the period of illumination will reduce the oxidative stress.

A model of MPT

The work presented in this thesis describes how the fluorescent, potentiometric probe, TMRE, may be used to signal variations in $\Delta\psi_m$ in single, living cells. Additionally, the oxidative properties of the illuminated probe were used to induce an oxidative stress that originated

from within mitochondria, in contrast to exogenously-added pro-oxidants. Imaging of TMRE-loaded cells revealed spontaneous depolarisations of the mitochondrial membrane, both transient and long-lasting. Spontaneous mitochondrial depolarisations are shown to be flickerings of the MPT pore, moreover, these brief openings are shown to progress to a complete dissipation of $\Delta\psi_m$ if the oxidative stress is increased. Using this model, the effects of the MPT on Ca^{2+} signalling events were investigated. Finally, the fate of the cells was examined, and the consequences of MPT, both transient and long-lasting, on cell viability were assayed.

Chapter 2: general methods

In this chapter I set out the general methods I have employed throughout the thesis and describes the equipment used to acquire the data presented. Some minor modifications of equipment or technique were carried out in a few individual experiments and these are described in later chapters. Unless otherwise stated, all experiments were performed on adult rat cortical astrocytes.

2.1 Cell culture

2.1.1 Preparation of adult rat cortical astrocytes.

Adult Sprague-Dawley rats (5-8 weeks old, 120-140 gm body weight) were killed by decapitation. A craniotomy was performed using scissors and tweezers and the brain removed to a dish of sterile, ice-cold Earle's balanced salt solution (EBSS). Under a tissue culture hood, the cerebral hemispheres were dissected free from the optic nerves, the brain stem and the hippocampi using a small spatula. The meninges and superficial blood vessels were then removed by gently rolling the isolated hemispheres over discs of sterilised filter paper. The cerebra were washed in EBSS.

Under a cell culture hood, the hemispheres were transferred to a pot containing a small volume of EBSS where they were chopped using scissors and triturated until apparently homogenous. This suspension was then passed through a 297 μm mesh (Sigma Chemicals Co.), resuspended in EBSS and washed by centrifugation at 400 *g* for 4 minutes at room temperature. The resulting pellet of tissue was suspended in a warmed, nominally Ca^{2+}, Mg^{2+} -free EBSS solution containing 50,000 Uml^{-1} trypsin (Type III, porcine pancreas, Sigma ref. T-7418), 336 Uml^{-1} DNAse 1(Type IV, bovine pancreas, Sigma ref. D-5025), and collagenase 1.033 Uml^{-1} (Type XI, Sigma ref. C-9407) and placed in an incubator (36°C, 95% air, 5% CO_2). The enzymatic digestion was stopped after 15 minutes by the addition of foetal calf

serum (10% of final volume) and the suspension filtered through a 140 μm metal mesh. The filtrate was resuspended in EBSS and centrifuged at 400 *g* at room temperature for 6 minutes. The pellet was resuspended in EBSS, gently layered onto 20 ml 0.4 M sucrose (molecular biology grade, BDH Chemicals Ltd.) in EBSS and centrifuged at 400 *g* for 10 minutes. The resulting pellet was washed twice in EBSS by centrifugation at 400 g for 6 minutes and finally in D-valine based minimal essential medium (MEM) with Earle's salts and supplemented with 5% foetal calf serum. The use of D-valine inhibits the growth of fibroblasts which could potentially overgrow the astrocytes.

The pellet was suspended in 12 ml pre-warmed D-valine MEM supplemented with 5% foetal calf serum, 2 mM glutamine and 1 mM malate and transferred to two 25 cm^2 tissue culture flasks precoated with 0.01% poly-D-lysine. The flasks were placed in an incubator for 24 hours after which time the medium was refreshed. After 6 days in culture the D-val-containing medium was replaced by MEM supplemented with L-valine.

2.1.2 Plating of cells

The cultured astrocytes usually reached confluence in the tissue flasks by about 14 days by which time they could be reseeded onto 24 mm glass coverslips for mounting on a microscope stage.

Glass coverslips (BDH) were soaked overnight in a 20% solution of nitric acid, washed with several changes of distilled water and then soaked in pure acetone for 2 hours. This procedure removes traces of grease, solvent and salts from the glass. Coverslips were then sterilised by irradiation with ultraviolet light for one hour, placed in 35mm Petri dishes, and coated with poly-D-lysine 0.01%. Excess poly-D-lysine was removed by washing with sterile distilled water.

Astrocytes were harvested by removing the culture medium from the tissue flasks and the cells were washed with Ca^{2+}, Mg^{2+} -free EBSS to remove any remaining serum. A 5 ml aliquot

of trypsin solution (0.05% trypsin, 0.5mM EDTA in Ca^{2+}, Mg^{2+} -free EBSS) was added to the flask and the flask returned to the incubator. After 10 minutes the cells were gently detached from the flask wall by scraping with a rubber spatula and transferred to a sterile centrifuge tube. The enzyme action of the trypsin was halted at this stage by the addition of 500 μl foetal calf serum. The suspension was centrifuged for 4 minutes at 400 *g* and the resulting pellet resuspended in 1 ml prewarmed L-valine MEM supplemented with 5% foetal calf serum. The cells were washed twice more in MEM and resuspended before plating. A single drop of this suspension was placed on each coverslip. After allowing the cells to settle for few hours, 1.5 ml L-valine MEM was added to each coverslip and the cells left in the incubator for 3-4 days before use in experiments.

Cells were fed every 3 days by exchanging culture medium with fresh, prewarmed L-valine MEM supplemented with 5% foetal calf serum.

2.2 Dye loading

Immediately prior to experimentation the coverslips were removed from their medium and mounted on custom-built alloy chambers. These mounts consisted of a circular base which held the 24 mm coverslips and a threaded top which, when screwed into the base, formed a water-tight well for bathing the cells in dyes or salines. The provision of a rubber 'O'-ring and Teflon spacer between the top and bottom ensured that there was no fluid leak of well contents onto the objective lens.

All solutions were based on a saline (termed 'recording medium') which composed NaCl 156 mM, KCl 3 mM, $MgSO_4$ 2 mM, KH_2PO_4 1.25 mM, $CaCl_2$ 2 mM, and D-glucose 10 mM. The pH was adjusted to 7.35 and buffered by addition of HEPES 10 mM. When a calcium-free medium was required, $CaCl_2$ was replaced with $MgCl_2$ 2 mM and EGTA 0.5 mM was added.

The membrane-permeant dye tetramethylrhodamine ethyl ester (TMRE) is a highly lipid-soluble cation and passes easily through cell membranes, however the free acid moieties of

other dyes (e.g. fura-2, fluo-3, rhod-2) are negatively charged and water-soluble and thus pass through polar membranes with difficulty. These latter dyes were therefore loaded as their acetoxy-methyl (AM) esters. The esterified derivatives are membrane-permeant and once exposed to endogenous cell esterases the AM esters are cleaved, leaving the fluorophore in the cytosol and/or other cell compartments. Initial dissolving of the AM esters in the aqueous recording medium required the addition of the surfactant Pluronic F-127 which aids the dispersion of water-insoluble molecules in aqueous media.

After the loading period, cells were washed 5 times with 0.5 ml aliquots of recording medium to remove background dye and left in 0.75 ml recording medium for the duration of the experiment.

- TMRE (MW 515) was loaded by immersing cells in a 1.5 μM dye solution for 15 minutes at room temperature followed by washing. In some experiments, cells were equilibrated in a 50 nM solution for 15 minutes. If used at the lower concentration, cells were not washed after equilibration and 50 nM TMRE was left in the recording medium.
- Fluo 3 AM (MW 1130) was loaded in a 4.4 μM solution in the presence of Pluronic F-127 0.005%. Cells were loaded for 30 minutes at room temperature.
- Fura-2 AM (MW 1002) was loaded in a 5 μM solution in the presence of Pluronic F-127 0.005%. Cells were loaded for 30 minutes at room temperature.
- Rhod-2 AM (MW 1124) was loaded in a 4.4 μM solution in the presence of Pluronic F-127 0.005%. Cells were loaded for 30 minutes at room temperature.

2.3 Pressure application of drugs

Application of short-acting drugs (e.g. FCCP, ATP) by pressurised puffer pipette was used to maintain a local effect of the drugs, the applied pressure was adjusted to limit the area of drug application to just a few cells. Glass pipettes (GC150TF-10 borosilicate glass capillaries, Clark Electromedical Instruments, Reading, UK) were drawn out to a tip diameter of 2 - 4 μM using a Model P-87 Flaming/Brown micropipette puller (Sutter Instrument Co, Novato, USA)

and connected to a Picospritzer II (General Valve Corp., Colorado, USA) pressure injector (an Eppendorf Transjector 5246 [Eppendorf, Hamburg, Germany] was used during confocal studies). Pipettes were filled with the relevant drug, tips were brought close (c. 20 μm) to the cells of interest by hydraulic micromanipulator (Narishige, Japan or Eppendorf Micromanipulator 5171) and air pressure (< 0.5 bar) used to apply the drug.

2.4 Fluorescence measurement

Four methods of collecting fluorescence signals were used in the laboratory, each according to its spatial or temporal resolution. When optimal temporal resolution was required in an experiment, the fast-response photomultiplier tubes were used. If fine spatial resolution was required then the confocal or slow scan CCD camera were used.

2.4.1 Microfluorimetry system

This system was based around an inverted, epifluorescence microscope (Nikon Diaphot 300) equipped with a x40 oil immersion, quartz objective lens (numerical aperture 1.3). Cells were continuously transilluminated by red (> 610 nm) light and monitored by video camera to allow direct visualisation of the preparation during experiments. An adjustable diaphragm on the output port of the microscope enabled masking of unwanted areas in the plane of focus, the diaphragm could be set around the image of a single cell (or group of cells) so that the background area was minimised. Fluorescence was excited by a 75 W xenon arc lamp, the light from which passed through a spinning filter wheel (Cairn Research, Faversham, UK) which rotated at 12 Hz. This arrangement allowed rapid sequential excitation of fluorescence through six 10 nm bandpass filters centred at 340, 360, 380 and 490 nm. Excitation light was separated from emission light by a dichroic mirror and the light emitted from the fluorescing preparation was measured by two photomultiplier tubes (PMTs) separated by a second dichroic mirror (see Figure 2.1). Thus excitation wavelengths could be changed within 14 msec and two emission signals could be measured simultaneously. Cells could therefore be loaded with more than one dye and/or dyes with dual emission or excitation could be used. The optical arrangements for individual experiments are detailed in Table 2.1.

Figure 2.1: schematic of microfluorimetry setup. The filter wheel spinning at 12 Hz allowed rapid sequential excitation at up to 6 wavelengths, while the 2 PMTs and the dichroic mirrors allowed simultaneous measurement of two emission wavelengths.

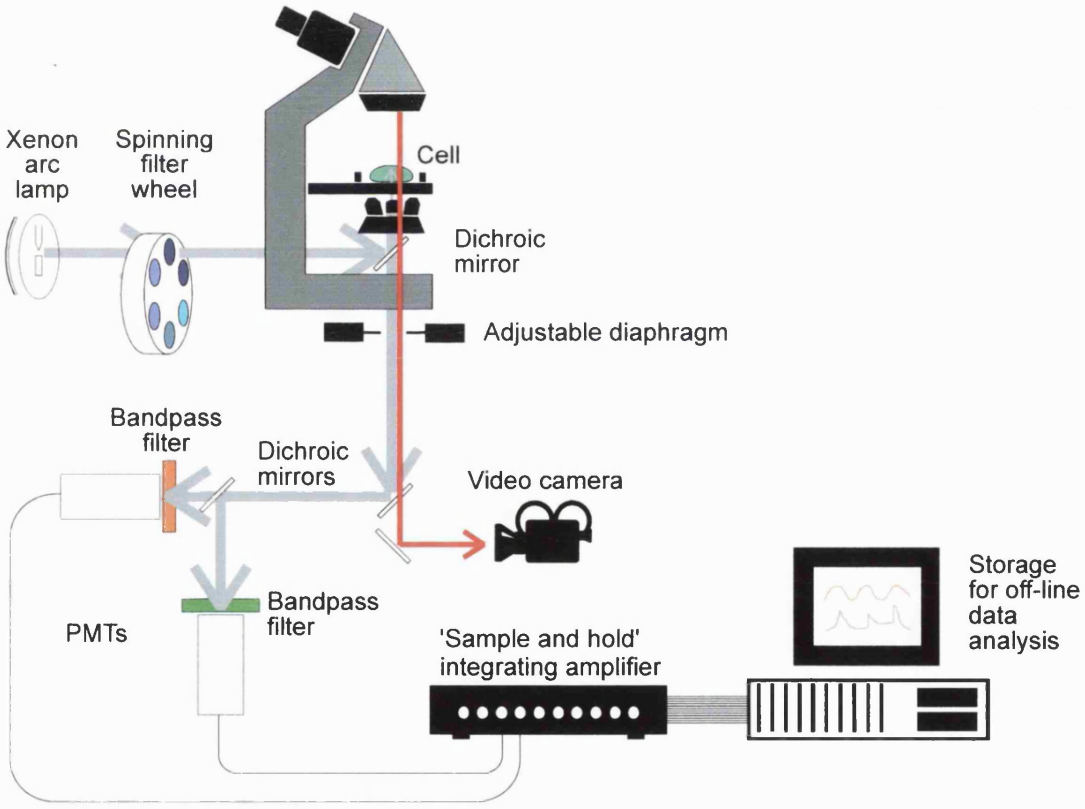

Fluorophore	*Excitation filter wavelength (nm)*	*Microscope dichroic (nm)*	*PMT Dichroic (nm)*	*PMT bandpass filters (nm)*
Fura-2	340/380	400 or 510	none	530 or 540 SP
TMRE	490	510	none	590
TMRE / fura-2	340/380/490	510	510	590 (TMRE) 530 (fura-2)
TMRE /H_2DCF	490	510	540	590 (TMRE) 530 (H_2DCF)

Table 2.1: optical setup for PMT experiments. A dichroic mirror in the microscope separated excitation from emission light, and a second dichroic mirror positioned between the PMTs allowed simultaneous measurement of 2 signals. When cells were loaded with two dyes, the signal from each was measured by a separate PMT, each with an appropriate bandpass filter.

The signals from the PMTs at each wavelength were extracted using a synchronised, integrating 'sample and hold' circuit (Cairn Research). This step was necessary as the signal transduced by the PMTs was parabolic in nature due to the passage of the rotating filter in front of the light source and contained signals elicited from all six excitation filters. The sample and hold circuit sampled the voltage output from each PMT, separated the six channels, integrated this varying signal and then 'held' the maximum signal until the relevant filter reappeared on its rotation. Thus an apparently constant signal was extracted from an interrupted source.

The integrated signals were collected via a Tecmar DMA Labmaster-TL1 interface board controlled by Labtech Notebook software (Laboratory Technologies Corp., Wilmington, USA). Data were imported into Microcal Origin 4.1 software for off-line analysis.

For spectral analysis of dyes loaded into cells, the light path to the PMTs was diverted to an imaging spectrograph (Oriel InstaSpec IV). Cells were illuminated as before but with the filter wheel in a fixed position. Fluorescence emission was scanned using a rotating grating and

the resultant spectrum imaged onto a cooled charge coupled device (CCD) chip. These data were analysed using InstaSpec software.

2.4.2 Frame transfer imaging camera

This imaging system was based around an inverted, epifluorescence microscope (Nikon, Diaphot TMD) equipped with x40 and x60 oil immersion, quartz objective lenses (NA 1.3 and 1.4, respectively). Cells were mounted on the microscope stage and fluorescence excited by a 75 W xenon arc lamp, the light from which passed via a computer-controlled shutter through a stepping filter wheel (Cairn Research). This filter wheel steps through a programmed sequence of 10 nm bandpass filters centred at 340, 380, 490 and 530 nm for any combination of dwell times and was controlled by Acquisition Manager software (Kinetic Imaging, Liverpool, UK). Excitation light was separated from emission light by a dichroic mirror (see Figure 2.2) and the fluorescence emitted focussed on the CCD chip of an imaging camera (Digital Pixel, Brighton, UK). To reduce background noise, the camera was cooled by a Peltier element to a temperature of -20°C. The data were read out by frame transfer, whereby half of the chip (an array of 600 x 800 pixels, pixel size 16 μm) was read out to the computer while the other half was exposed to the light path from the objective. This method of data transfer limited image acquisition to around 1 Hz but acquisition speed could be improved by 'binning' the pixels so that the signal from square arrays of 4 or 9 pixels was averaged and read out as a single data point, although reducing the effective number of pixels degraded the spatial resolution. In addition, regions of interest could be selected within images reducing the number of pixels exposed per image and hence increasing readout time. Due to the large number of pixels and the excellent optics of the setup the spatial resolution of this system was very good, mitochondria were easily resolved (see Figure 2.3) and it was used extensively in the initial characterisation of the mitochondrial depolarisations and in experiments when two fluorescent dyes were used concurrently.

Figure 2.2: schematic of Digital Pixel ('slow-scan') CCD camera system.

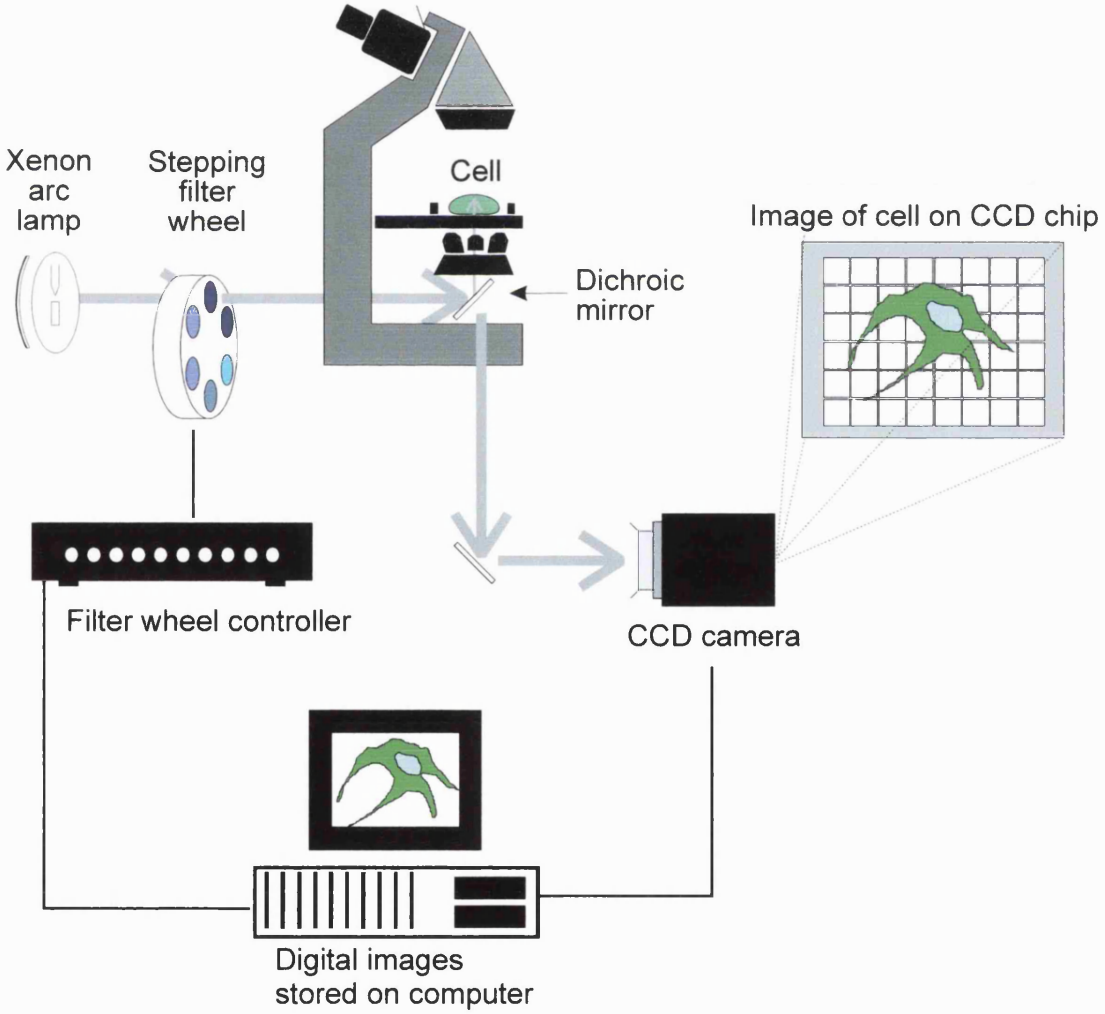

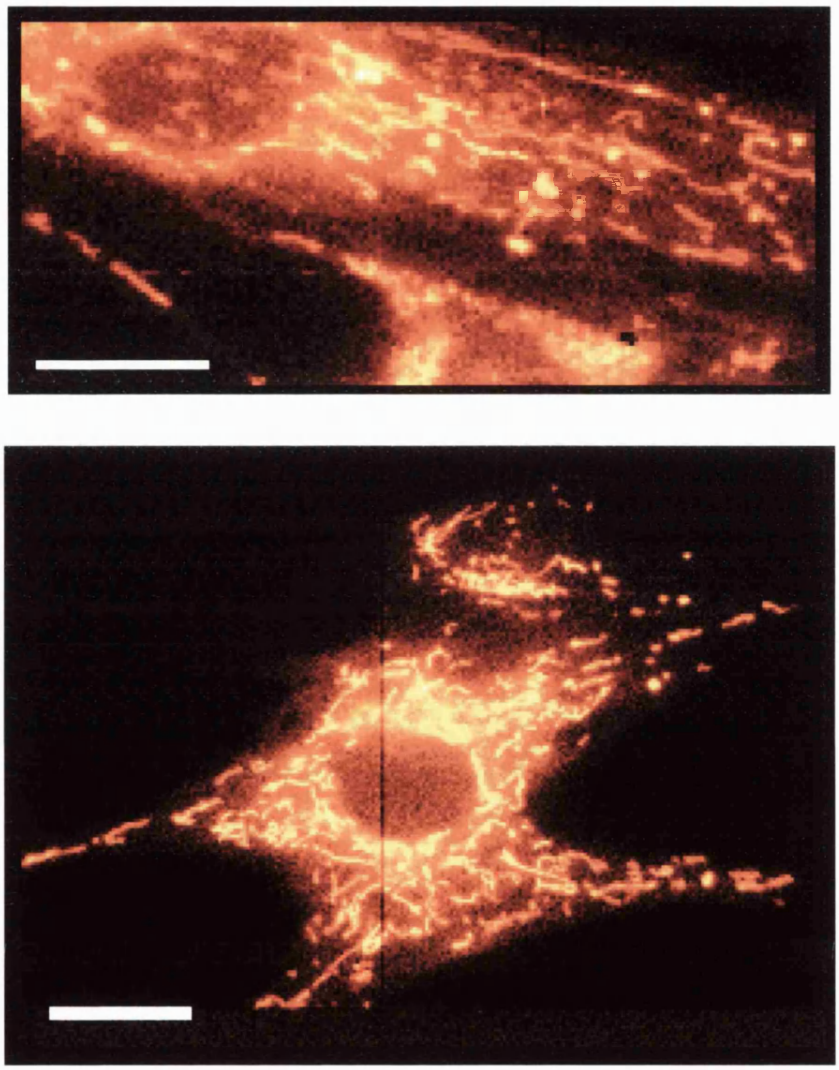

Figure 2.3: digital images of TMRE-loaded astrocytes. These images were obtained using the Digital Pixel frame transfer CCD camera. A 63x objective lens was used. Individual mitochondria can clearly be seen surrounding the dye-free nucleus. The scale bars denote 10 μm.

2.4.3 Interline transfer imaging setup

This imaging system was based around an inverted, epifluorescence microscope (Zeiss Axiovert 100 TV) equipped with x40 and x63 oil immersion, quartz objective lenses (NA 1.3 and 1.4, respectively) as well as a x40 long working distance lens (NA 0.68). Cells were mounted on the stage and fluorescence was excited by a 75W xenon arc lamp, the light from which passed through a slider holding three sets of excitation, dichroic and emission filters (see Table 2.2).

Filter Set	*Excitation filter (nm)*	*Dichroic mirror (nm)*	*Emission filter (nm)*
1	546	580	590
2	355	395	420
3	450-490	510	520

Table 2.2: filter sets in Zeiss Axiovert slider. All emission filters were longpass – light of wavelength longer than the quoted value passes through the filter.

In some experiments the arc lamp was replaced by a monochromator (Monokromator, Kinetic Imaging) connected to the microscope by a fibre optic (see Figure 2.4). The monochromator light source was also a 75 W xenon arc lamp, but by means of a rotating grating (1200 lpmm), wavelengths of between 300 and 700nm (bandwidth 12nm) could be selected using the computer interface. The monochromator drivers were interfaced with those of the CCD camera, allowing integrated imaging of wavelength switches at up to 3 msec between any two wavelengths. Excitation intensity was adjustable by means of a slider, controlled by a micrometer, which could be positioned in the light path. The CCD camera (Hamamatsu C4880-80) employed a chip with an array of 656 x 494 pixels (pixel area 9.9 μm^2). In contrast to the frame transfer (Digital Pixel) camera, this device used an interline transfer method of data read-out. This involved using alternate, masked columns of pixels as 'data sinks', cutting the read-out time and improving the acquisition rate. The presence of micro-lenses on the chip meant that light was focused on the matched pixel in the adjacent row, so that no signal

Figure 2.4: schematic of the Hamamatsu interline transfer cooled CCD camera setup. The camera could acquire data at up to 500 Hz but maintaining spatial resolution of mitochondria limited acquisition rates to under 30 Hz. The monochromator stepped through wavelengths between 300 and 700 nm.

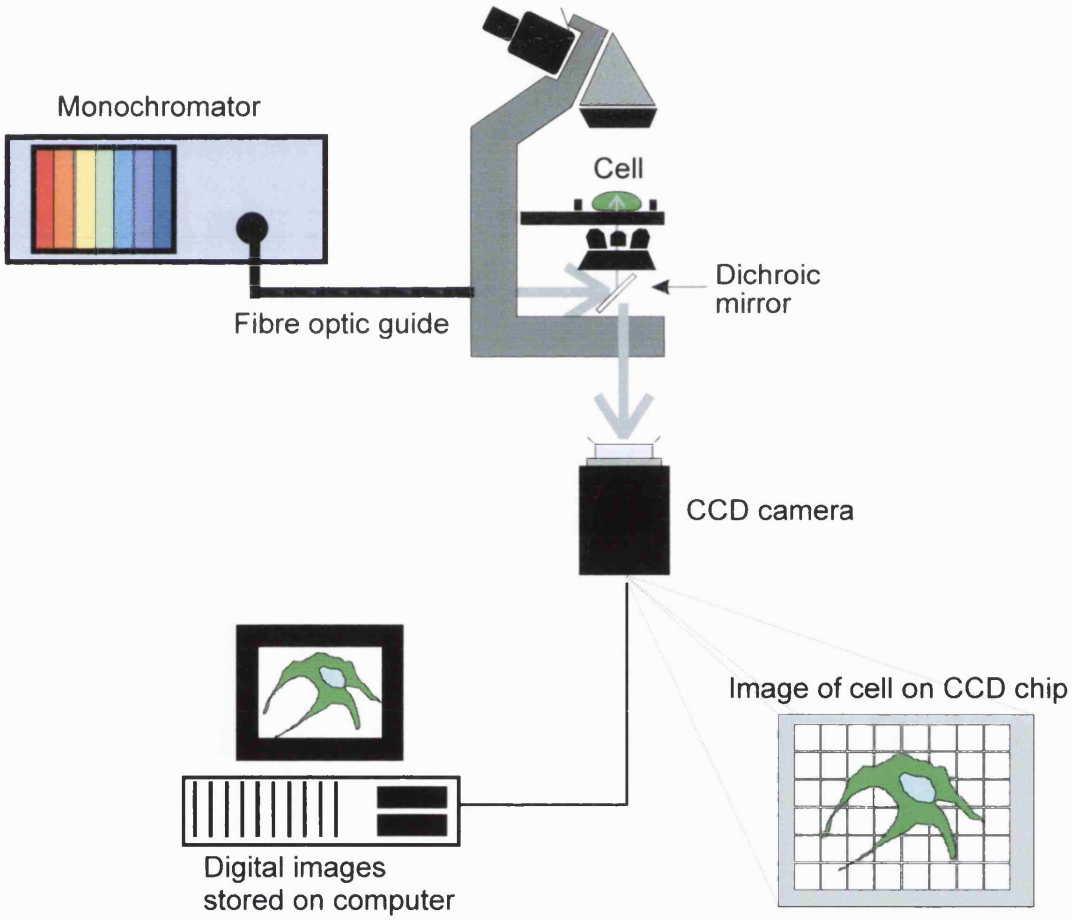

was lost. Moreover, the rate of digitisation of the analogue signal was extremely high as data could be digitised to either 10- or 12-bit and the acquisition software could be used in 8-bit mode. Using the 8-bit mode the 10-bit raw data could be read out even more quickly by discarding unwanted information at either the high or low end of the scale. When imaging with the camera at 10-bits, the data acquisition software set at 8-bit, and data binned into 4-pixel groups, images were acquired at around 30 Hz. Acquisition rates could be much greater than this (up to 500 Hz), but at higher rates all spatial resolution was lost with the pixels binned into a single group. In this mode the camera was acting essentially as a fast-response PMT. To maintain spatial resolution and allow adequate exposure times, the fastest acquisition rates were below 50 Hz but still appreciably faster than the Digital Pixel camera. This system was particularly useful when analysing the kinetics of the mitochondrial depolarisations.

2.4.4 Confocal Imaging

Confocal images were produced using the Zeiss LSM 510 laser scanning microscope. This is based around a Zeiss Axiovert 100 M inverted epifluorescence microscope equipped with x40 and x63 oil immersion lenses (NA 1.3 and 1.4, respectively) as well a x63 water immersion lens (NA 1.2). The water immersion lens was corrected for chromatic aberration. Fluorescence was excited using one or more of three laser types – a UV argon (lines at 351 and 364 nm), an argon (lines at 458, 488 and 514 nm) and two helium-neon lasers (lines at 543 and 633 nm).

The confocal principle is based around the use of a point source of excitation illumination in combination with an adjustable aperture (the 'pinhole diaphragm') placed in the emission light pathway (see Figure 2.5). The laser light source is focussed on the specimen so that only a small fraction is illuminated at any one time and a scanning module (a silvered mirror) rapidly scans this point back and forth across the area being imaged. The emission signal is scanned concurrently by the same module and the pinhole placed in the emission pathway limits the light falling on the PMT to a similar single point. Thus, light from out of focus layers is rejected, resulting in images that are less blurred, and allowing optical sections of the

Figure 2.5: schematic of laser scanning confocal microscope. For clarity, only one laser and two PMTs are shown. The Zeiss LSM 510 has four of each, allowing truly simultaneous imaging of several fluorescent probes

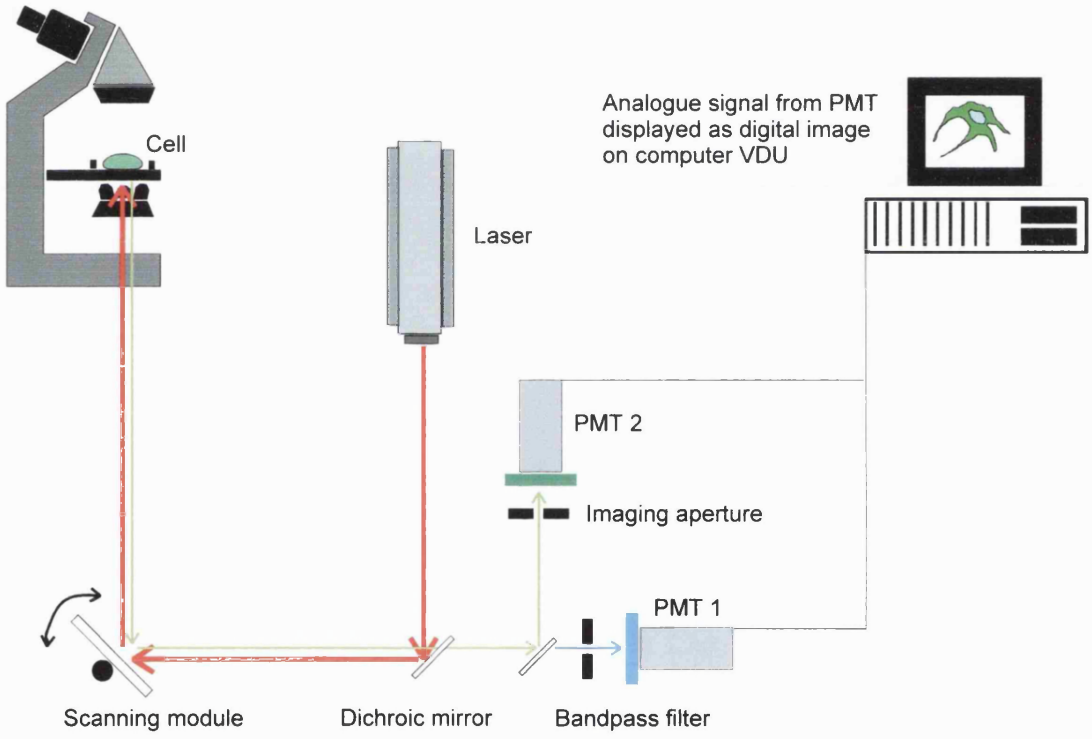

preparation to be obtained non-invasively (in practice, optical sections of around 1 μm thickness were imaged). In addition, the fact that the LSM 510 is equipped with four lasers and four PMTs allows truly simultaneous imaging using up to seven excitation wavelengths and up to four emission wavelengths. The presence of an acousto-optic tunable filter meant that the intensity of each laser line could be independently controlled.

2.5 Image processing

Images were collected using Kinetic Imaging 'Acquisition Manager' software (for data created by CCD cameras) or by Zeiss 'LSM' software (for data created by the confocal imaging system). All images were analysed using Kinetic Imaging 'Lucida' software.

2.5.1 Digitisation

The signal emitted by the fluorescing cell was digitised to 12-bit for the majority of the experiments performed. In those experiments where temporal resolution was of more interest than the spatial information, data were digitised to 10-bit and stored as 8-bit; these steps allowed faster readout of data from the CCD chip.

2.5.2 Mapping

In order to assess all the information contained in the images, frequent 'remapping' was required. There are 4096 grey levels in a 12-bit image, but as computer visual display units operate at 8-bit (256 grey levels) much of this digital information may be lost when images are displayed on a monitor. If the range of the signal change is small an event may be invisible as displayed and its significance overlooked. The mapping process essentially 'stretches' or 'compresses' the data display to fit the available grey levels (see Figure 2.6). The original data are unchanged, it is the contrast of the *display* that is being adjusted. By remapping, both small and large events may be analysed from a single image series, providing the image signal is not saturating.

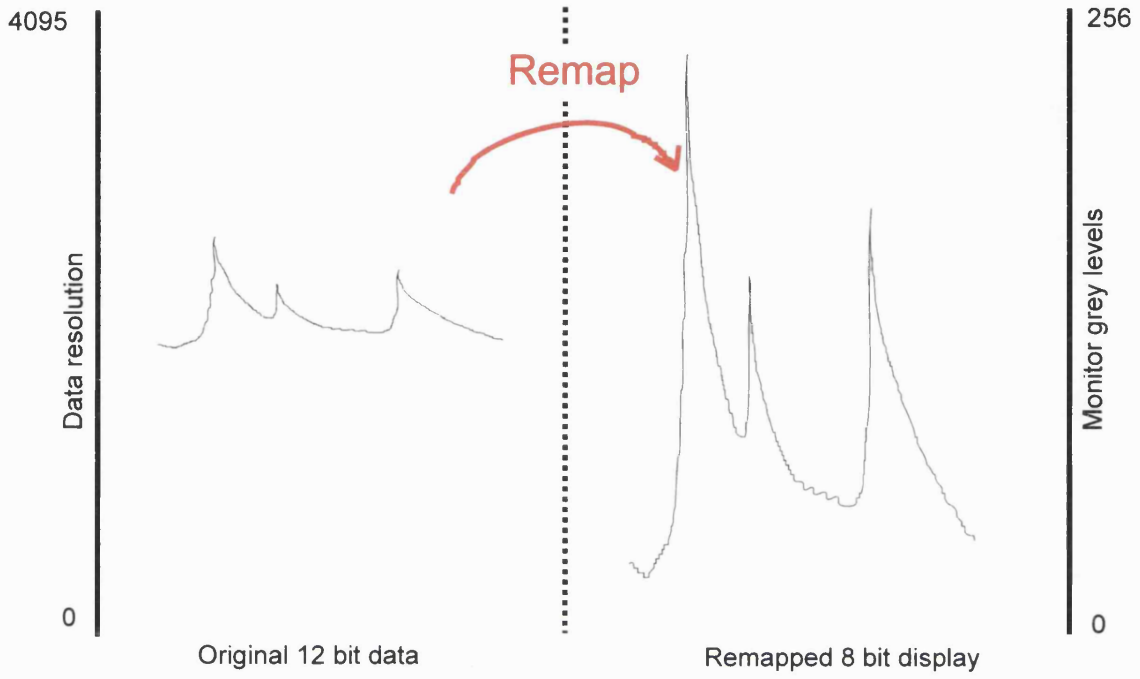

Figure 2.6: the principle of remapping. Original values remain unchanged but the image representation is adjusted to maximise the display in 8 bits of 12 bit data.

2.5.3 Lookup tables

Digital images are monochrome. The pixels of a CCD chip detect only light levels, not wavelengths, and these are displayed as a monochrome image. The human eye, however, can detect more information in a coloured image as we can only distinguish about 64 grey levels. To improve image quality, false colour was added to images by applying 'lookup tables', spectra of colour correlated to image intensity. Typically, warmer colours (red, orange) reflect greater signal intensity.

2.5.4 Ratioing and differentiation of images

Calibration of fluorophores that have single excitation and emission wavelengths is difficult and laborious. A bright fluorescence may signal a high local calcium concentration (in the case of a calcium-sensitive fluorophore) or merely reflect a local accumulation of calcium-free dye. Each cell must be calibrated individually and the maximum and minimum fluorescence established for each fluorophore. Often, as in the case of calcium-sensitive probes, the plasma membrane needs to be permeabilised to allow entry of calibrating solutions, and permeabilising single cells without damaging their neighbours is very difficult. For this reason, fluorescence of single-wavelength dyes is usually represented on an arbitrary scale, enabling qualitative but not quantitative analysis. This system has been used in this thesis.

Normalising image series allows signal changes in time to be assessed more easily, and dividing a time series by the first image in that series will emphasise how the signal has changed with time. However, it is possible that the first image could contain transients that would confound ratioing of the time series. For example, if a brief calcium transient appeared in the first image, using this fluorescence value as a denominator for ratioing of a time series would underestimate the relative fluorescence at that point for the entire series. In other words, spatial as well as temporal changes need to be controlled for. One way of doing this is to use a 'darkest image' denominator, on the assumption that minimum TMRE fluorescence reflected maximum mitochondrial membrane potential (see Chapter 3). To construct a darkest

image, the image series was interrogated by the software and the point in time at which each pixel was at its darkest was established. The individual pixels were then combined to form a 'virtual image' which reflected minimum signal. This darkest image was used in ratioing image series to reveal how the signal had changed from a baseline of minimum fluorescence.

For relatively slow physiological events, for example a global rise in cell calcium, ratioing images against a first or darkest image will show how the signal has changed in time. However, rapid transients that may occur several times at the same place in quick succession may be lost in this process, especially if the interval between successive events is short. In such cases, differentiation of image series was performed in order to emphasise a change in signal from one image in a series to the next. Images were serially subtracted from their immediate predecessor and the serial product displayed.

Chapter 3: verification of fluorophore wavelengths and the use of TMRE as a probe of mitochondrial membrane potential.

The fluorescent, potentiometric probe, TMRE, was used to signal mitochondrial depolarisations in intact cells, and these depolarisations were detected and analysed using digital imaging techniques. In order to establish the spectra and behaviour of the dye, and to establish whether it could be used as a reliable indicator of $\Delta\psi_m$, experiments were performed as set out in this chapter. Additionally, other dyes used in this thesis were examined and their *in vivo* spectra measured.

3.1 Determination of the *in vivo* spectra of fluorescent dyes.

The excitation and emission spectra of commercially available fluorescent probes are supplied by the manufacturing companies, however the majority of these spectra are determined *in vitro* and in some cases (as with TMRE) the spectra of a similar compound are supplied in place of those of the relevant dye. Although 'differences between the spectra displayed and those of (TMRE) are not expected to be significant' (Molecular Probes website) the spectra of dyes to be used in experiments were checked *in vivo* to determine whether there were any spectral shifts in living cells (Kalenak, McKenzie & Conover, 1991; Stevens, Fouty, Cornfield & Rodman, 1994). In addition, it is possible that some compounds may cause spectral shifts in dyes, obfuscating interpretation of fluorescence intensity measurements. Therefore, the drugs that were to be commonly used in experiments, e.g. carbonyl cyanide p-trifluoromethoxyphenyl hydrazone (FCCP) to induce mitochondrial depolarisation, were applied to ascertain their effects on the fluorophore spectra.

3.1.1 Experimental procedures

i. Emission spectra.

Cortical astrocytes were loaded with a series of fluorescent probes following the dye-loading protocol set out in Chapter 2, Section 2.2. Coverslips containing dye-loaded cells were mounted on the stage of the microfluorimetry setup with the InstaSpec IV spectrograph attached to the emission port of the microscope. Background dark current was determined by taking a spectrum while the spectrograph's integral shutter was closed and this value was subtracted on-line from the acquired data. Fluorescence of each probe was elicited using the filter wheel - an excitation wavelength was chosen with reference to the literature accompanying the probe. Using the video monitor, the diaphragm on the microscope emission port was closed around an image of the cell to exclude as much background as possible and the emission signal was scanned by the spectrograph. Suitable dichroic mirrors were inserted for each excitation wavelength in order to separate the excitation from the emission signal. Data were stored on computer and analysed using InstaSpec software.

Agonists were added by puffer pipette to some cells in order to check whether their action brought about a change in the emission wavelength for the relevant fluorophore. To this end, FCCP 1 μM was added to TMRE-loaded cells and ATP 100 μM (an agonist of IP_3-mediated calcium release in these cells) was added to rhod 2- and fura 2-loaded cells.

ii. Excitation spectra.

Cortical astrocytes were loaded with the same dyes as above and mounted on the stage of the Hamamatsu CCD system. The monochromator was set to ramp through excitation wavelengths in 5 nm steps (from 300 to 700 nm, inclusive) and images were collected at each wavelength step by the CCD camera. Suitable dichroic mirrors were chosen to separate the excitation from the emission light. In some cases drugs were applied by puffer pipette to the cells to check whether their action brought about a change in the excitation wavelength: FCCP 1 μM was added to TMRE-loaded cells, ATP 100 μM was added to rhod 2- and fura 2-loaded cells.

Images were analysed using Lucida software as follows: a cell-free area of the image was chosen and the signal over that area measured, designated as the background and subtracted from the image series. A region of interest was drawn around a cell, excluding background, and the mean fluorescence signal over this region plotted against the changing excitation wavelength. For each dye, the signal from several cells were collected in this way. Plots were imported into a spreadsheet (Origin), an average fluorescence for the number of cells studied calculated, replotted against the excitation wavelengths and the maxima noted.

3.1.2 Results

TMRE

An emission spectrum of a TMRE-loaded astrocyte is illustrated in Figure 3.1, Panel A. The cell was illuminated with 490 nm light and a 510 nm ('Tsien') dichroic mirror was used to separate excitation light from the fluorescence signal. The emission signal peaks at 590 nm in the resting cell (as it did in all cells examined).

As FCCP was frequently used to depolarise mitochondria, the effect of this drug on TMRE emission wavelength was checked. As can be seen from Figure 3.1, Panel B, the addition of FCCP to a TMRE-loaded astrocyte increases the signal (see Chapter 4), but the peak emission wavelength of the TMRE before and after FCCP was 590 nm.

Figure 3.1, Panel C illustrates the effect of ATP 100 μM on TMRE fluorescence *in vivo*. As an agonist of IP_3-mediated calcium release in these cells, ATP was often applied in later experiments. There was a rise in fluorescence, signalling a mitochondrial depolarisation consistent with electrogenic uptake of cytosolic calcium (Duchen, 1992; Peuchen, Clark & Duchen, 1996a). The peak emission signal was at 588 nm in the resting cell and 590 nm after addition of ATP.

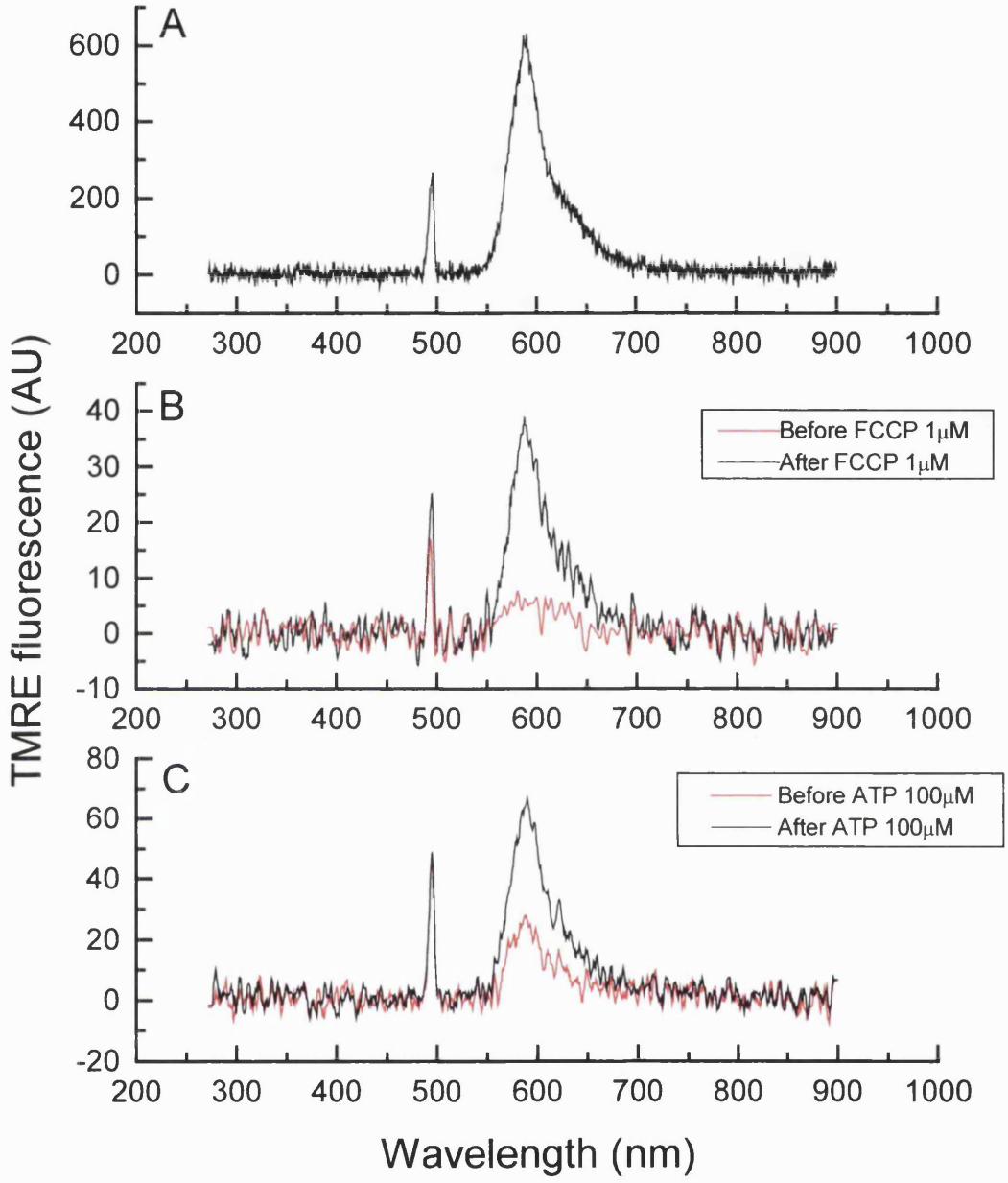

Figure 3.1: Emission spectra recorded from TMRE-loaded cortical astrocytes. Panel A, typical emission spectrum from a single cell. The sharp peak at 495 nm is not fluorescence from the fluorophore but breakthrough of excitation light centred at 490 nm. Panel B, FCCP causes a rise in fluorescence but no change in emission wavelength. Panel C, ATP causes a rise in fluorescence, due to mitochondrial calcium uptake and loss of $\Delta\Psi_m$, but no change in emission wavelength.

Hence mitochondrial depolarisation, whether by action of a protonophore or by physiological uptake of calcium caused a rise in the TMRE fluorescence but did not cause a shift in emission wavelength peak.

The mean excitation spectrum of 12 TMRE-loaded astrocytes is shown in Figure 3.2. Peak excitation was at 555 nm, although some excitation extended down as far as 480 nm. There were small peaks at 330 nm and 405 nm. The peak was consistently at 555 nm, but the error bars reveal a wide range in amplitudes, reflecting variability in dye loading. The peak excitation wavelength of astrocytes treated with FCCP and ATP did not change (see Table 3.1).

Fluorescence emission and excitation wavelengths for astrocytes loaded with rhod-2 AM, fluo-3 AM, and fura-2 AM were measured using the same method. ATP was added to cells loaded with rhod-2 AM and fura-2 AM to check for excitation wavelength shifts on calcium release. It was found that the efficiency of the spectrograph was too low to image changing fluorescence over a few seconds, prohibiting assessment of a short-lived signal change (as when calcium release agonists were applied). For this reason, emission characteristics of calcium-bound dyes could not be assessed. The signal change of dequenched TMRE, however was large and sustained enough to be measured.

Finally, the autofluorescence of the glass coverslips in combination with the standard recording medium was measured.

The data from these experiments are summarised in Tables 3.1a and 3.1b.

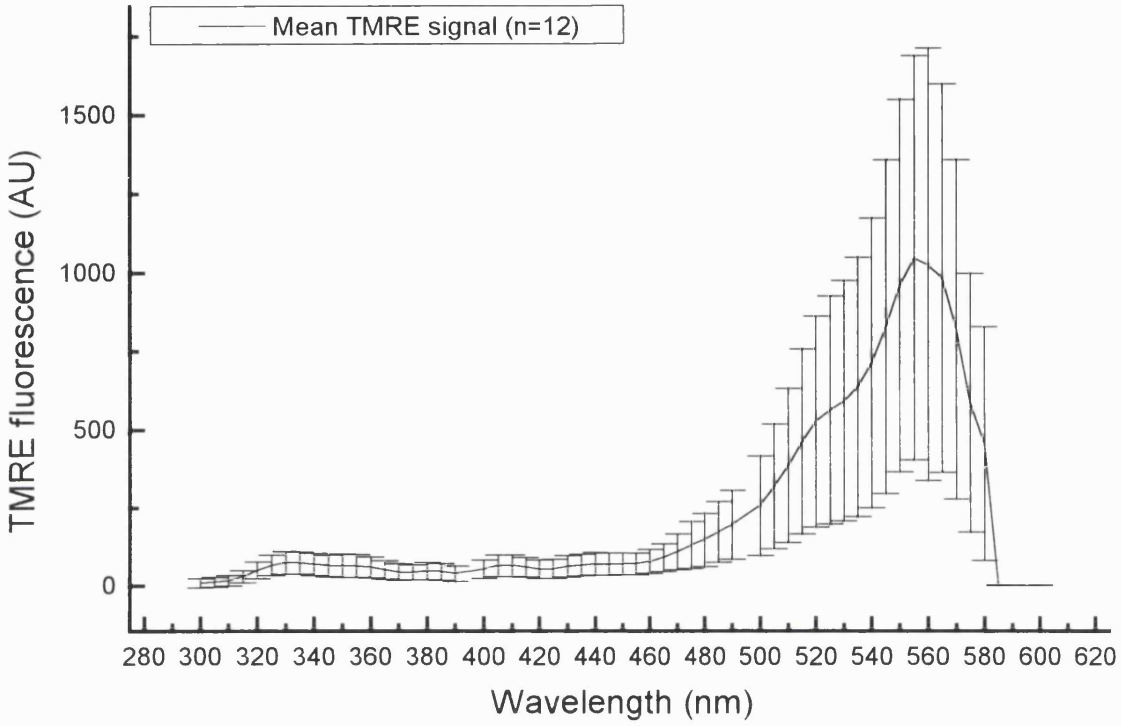

Figure 3.2: mean excitation spectrum of 12 cortical astrocytes loaded with TMRE 1.5 μM.

Error bars denote standard deviations.

Table 3.1a: excitation spectra of dyes used in this thesis

Fluorophore	*Dichroic mirror*	*In vitro excitation peak*	*Excitation peak (resting cell)*	*Drug added*	*Excitation peak (stimulated cell)*
TMRE	580	549	555-560	FCCP /ATP	555-560
Fluo –3	510	506	490	-	-
Fura-2	395	363/355	357	ATP	355
Rhod-2	580	550	555	ATP	570
Glass and saline	395	-	355-375	-	-

Table 3.1b: emission spectra of dyes used in this thesis

Fluorophore	*Excitation λ*	*Dichroic mirror*	*In vitro emission peak*	*Emission peak (resting cell)*	*Drug added*	*Emission peak (stimulated cell)*
TMRE	490	510	574	590	FCCP /ATP	590
Fluo -3	490	510	526	530	-	-
Fura-2	340/380	510	505	540	-	-
Rhod-2	490	510	571	586	-	-

Tables 3.1a and 3.1b. Summary of the excitation and emission peaks of fluorophores used in following experiments. The effect of ATP 100 μM and FCCP 1 μM on wavelength are shown, where measured. The cut-off point of the dichroic mirror used in each experiment is included as reference to this explains why there are sharp drops in signal at wavelengths approaching this value (see Figure 3.1). *In vitro* values were obtained from literature accompanying the fluorophores. Some autofluorescence of the glass coverslip and the saline was noted (excitation peak 355 – 375 nm), but the signal amplitude was so small it was unlikely to significantly contribute to the signal emitted by the fluorophores under experimental conditions.

3.2 Imaging of TMRE-loaded astrocytes

3.2.1 Experimental procedures

Cortical astrocytes were loaded with TMRE 50 nM ('low dose') or 1.5 μM ('high-dose') for 15 minutes at room temperature. Images were collected by CCD camera and by confocal microscopy and were analysed using Lucida software. The analogue signals were converted to 12-bit digital data and TMRE fluorescence is shown on an arbitrary scale, where a saturating signal would be 4095.

As TMRE is a lipophilic, diffusible cation, it should distribute intracellularly in a Nernstian fashion (Ehrenberg, Montana, Wei, Wuskell & Loew, 1988). That is, the TMRE was expected to distribute across cell membranes according to its electrochemical gradient, accumulating in a negatively-charged environment until a concentration of molecules was reached that created an electrochemical equilibrium. Thus, dissipation of mitochondrial inner membrane potential ($\Delta\Psi_m$) would be expected to cause a redistribution of the dye as the electrical component of the Nernst effect is dissipated. To test for this, 1 μM (FCCP) was applied by puffer pipette brought close to the cells being imaged. FCCP is a highly diffusible, amphipathic protonophore that discharges the proton gradient across the inner mitochondrial membrane, uncoupling mitochondrial respiration and dissipating $\Delta\Psi_m$.

Mitochondria may also be depolarised by inhibiting electron transport. The addition of pharmacological inhibitors of the enzymes in the electron transport chain prevents electron transport and thus proton translocation at Complexes I, III, and IV. The inhibition of proton translocation, together with proton leak and re-entry via the ATP synthase, depolarises the membrane potential leaving the integrity of the inner mitochondrial membrane unaltered. As an alternative to FCCP-induced depolarisation, the Complex I inhibitor, rotenone, was applied to TMRE-loaded cells to investigate the behaviour of the dye. Rotenone 2 μM was applied by puffer pipette and the fluorescence signal change was measured. As the dissipation of the proton gradient may cause ATP synthase to operate in reverse in some cell types, consuming

ATP and expelling protons, the ATP synthase blocker, oligomycin, was added. The presence of oligomycin 2.5 μgml^{-1} prevented the maintenance of $\Delta\psi_m$ by ATP synthase reversal.

Results

Loading of cortical astrocytes with TMRE, whether as a low or a high dose, revealed many selectively stained, vermiform structures distributed throughout the cells, often occurring more densely around the nuclei (see Figure 3.3).

Confocal imaging of the cells loaded with low dose TMRE showed a bright, stable signal over the fluorescing organelles, and much dimmer, but stable, signals over the cytosol and nucleus. Application of FCCP produced a rapid reduction in the signal recorded over the fluorescing structures with a concomitant rise in the signal recorded over nearby cytosol (see Figure 3.4). As FCCP acts to abolish $\Delta\Psi_m$, these observations are consistent with a mitochondrial loading of the dye which is reversed by the FCCP-induced dissipation of the $\Delta\Psi_m$ causing a redistribution into the cytosol. The action of FCCP is reversible over a period of time, and the mitochondria were seen to reabsorb the TMRE soon after the FCCP application.

The pattern of signal change over the cells loaded with the high dose TMRE was quite different. In Figure 3.5, the background-subtracted confocal images (Panel A) clearly show that FCCP 1 μM induced a *rise* of whole-cell fluorescence and loss of definition of the mitochondria. Thus, depolarisation of the mitochondria caused a dequench of the TMRE fluorescence. The image pair in Panel B are ratioed against a darkest image. This process reveals the *proportional* change in signal in each pixel induced by FCCP and the darker mitochondria in this image confirm a proportionally smaller rise in fluorescence over the depolarised organelles as compared with that seen over the cytosol. These data are consistent with dye efflux from the mitochondria into the cytosol coincident with fluorescence dequench.

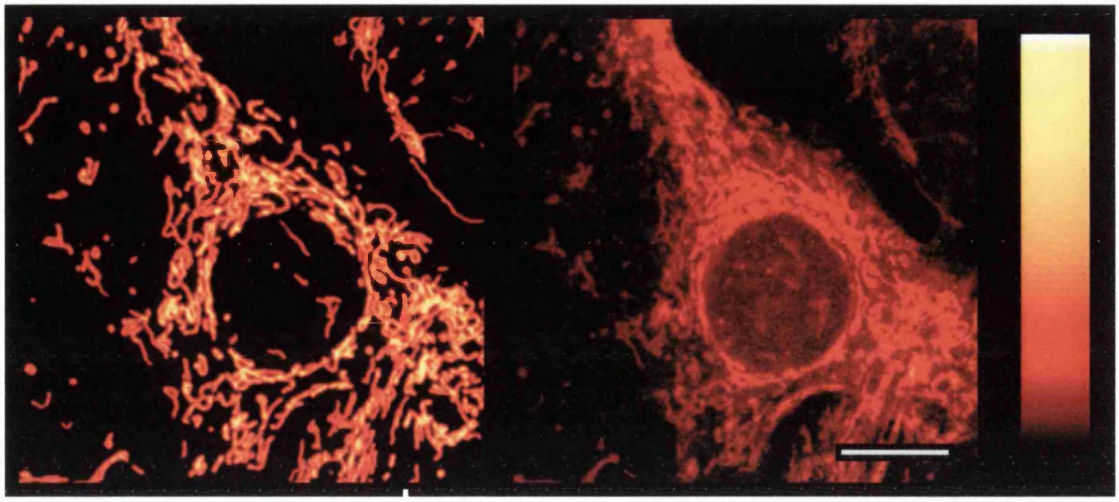

Image a Image b The scale bar represents 10 μm.

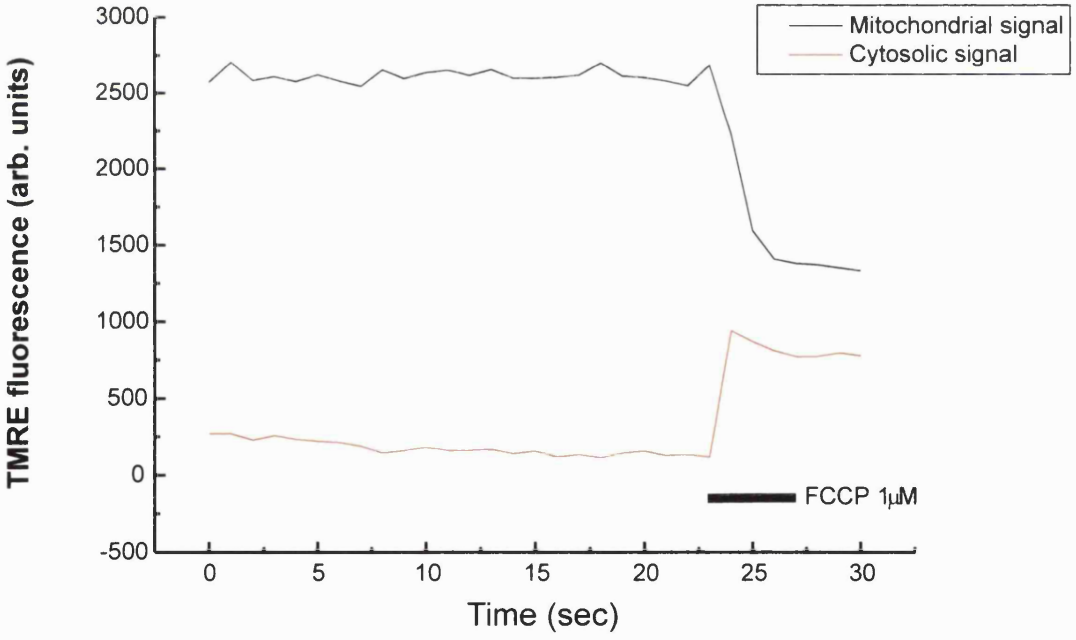

Figure 3.4: application of the protonophore FCCP dissipates the TMRE signal over mitochondria and induces a concomitant rise over nearby cytosol. Confocal images (upper panel) of astrocytes loaded in 50 nM TMRE demonstrate the loss of mitochondrial staining on dissipation of $\Delta\psi_m$ (image b). The dye leaves the mitochondria and redistributes into the cytosol.

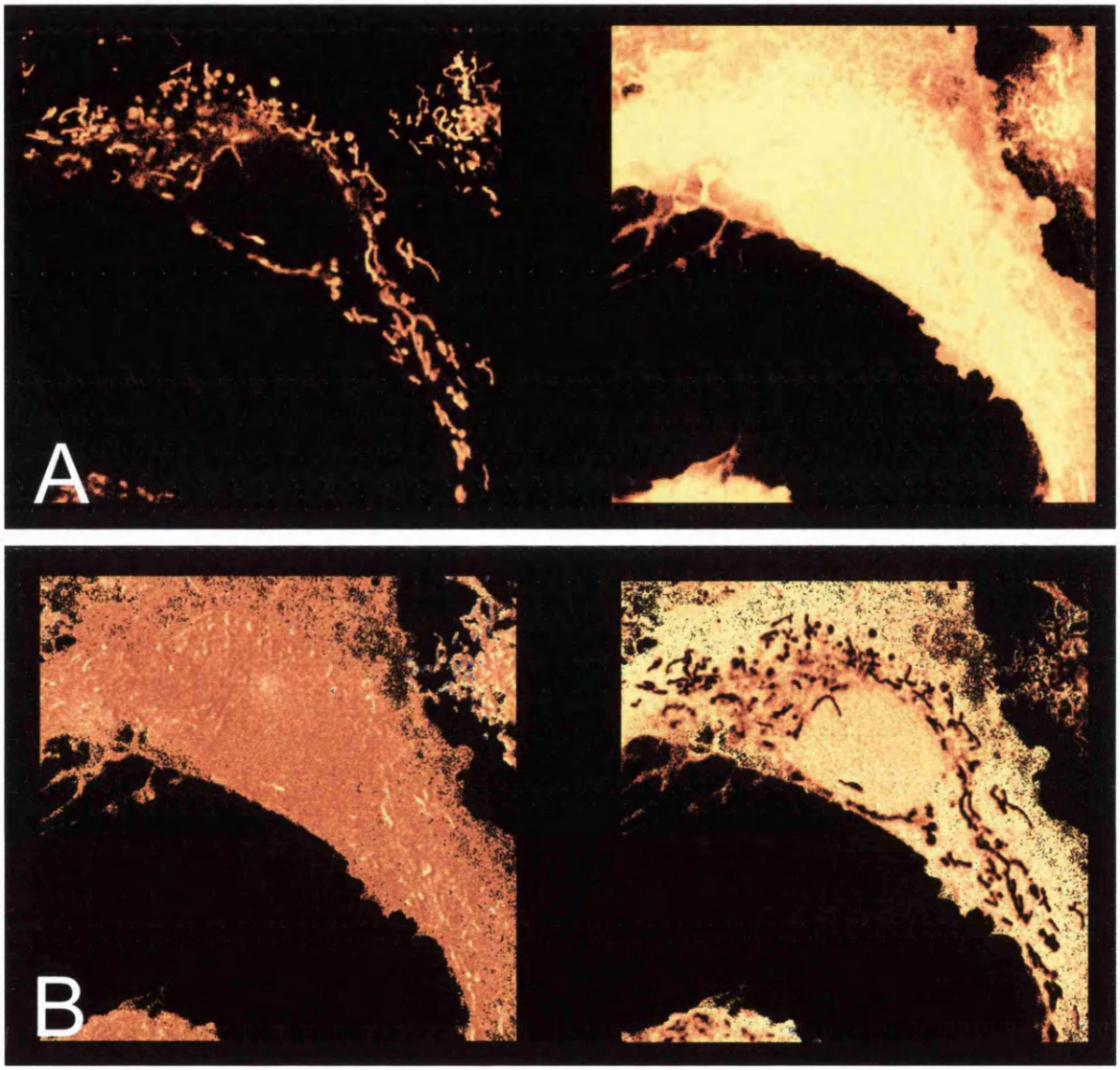

Figure 3.5: dissipation of $\Delta\psi_m$ with FCCP causes a redistribution of TMRE and a dequench of the fluorescence. Panel A - raw images, the dequench of the TMRE signal engulfs the whole cell. Panel B - images ratioed against the darkest image showing the proportional change in signal after FCCP. Mitochondria are revealed as dark bodies, and the large signal change over the cytosol confirms dye redistriburtion.

Similarly, depolarisation of the mitochondrial membrane by rotenone, an inhibitor of Complex I of the electron transport chain, caused efflux of TMRE from mitochondria and dequench of the fluorescence. The addition of rotenone 2 μM, in the presence of oligomycin, to TMRE-loaded cells induced a 147 ± 80% rise in fluorescence signal (mean ± SD, n = 13 cells). Data acquired using the cooled CCD camera and are illustrated in Figure 3.6. The images demonstrate that dissipation of $\Delta\psi_m$, whether by protonophore or Complex I inhibition, causes a dequench of TMRE signal.

Thus TMRE may be used to signal mitochondrial polarisation, and depolarisation, but the direction of fluorescence change is dependent upon the loading concentration of the dye and whether the fluorescence is quenched by concentration within mitochondria.

Mitochondrial flicker and global TMRE dequench

Imaging of cells loaded with high dose TMRE also revealed that the signal from individual mitochondria appeared to flicker – there were repeated, transient increases in TMRE fluorescence over single organelles. Additionally, in some cells there was a gradual increase in the global TMRE signal, whether measured over the nucleus or the cytosol. In other cells the signal rise reached a plateau that did not respond to addition of FCCP (Figure 3.7). These observations suggested that in the imaged cells $\Delta\psi_m$ was fluctuating and that in some cells there was a progression to a global mitochondrial depolarisation. These phenomena are further described in Chapter 4.

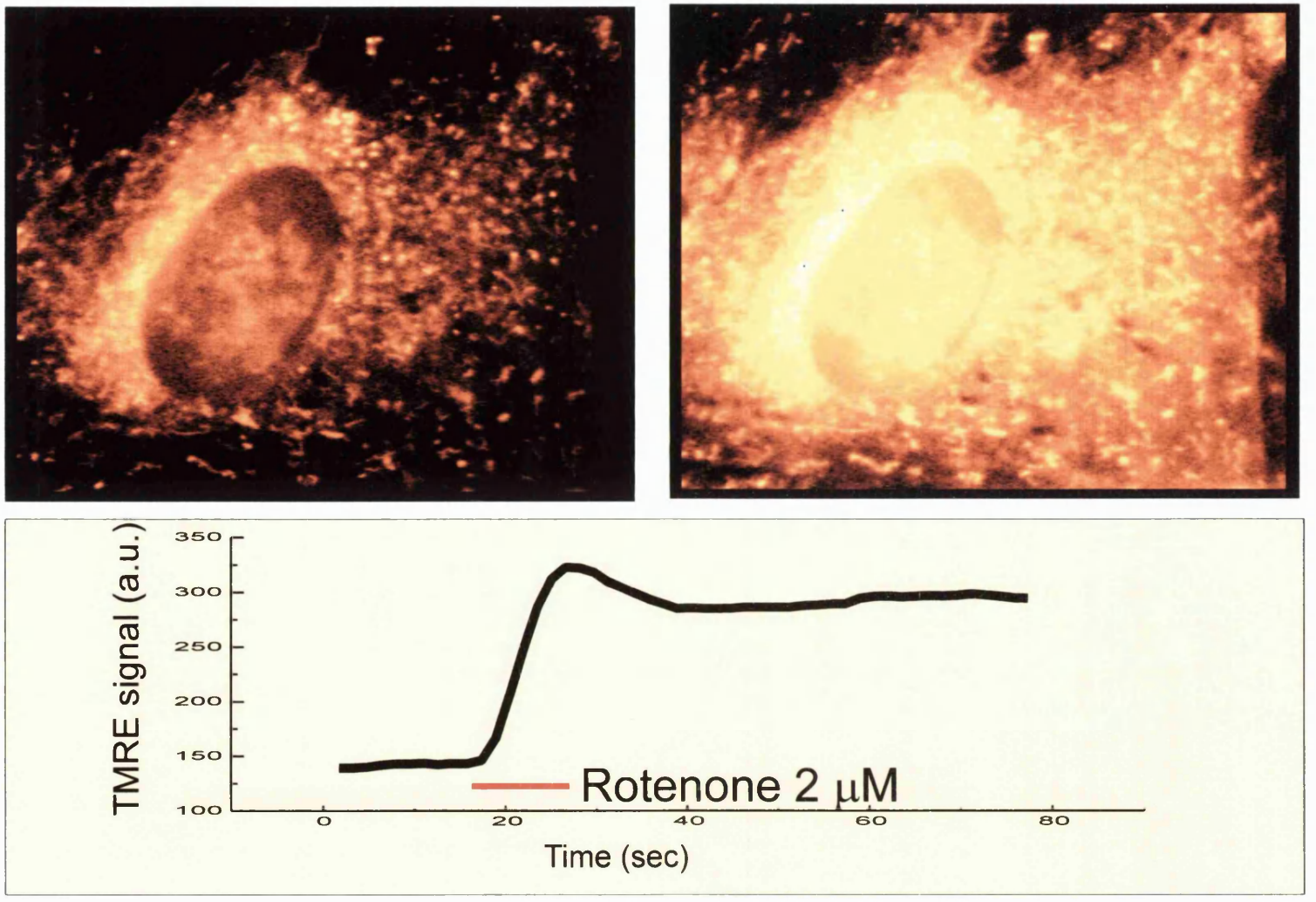

Figure 3.6: rotenone (in the presence of oligomycin) induced a dequench of TMRE fuorescence and a redistribution of the dye.

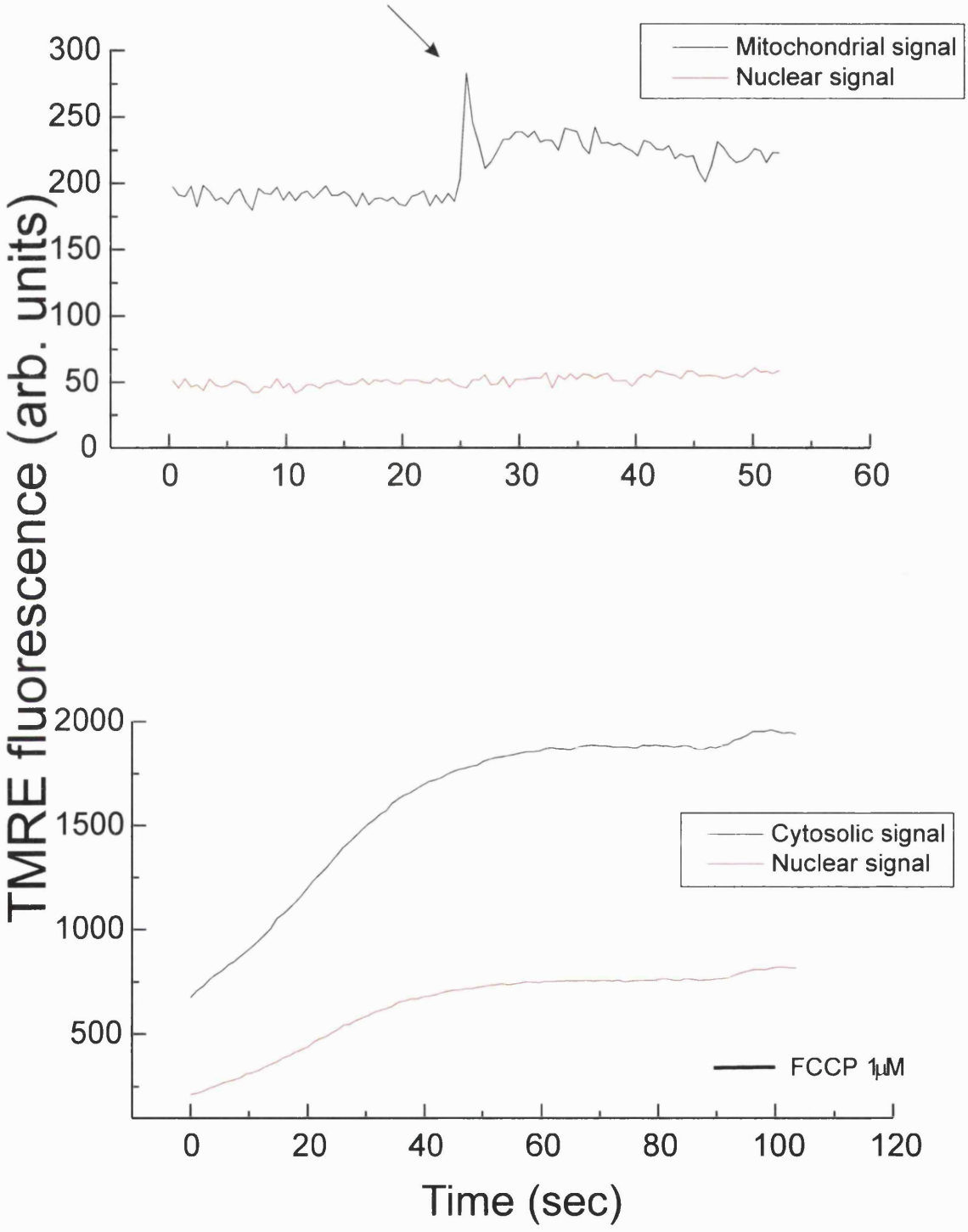

Figure 3.7: imaging of astroytes loaded with TMRE 1.5 μM revealed transient flickers over individual mitochondria. No flickers appeared over the mitochondrion-free nucleus (upper plot). In some cells, plotting of the TMRE signal from the whole cytosol revealed a gradual rise in fluorescence over time. There was a similar rise in nuclear signal in these cells (lower plot).

3.3 Conclusions

There were slight variations from the published data in the excitation and emission peaks of the dyes studied, however these had little effect on qualitative use of the dyes *in vivo*. As the fluorescence signal was being collected at all wavelengths longer than the relevant dichroic mirror (see Tables 3.1a and 3.1b), the emission shifts were unimportant. That is, there was still a change in signal *amplitude* as collected by the CCD chip or PMT. Wavelength shifts in optimum excitation light could potentially be more troublesome as the relatively narrow band (c. 10 nm in most cases) of filter used to select the excitation light could have resulted in illumination at an inefficient point on the dye's excitation spectrum. However, as can be seen from the excitation spectrum of TMRE, the excitation spectra were broad, indeed significant emission signal could be obtained if the dyes were excited some distance from their excitation maxima. For example, it was perfectly feasible to excite TMRE-loaded cells (optimum λ_{Ex} 555-560 nm) at 490 nm and record strong fluorescence.

Importantly, the addition of ATP or FCCP did not appear to alter either the excitation or emission wavelengths of the dyes studied. As these reagents would be added during microfluorimetric measurements, an artifactual shift in either wavelength could have confounded analysis of the fluorescence signals.

These data showed that the fluorescent probes studied could be used *in vivo* with the fluorimetry and imaging setups as described. Application of commonly-used drugs did not induce artifactual changes in fluorescence.

Imaging of TMRE-loaded adult cortical astrocytes revealed selective loading of the dye into mitochondria. In cells loaded with 50 nM TMRE, the application of the protonophore FCCP 1 μM, which dissipates the $\Delta\Psi_m$, immediately attenuated the mitochondrial fluorescence, confirming mitochondrial loading of the fluorophore. In contrast, application of FCCP 1 μM to cells loaded with 1.5 μM TMRE caused a rise in signal, suggesting that the dye had been quenched by loading into mitochondria. Examination of processed images confirmed dye loss

from the mitochondria in response to FCCP and increase in fluorescence signal as TMRE diluted in the cytosol.

The application of the Complex I inhibitor, rotenone, in the presence of oligomycin, induced a similar dequench of TMRE fluorescence in cells equilibrated with TMRE 1.5 μM, providing further evidence that the dissipation of $\Delta\psi_m$ was responsible for the change in fluorescence.

Of note were flickerings of the TMRE signal which could be repeated and restricted to individual mitochondria. Additionally, in some cells there was a steady rise in TMRE signal seen before application of FCCP suggesting an on-going mitochondrial depolarisation before the addition of the protonophore.

Chapter 4: mitochondrial depolarisations, transient and sustained, were imaged in TMRE-loaded cells.

Imaging of TMRE-loaded astrocytes revealed that the fluorescence signal from these cells was far from quiescent. Although the cells were unstimulated and imaged at room temperature, conditions where one might expect mitochondria to have a steady-state membrane potential, frequent, transient increases in TMRE signal were seen. These 'flickers' were restricted to individual organelles, or occasionally, small groups of mitochondria. No equivalent transients were seen over mitochondrion-free areas of cytosol, nor over the nucleus. As dequenching of TMRE fluorescence reflects mitochondrial depolarisation, it seemed that these mitochondria were depolarising and then repolarising in succession, often several times in the few seconds that they were imaged. Other organelles flickered only once, or would show transient depolarisations super-imposed on a rising baseline of fluorescence. If the signal over a whole cell, as opposed to that over individual mitochondria, was measured, the TMRE fluorescence was seen to rise steadily, often reaching a plateau. In these cases, the application of FCCP by puffer pipette caused no further rise in fluorescence, confirming complete dissipation of mitochondrial membrane potential throughout the cell.

The nature of these mitochondrial depolarisations was investigated. Confocal microscopy was used to optimise spatial resolution of the individual organelles studied, and the interline transfer CCD camera was used to increase speed of image acquisition and thus optimise the temporal resolution of the depolarisations.

4.1 TMRE-signalled mitochondrial flicker

4.1.1 Experimental procedures

Confocal images were obtained as previously described. Briefly, astrocytes loaded in TMRE 1.5 μM were mounted on the stage of the confocal imaging system. TMRE fluorescence was excited with a laser line at 543 nm and the laser power was attenuated to 3% of total power. Images were collected at a rate of c. 1Hz and stored to disc. A 63x oil immersion objective was used.

Fast scan images were collected by mounting astrocytes (loaded in TMRE 1.5 μM) on the stage of the fast readout CCD camera. Fluorescence was excited by illumination at 546 nm, incident light was attenuated to 5% of total output and images collected at wavelengths longer than 590 nm. A 63x oil immersion objective was used. To increase the speed of image acquisition, images were collected at 10 bits and pixels were binned into 4x4 arrays. Camera exposure time was 38 msec. A preliminary still image was taken so that regions of interest could be selected for acquisition of the time series data. Selecting a region of the cell for imaging limited the amount of data collected, speeding the readout. This arrangement optimised temporal resolution at the expense of spatial resolution, but images could be collected at 25-30 Hz. Two sets of images were acquired of each field of cells; in the first, images of flickering were acquired at high speed, in a second series collected at 3 Hz, FCCP 1 μM was applied by puffer pipette in order to measure the maximum TMRE signal achieved on complete mitochondrial depolarisation.

4.1.2 Results

Confocal and slow-scan imaging

Examination of the images acquired by CCD camera confirmed that there were spatial and temporal inhomogeneities in the TMRE signal. Brief, transient flashes were seen over mitochondria, sometimes occurring several times over a single organelle (see Figure 4.1). In other images a rapid increase in signal over the whole cell often overwhelmed the transients, however

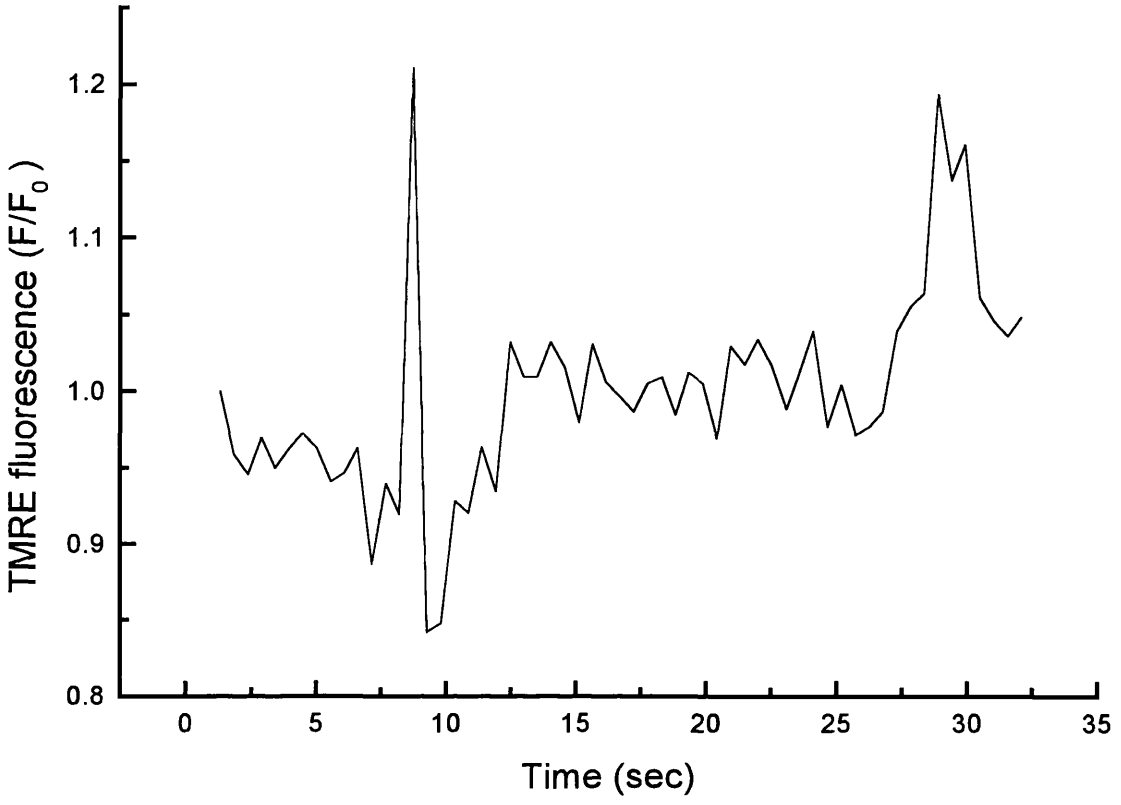

Figure 4.1: imaging of TMRE-loaded cells revealed multiple brief transients over mitochondria. The transients, or flickers, could occur several times over individual mitochondria and could not be ascribed to movement of the organelles. Cells were loaded by exposure to 1.5 μM TMRE, thus the TMRE fluorescence within the mitochondria was quenched. Depolarisation of the mitochondrion thus induced a rise in TMRE signal. The fluorescence signal is normalised against the value in the first frame of the time series (F_0).

even in some of these, transients were evident in the initial images, superimposed upon the rise in fluorescence (see Figure 4.2). A steady increase in fluorescence over the nucleus was seen which was similar in pattern to the change in signal over the cell as a whole.

That the flashes of fluorescence (or 'flickers') were due to spontaneous depolarisations of TMRE-loaded mitochondria, rather than sudden movement of the organelles, was evident from confocal images of similar events. The images illustrated in Figure 4.3 are drawn from a confocal series where the optical slice was maintained at less than 1 μm Flickers are clearly localised over mitochondria which are stable in position. Some mitochondria were seen to move during the image sequence, but the pattern of fluorescence over these organelles was quite different; the sudden increase in signal was absent and there was lateral as well as vertical motion, the mitochondria clearly moving from the region of interest. In addition, if the image series shown in Figure 4.3 is differentiated, so that the pixels that have changed since the preceding image are emphasised (illustrated in Figure 4.4), redistribution of the TMRE into the cytosol around the depolarising mitochondria – seen as small 'clouds' of fluorescence in the vicinity of the organelle – can clearly be seen. These images are consistent with spontaneous, brief depolarisations of mitochondria in illuminated, TMRE-loaded astrocytes. The resultant efflux of the fluorophore from the mitochondrial matrix caused a dequench of fluorescence typically around 10 – 50% of that seen when FCCP was applied to fully depolarise the mitochondria.

It appeared from the images that single mitochondria could flicker several times and that this reflected multiple depolarisations and subsequent repolarisations resulting in TMRE efflux and reuptake. Figure 4.5 shows such an event. These repeated events were frequently seen and the fact that the signal often returned to baseline (or even below) implied that the repolarisations could be complete. In addition, the fact that the flicker amplitudes were typically 50% or less than the signal change seen on complete mitochondrial depolarisation with FCCP suggested that $\Delta\Psi_m$ was not completely dissipated by the transient events.

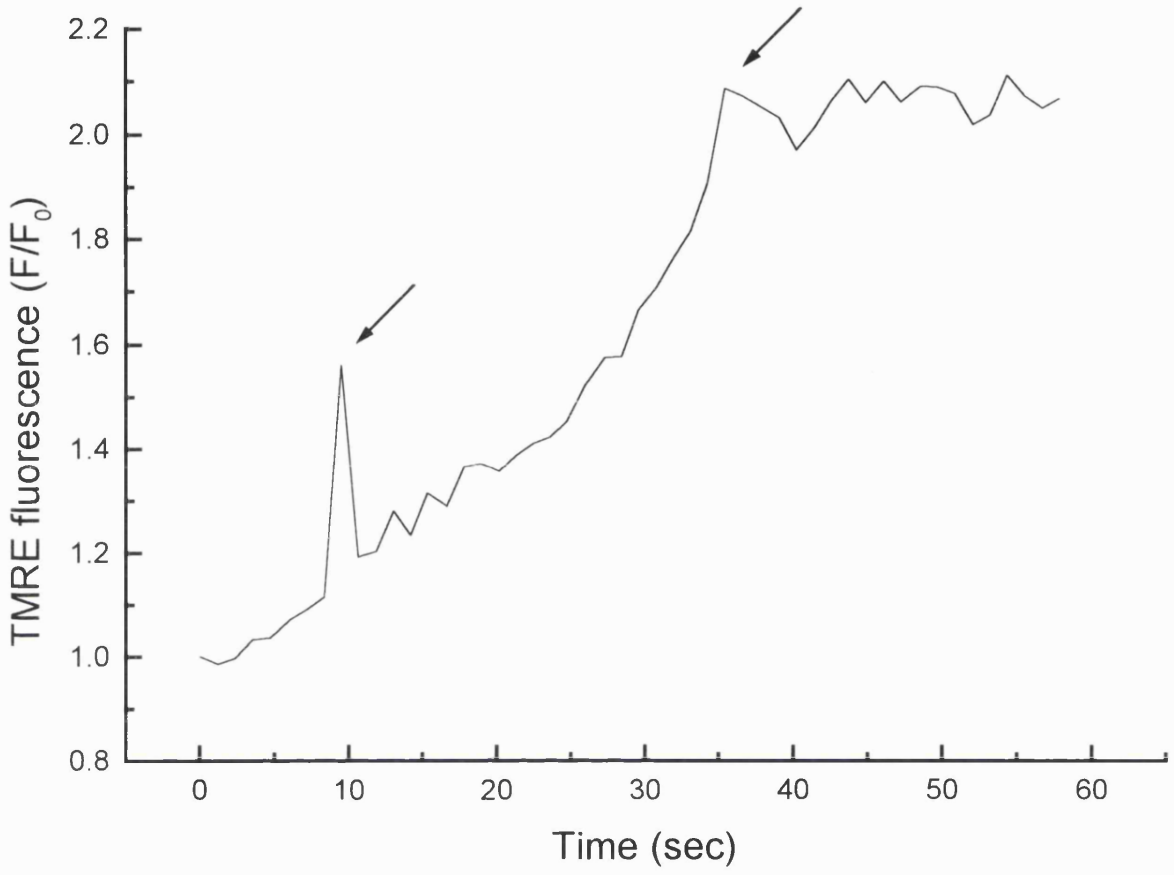

Figure 4.2: multiple flickers superimposed on a global rise in TMRE signal recorded over a single mitochondrion in a cortical astrocyte.

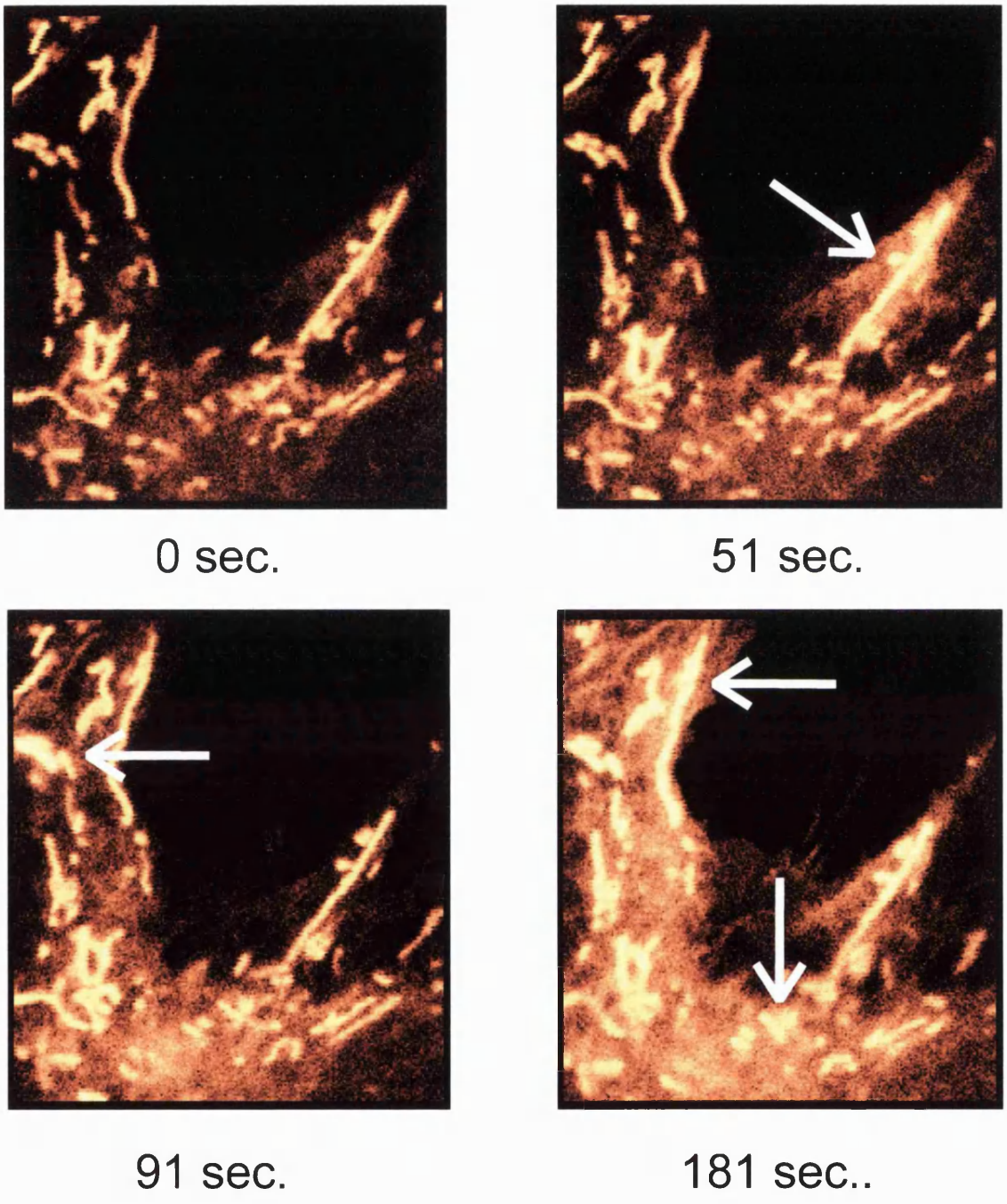

Figure 4.3: mitochondrial flicker seen in a TMRE-loaded astrocyte. Confocal images revealed multiple transients in TMRE signal over individual mitochondria (arrowed).

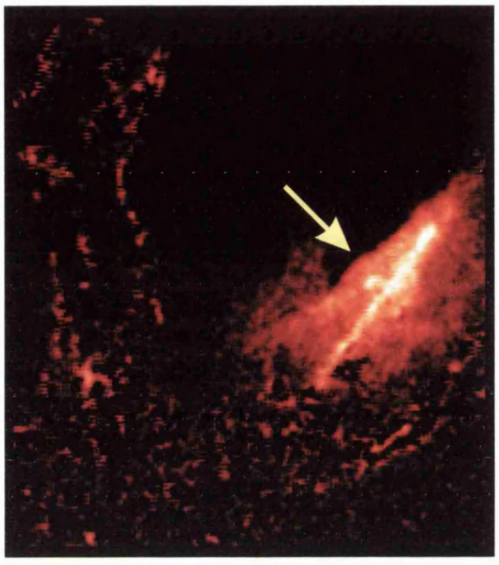

51 sec

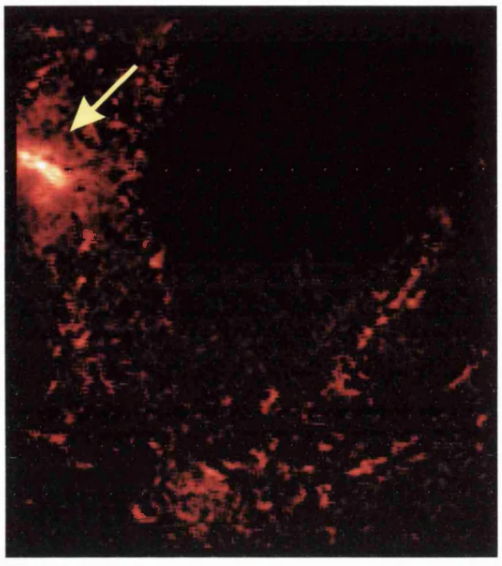

91 sec

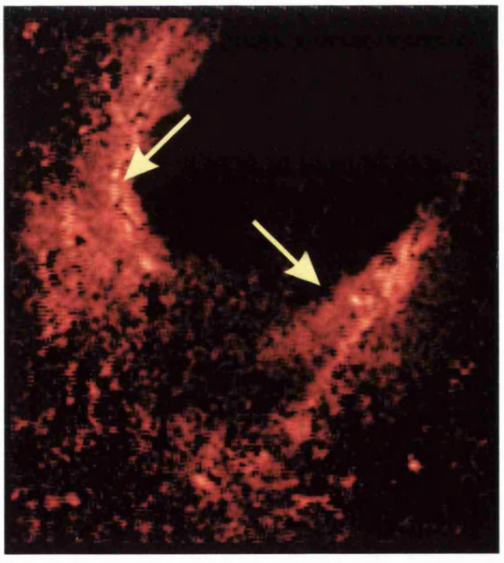

181sec

Figure 4.4: Differentiation of the images (subtracting each pixel value from its corresponding predecessor in the time series) shows how the fluorescence pattern has changed over time. This process reveals how TMRE leaves the mitochondria and redistributes into the cytosol.

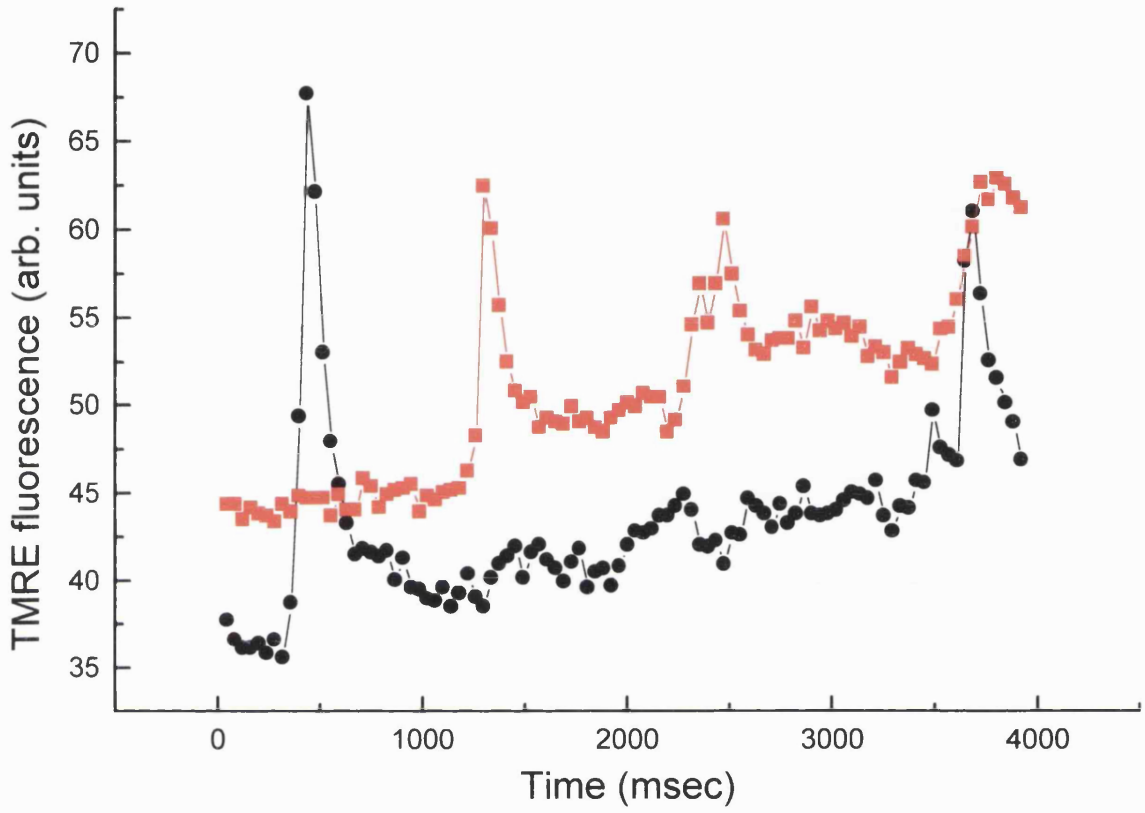

Figure 4.5: examples of TMRE-induced flicker of single mitochondria collected at 25 Hz. Individual organelles were frequently seen to depolarise several times in succession, as can be seen from these traces.

Fast scan imaging

In order to study the time course of these mitochondrial depolarisations, the flickers were imaged using the fast interline transfer CCD camera. Although the excellent spatial resolution of the confocal system enabled detailed analysis of the pattern of the events in the spatial domain, the maximum rate of image acquisition was around 5–10 Hz. The fast scan CCD camera in effect traded spatial for temporal resolution, providing images that were much less detailed in the spatial domain but which could be collected at rates approaching 30 Hz (Figure 4.5).

Figure 4.5 shows plots of TMRE fluorescence recorded over two mitochondria in the same cell extracted from images collected at 26 Hz. The high frequency of data points obtained in these images allowed detailed analysis of the time to peak as well as the decay time of the individual flickers. Figure 4.5 also emphasises that the flickers were independent in time and did not reflect a global loss of $\Delta\psi_m$. Ninety one events in 58 cells were analysed and a histogram of the frequency distributions of the times to peak of the flickers analysed is shown in Figure 4.7 The acquisition rate limited the temporal resolution, but within these constraints the mean time from baseline to peak fluorescence in single flickers was 257.5 msec ± 153.5 msec (n = 91), although the histogram reveals a distribution skewed towards a time to peak of around 150 msec.

Flicker decay

The decay times of the flickers were best analysed by fitting first-order exponential decays to plots of the TMRE signal, an example is shown in Figure 4.8. The mean decay time was 182.9 msec ± 89.5 msec (n = 76). When the frequency distribution of the decay times was plotted (Figure 4.9) it became apparent that there were two populations of decay time constant in the flickers studied, one centred at 140 msec, the other at 268 msec.. These data suggest that there were at least two modes of fluorescence dissipation after the initial dequench. As multiple flickers over single organelles were frequently seen it is likely that repetitive depolarisations were possible. Thus one time constant may reflect the reuptake of

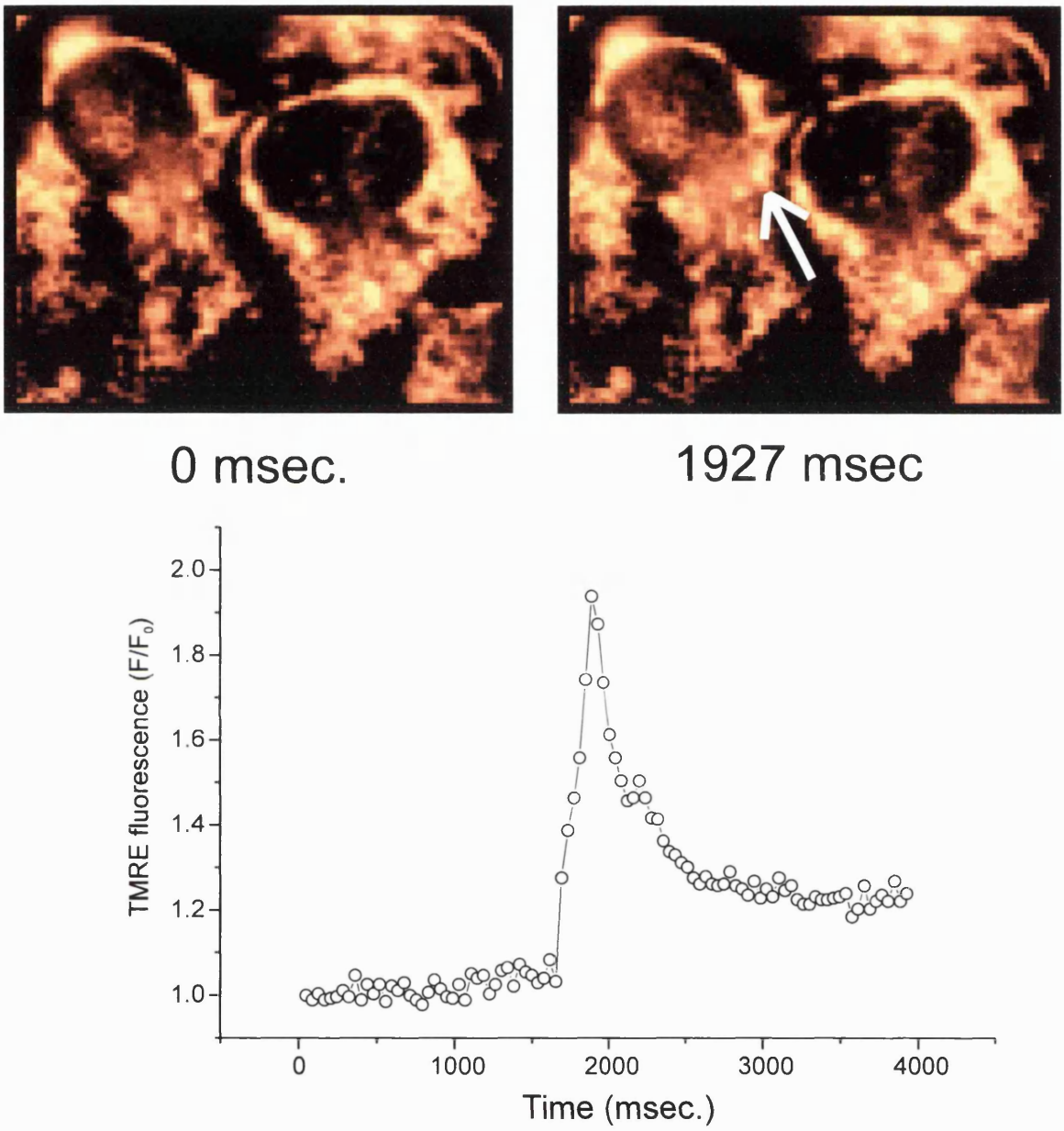

Figure 4.6: fast scan imaging of TMRE-loaded astrocytes sacrifices spatial resolution but images can be collected at over 25 Hz. Despite the poor spatial resolution, mitochondrial flicker may still be identified and an example is arrowed in the second image. A plot of the fluorescence change over this mitochondrion is shown.

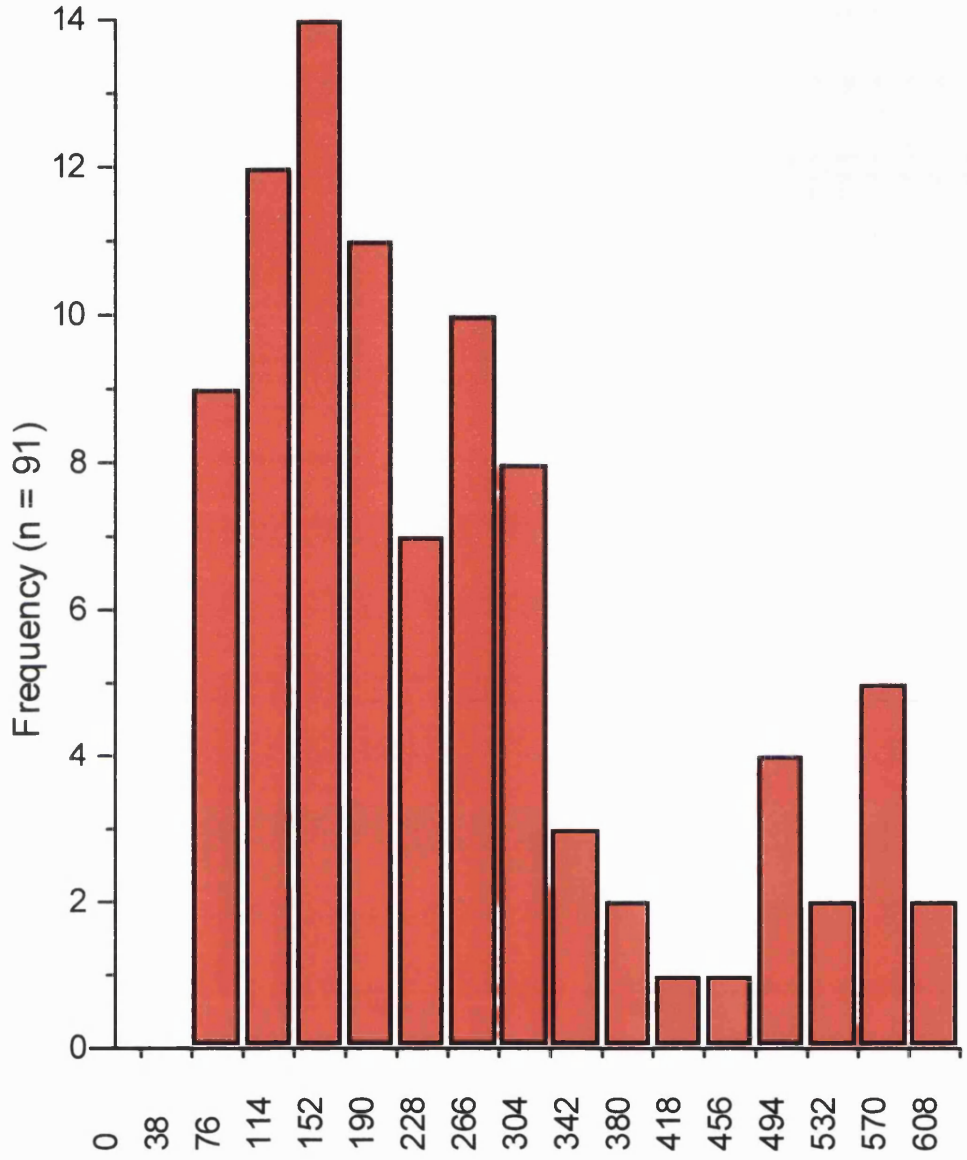

Figure 4.7: frequency distribution of time to peak from baseline for individual TMRE flickers. Times to peak were all multiples of 38 msec. as this was the exposure time of the CCD camera when imaging, hence temporal resolution was restricted to 38 msec. Abscissa labels – '0' for 0 – 37 msec. group, '38' for 38 – 75 msec. group, etc.

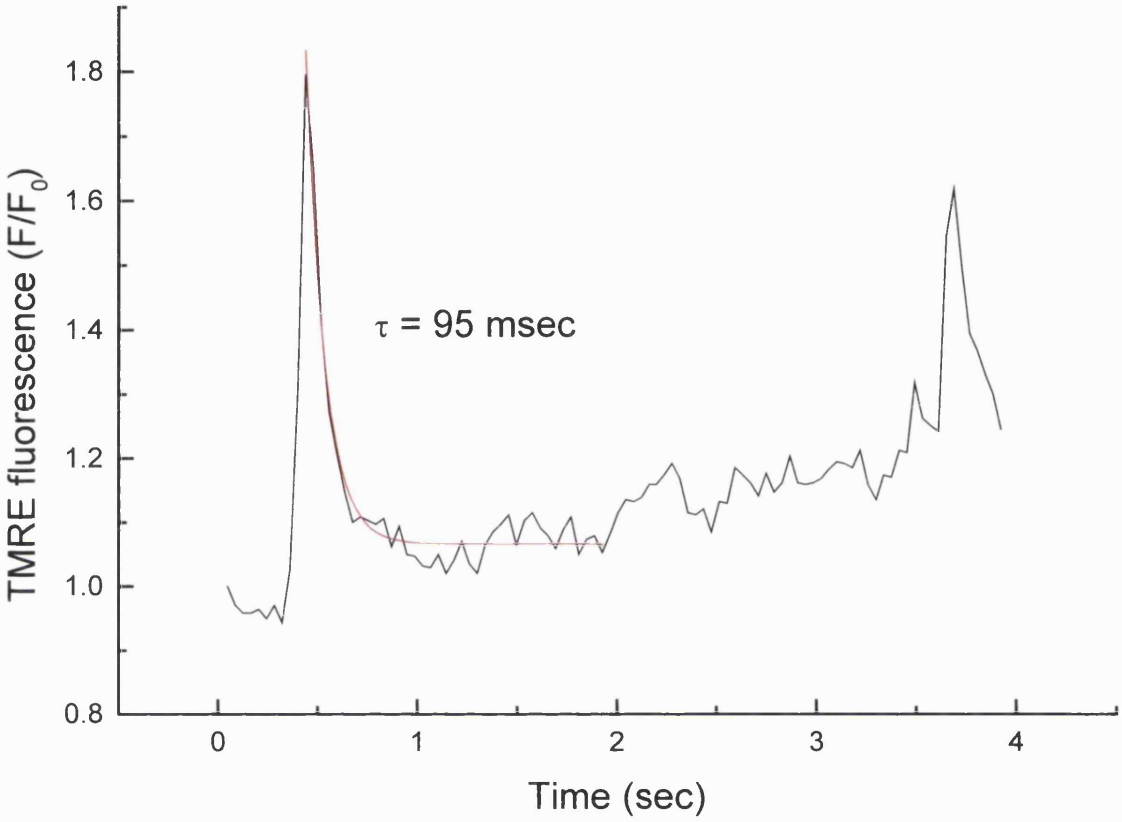

Figure 4.8: fitting of a single order exponential decay to a TMRE flicker. In this case the time constant (τ) was 95 msec. This trace illustrates another example of the fluorescence returning almost to baseline followed by a second event. As this plot was taken from a region of interest limited to a single mitochondrion, this strongly suggests multiple depolarisations followed by repolarisation in individual organelles, as opposed to one-off events.

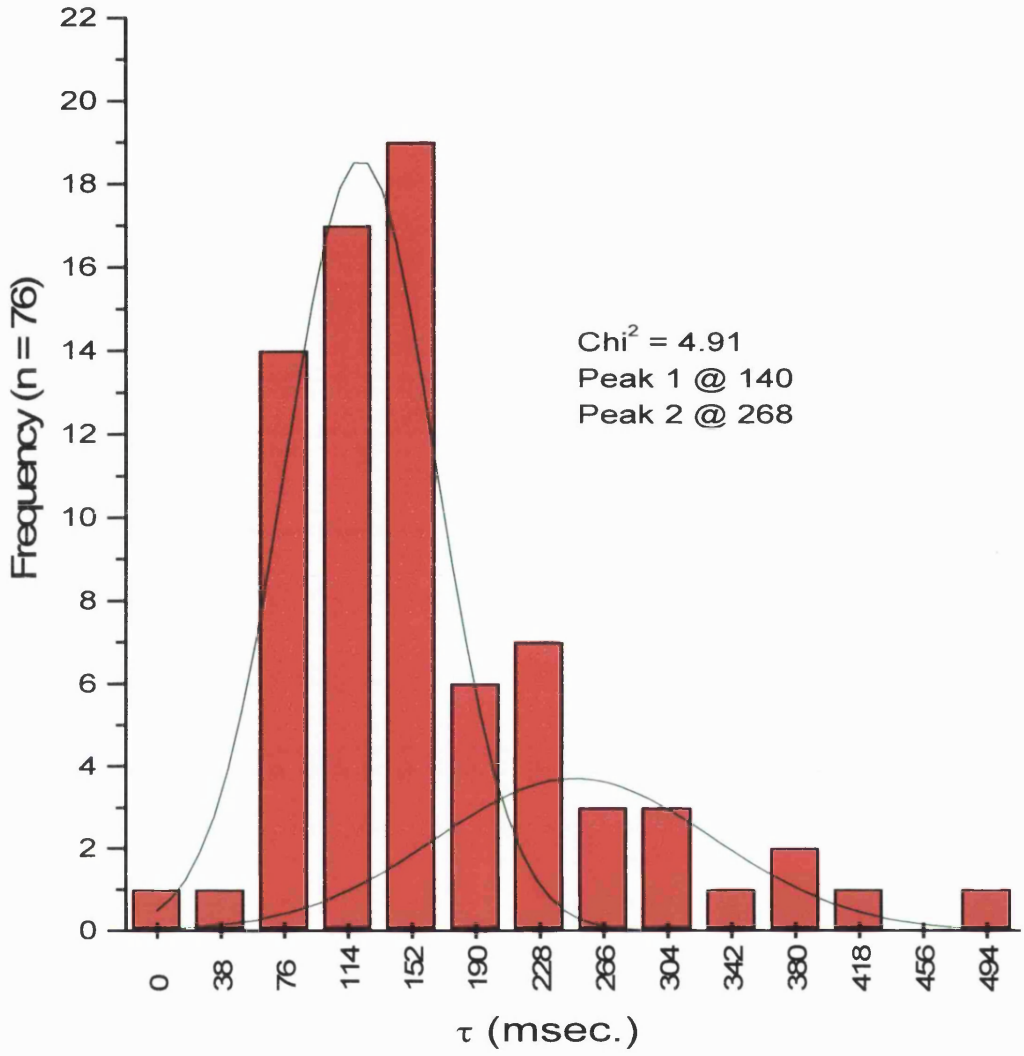

Figure 4.9: frequency distribution of time constants of first order exponential decays fitted to flickers. The best Gaussian fit (Chi^2 = 4.91) was achieved by fitting two curves with peaks at 140 msec and 268 msec.

TMRE into the repolarised mitochondrion (and hence its requench), while the other may be related to dye dilution in the cytosol.

Flicker amplitude

In each cell studied, FCCP 1 μM was applied in a second image series in order to gauge the maximum TMRE signal achieved on complete mitochondrial depolarisation. The amplitudes of the flickers were expressed as a percentage of this maximum, the mean amplitude being 39.4% ± 17% (n = 100). The frequency distribution of the flicker amplitudes is illustrated in Figure 4.10.

4.2 Attenuation of excitation light

The occurrence of the transient events appeared to increase in frequency as the cells were imaged, from occasional depolarisations at first, to more and more frequent flickers that culminated in the complete dissipation of $\Delta\psi_m$ in the whole cell. If the signal over the whole cell was measured, fluorescence increased steadily with time, culminating in a plateau which was unaffected by the application of FCCP. The rise in global TMRE signal seemed to be composed of an integration of many smaller events. These events were imaged in cortical astrocytes under resting conditions, there was no pharmacological stimulation of the cells during imaging. However, in order to obtain fluorescent images, cells have to be illuminated, by laser for confocal microscopy or by Xenon arc lamp for the CCD cameras. Illumination of biological material is not entirely benign, as the photon energy which is utilised to excite fluorescence may also cause heating or induce the production of highly reactive free radicals. As it was evident that the fluorescence measured over single cells increased as the cells were imaged, the possibility of a light-induced effect on the frequency of the depolarisations was investigated.

4.2.1 Experimental procedures

Cortical astrocytes were loaded with TMRE by immersion in a 1.5 μM solution for 15 minutes followed by washing. Dishes of cells were mounted on the stage of the interline transfer

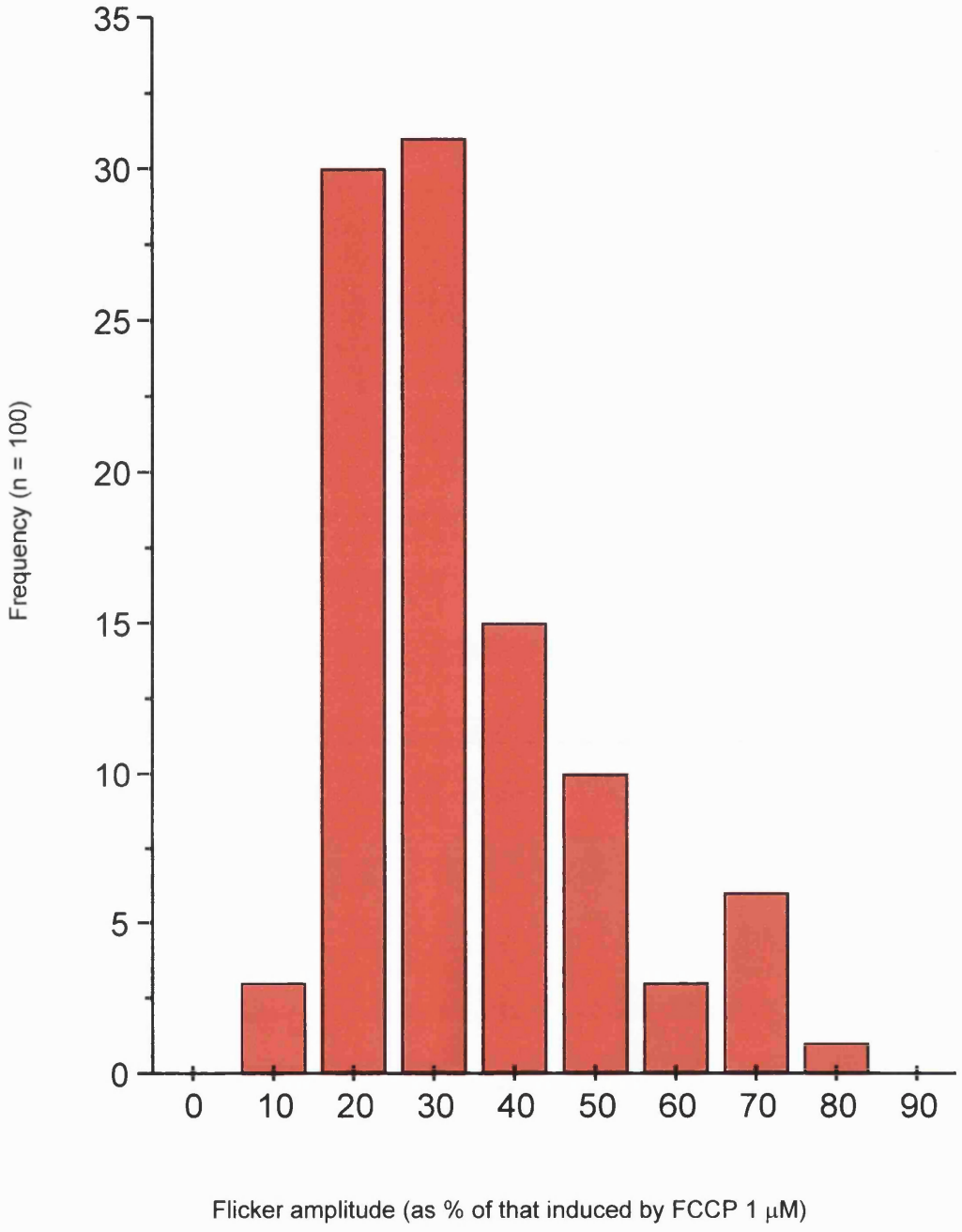

Figure 4.10: frequency distribution of flicker amplitudes expressed as a percentage of the dequench in TMRE fluorescence seen on application of FCCP 1 μM

imaging system and fluorescence was excited using 546 nm light. Images were collected at wavelengths longer than 590 nm. The excitation light was attenuated using neutral density filters (1%, 3.5% and 5% transmission) placed in the light path between the light source and the preparation. These filters are part-silvered and work by reflecting incident light, thus a 5% neutral density (ND) filter reflects 95% of the incident light and allows passage of the remaining 5%. Images were recorded of the TMRE dequench over time using the different filters and FCCP was applied by puffer pipette to each cell towards the end of illumination to check for further depolarisation. Background-subtracted images were normalised by dividing the image series by the first image in order to control for variable loading of the TMRE. Plots of dye dequench were then compared.

4.2.2 Results

The rate of onset of TMRE dequench in the astrocytes was clearly related to the intensity of the incident light (see Figure 4.11). The cells illuminated with the 5% ND filter completely dequenched within 60 seconds and the TMRE signal then slowly declined. The mean peak signal was 270 ± 100% (n = 38, mean ± SD) of that at the start of illumination. Application of FCCP 1 μM to these cells at 230 seconds did not produce a further dequench, suggesting that the subsequent loss of signal was not due to re-uptake of TMRE into mitochondria and requench. The cells illuminated using a 3.5% ND filter (n = 27) took longer to dequench, 165 seconds to reach maximum (264 ± 62% of fluorescence at T_0), followed by a similar loss of signal. There was little response to FCCP at 230 seconds, again suggesting that there had been no significant re-accumulation of the TMRE into polarised mitochondria. The cells that were illuminated with 1% of the arc lamp output (n = 46), however, showed only a 56% increase in signal during image acquisition and the application of FCCP induced a large and precipitant rise in TMRE signal (to 316 ± 137% of fluorescence at T_0).

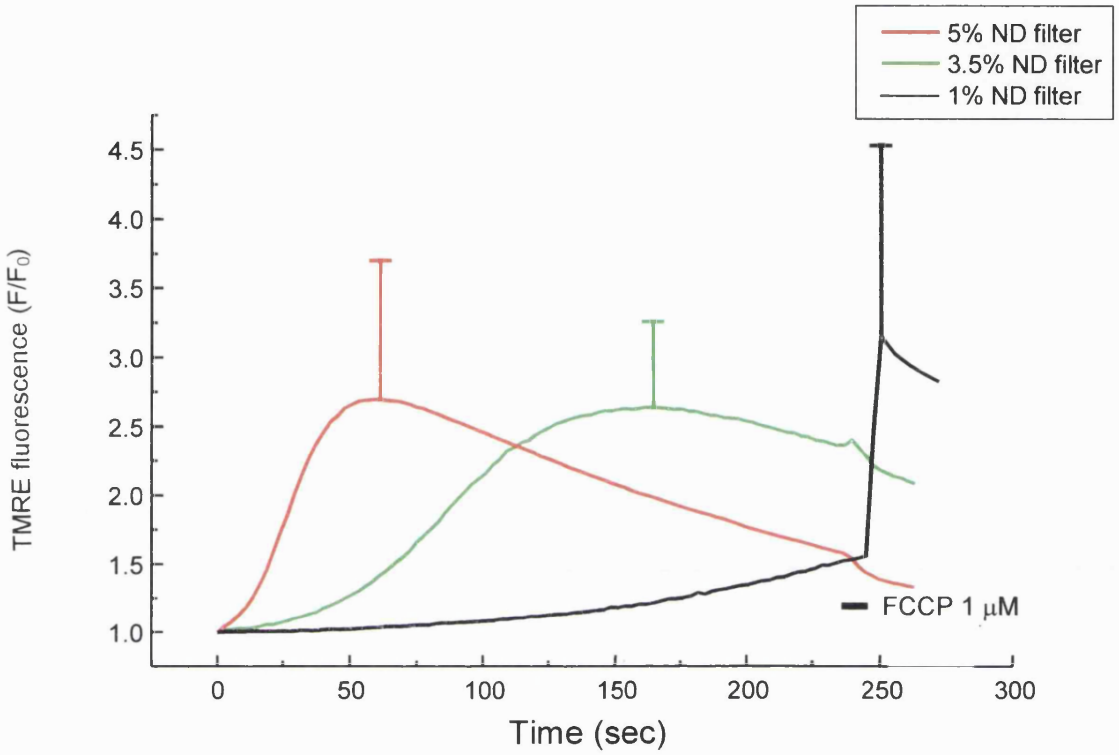

Figure 4.11: attenuating the intensity of the excitation light reduced the rate of global TMRE dequench. FCCP applied by puffer pipette at 230 sec. did not cause any further dequench in cells illuminated with 3.5% or 5% filters, suggesting that $\Delta\psi_m$ had been completed dissipated in these cells. Hence, as the global signal reflects a summation of many individual mitochondrial depolarisations, increased light intensity accelerated the individual depoarisations. 46, 27 and 38 cells were studied (1%, 3.5% and 5% groups, respectively) and the error bars denote standard deviations.

The rate of onset of TMRE dequench was analysed in each cell by fitting a line to the steepest part of the slope and comparing the slopes between groups. This rate of onset of dequench was significantly different in each group ($p < 0.0001$, Kruskal-Wallis Non-parametric ANOVA test), see Figure 4.12.

Additionally, as the TMRE dequenched the punctate distribution of the dye became less defined (see figure 4.13) and the fluorescence measured over mitochondrion-free areas of the cytosol and nucleus also increased (see figure 4.14). These data are reminiscent of those seen on application of FCCP and are consistent with a progressive depolarisation of the mitochondria, loss of $\Delta\Psi_m$ in the whole cell, and redistribution of the TMRE from mitochondria into other parts of the cell.

Thus illumination of TMRE-loaded astrocytes by more intense light accelerated the mitochondrial depolarisations, as reflected by the global rise in fluorescence.

Comparison of flicker frequencies.

If the factors underlying the (patho)physiology of these transient mitochondrial depolarisations were to be investigated, a method of comparing probability of flickering needed to be established. As was seen in Section 4.2.2, one way of assessing the change in TMRE signal seen under different conditions was to measure the slopes of the onset of TMRE dequench seen in different cells and compare these. As a method of looking at the overall mitochondrial depolarisation in a cell this method worked well, and was relatively easy to do, however, taking this approach involved assuming that the overall dequench was directly related to the individual flickers seen and described above. Whilst it is possible that the global signal change represented a summation of the individual flickers seen over single mitochondria (so-called 'ensemble behaviour', Hüser, 1998) it could also be proposed that flickers represented transient events that were overwhelmed by a separate, complete mitochondrial depolarisation signalled by the global change. In order to

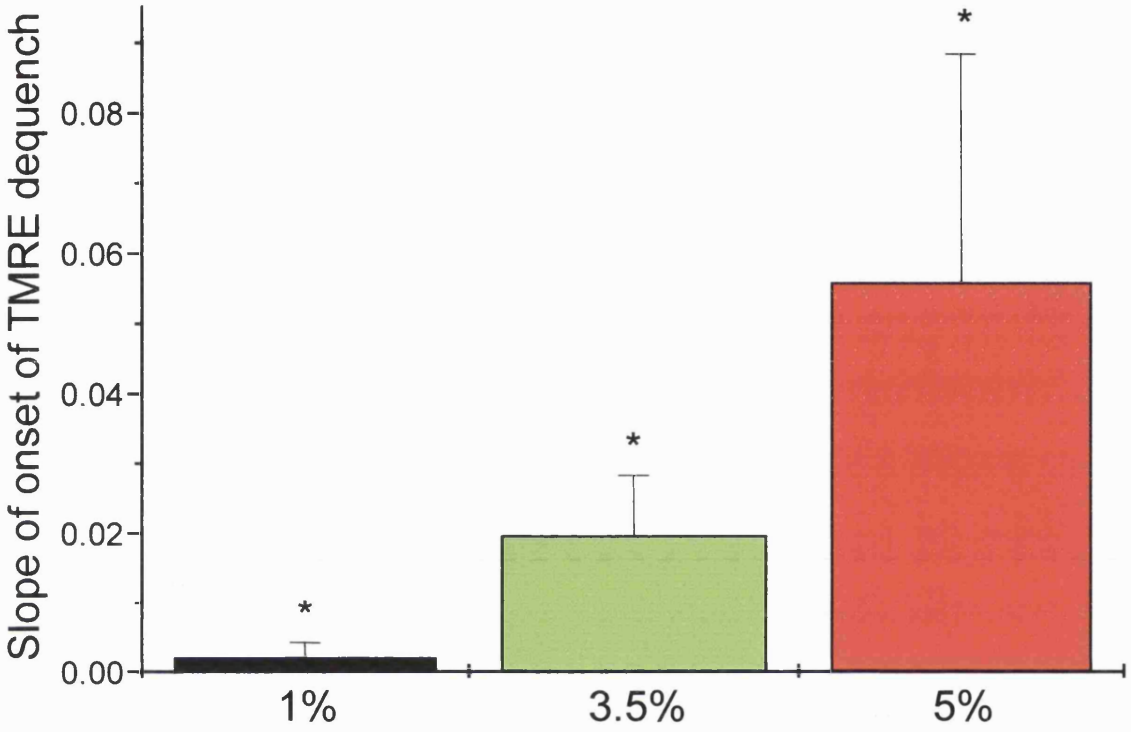

Figure 4.12: mean slope of onset of dye dequench measured in astrocytes loaded with TMRE. Standard deviation bars are shown and significant difference between column heights denoted by * ($p < 0.0001$, Kruskal-Wallis non-parametric ANOVA test).

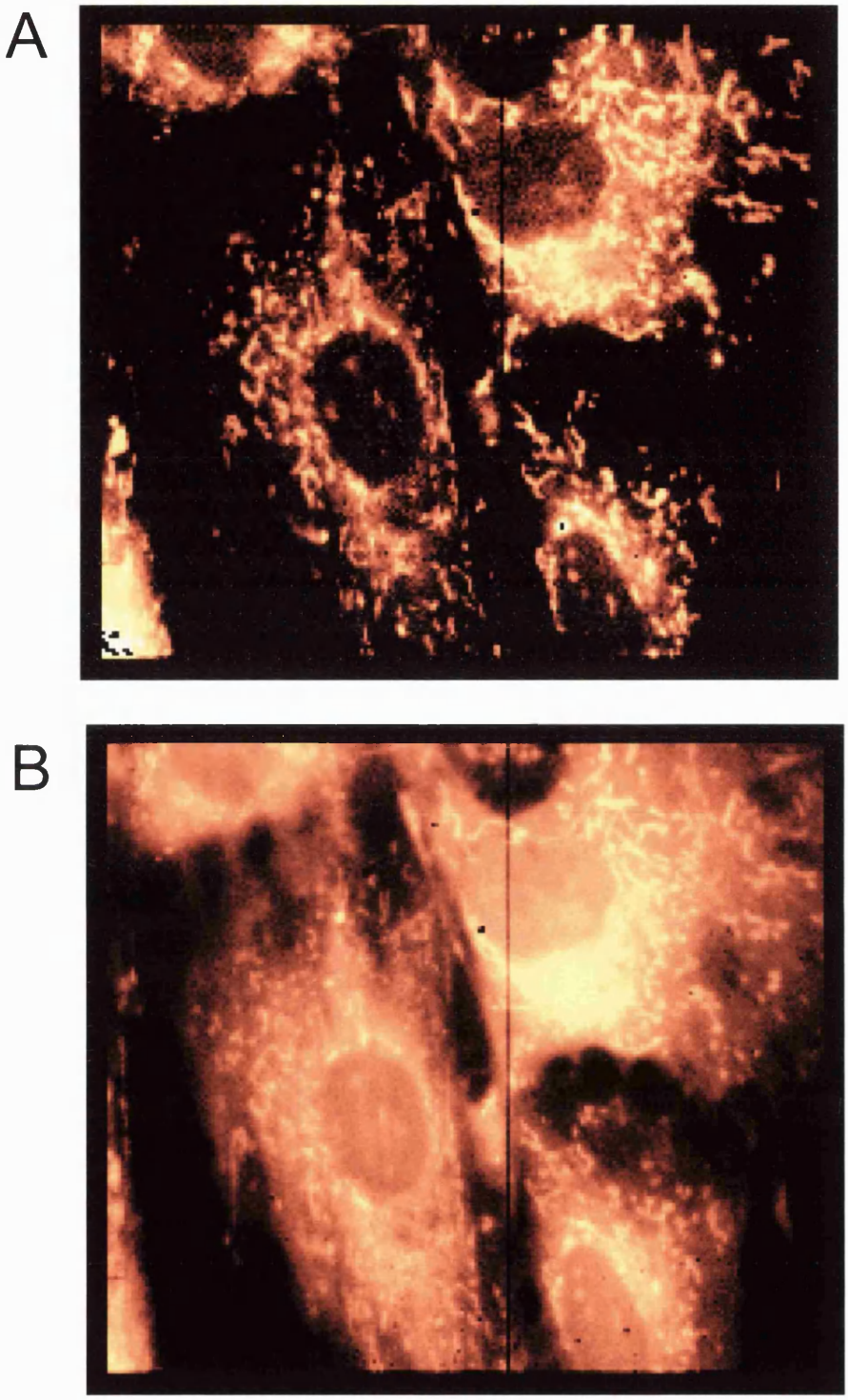

Figure 4.13: illumination of TMRE-loaded astrocytes caused a redistribution of dye. Early images (eg Panel A, at 1 second) show a punctate pattern of fluorescence as the dye is sequestered within mitochondria. After 100 seconds of illumination (Panel B) the TMRE has spread into the nucleus and neighbouring cytosol. The redistribution causes a dequench in TMRE fluorescence, so Panel B was remapped to improve spatial resolution.

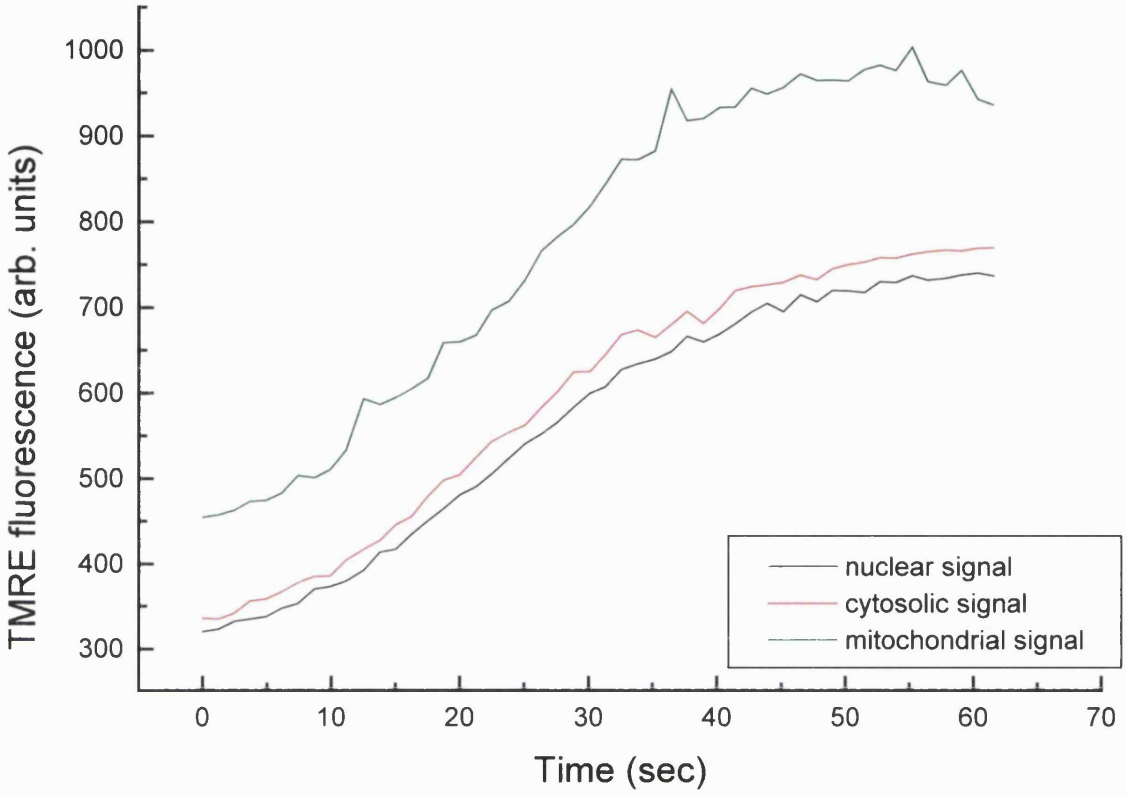

Figure 4.14: when the rate of mitochondrial depolarisations was increased by increasing the intensity of illumination, the nuclear and cytosolic signal also rose confirming efflux and redistribution of TMRE from depolarised mitochondria.

differentiate between the two types of signal, and to provide an index of mitochondrial flickering, a system of analysing the flickering images was devised.

Proportional changes in signal in background-subtracted image sequences were created by dividing the time series by a 'darkest image' as described in the General Methods section. This procedure is based on the assumption that maximum mitochondrial polarisation is reflected by a minimum TMRE signal, and so the darkest image reflects a natural baseline. Division of the time series by this darkest image produced an image series where each pixel value represented a proportional change in $\Delta\psi_m$ from maximum $\Delta\psi_m$. By averaging the time series a single image was obtained where each pixel value represented a proportional change in $\Delta\psi_m$ from maximum $\Delta\psi_m$ over time. If there had been little mitochondrial activity in the time series then average pixel value was close to unity. A great deal of activity (that is, many TMRE-signalled flickers) raised the value, typically by 20 – 30%. By drawing a region of interest around a cell so that no background was included, the average mitochondrial activity in time could be calculated for each cell. Care had to be taken to exclude background and nucleus as these areas, by taking up TMRE from depolarised mitochondria could rise in value dramatically, confounding this system of image analysis. Therefore, regions of interest from which data were drawn were limited to the cytosol where mitochondria were present. The value obtained for mitochondrial activity by this process was dubbed the 'index of variation' and reflected the subjective impression of the frequency of transient events. While time-consuming, calculating an index of variation for TMRE flicker in different conditions allowed direct comparison of cells in different conditions and thus provided a way of quantifying the contributory events. Figure 4.15 illustrates the image processing required to produce an index of variation.

To separate the assessment of flicker from the global rise, a set of conditions were established whereby illuminated, TMRE-loaded astrocytes would flicker but there would be minimal (or no) rise in overall fluorescence. These conditions varied from culture to culture, probably due to variable loading of the TMRE, and so had to be established on a daily basis. In practice this meant attenuating the light source to a point where flickering occurred but

Figure 4.15: calculation of the Index of Variation

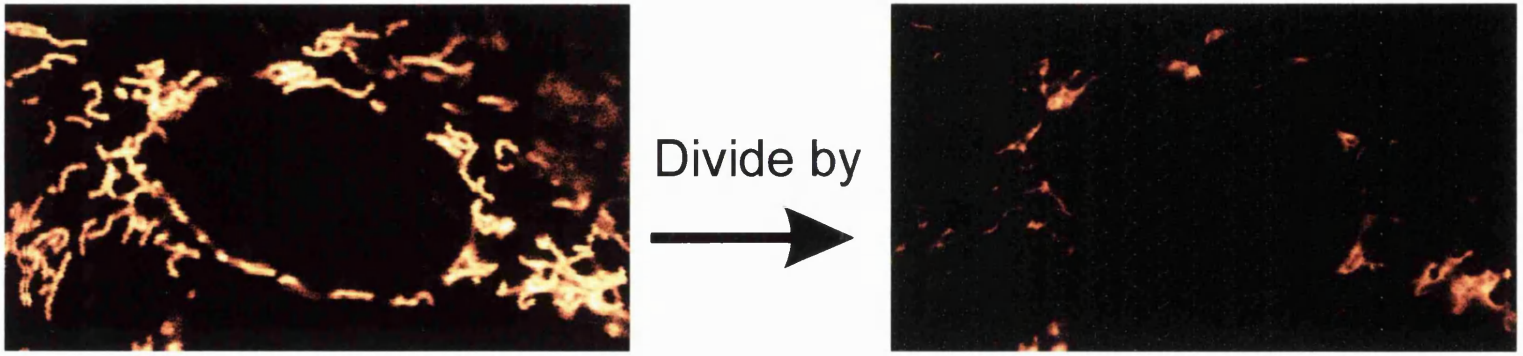

Image series

Digitally-constructed
'darkest image'

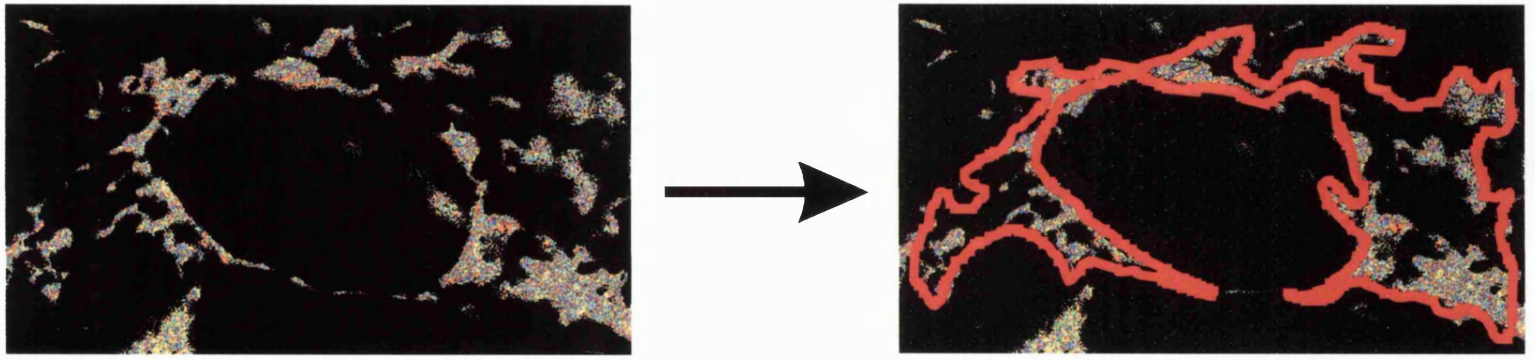

Average of ratio series

Calculate pixel value
inside region of interest

where the overall TMRE signal did not rise. Although reduction of light intensity slowed the global signal rise, it proved very difficult to attain mitochondrial flickering without a change in the cytosolic signal, presumably as dequenched TMRE released from flickering mitochondria accumulated in the cytosol. Therefore, only those cells where the overall rise over the course of imaging was less than 10% of the initial value were analysed for the index of variation. Any movement excluded a cell from this type of analysis.

Throughout this thesis, the index of variation has been presented in bar charts, with the percentage change from unity plotted. For example, a mean index of variation of 1.2 would be presented as a 20% increase from baseline. All error bars represent standard deviations.

Conclusions

Imaging of TMRE-loaded astrocytes revealed marked fluctuations in the TMRE signal over time. These changes were of two types, a gradual rise in fluorescence as measured over the whole cell, and small, transient flashes of fluorescence measured over single mitochondria. The rise in TMRE fluorescence signalled mitochondrial depolarisations. Over single organelles the frequent, brief, transients could occur several times. This, in conjunction with the observation that the amplitudes of the flickers averaged around 40% of the signal change seen with FCCP, suggested that mitochondria were undergoing repeated, partial depolarisations and repolarisations.

If the TMRE signal over the whole cell was measured, the signal increased gradually to reach a plateau, after which application of FCCP did not induce any further change in signal, suggesting a complete dissipation of $\Delta\psi_m$. The gradual rise in the global TMRE fluorescence was consistent with a summation of many, individual transient depolarisations. The rate of rise of the global signal, was related to the intensity of the incident light. With greater intensities the global signal rose more quickly, implying that the stronger light was accelerating the frequency of the individual depolarisations.

Chapter 5: integrity of intraceilular caicium stores is necessary for the mitochondrial depoiarisations

The data presented in Chapter 4 show that mitochondria in TMRE-loaded astrocytes may undergo repeated, spontaneous depolarisations, so possible causes for the events were investigated. It is well established that mitochondria have a calcium-uptake pathway (reviewed in Chapter 1) and that this uptake of calcium is electrogenic. Accumulation of the positively-charged ion may cause a depolarisation of the mitochondrial membrane and the depolarisation is transient. Indeed it has been shown that physiological mobilisation of stored Ca^{2+} in cortical astrocytes causes a global dissipation of $\Delta\psi_m$ (Peuchen *et al.*, 1996b).

Much recent work has centred on the phenomenon of focal Ca^{2+} release, where Ca^{2+} held in intracellular stores (generally accepted to be the endoplasmic reticulum, ER) may be released in a quantal fashion from ER Ca^{2+}-release channels (for review, see Berridge, 1997). As elementary Ca^{2+}-release events may be highly localised, resulting in microdomains of high $[Ca^{2+}]_{cyt}$, it seemed possible that the mitochondrial depolarisations in the astrocytes may be in some way linked to Ca^{2+} uptake following elementary, intracellular Ca^{2+} events. The possible link between ER Ca^{2+}-release and the mitochondrial depolarisations was therefore investigated.

Astrocyte calcium stores

Release of calcium from internal stores may be mediated by the second messenger inositol 1,4,5 trisphosphate (IP_3), a highly diffusible product of the hydrolysis of membrane-bound phospotidylinositol bisphosphate. Binding of IP_3 to its receptor on the endoplasmic reticulum induces opening of calcium channels and consequent release of calcium into the cytosol. The receptors themselves are calcium-sensitive, and calcium release from one, or a group of, channels increases the open probability of nearby channels (Bezprozvanny, Watras & Ehrlich, 1991; Kaftan, Ehrlich & Watras, 1997). This regenerative action may be the basis of the calcium wave and calcium spike formation described in astrocytes (Nadal, Fuentes, Pastor &

McNaughton, 1997; Boitier *et al.*, 1999) and other cells. ATP, acting at P_{2U} receptors is a reliable stimulus for the release of stored calcium by IP_3 in these cells (Peuchen *et al.*, 1996a)

ER calcium stores may also be sensitive to the plant alkaloid, ryanodine (for review see Shoshan-Barmatz & Ashley, 1998). These stores are insensitive to IP_3 and are typically involved in calcium induced calcium release (CICR). The ryanodine receptor (RyR) is sensitive to caffeine (although the pharmacology of the action of caffeine upon the receptor is complex (Sandler & Barbara, 1999; Zhang, Williams & Sitsapesan, 1999) and there is evidence that its action may be enhanced by cyclic ADP ribose (Sitsapesan, McGarry & Williams, 1995). Low concentrations of ryanodine (sub-micromolar) can induce release of calcium from stores, while higher concentrations (10 μM or more) have been shown to inhibit release, possibly by maintaining the channels in a closed conformation (Shoshan-Barmatz & Ashley, 1998). Some investigators report the presence of RyRs in astrocytes (Langley & Pearce, 1994), while others have failed to see calcium release in these cells with either ryanodine or caffeine (Peuchen *et al.*, 1996a).

Thus astrocytic mitochondria may be exposed to Ca^{2+} originating from IP_3-sensitive intracellular Ca^{2+} stores or, in some cases, ryanodine-sensitive Ca^{2+} stores, and the mitochondria may transiently depolarise on taking up Ca^{2+} under physiological conditions. Influx of Ca^{2+} from extracellular fluid may also provoke Ca^{2+} uptake by mitochondria, so potential sources of $[Ca^{2+}]_i$ rises in the astrocytes were investigated and the possibility that the TMRE-signalled depolarisations were due to mitochondrial Ca^{2+} uptake was examined.

Experimental methods

Measurement of intracellular calcium.

Cells were loaded with fura-2 AM 5 μM for 30 minutes at room temperature and the cell dish was mounted on the stage of the microfluorimetry system. Fluorescence was excited at 340, 360 and 380 nm using the spinning filter wheel. A 510-540 nm band-pass filter was placed in

front of the PMT and a dichroic block with a cut-off at 510 nm excluded excitation light. Data were then digitised and saved to disc.

Removal of extracellular calcium

To establish whether extracellular calcium was necessary for the mitochondrial depolarisations, cells were loaded with TMRE 1.5 μM for 15 minutes. The cells were washed and bathed in the recording medium detailed in Section 2.2. Control images were acquired, establishing that the cells showed mitochondrial flickering as usual. The recording medium was removed and replaced with a calcium-free medium. This solution was identical to the standard recording medium except for the replacement of the 2 mM CaCl with 2 mM MgCl. The calcium chelator EGTA was added at a concentration of 0.5 mM to bind any calcium present in solution. Image acquisition was then repeated and the data compared with controls.

Effect on mitochondrial flickering of chelating cytosolic Ca^{2+}

Cells were loaded with TMRE and control images acquired as described above. Cytosolic Ca^{2+} was chelated using the membrane-permeant EGTA analogue, 1,2-bis(o-aminophenoxy)ethane-N,N,N'N'-tetraacetic acid, (BAPTA). The BAPTA was loaded as its AM ester and was made up to a concentration of 10 μM using the calcium-free recording medium described above. The chelator was loaded for 30 minutes and the cells were left in an incubator at 36ºC to optimise the efficiency of the esterases and hence BAPTA loading. Cells were then imaged once more and the data compared with controls.

Emptying of intracellular calcium stores

The sequisterpine lactone thapsigargin, derived from the plant Thapsia garganica, is an inhibitor of the sarcoplasmic/endoplasmic reticulum calcium ATPases (SERCA pumps) that pump calcium from the cytosol into the endoplasmic reticulum (ER). This leads to emptying of the stores, suggesting that Ca^{2+} may be cycled constantly through the ER, or that a build-up of local $[Ca^{2+}]_{cyt}$ may induce CICR and store emptying. The action of thapsigargin on the SERCA pumps is thought to be irreversible.

Intracellular calcium stores were emptied by applying a 200 nM solution of thapsigargin for 10 minutes. The thapsigargin was made up in calcium-free recording medium or standard recording medium depending upon the requirement for extracellular calcium in each experiment.

Blocking mitochondrial calcium uptake with Ru360

An alternative approach to assessing the involvement of Ca^{2+} on the transient depolarisations is to block mitochondrial Ca^{2+} uptake at the uniporter. There are, however, few available ligands of the calcium uniporter. The best known of these, ruthenium red (ammoniated ruthenium oxychloride), is a complex, cationic molecule which has frequently been shown to inhibit mitochondrial calcium uptake in isolated mitochondria (Al-Nasser & Crompton, 1986), endothelial cells (Jornot, Maechler, Wollheim & Junod, 1999), hepatocytes (Hajnóczky, Hager & Thomas, 1999), neurones (Kunz, Goussakov, Beck & Elger, 1999) and cardiomyocytes (Griffiths-EJ, 1999). However, the use of ruthenium red in intact cells is limited due to its poor membrane permeability and its inhibitory effects on sarcoplasmic reticulum calcium release (Chamberlain, Volpe & Fleischer, 1984; Vassilev, Kanazirska, Charamella, Dimitrov & Tien, 1987). There is also evidence that ruthenium red inhibits SR Na^{+}/Ca^{2+} exchange in isolated, perfused rat hearts (Gupta, Innes & Dhalla, 1988). Recently, Ru 360, an oxygen-bridged, dimeric ruthenium amine complex, has been shown to inhibit calcium-stimulated mitochondrial respiration (Ying, Emerson, Clarke & Sanadi, 1991). In addition, it has been demonstrated that Ru 360 (which is cell permeant) is highly specific in its actions, as very little effect of the compound was found on SR calcium release, SR Na^{+}/Ca^{2+} exchange, or cardiomyocyte contractility (Matlib *et al.*, 1998). In view of these actions, the potential use of Ru360 as a modulator of mitochondrial flickering was investigated.

Confocal imaging of cells co-loaded with TMRE and fluo-3

The confocal imaging system allows truly simultaneous imaging of up to four fluorophores. To investigate the possible co-localisation of calcium transients and mitochondrial depolarisations, cells were co-loaded with TMRE (by immersion in a 1.5 μM solution) and

fluo-3 AM (by immersion in a 4.4 μM solution). At the time of these experiments rat cortical astrocytes were unavailable, so neonatal rat cardiomyocytes, which were being used in other studies were substituted. Previous work in the lab has established that cardiomyocytes exhibit the same mitochondrial flickering pattern as astrocytes and that in these cells intracellular calcium stores are involved in the phenomenon (Duchen *et al.*, 1998). The dye-loaded cells were illuminated using the 488 nm laser line and the laser power was attenuated to around 3% of total power. Fluorescence emission was measured via a band-pass filter at 505-550 nm (fluo-3) and a long-pass filter at 585 nm (TMRE). The acquisition time for each frame of the image sequences was in the region of 1 second. The 63x objective lens was used and the acquired images were collected at either 8 or 12 bits.

Results

1. Removal of extracellular calcium

Removal of extracellular calcium did not affect the mitochondrial depolarisations

The chelation of extracellular calcium by immersing TMRE-loaded cells in a calcium-free saline did not attenuate the mitochondrial flicker. There was no change in the index of variation. The P value, calculated by an unpaired, two-tailed t test, was 0.285, not significant The index of variation is illustrated in Figure 5.1, where the error bars represent standard deviations, as they do in all the histograms in this thesis.

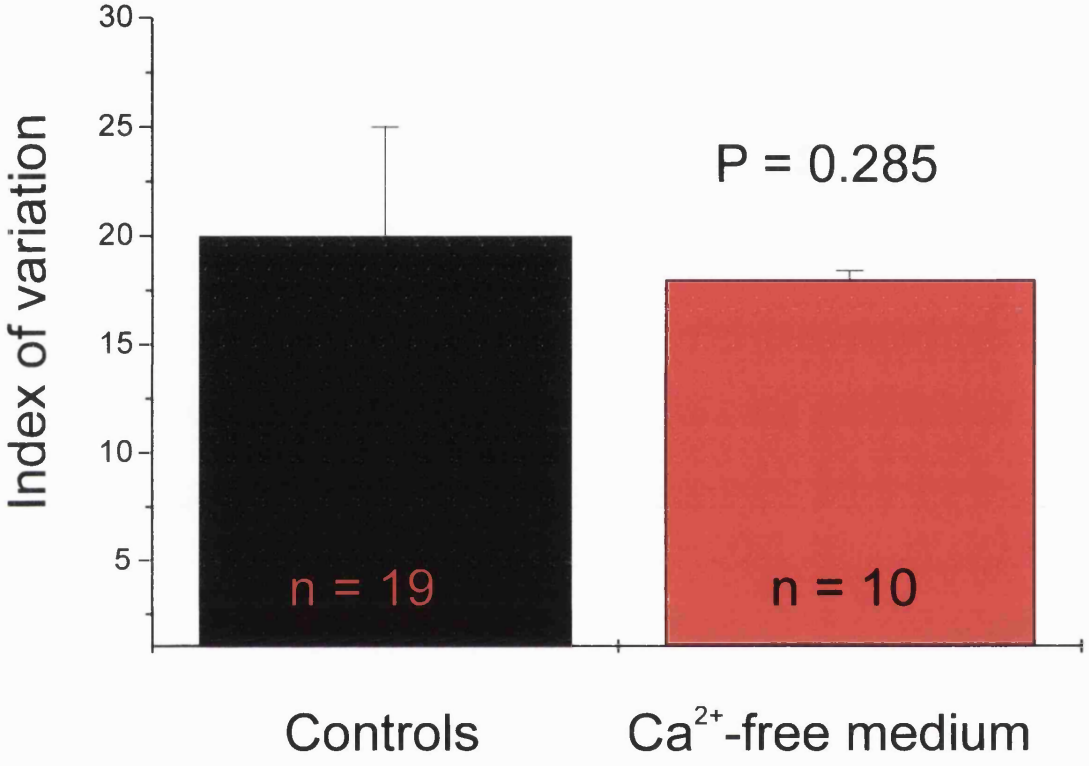

Figure 5.1: removal of extracellular Ca^{2+} did not attenuate the flickering

2. Buffering of intracellular Ca^{2+}

Treatment with BAPTA did not suppress the flickering but did slow the global depolarisation

Treatment of cells with BAPTA-AM had no effect on mitochondrial flickering, as assessed by calculating index of variation. The two-tailed P value, calculated by Mann-Whitney U test, was 0.979, not significant. The data are summarised in Figure 5.2.

Treatment with BAPTA-AM attenuated calcium mobilisation

In order to test that this protocol did indeed effectively buffer $[Ca^{2+}]_i$, responses to Ca^{2+} mobilisation in BAPTA-loaded cells were checked using the fluorimetric system. In astrocytes that had been loaded with the ratiometric calcium indicator fura-2, application of ATP 100 μM by puffer pipette induced brisk, robust rises in Ca^{2+} (fura-2 ratio) in all of the cells studied (Figure 5.3a). This response was independent of $[Ca^{2+}]_o$ and so reflected mobilisation of ER Ca^{2+}. Occasional calcium oscillations were seen after application of ATP. The Ca^{2+} rise in response to ATP was completely ablated in nine of ten cells studied (Figure 5.3b), and the rise in fura-2 ratio on stimulation of this single cell was greatly attenuated, confirming that treatment with BAPTA-AM attenuated $[Ca^{2+}]_{cyt}$.However, loading of the cells with BAPTA-AM significantly reduced the rate of change of global TMRE signal in all of the cultures studied (Figure 5.4).

Hence treating TMRE-loaded astrocytes with BAPTA-AM 10 μM did not affect the mitochondrial flicker but did reduce the rate of global mitochondrial depolarisation as measured over the whole cell.

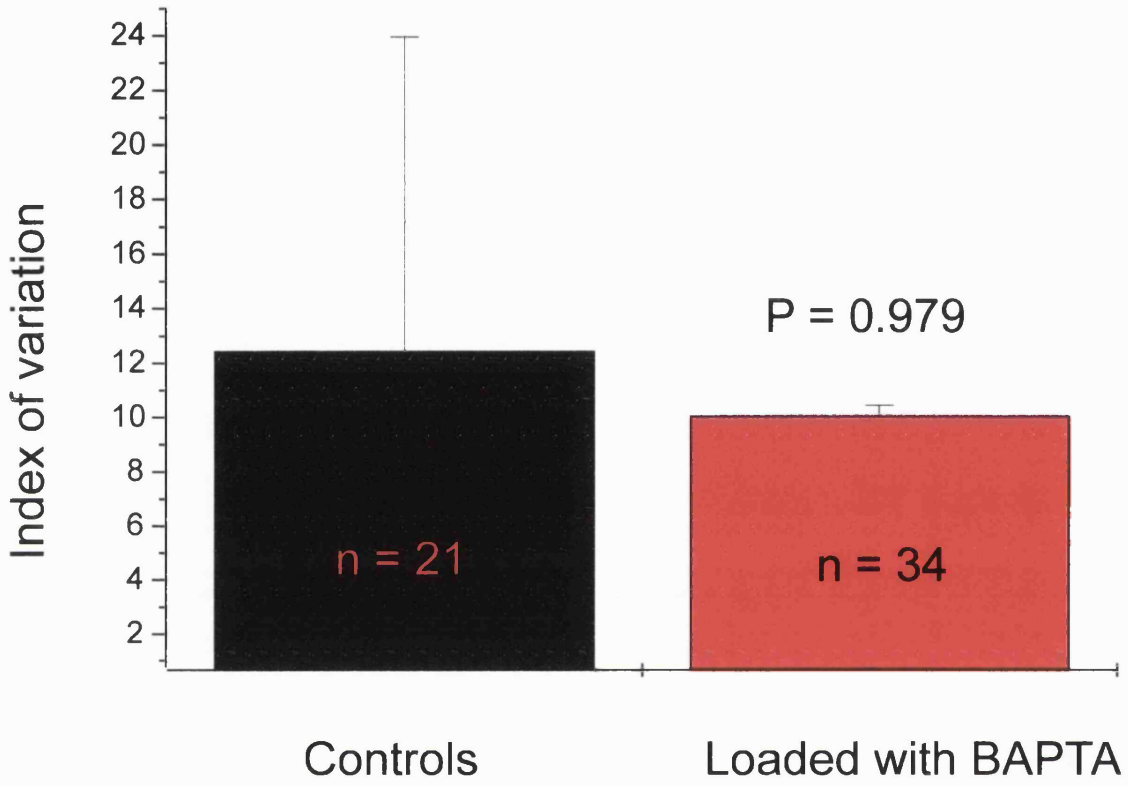

Figure 5.2: Treatment with BAPTA-AM 10 μM
did not reduce the index of variation

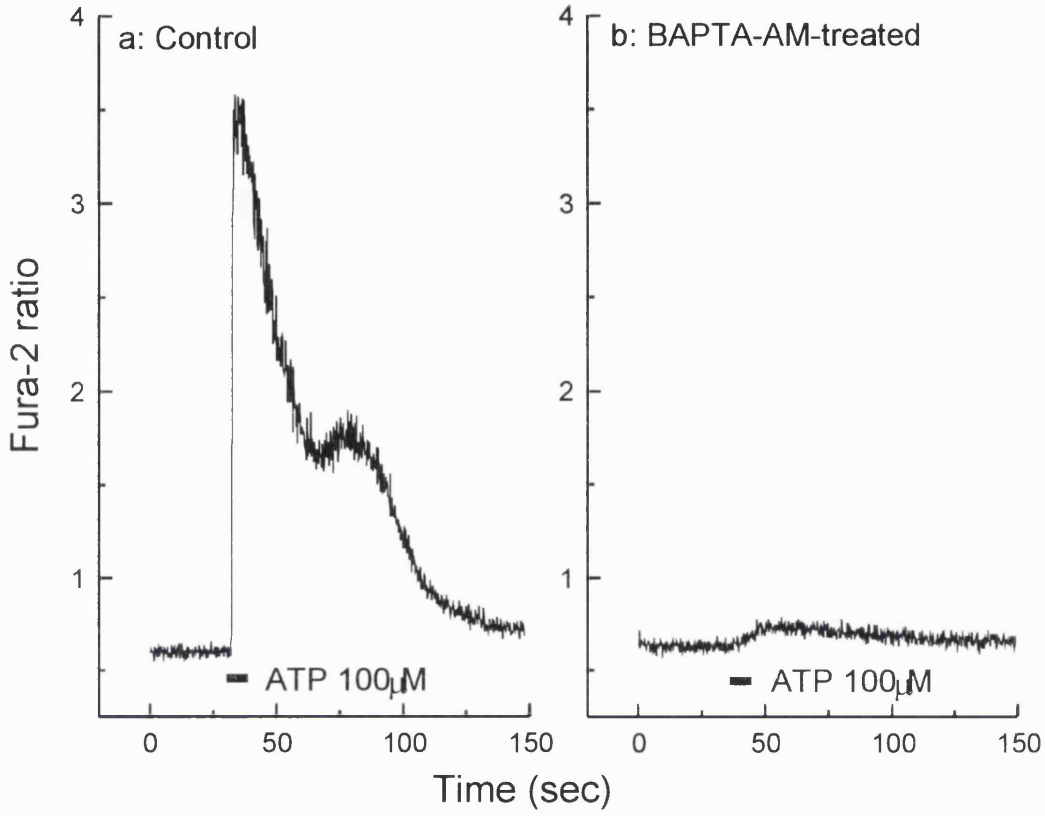

Figure 5.3: astrocytes loaded with fura-2 AM 5 μM showed a robust response to ATP 100 μM. Treatment with BAPTA-AM 10 μM completely ablated this response in most cells. The response shown in Panel b was the maximum seen in BAPTA-treated cells.

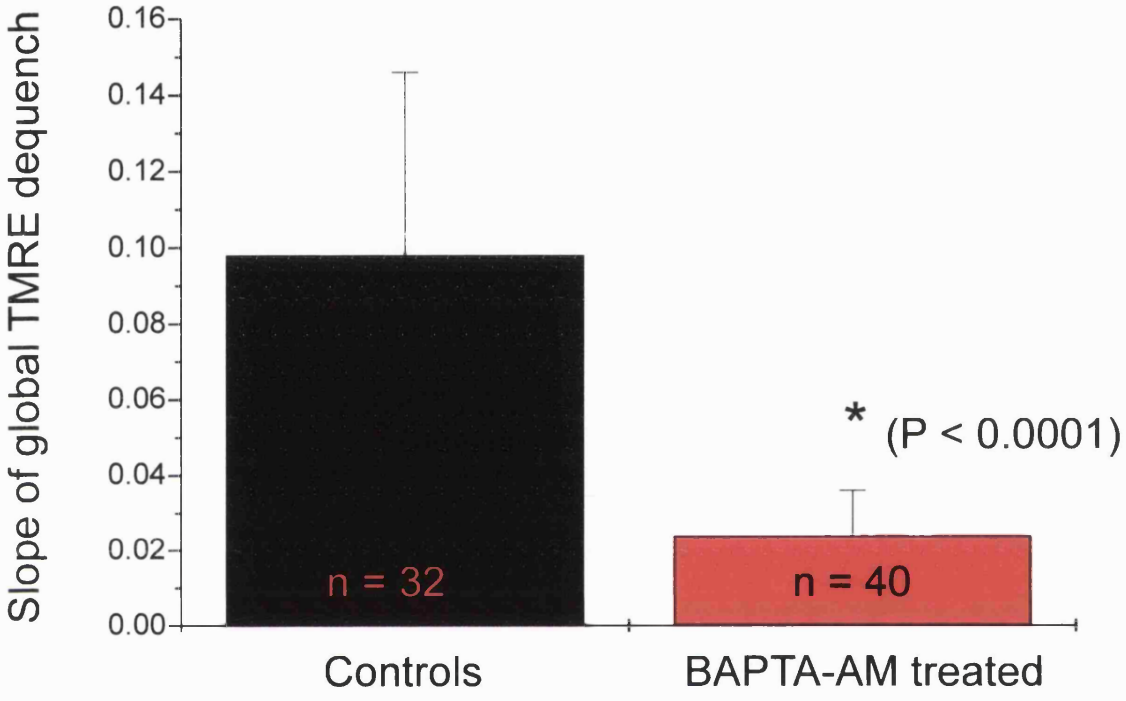

Figure 5.4: treatment with BAPTA-AM significantly slowed the global depolarisation

3. Emptying of intracellular Ca^{2+} stores

The buffering of $[Ca^{2+}]_{cyt}$ slowed the time to global mitochondrial depolarisation, suggesting involvement of intracellular Ca^{2+} in the mitochondrial depolarisations. There is evidence that mitochondria may be loaded with Ca^{2+} directly from internal stores (Rizzuto, Brini, Murgia & Pozzan, 1993; Gallitelli, Schultz, Isenberg & Rudolf, 1999) and a privileged pathway for Ca^{2+} movement from ER to mitochondria may explain the inability of BAPTA-AM to attenuate the index of variation. Therefore the possibility of suppressing flicker by emptying ER of stored Ca^{2+} was investigated. Thapsigargin blocks the action of SERCA pumps, leading to depletion of stored $[Ca^{2+}]$, so the actions of thapsigargin on $[Ca^{2+}]_i$ in the astrocytes were investigated with a view to using the compound to further deplete $[Ca^{2+}]_i$.

Treatment with thapsigargin raised $[Ca^{2+}]_i$

Addition of thapsigargin 200 nM to the cell dish caused a steady but small rise in $[Ca^{2+}]_i$, as measured by fura-2 ratio (Figure 5.5, Panels A and B). This suggests that there is a constant Ca^{2+} leak from ER and subsequent reuptake; Ca^{2+}-cycling that is blocked by thapsigargin. Hence treatment with thapsigargin causes Ca^{2+} efflux from ER.

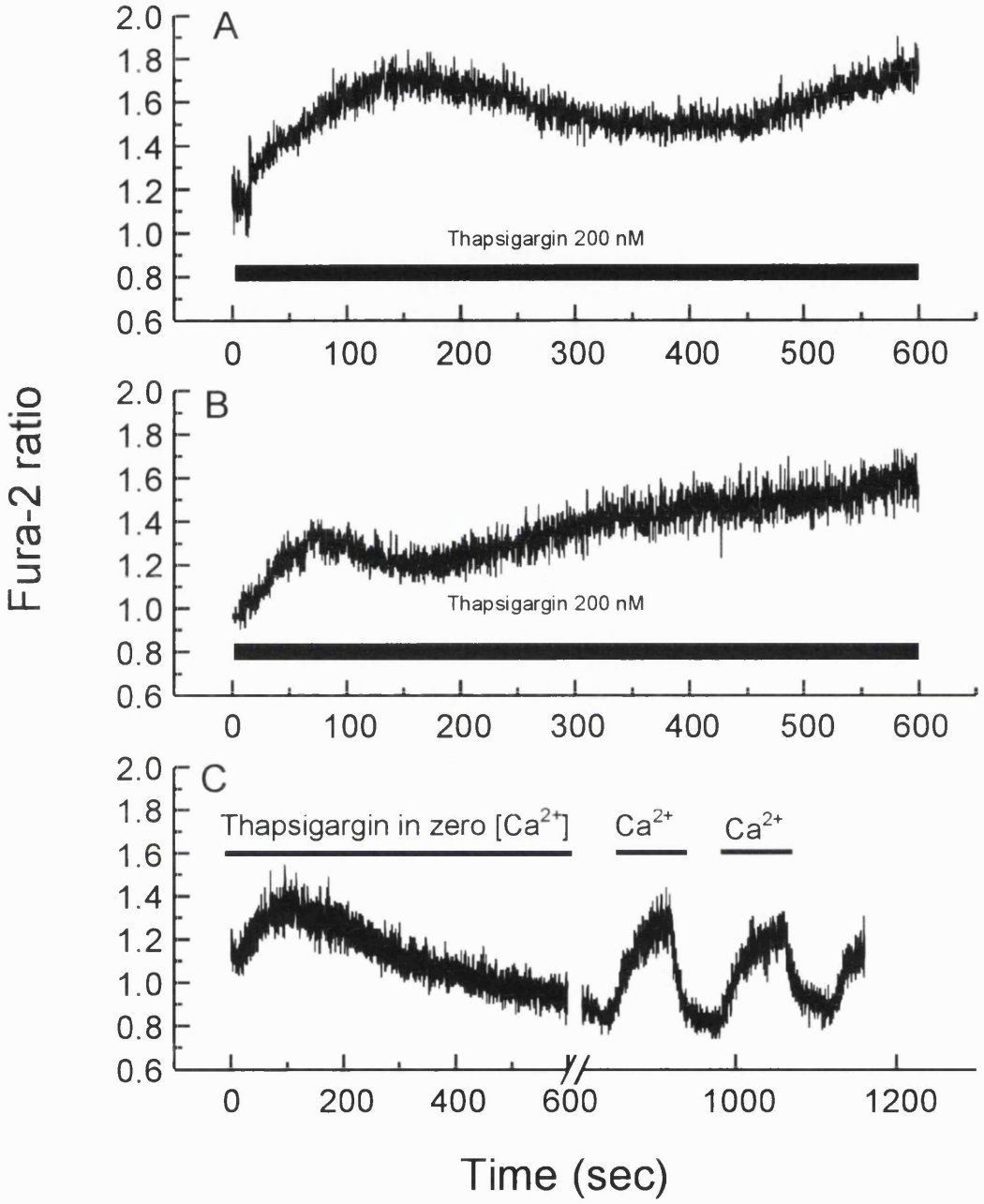

Figure 5.5: the effect of thapsigargin 200 nM on $[Ca^{2+}]_i$ in fura-2-loaded astrocytes. In those cells treated with thapsigargin (200 nM for 10 minutes) in a calcium-containing medium, the rise in $[Ca^{2+}]_i$, was biphasic, after a short recovery (Panels A and B). Treating cells with thapsigargin in a Ca^{2+} -free medium (Panel C) ablated the secondary rise, suggesting that Ca^{2+} influx from the extracellular medium was being activated by emptying of internal stores. Washes with saline containing calcium reinstated the rise in $[Ca^{2+}]_i$ in these cells.

After a small recovery in $[Ca^{2+}]_i$, the fura-2 signal began to rise slowly. That this latter rise in $[Ca^{2+}]_i$ was due to capacatative influx of extracellular calcium was demonstrated by removal of Ca^{2+}_o (Figure 5.5, Panel C). The initial rise in $[Ca^{2+}]_i$ to thapsigargin was unchanged, confirming that this was release from internal stores but the secondary rise was abolished in the absence of Ca^{2+}_o. Return of Ca^{2+}_o caused an immediate rise in $[Ca^{2+}]_i$. The transient recovery in $[Ca^{2+}]_i$ (eg between 180 and 400 seconds in the cell illustrated in Figure 5.5A) was due to calcium extrusion at the plasmalemma, as addition of FCCP 1 μM did not abolish the fall in ratio, suggesting that mitochondrial calcium uptake could not account for the temporary drop in $[Ca^{2+}]_i$.

Thus thapsigargin treatment alone, while emptying Ca^{2+} stores, may nevertheless raise $[Ca^{2+}]_{cyt}$ and this in turn might lead to mitochondrial Ca^{2+} loading. In order to remove all sources of intracellular Ca^{2+} a combination of thapsigargin and BAPTA-AM was used to empty the stores, buffer released Ca^{2+} and limit Ca^{2+} loading by capacitative influx. Under these conditions, basal fura-2 ratio was unchanged ($P = 0.540$, unpaired t test) and stimulation with ATP failed to evoke any response at all (Figure 5.6). This combination of agents seem the most effective way to limit movement of intracellular Ca^{2+}.

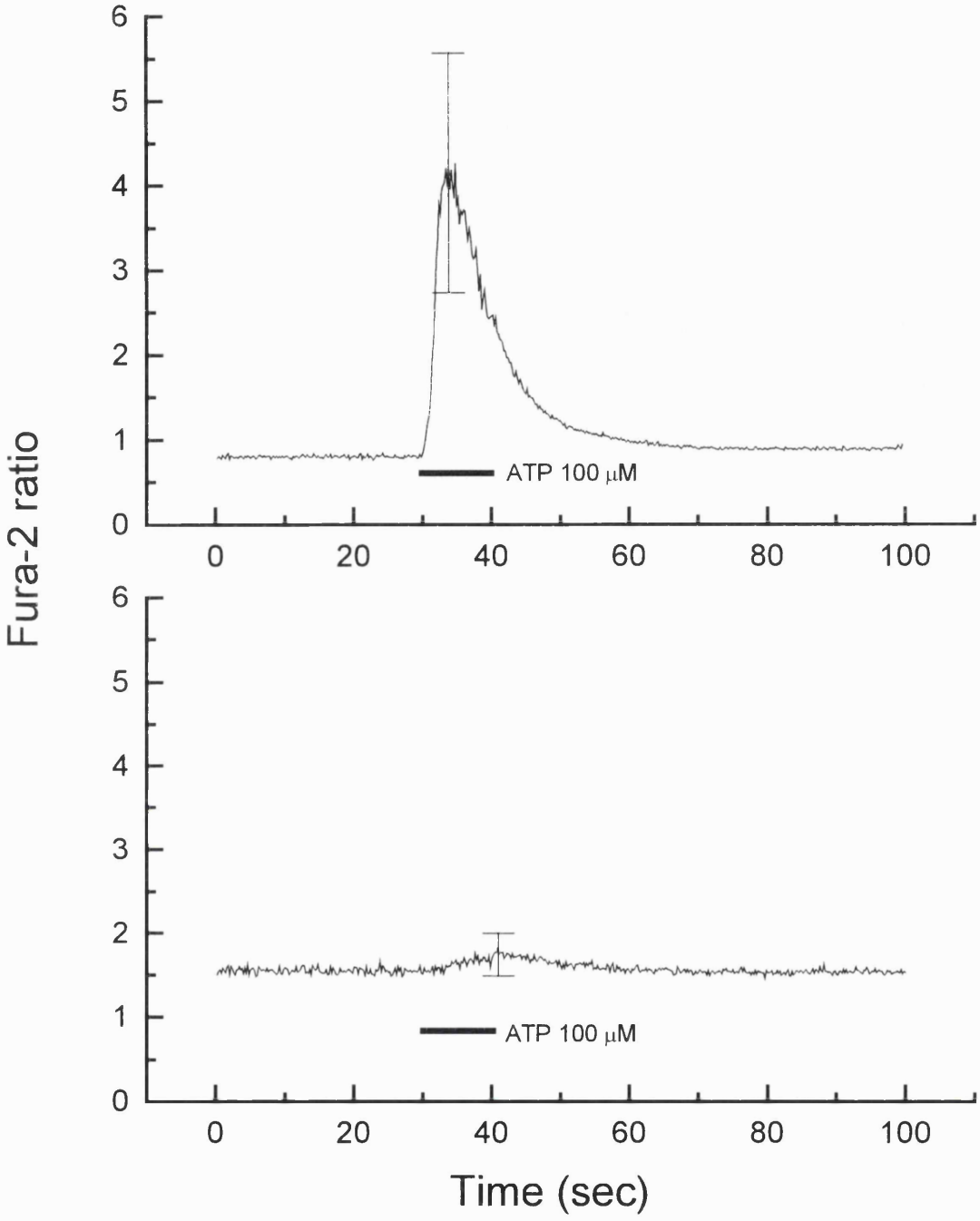

Figure 5.6: the effect of treatment with thapsigargin 200 nM and BAPTA-AM 10 μM on ATP-stimulated Ca^{2+} release. Cells were loaded with BAPTA-AM by equilibration in a 10 μM solution and then immersed for 10 minutes in thapsigargin 200 nM (lower panel). Application of ATP 100μM evoked no change in fura-2 ratio, indicating that intracellular Ca^{2+} stores were emptied and chelated by this protocol.

Treatment with both thapsigargin and BAPTA attenuated mitochondrial flickering

Treatment of astrocytes with BAPTA-AM 10 μM and thapsigargin 200 nM, as outlined above, significantly reduced the mitochondrial flickering seen in TMRE-loaded, illuminated cells - $P < 0.0001$, Mann-Whitney test (Figure 5.7a)

In Figure 5.8, line and surface plots illustrate how treatment with thapsigargin and BAPTA could attenuate the mitochondrial flickering. The figures are drawn from single cells imaged using the confocal microscope. In order to show how events in the spatial domain vary with time (that is, illustrate a three dimensional event on the two dimensional page) line plots are frequently used. Once the image of the cell has been collected, a line is drawn through the image, using the analysis software. The values of the individual pixels along that line may then be plotted against time and the resultant rectangular image demonstrates in two dimensions how the pixel values along the line varied during the imaging. Hence, with reference to the lower left panel of Figure 5.8, it can be seen that there was a large, isolated event 40 μm from the start of the line, both at 4 seconds and at 44 seconds; an illustration of how a single mitochondrion depolarised twice during the image sequence. There are similar events at different points along the line at 11, 23 and 26 seconds. Additionally, the hotter colours towards the end of the sequence, after about 30 seconds, emphasise how the TMRE signal rose in the cytosol as the dye left depolarising mitochondria. Finally, there are a flurry of events around 45 seconds. If the line plot is rendered as a surface plot (upper left panel) the amplitude of the signal changes may be more clearly seen. By contrast, in the thapsigargin/BAPTA treated cell, right-hand pair of images, there was only one depolarisation (at 26 seconds) on the line during the 45 seconds that the cell was imaged.

There was no difference in the dequench of TMRE when FCCP 1 μM was added to either of the groups (Figure 5.7b), suggesting similar dye loading in each group ($P = 0.151$, unpaired t test).

Hence, emptying of intracellular calcium stores, in the presence of intracellular BAPTA, significantly reduced both the mitochondrial flicker and the rate of progression to global

Figure 5.7a: treatment with thapsigargin and BAPTA-AM significantly reduced the index of variation

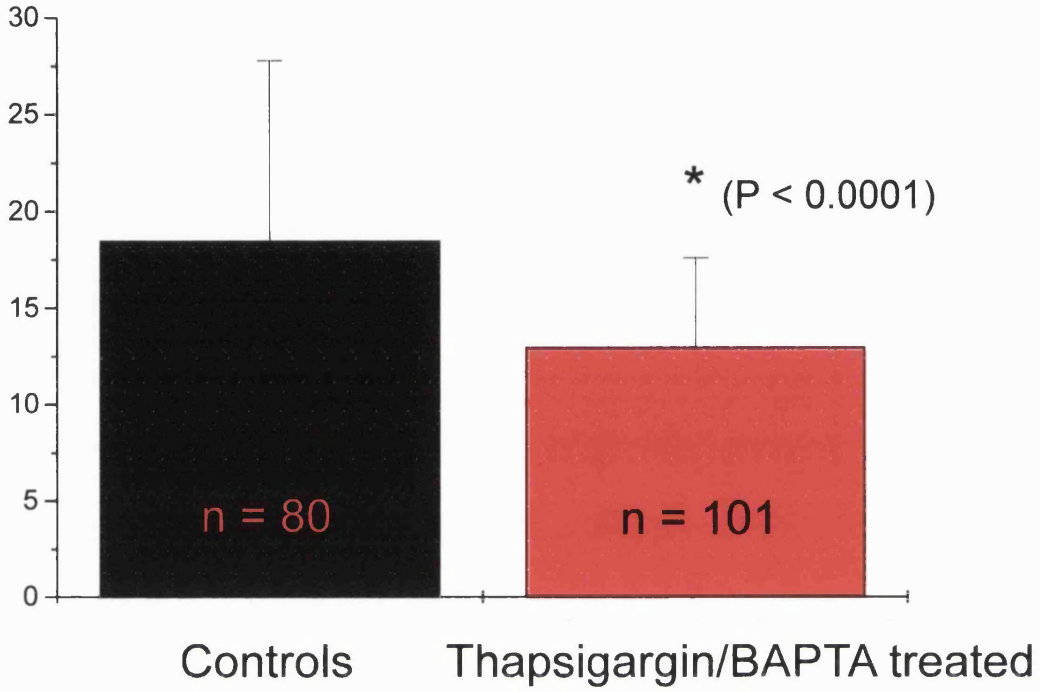

Figure 5.7b: there was no difference in TMRE dequench on application of FCCP

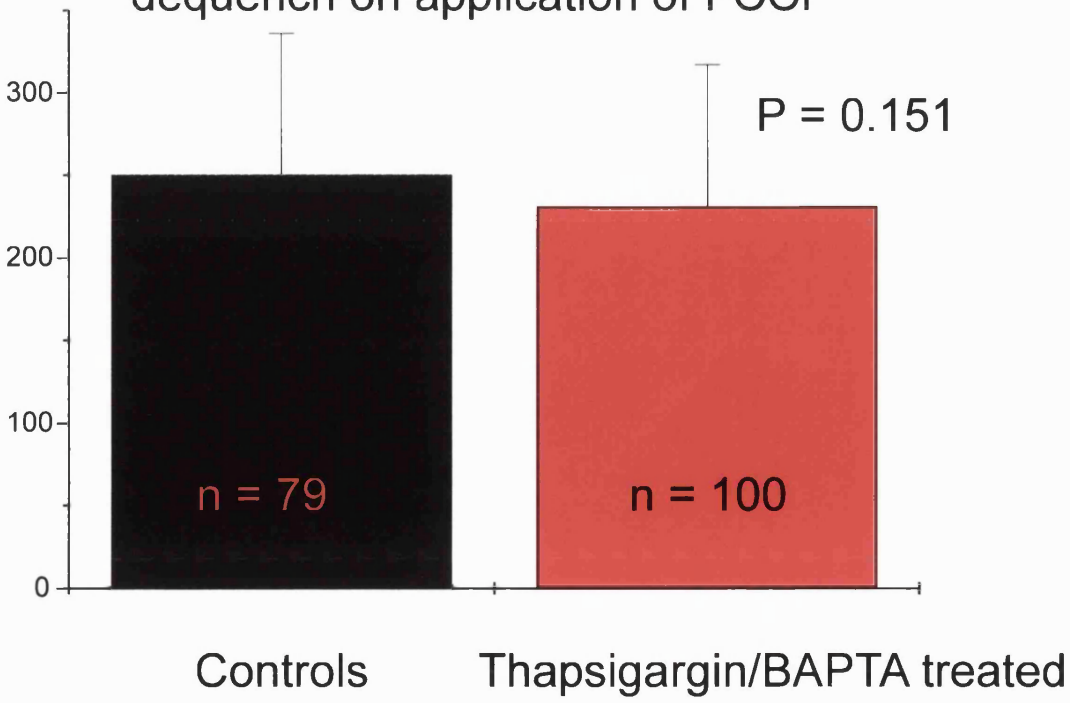

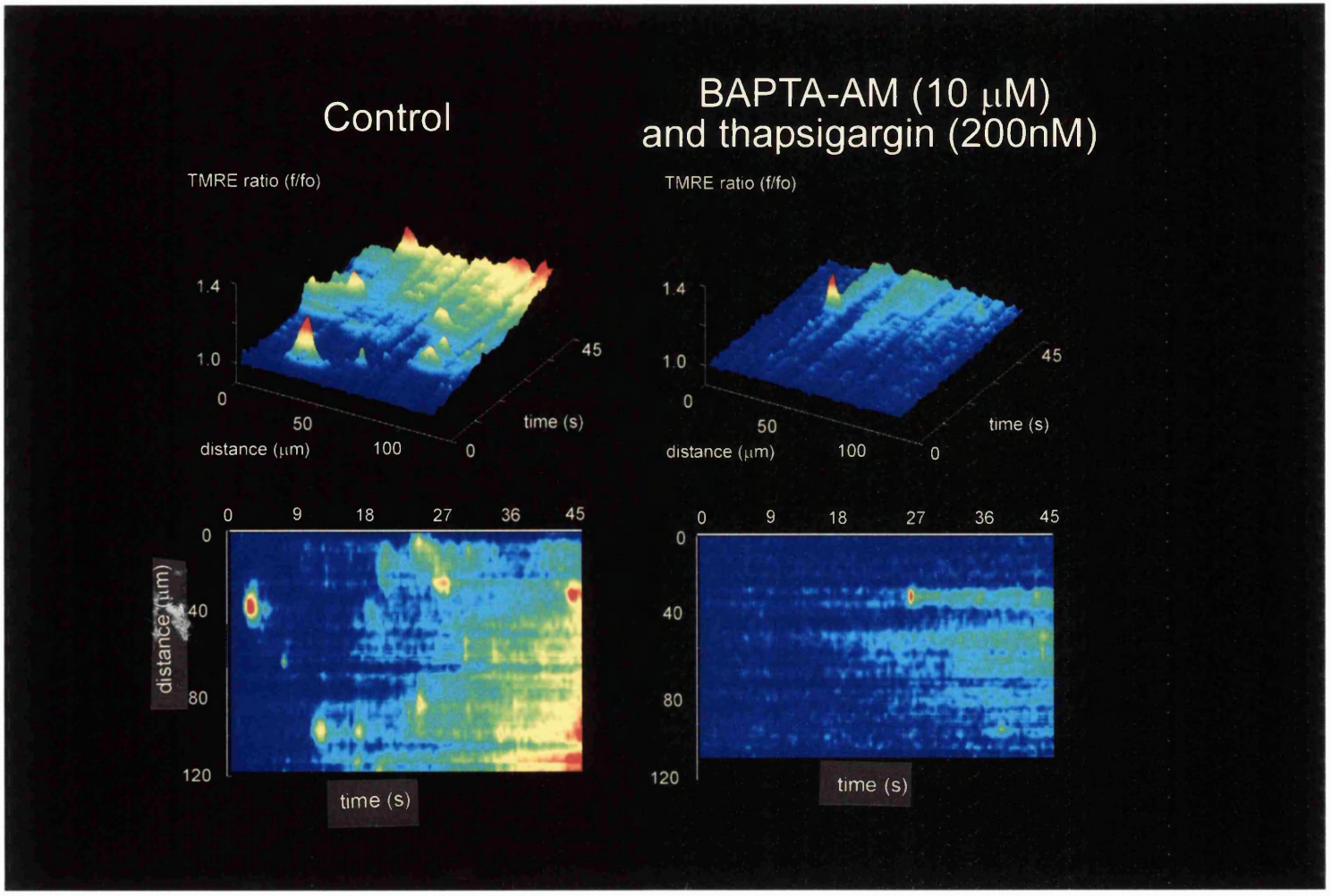

Figure 5.8: treatment with thapsigargin and BAPTA-AM attenuated the mitochondrial flickering. Line images are taken from confocal images of single astrocytes loaded with TMRE and the signal has been ratioed against the first image of the series. The mitochondrial flickers can clearly be seen in both the control line image (below) and surface plot (above). The flickers are almost entirely absent in the cell treated with thapsigargin and BAPTA.

mitochondrial depolarisation, suggesting that *stored* calcium made a significant contribution to the mitochondrial flickering.

4. Treatment with Ru360

As stored Ca^{2+} contributes to mitochondrial flickering, it seems likely that mitochondrial uptake of released Ca^{2+} could account for the transient depolarisations. Pharmacological blockade of the calcium uniporter would be expected to prevent the flickering. The novel inhibitor of the mitochondrial uniporter, Ru360, has been shown to block mitochondrial Ca^{2+}uptake in cardiomyocytes (Matlib *et al.*, 1998). In order to establish the efficacy of this compound in astrocytes, cells were loaded with rhod-2 to monitor mitochondrial Ca^{2+} uptake. Cells were stimulated with ATP and the signal was measured over individual mitochondria. Additionally, as some rhod-2 partitions within the nucleus, the signal here was measured to assess Ca^{2+} transients not affected by mitochondria.

Ru360 attenuated the rhod-2 response to ATP

Rhod-2-loaded astrocytes were stimulated by puffer application of ATP 100 μM. In the control cells this stimulation induced a rise in rhod-2 signal over the mitochondria of 58% ± 47%, mean ± SD, n = 92 cells (Figure 5.9 and Figure 5.10, upper panel). Ru360 100 μM was added to the dish of cells and the stimulation repeated after 30 minutes. The rise in signal over mitochondria was 51% ± 34% (n = 27), not different from the controls (P = 0.47, two-tailed t test). After 75 minutes, however, the rise in signal was only 16% ± 13%, significantly less than that seen in controls (P < 0.001, two-tailed t test, n = 26). At 90 minutes (Figure 5.10, middle panel) there was no rise in rhod-2 signal on addition of ATP and the Ru360 solution was removed and the cells washed. Within 10 minutes the mitochondrial rhod-2 response to ATP had returned, the rise in signal was 78% ± 51% (n = 18).

These findings initially suggested that the Ru360 was reversibly blocking mitochondrial calcium uptake after about 75 minutes loading, however analysis of the concurrent rhod-2 signals over the nuclei, used as an index of $[Ca^{2+}]_{cyt}$, revealed that there was no change in rhod-2 signal here when the cells were stimulated (Figure 5.10, lower panel). In other words,

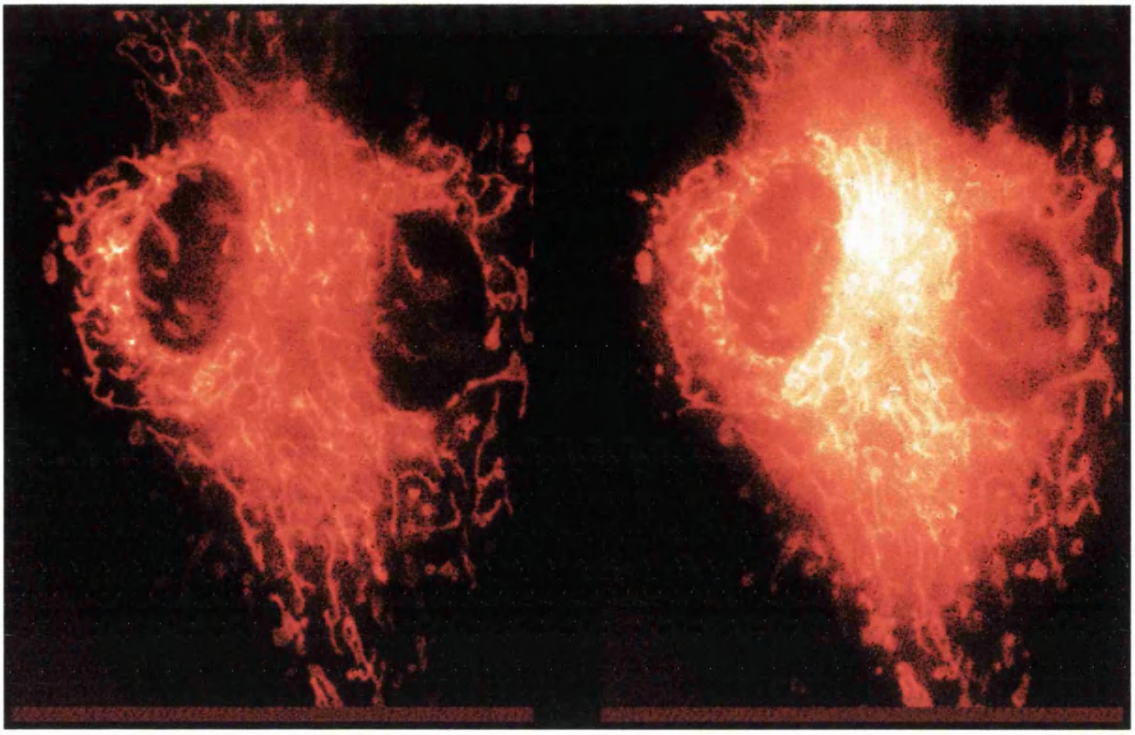

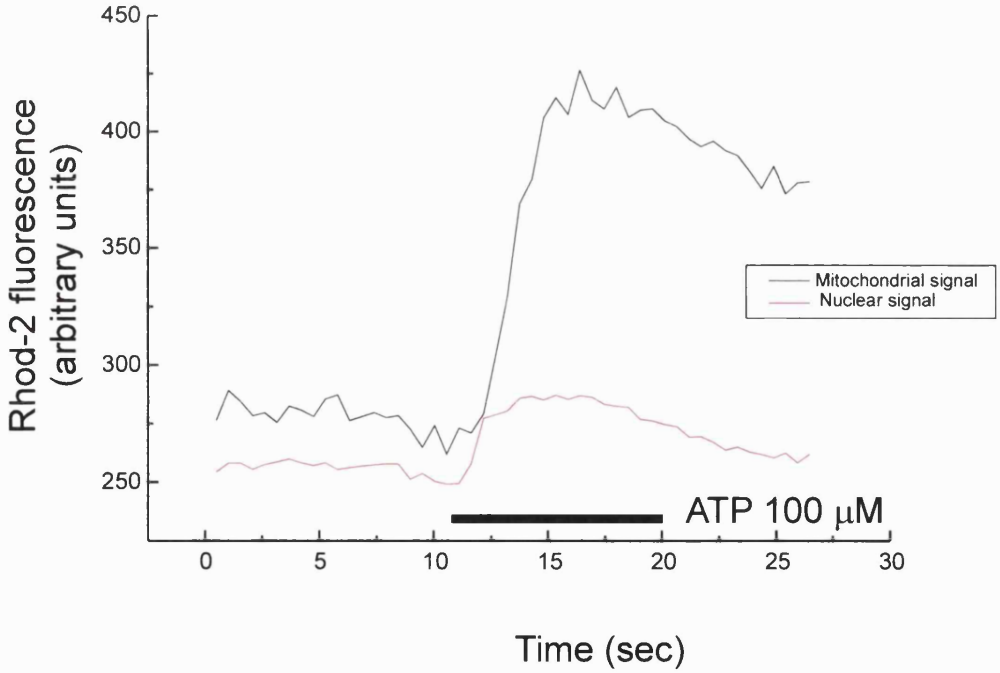

Figure 5.9: application of ATP 100 μM to rhod-2 loaded astrocytes induced a rise in mitochondrial rhod-2 signal of 58 ± 47% (n = 92 cells) confirming mitochondrial Ca^{2+}-loading on mobilisation of stored Ca^{2+}. There was a concomitant, but proportionally smaller, rise in rhod-2 signal over the mitochondrion-free nucleus.

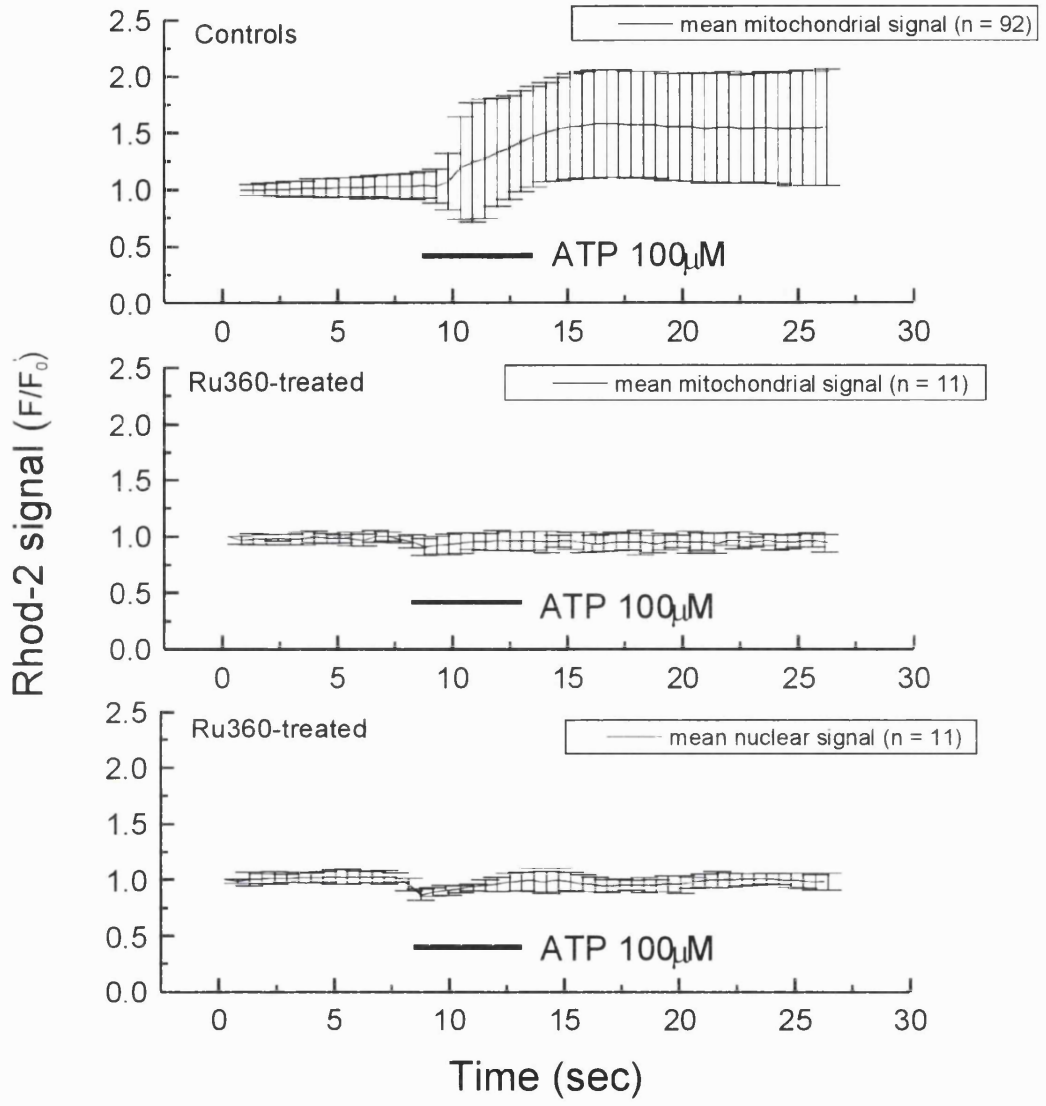

Figure 5.10: after 90 minutes, treatment of rhod-2-loaded astrocytes with Ru 360 completely suppressed the change in mitochondrial rhod-2 signal after stimulation with ATP 100 μM. However, the rhod-2 signal over the mitochondrion-free nucleus was also attenuated, suggesting that, in these cells, Ru 360 had pharmacological effects other than blockade of the calcium uniporter.

the Ru360 appeared to be blocking calcium release in response to ATP as the calcium indicator in the nucleus should have signalled a rise in $[Ca^{2+}]_i$.

Ru360 prevented Ca^{2+} mobilisation in response to ATP

To investigate this further, and to determine whether the Ru360 was somehow quenching the rhod-2 fluorescence, cells were loaded with the fluorescent calcium indicator fluo-3 AM and then treated with Ru360 as before. The fluo-3 signal was measured over a large area of cytosol and thus reflected intracellular calcium mobilisation as a whole rather than just the change over a single organelle. Stimulation of these cells confirmed that calcium mobilisation in response to ATP was significantly reduced after 75 minutes treatment with Ru360, the rise in fluo-3 signal in the controls being 300% ± 47% (mean ± SD, n = 8) whereas in the Ru360-treated cells the change in signal was 102% ± 85% (n = 9), $P < 0.0001$, two-tailed t test. The resting fluo-3 fluorescence in the unstimulated cells was not different after treatment with Ru360 ($P = 0.238$, two-tailed t test) suggesting that the compound was not quenching the fluo-3 signal.

Ru360 emptied intracellular calcium stores

To ascertain whether the Ru360 was disrupting the ATP-mediated signalling pathway or was emptying intracellular calcium stores, the calcium ionophore ionomycin was applied to cells before treatment with Ru360 and the fluo-3 response compared with that seen after 90 minutes in 100 μM Ru360. Figure 5.11 confirms that the application of ionomycin 10 μM mobilises calcium from internal stores in the absence of external Ca^{2+}. After treatment with Ru360 the response to ionomycin had completely disappeared, confirming an action of Ru360 on the stores. Removal of the Ru360 solution and restoration of the $[Ca^{2+}]_o$ to 2 mM once again initiated refilling of the internal stores, as application of ATP 100 μM an hour later induced a rise in fluo-3 signal of 150% ± 100% (n = 15).

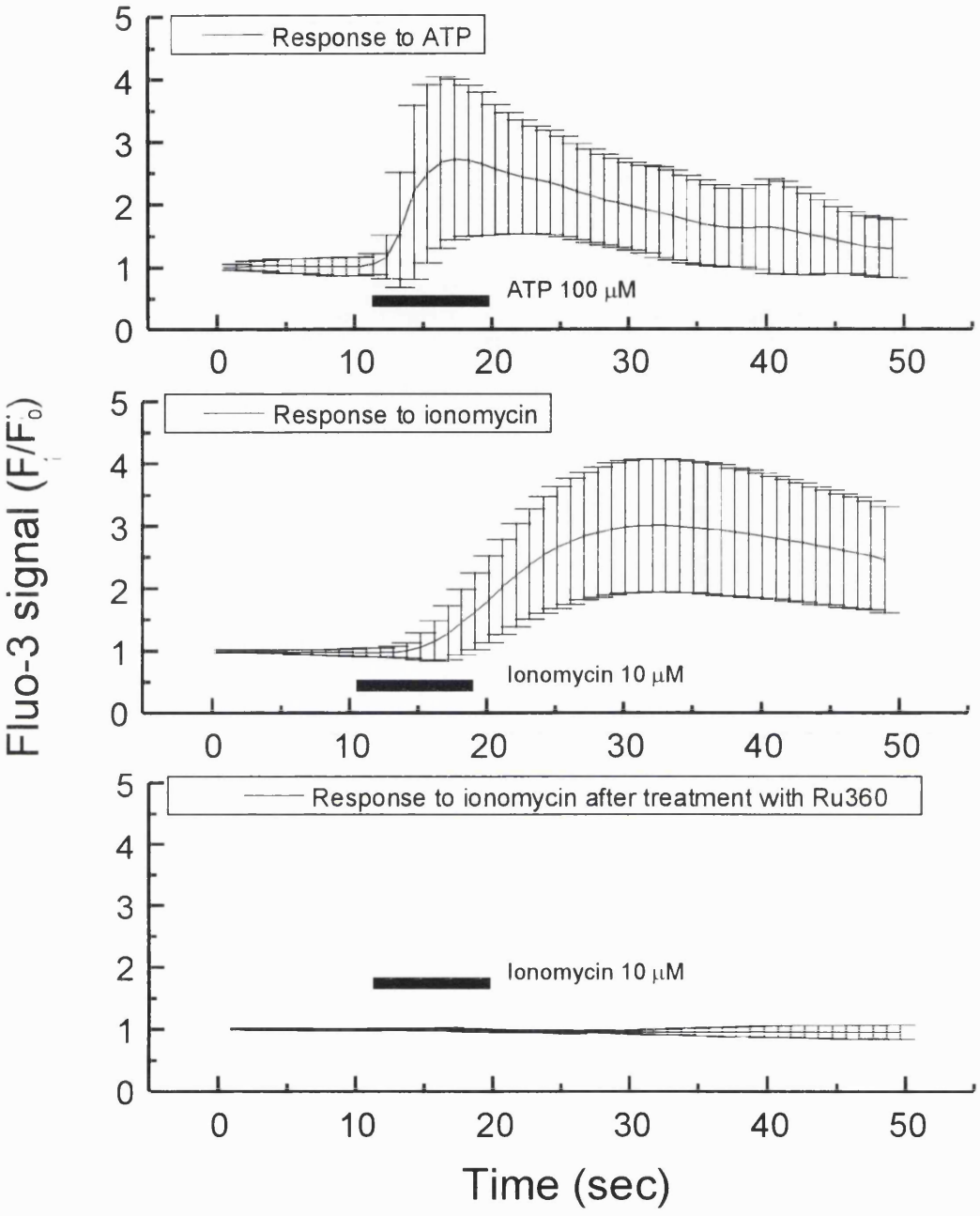

Figure 5.11: application of the calcium ionophore induced a rapid rise in fluo-3 signal which was similar in amplitude to that seen on application of ATP. However, after 90 minutes in Ru360 the response to ionomycin completely disappeared, suggesting that this compound depletes intracellular calcium stores in cortical astrocytes.

In summary, these results suggest that Ru360 is not a suitable compound for pharmacological manipulation of mitochondrial calcium uptake in these cells as it appears to temporarily deplete the intracellular calcium stores.

5. Cortical astrocytes contain ryanodine-sensitive Ca^{2+} stores

As Ca^{2+} derived from intracellular stores is necessary for the mitochondrial depolarisations, the identity of those stores was investigated. This is important as the ryanodine receptor (RyR) has a larger conductance than the IP_3 receptor and so would mediate greater local $[Ca^{2+}]$ changes than release from IP_3 receptors. Additionally, the RyR has a well established sensitivity to reactive oxygen species (see Chapter 6), while the sensitivity of the IP3 receptor to oxidative modulation is less well established.

Peuchen and colleagues demonstrated that adult rat cortical astrocytes contain IP_3-mediated Ca^{2+} stores and that stored Ca^{2+} is released upon activation of the P_{2U} receptor by ATP (Peuchen *et al.*, 1996a). No rise in $[Ca^{2+}]_i$ was seen on application of caffeine (however caffeine inhibited $[Ca^{2+}]$ responses to ATP) and there was no response to ryanodine. However other investigators have shown that a sub-population of rat cortical astrocytes do exhibit ryanodine-sensitive Ca^{2+} release (Langley & Pearce, 1994).

Ryanodine evoked a rise in $[Ca^{2+}]_i$

Local application of ryanodine by puffer pipette induced a rise in $[Ca^{2+}]_i$ in many of the astrocytes examined. Not all cells responded (in contrast ATP nearly always produced a response), but the responses were robust, where present. Figure 5.12 illustrates the fura-2-signalled changes in $[Ca^{2+}]_i$ seen on addition of various concentrations of ryanodine. Removal of extracellular calcium did not attenuate the response to ryanodine, indicating that release from intracellular Ca^{2+} stores was responsible for the change in fura-2 ratio.

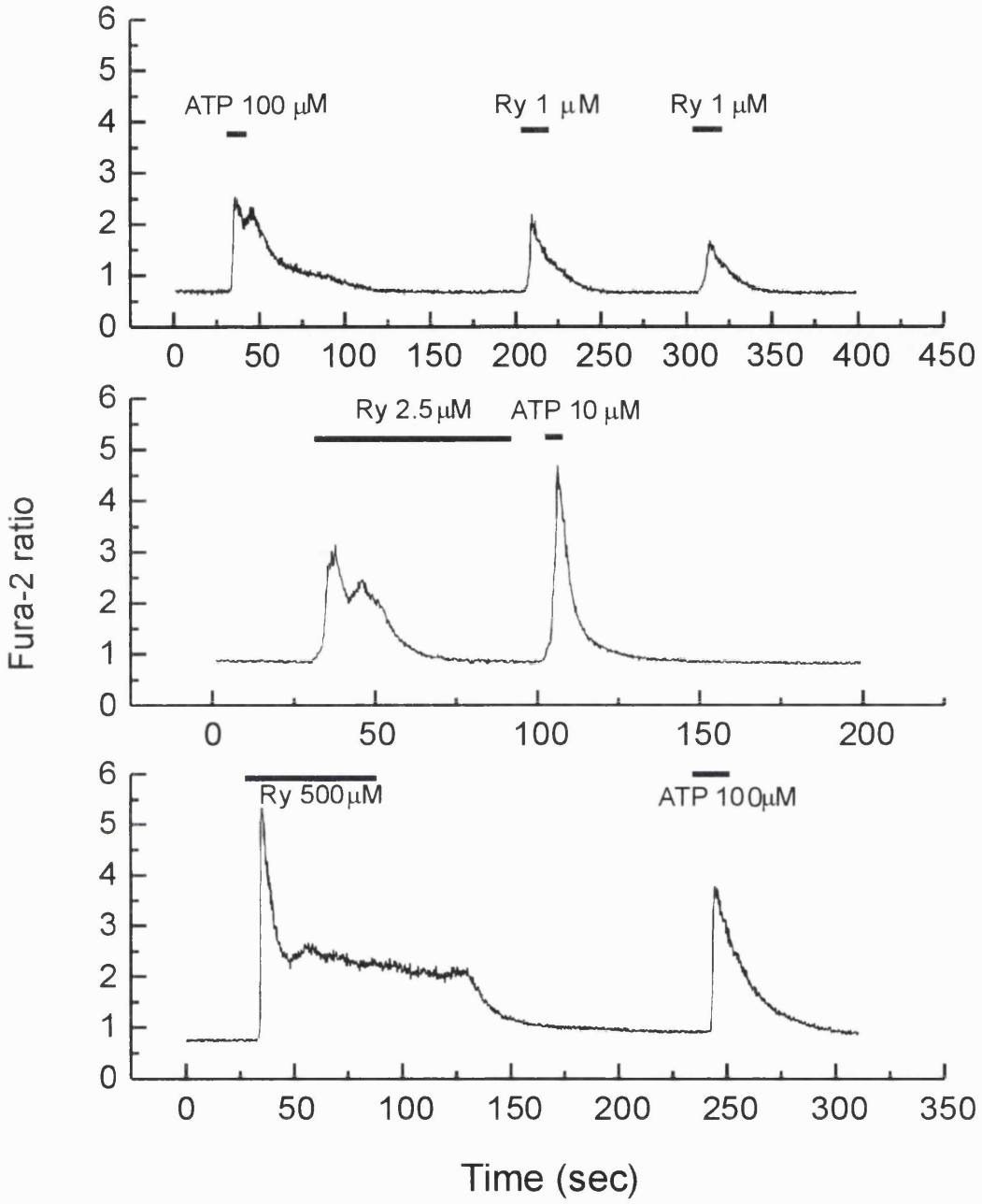

Figure 5.12: ryanodine at all the concentrations tested (1 500 μM) induced calcium release from internal stores in some of the astrocytes. Other cells showed no response to any concentration of ryanodine but reacted to application of ATP 100 μM. No concentration of ryanodine was found that would reliably block calcium release in the astrocytes.

Experiments were carried out in the presence of extracellular Ca^{2+}.

Ryanodine-sensitive Ca^{2+} stores are distinct from the IP3-sensitive Ca^{2+} stores

Repeat applications of ryanodine, where a pulse of the agonist was immediately followed by a second, did not evoke repeated rises in $[Ca^{2+}]_i$, presumably because some time for store refilling was required (data not shown). However, addition of ATP 100 μM immediately after stimulation by ryanodine induced further rises in $[Ca^{2+}]_i$, sometimes superimposed upon the response to ryanodine, suggesting that the calcium was derived from separate stores. Additionally, the rise in fura-2 ratio with ATP was invariably faster and larger than that seen with ryanodine.

High concentrations of ryanodine did not block Ca^{2+} release

Ryanodine binds to multiple binding sites on the ryanodine receptor in a Ca^{2+}-dependent manner. In both skeletal and cardiac muscle SR [^{3}H] ryanodine binding studies have identified a high affinity site with an apparent K_D between 2 and 200 nM and a low-affinity site with apparent K_D values between 30 nM and 4 μM (Shoshan-Barmatz & Ashley, 1998). The activity of the channel is modulated by ryanodine in a biphasic manner, with low concentrations activating the channel and high concentrations (> 100 μM) inhibiting it. Although ryanodine was applied at various concentrations, up to 500 μM, no concentration was found that routinely blocked calcium release as some cells reacted to all concentrations of ryanodine (see Table 5.1).

[Ryanodine] μM	*Number of cells tested*	*% reacting to ryanodine*
1	6	33
2.5	13	77
20	10	50
500	10	90

Table 5.1: the response (as determined by fura-2 ratio) of cortical astrocytes to various concentrations of ryanodine. All cells responded to ATP 100 μM with a rise in fura-2 ratio, while the responses to ryanodine were less robust.

Bath application of ryanodine attenuated the global depolarisation in TMRE-loaded cells

As a proportion of the astrocytes demonstrated responses to ryanodine, the effect of the compound on the global mitochondrial depolarisation was investigated. TMRE-loaded cells were imaged and the rate of overall mitochondrial depolarisation was assessed by measuring the slope of the TMRE signal change with time. A solution of 100 μM ryanodine was added to the dish and the imaging procedure repeated.

The rate of global depolarisation upon illumination (Figure 5.13), was significantly reduced ($P = 0.0025$, two-tailed t test). The slope in the control group was 0.049 ± 0.012, (mean ± SD, $n = 9$), the slope in ryanodine group 0.023 ± 0.019 ($n = 10$). However, the responses were very heterogeneous and the lower panel in figure 6.7 illustrates the variety of response seen in these cells – two adjacent cells were imaged, in one the mitochondria depolarised rapidly and completely within a minute, while in the second, there was minimal depolarisation until the FCCP was applied. Thus, bath application of 100 μM ryanodine significantly lengthened the time taken to global depolarisation when the cells were loaded with TMRE and illuminated. These data suggest that in some cells ryanodine-sensitive Ca^{2+} stores were involved in the mitochondrial depolarisation.

Evidence for focal calcium release.

A possible origin of the mitochondrial depolarisations seen in the illuminated astrocytes is focal calcium release from intracellular stores. It is established that mobilisation of intracellular Ca^{2+} stores transiently depolarises mitochondria in many cell types. Application of ATP 100 μM to TMRE-loaded astrocytes reliably caused a dequench of the TMRE fluorescence (Figure 5.14), signalling that electrogenic uptake of Ca^{2+} in these cells caused a dissipation of $\Delta\psi_m$. Consequently, mitochondrial Ca^{2+} uptake after highly localised Ca^{2+} release might be responsible for the TMRE-signalled flickering. Confocal imaging of cells co-loaded with TMRE and the calcium indicator, fluo-3 was therefore performed in an attempt to identify focal calcium events and to investigate whether these could be associated, temporally and spatially, with mitochondrial

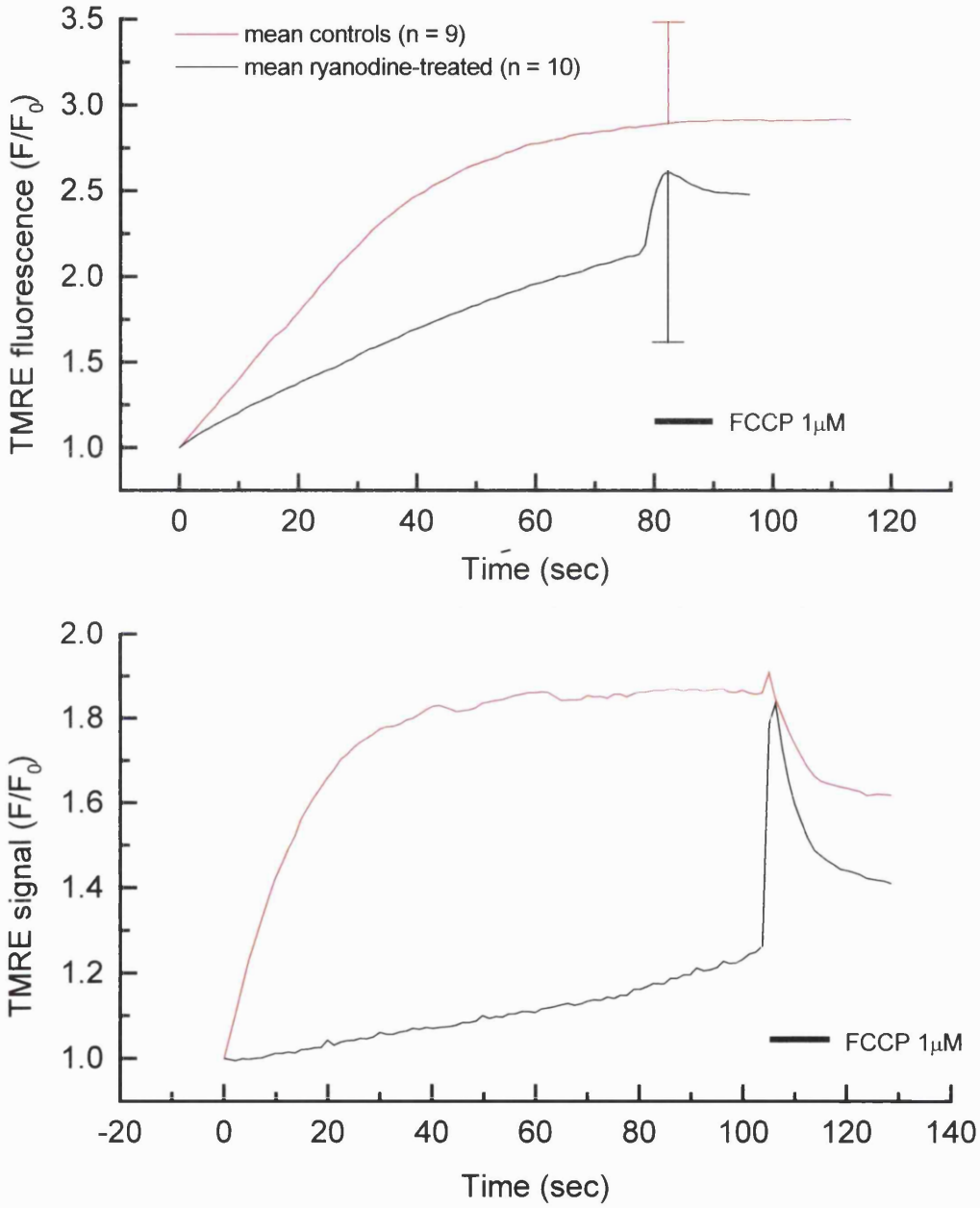

Figure 5.13: the effect of bath-application of ryanodine 100 μM on the rate of TMRE dequench in illuminated astrocytes. The slope of the TMRE dequench was significantly (P = 0.0025) less in the ryanodine-treated cells, reflecting the slower depolarisation in this group. The lower panel shows the fluorescence changes recorded over two adjacent cells, illustrating the inconsistency of response to ryanodine in these cells.

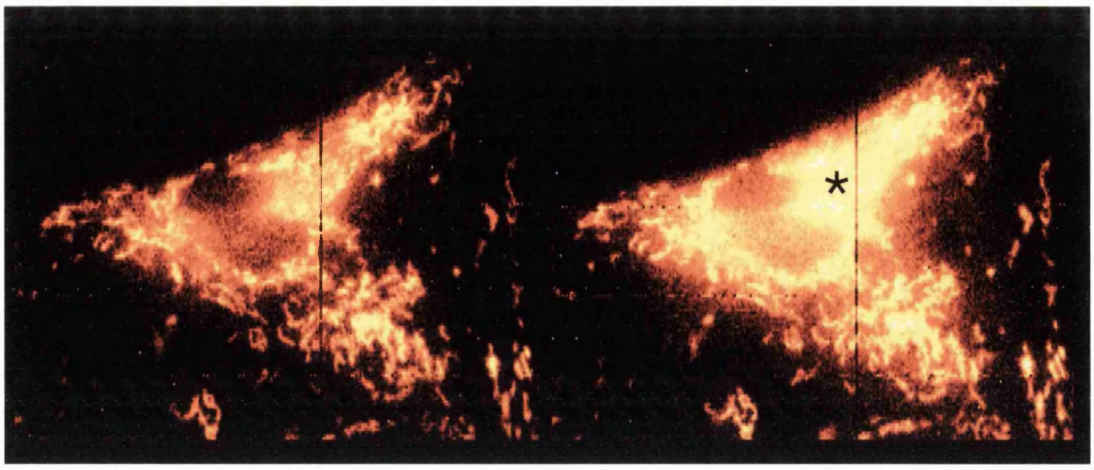

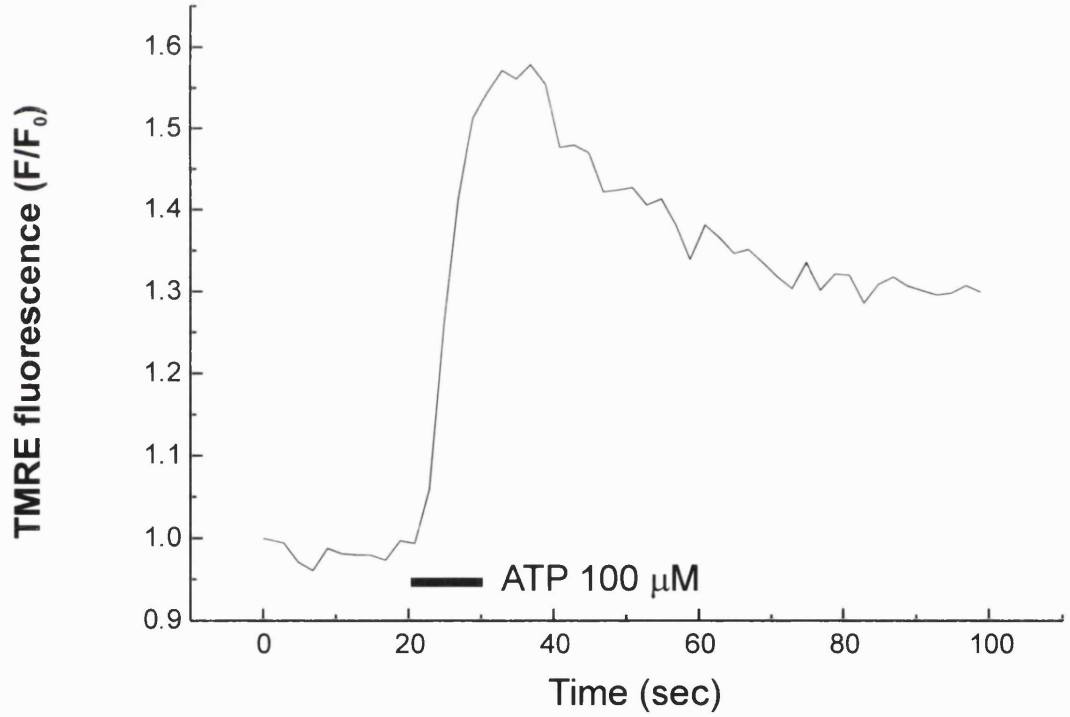

Figure 5.14: physiological mobilisation of intracellular Ca^{2+} depolarises mitochondria. The images show a TMRE-loaded astrocyte and the application of ATP induces a dequench of the fluorescence, signalling loss of $\Delta\psi_m$. The plot is of the fluorescence change over a single mitochondrion (asterisk *).

depolarisations. The use of the confocal microscope allows truly simultaneous imaging of the two dyes, and thus correlation of calcium and mitochondrial events could be studied.

Many local Ca^{2+} transients were seen, of varying duration, and although these could not always be associated with TMRE flickers, some were quite clearly occurring at the same time in the same region of the cell as the TMRE transients. Ca^{2+} transients over mitochondria were measured concurrently with a second region of interest 1 μm away to establish whether any rise in $[Ca^{2+}]_m$ was restricted to the organelle or the cytosolic volume around it.

1. Short calcium transients restricted to mitochondria

The four traces shown in Figures 5.15a and 5.15b are examples of calcium transients that were restricted to mitochondria and which have associated mitochondrial depolarisations. In 5.15A the small fluo-3 spike at 47 seconds (denoted number 1) was isolated to the mitochondrion, there was no accompanying rise in the peri-mitochondrial fluo-3 signal. The TMRE signal rise was coincident with the fluo-3 transient.

In Figure 5.15B there was a small calcium transient at 11 seconds (1) that is coincident with a 14% rise in the TMRE signal. The two larger calcium transients at 51 and 58 seconds (2 and 3) appeared to induce a depolarisation that initially recovers and then one that does not; in both cases there was no change in the peri-mitochondrial fluo-3 signal.

The volley of focal calcium transients in Figure 5.15C were accompanied by small rises in peri-mitochondrial calcium, but the difference in fluo-3 signal over a distance of 1 μm, or less, serves to emphasise how localised such calcium changes can be. Most of these transients were associated with mitochondrial depolarisations, however that at 30 seconds (1) was not. In addition, no calcium change was detected at 49 seconds (2) when there was a 90% transient rise in TMRE signal (160 to 304 arbitrary units).

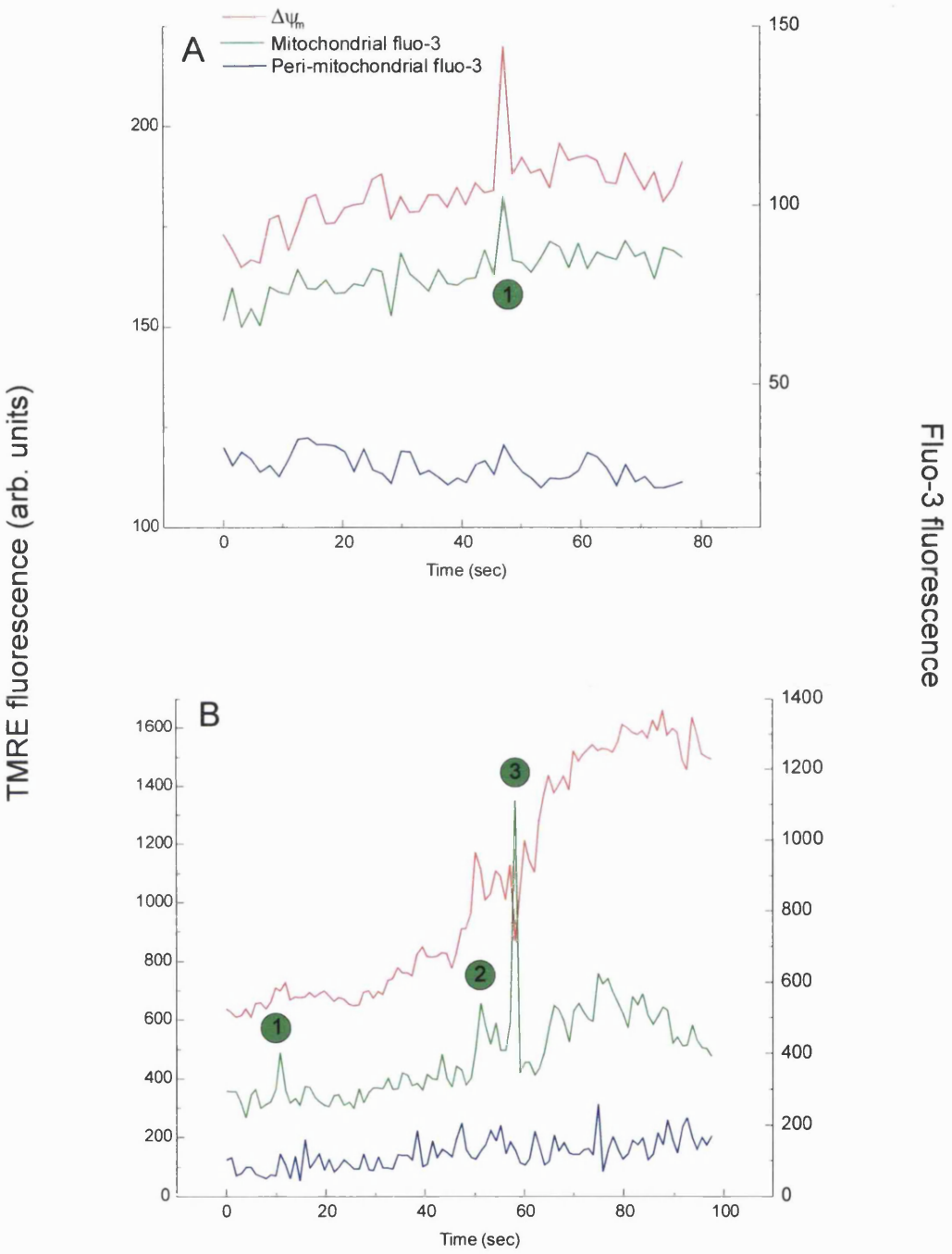

Figure 5.15 a,b: confocal imaging of cells co-loaded with TMRE and fluo-3 revealed some mitochondria depolarisations that were coincident in time and space with calcium transients. That these transients were highly localised to individual mitochondria was shown by analysis of nearby (< 1 μm away) cytosol. As can be seen, the calcium transients over individual organelles (green traces) could be very much larger than any concomitant signal change nearby (blue traces).

Images and traces drawn from neonatal rat cardiomyocytes coloaded with TMRE and fluo-3.

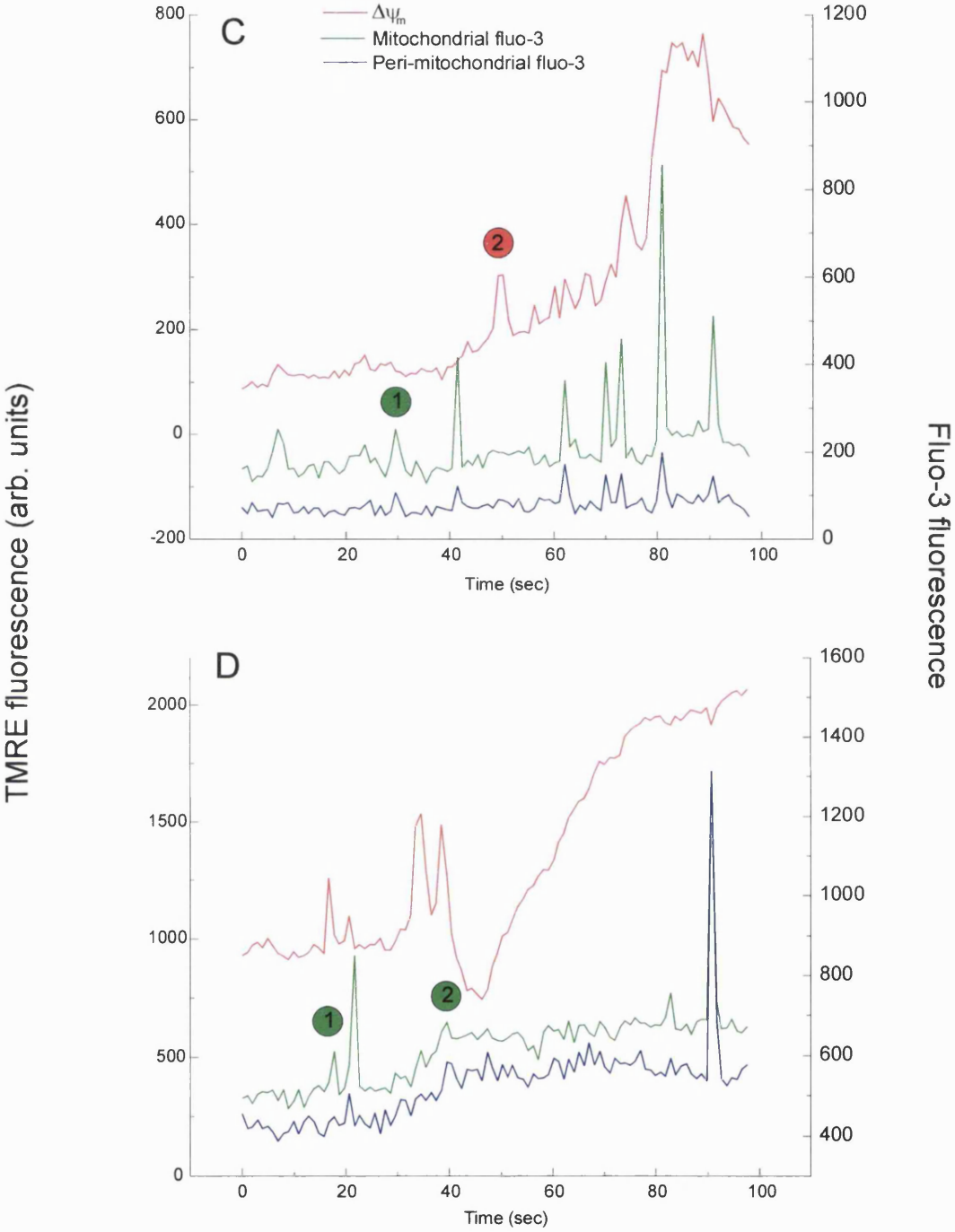

Figure 5.15 c,d: confocal imaging of cells co-loaded with TMRE and fluo-3 revealed some mitochondrial depolarisations that were coincident in time and space with calcium transients. That these transients were highly localised to individual mitochondria was shown by analysis of nearby (< 1 μm away) cytosol. As can be seen, the calcium transients over individual organelles (green traces) could be very much larger than any concomitant signal change nearby (blue traces).

Images and traces drawn from neonatal rat cardiomyocytes coloaded with TMRE and fluo-3.

The two initial calcium transients in 5.15D (at 18 and 21 seconds (1)) are accompanied by mitochondrial depolarisations, but the slower, more sustained rise in mitochondrial and peri-mitochondrial calcium at 33 seconds (2) provoked larger depolarisations that recovered at first and then recurred. The transient calcium changes appear only over the mitochondrion, while the more prolonged increase in fluo-3 signal is associated with a rise in the signal over nearby cytosol.

Images taken from neonatal rat cardiomyocytes are illustrated in Figure 5.16. Note the rise in fluo-3 signal over the depolarising mitochondrion, a calcium transient coincident with the depolarisation but which is not reflected in the signal measured over the cytosol less than 1 μm distant.

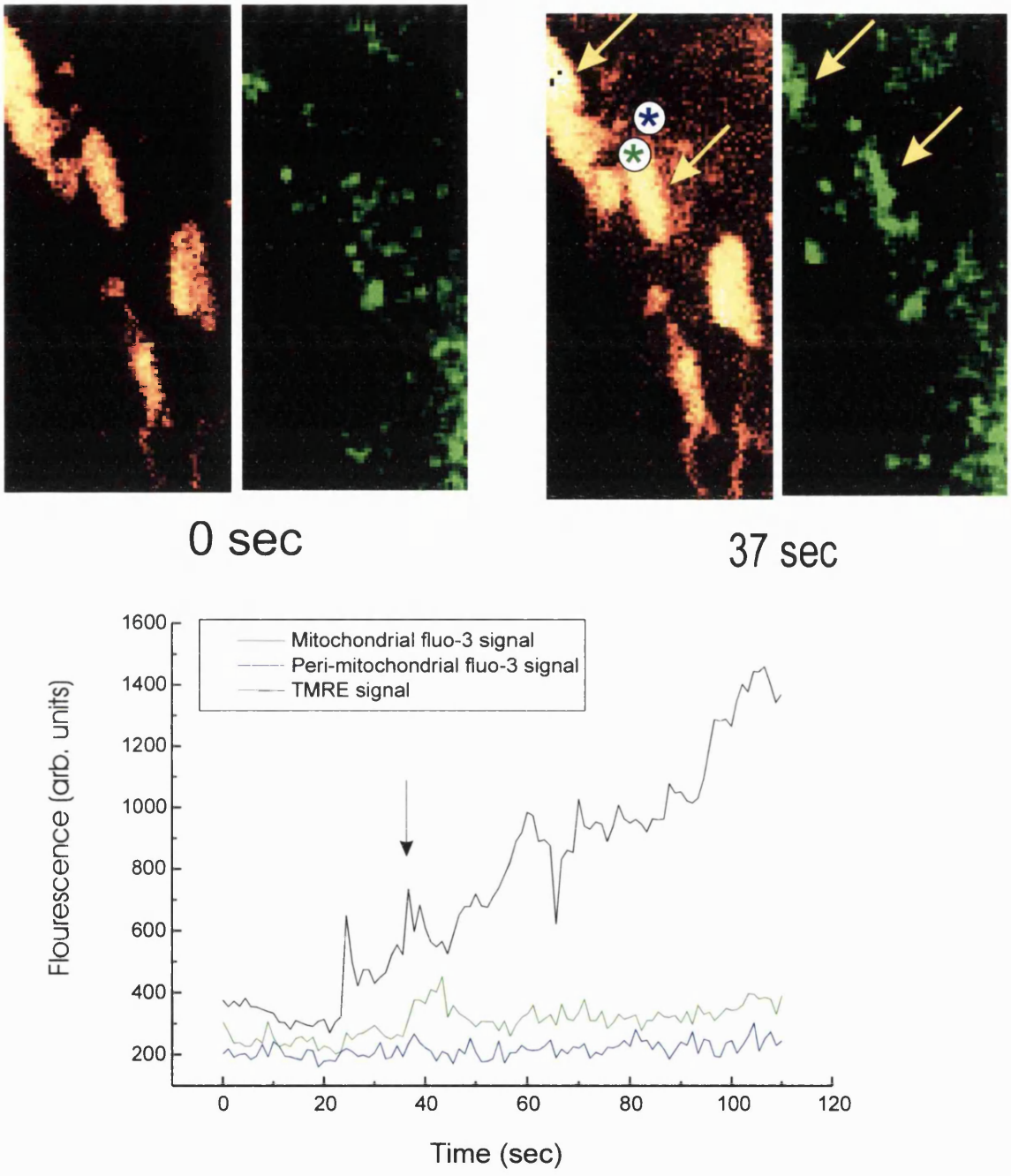

Figure 5.16: confocal images of mitochondrial depolarisations (yellow arrows) accompanied by highly localised changes in calcium (also arrowed). The fluo-3 signal, measured simultaneously, was assessed over the mitochondrion (arrowed and marked with a green asterisk) and an area of cytosol less than 1 μm away (blue asterisk). The fluorescence signals, measured at the points asterisked, are represented in the plot. The black arrows marks 37 seconds, the time at which the second pair of images were extracted.

Images and traces drawn from neonatal rat cardiomyocytes coloaded with TMRE and fluo-3.

2. Prolonged calcium changes restricted to mitochondria

While the calcium transients recorded over the mitochondria could be very brief, the peak signal appearing in only one frame of the confocal image, many were more prolonged, lasting for several seconds. In Figure 5.17A, the large transients in fluo-3 signal at 19 and 41 seconds (1 and 2) were not restricted to the mitochondrion but the more sustained increase, beginning at 92 seconds (3), was. There was a TMRE-signalled depolarisation associated with this later calcium rise.

The prolonged rise in mitochondrial calcium in Figure 5.17B (again isolated from any change in the fluo-3 signal measured 1 μm distant) was accompanied by a 42% drop in TMRE signal. The fact that there was a later depolarisation (1) of this mitochondrion suggests that this drop in signal was not dye diffusing away from a depolarised organelle, rather an enhanced quench of fluorescence. Hence the rise in calcium may have hyperpolarised this mitochondrion. There was no evidence of a rise in cytosolic calcium measured over the peri-mitochondrial area.

The brief calcium flashes in the first 30 seconds of Figure 5.17C were associated with small mitochondrial depolarisations, however, the more sustained rise in mitochondrial calcium at 33 seconds (1) was accompanied by a much larger change in TMRE signal. The peri-mitochondrial fluo-3 signal (1 μm away) rises in concert with that over the mitochondrion, but quickly recovered.

3. Mitochondrial depolarisations not associated with measurable calcium transients

TMRE flickers, and longer depolarisations, were frequently seen that could not be associated with any local change in fluo-3 signal. Figure 5.18A illustrates two large mitochondrial depolarisations (at 4 and 19 seconds (1 and 2)) that were not associated with any change in fluo-3 fluorescence, although the depolarisation at 47 seconds (3) was coincident with a volley of global calcium spikes. Likewise, there was no change in fluo-3 signal associated with the depolarisation at 19 seconds in Figure 5.18B.

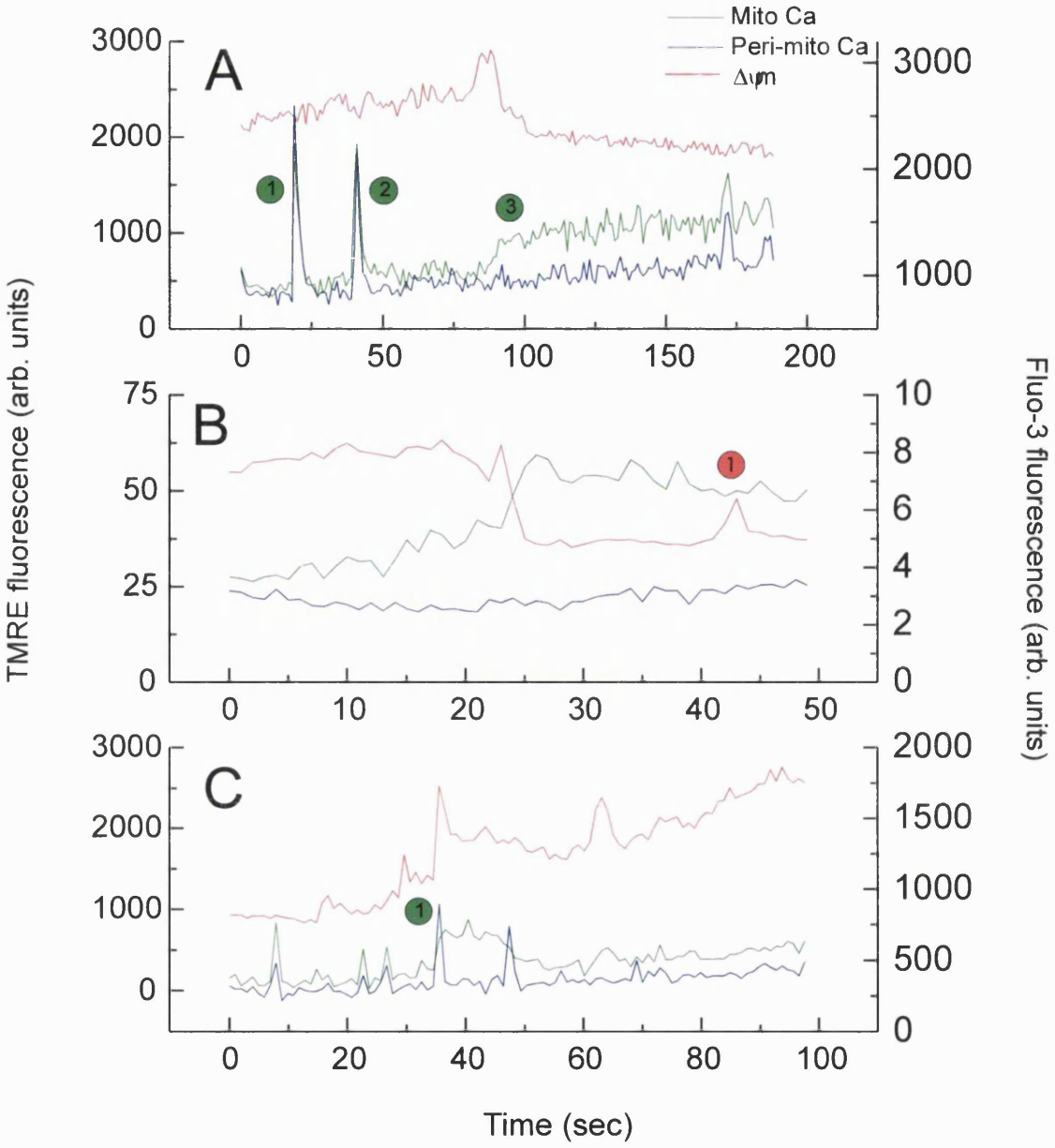

Figure 5.17: plots derived from confocal imaging of cells co-loaded with TMRE and fluo-3. Some of the TMRE-signalled mitochondrial depolarisations were accompanied by highly localised rises in [Ca^{2+}] which could be be prolonged even after the mitochondrion had depolarised. Note that the fluo-3 signal measured over nearby cytosol (blue trace) did not always change in concert with that over the mitochondrion (green trace), further evidence for spatially-restricted [Ca^{2+}] transients.

Images and traces drawn from neonatal rat cardiomyocytes coloaded with TMRE and fluo-3.

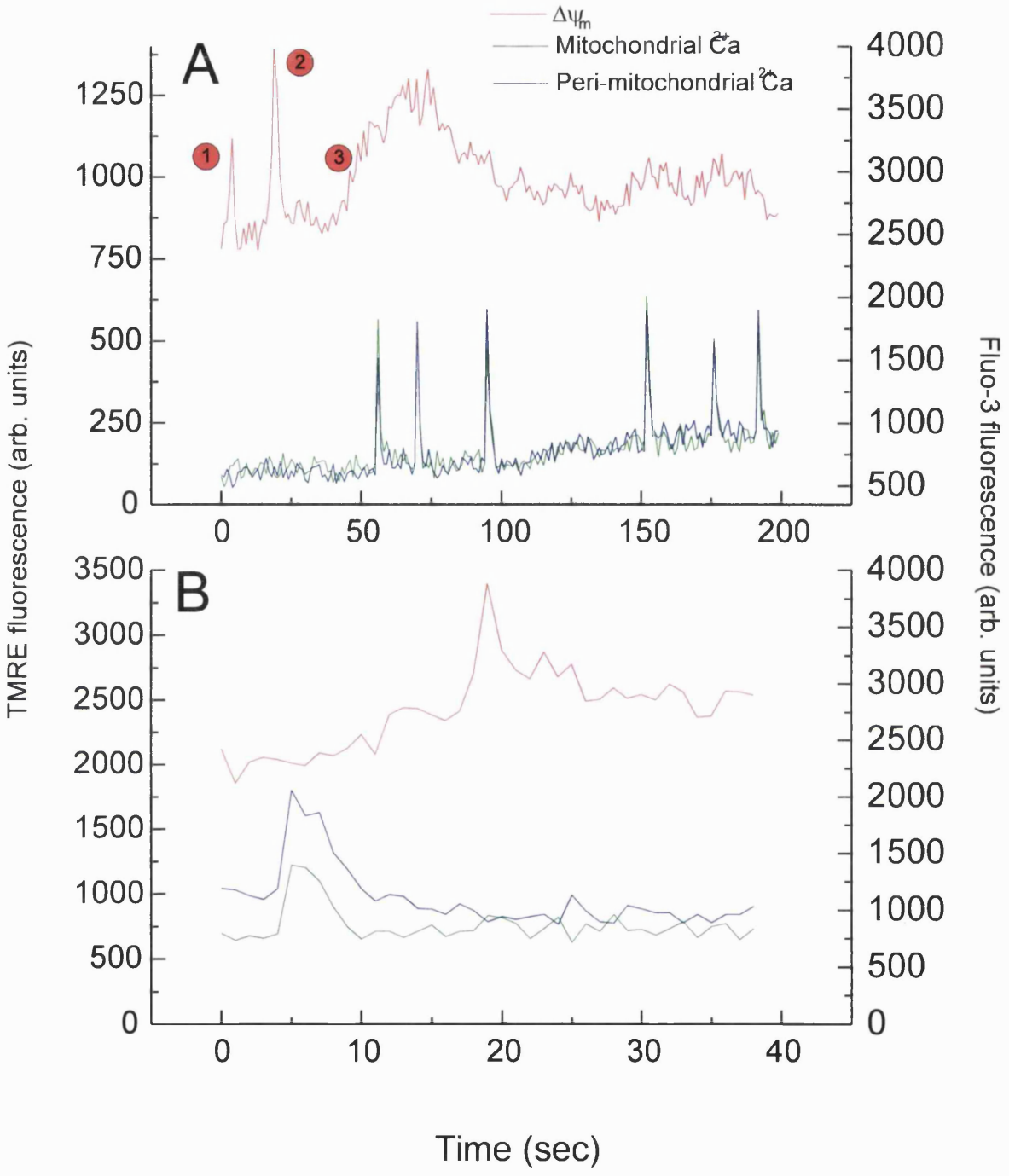

Figure 5.18: confocal imaging of cells co-loaded with TMRE and fluo-3 revealed many mitochondrial depolarisations that could not be associated with local changes in fluo-3 signal

Traces drawn from neonatal cardiomyocytes coloaded with TMRE and fluo-3.

4. Calcium transients that did not initiate mitochondrial depolarisations.

Many transient changes in fluo-3 signal were not associated with a TMRE dequench. Illumination of fluo-3-loaded cells revealed multiple events occurring in many cells. These calcium changes could be global (associated with a twitch in the neonatal cardiomyocytes) or spatially restricted, the change in fluorescence being limited to a few μm^2. Calcium transients over single mitochondria were frequently identified (see those at 30 seconds in Figure 5.15C, 22 seconds in Figure 5.15A) which did not induce a change in the TMRE signal.

Hence, confocal imaging of cells loaded both with TMRE and fluo-3 revealed a variety of calcium signals and a variety of mitochondrial responses to those signals. It is evident that changes in calcium can be restricted to tiny volumes of the cell and frequent transients occurred over individual mitochondria that were isolated to those organelles – there was no accompanying change in fluo-3 signal from the peri-mitochondrial area, less than 1 μm away. Given the evident Ca^{2+}-dependence of the TMRE-signalled flickers, these data suggest a privileged pathway for mitochondrial calcium uptake, in some cases, where calcium released from internal stores is quickly taken up by mitochondria with little, or no, change in the nearby $[Ca^{2+}]_{cyt}$. These data provide an explanation for the fact that treatment with BAPTA-AM alone did not attenuate the frequency of flickering in the mitochondria, and that a more complete inhibition of flicker required combined treatment with BAPTA and thapsigargin.

The rise in mitochondrial calcium could be associated with a mitochondrial depolarisation, as signalled by the dequench of TMRE. Less spatially-restricted calcium transients also occurred and these could also initiate a mitochondrial depolarisation. However, many depolarisations were identified that could not be associated with changes in fluo-3 signal and calcium transients were not invariably associated with mitochondrial depolarisations.

Conclusions

- Calcium ions are necessary for the TMRE-signalled mitochondrial depolarisations and these derive from intracellular calcium stores.

- Chelation of cytosolic calcium with BAPTA failed to halt the transient depolarisations but significantly slowed the global mitochondrial depolarisation, suggesting that a raised cytosolic calcium increases the rate of the flickers but that mitochondria may flicker constitutively in the absence of a raised cytosolic [Ca^{2+}].

- Emptying and chelation of intracellular calcium stores with thapsigargin and BAPTA, however, significantly reduced both the transient flickering and the progression to global depolarisation, confirming a role for stored calcium in the depolarisations.

- That the calcium release could be very localised, possibly by-passing the cytosol, was suggested by confocal imaging of cells co-loaded with TMRE and fluo-3. Calcium transients were not always associated with mitochondrial depolarisations, however when they were they could be restricted to single organelles.

Chapter 6: reactive oxygen species are necessary for the mitochondrial depolarisations

(i) Introduction

Generation of reactive oxygen species by illumination of fluorophores

Excitation of a fluorophore is induced by absorption of energy from incident photons. Electrons are raised from the ground state to a higher energy orbit and as a result of their subsequent return to a ground state, energy is released as quanta of light. This is fluorescence.

Increased excitation intensity, however, does not always correlate linearly with increased fluorescence, as light may also induce molecular changes other than an excited, fluorescent state. Photodegradation of a fluorophore, photobleaching, is an example. Increasing intensities of excitation light can decrease fluorescence emission from some molecules, attenuating the total signal measured. The precise mechanisms behind photobleaching of fluorophores are unclear, but some studies show that photobleaching is decreased if oxygen is removed (Song, Hennink, Young & Tanke, 1995) suggesting that a reaction between molecular oxygen and the excited state of the dye may be involved. The fluorophore may combine with molecular oxygen forming a non-fluorescent product or energy transference from the excited fluorophore to ground state oxygen can generate the highly reactive singlet oxygen (Bunting, 1992). Singlet oxygen, in turn, can react with the fluorophore rendering it non-fluorescent, and treatment with antioxidants has been shown to diminish light-induced photobleaching. Indeed, commercially available 'antifade' solutions, designed to prolong fluorescence lifetime, consist of a mixture of antioxidants. Additionally, singlet oxygen may react with other molecules within the cell.

Oxidative stress

Highly reactive intermediaries of the reduction of oxygen to water, such as singlet oxygen, superoxide, hydrogen peroxide and the hydroxyl radical, are referred to collectively as

reactive oxygen species (ROS). As aerobic respiration entails the production of ROS, even under basal conditions, cells are continually exposed to varying amounts of ROS. These highly reactive molecules have been implicated in a variety of cell dysfunctions ranging from peroxidation of lipid membranes, to oxidative DNA damage and activation of apoptotic cell death pathways. Unsurprisingly, plant and animal cells have evolved a range of enzymatic and other defences that act as antioxidants, metabolising the pro-oxidant ROS and providing protection against oxidative damage. However, the steady state of pro-oxidants and antioxidants may be disrupted and an imbalance in favour of oxidation has been called 'oxidative stress' (Sies, 1985).

Oxidative stress and calcium homeostasis

Oxidative stress may affect the activity of ion channels, pumps, exchangers and co-transporters. There is evidence of both reductive and oxidative modulation of sulphydryl groups on the protein molecules that comprise these channels, resulting in disruption to intracellular [Na^+] (Bhatnagar, Srivastava & Szabo, 1990), [K^+] (Duprat *et al.*, 1995) and pH (Brisseau *et al.*, 1994). Reactive oxygen species have been especially implicated in modulating calcium homeostasis, proposed mechanisms including inactivation of L-type calcium channels (Cerbai *et al.*, 1991), increasing the open probability of ryanodine-sensitive SR calcium release channels (Boraso & Williams, 1994), and inhibition of the sarcolemmal Ca-ATPase (Kukreja, Kearns, Zweier, Kuppusamy & Hess, 1991). Mitochondria, as producers of reactive oxygen species (Chance *et al.*, 1979), have been implicated in the wider pathology of oxidative injury, particularly after reperfusion of hypoxic tissue (Halestrap *et al.*, 1998).

As ROS may induce Ca^{2+} release from intracellular stores, and Chapter 5 established that stored Ca^{2+} was necessary for the mitochondrial flickers, an interplay between ROS and intracellular Ca^{2+} stores seems possible. Indeed, previous experiments using the $[Ca^{2+}]_{mit}$ indicator, rhod-2, had revealed that the rhod-2 signal could increase steadily as unstimulated cells were being imaged (Duchen, Boitier, Jacobson, unpublished observations), suggestive of mitochondrial Ca^{2+} loading induced by fluorophore illumination. To investigate whether this effect was mediated by ROS production, the effects of antioxidants on rhod-2 fluorescence

were investigated. Additionally, as illuminated TMRE may produce ROS (Bunting, 1992; Hüser *et al.*, 1998), the potential involvement of ROS in mitochondrial flickering was investigated.

Experimental methods

Imaging of rhod-2–loaded cells

To investigate whether illumination alone of a fluorophore could cause mitochondrial Ca^{2+}-loading, astrocytes were loaded with rhod-2 AM (by 30 minute exposure to a saline solution containing 5 μM rhod-2 AM) and illuminated. Imaging was carried out on both the Digital Pixel or Hamamatsu imaging systems. Cells were illuminated with either 560 nm (Digital Pixel system) or 546 nm light (Hamamatsu system) and images collected at wavelengths longer than 590 nm through a 63x objective. Images were analysed to establish whether illumination alone caused an increase in the rhod-2 signal. To establish whether any change in signal was due to ROS production by the illuminated dye the experiment was repeated in the presence of free radical scavengers (below).

The effect of free radical scavengers on mitochondrial flickering

The effects of an array of free radical scavengers on mitochondrial flickering was investigated. Dishes of TMRE-loaded astrocytes were mounted on the stage of the Hamamatsu imaging system and fluorescence was excited using a 546 nm bandpass filter. The excitation light intensity was attenuated using a 1% neutral density filter to establish conditions where the mitochondria flickered but the global increase in TMRE signal was minimal. A 40x oil immersion lens was used and images were collected at wavelengths longer than 590 nm. Once control images had been collected, an array of antioxidants were added to the dish and left to equilibrate for 15 minutes. This array comprised ascorbate 1 mM, catalase 250 units ml^{-1}, TEMPO 500 μM, and Trolox 1 mM (see below). The image acquisition was repeated in the presence of the antioxidants. Three separate dishes of cells were examined. Images were analysed as described in section 4.2, and the index of variation was obtained for each cell in each of the groups (controls and those in the presence of antioxidants).

A second set of experiments compared the time to full dequench of the dye as measured over whole cells. TMRE-loaded cells were imaged using the Digital Pixel system. The cells were exposed to 530 nm light at an intensity that induced a global mitochondrial depolarisation in the controls. Using a 30% neutral density filter, the TMRE fully dequenched in around 60 seconds. FCCP 1μM was applied by puffer pipette towards the end of each imaging sequence to check for residual $\Delta\Psi_m$ in the illuminated cells. A 63x oil immersion objective was used. These experiments were then repeated in the presence of the antioxidant array detailed above. For each of the cells imaged, the rate of TMRE dequench was assessed by fitting a line to the linear part of the slope of the light-induced rise in signal. In addition, the change in TMRE signal from t_0 to full amplitude was measured and expressed as a percentage. The slopes of the signal change and the percentage change in signal were then compared.

The antioxidants

Ascorbate (vitamin C) is synthesised from glucose by most plants and animals. Humans and other primates, however, do not have one of the enzymes necessary to synthesise ascorbic acid and so rely on dietary intake of vitamin C. Ascorbic acid is required as a cofactor for several enzymatic processes including the biosynthesis of collagen and the conversion of dopamine to noradrenaline. The ascorbate molecule readily acts as an electron donor, and is a major *in vivo* antioxidant, present in millimolar concentrations in lung cells and the lens of the eye. It reacts readily with O_2^-,$OH^\cdot$, and singlet oxygen. Ascorbate in solution is cell membrane-permeant.

The catalases protect against damage by $OH^\cdot$ radicals. This class of enzymes, present in varying quantities in all animal organs, catalyses the reaction:

$$2H_2O_2 \rightarrow 2H_2O + O_2$$

As hydrogen peroxide (H_2O_2) readily dissociates to produce $OH^{\cdot}$ radicals, catalase provides important protection from one of the most reactive chemical species known. Catalase is a protein molecule and is unlikely to be membrane-permeant but may act to remove extra-cellular H_2O_2 (Peus *et al.*, 1998) which is thought to accumulate in some models of oxidative stress (McLeod & Sevanian, 1997).

Trolox is a water-soluble analogue of α-tocopherol (vitamin E). α-Tocopherol, being hydrophobic, tends to concentrate in membranes and it is known to be present in high concentrations in mitochondrial membranes. It reacts with $OH^{\cdot}$ and superoxide, but its major action is donation of a hydrogen ion to lipid peroxy and alkoxy radicals, terminating the chain reaction of lipid peroxidation. This reaction produces tocopherol radicals which in turn react with ascorbate. The hydrophobic side chain present in α-tocopherol is replaced with a hydrophilic -COOH group to form Trolox.

TEMPO (2,2,6,6-tetramethyl-1-piperidine-N-oxyl) is a membrane-permeant synthetic spin trap which dismutates superoxide (Krishna, Grahame, Samuni, Mitchell & Russo, 1992). Spin traps react with free radicals to form longer-lived, more stable radicals which are less reactive than their targets. The conversion is energetically favoured and is essentially irreversible.

Results

(i) The effects of free radical scavengers on mitochondrial Ca^{2+} and $\Delta\Psi_m$

1. Illumination alone induced a rise in rhod-2 signal

Illumination of rhod-2 loaded cells for 160 seconds using a 30% neutral density filter induced a rise in rhod-2 signal over mitochondria of 136 ± 123% (mean ± SD, n = 41 cells). Figure 6.1 illustrates that the pattern of rhod-2 fluorescence changed during the period of illumination. The initially weak, diffuse cytosolic signal became gradually brighter and more punctate as the illumination continued, suggesting that illumination of the dye initiated calcium uptake by mitochondria. Analysis of the fluorescence over the mitochondria revealed a range of responses to the illumination. Some mitochondria demonstrated a rise in fluorescence that

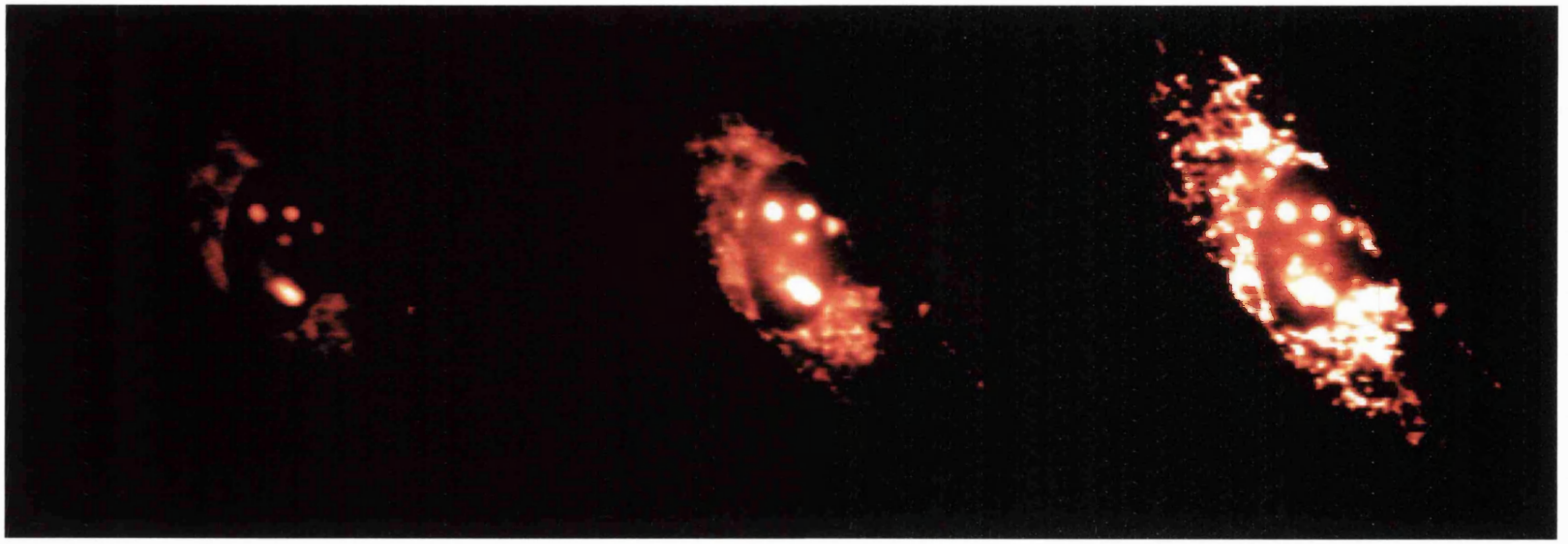

Figure 6.1: the illumination of rhod-2-loaded astrocytes revealed a gradual increase in fluorescence over punctate organelles. Rhod-2, a calcium indicator, loads into mitochondria and these data are consistent with mitochondrial calcium uptake on illumination of some fluorophores. Illumination was at 546 nm and a 30% neutral density filter was used to attenuate the excitation light intensity.

plateaued and remained high, while over others the signal gradually declined after an initial peak. In most cases these responses appeared to be reflecting the change in [Ca^{2+}] in the cell as a whole, as measurement of the rhod-2 signal over the mitochondrion-free nucleus revealed a similar pattern of signal change. In a few cases, however, the rhod-2 signal over mitochondria declined slowly after reaching a peak while that over the nucleus remained at a plateau. Some mitochondria flickered in a way that was reminiscent of the signal changes seen with illuminated TMRE-loaded cells (Figure 6.2).

2. Free radical scavengers slowed the increase in rhod-2 signal

Treatment of rhod-2 loaded cells with the antioxidant array significantly slowed the rate of increase in rhod-2 signal, two-tailed P value< 0.0001, Mann-Whitney U test (Figure 6.3). These results confirm that the mitochondrial Ca^{2+}-loading seen on illumination of rhod-2 loaded astrocytes is mediated by ROS. ROS produced by the illuminated fluorophore resulted in mitochondrial Ca^{2+} loading.

3. Antioxidants attenuated mitochondrial flicker in TMRE-loaded cells

Thus illumination of a fluorophore can result in mitochondrial Ca^{2+}-loading and this process may be prevented by treating the cells with an array of antioxidants. To investigate whether ROS were involved in the mitochondrial flicker, where stored Ca^{2+} is required, TMRE-loaded cells were treated with antioxidants and illuminated and compared with controls.

In the astrocytes that had been exposed to minimal excitation light, the control group showed mitochondrial flickering much as described in Chapter 4. There were many events over mitochondria, often several times over a single organelle. The events were brief and transient and by limiting the excitation light to 1% transmission, the great majority of the cells did not show an overall rise in TMRE signal during the illumination period of 25 seconds.

Indices of variation for each of the control cells were calculated as described in section 4.2. For the control group, consisting of 32 individual cells, the index of variation was 1.19 ± 0.07 (mean ± SD). In the cells that had been treated with the antioxidants there was a marked

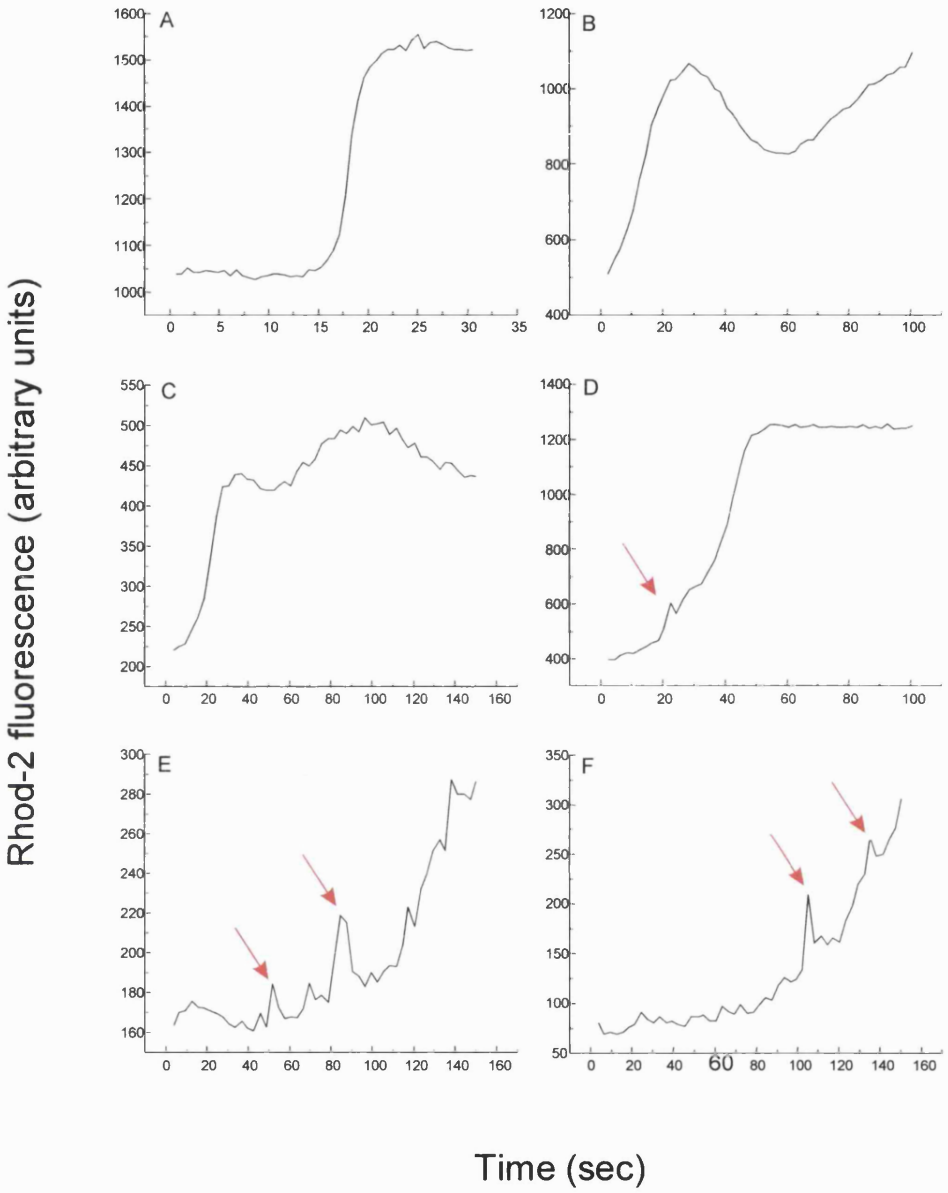

Figure 6.2: illumination of rhod-2 loaded cells revealed a rise in rhod-2 fluorescence over time, indicating mitochondrial calcium accumulation. The pattern of signal change varied widely, usually reflecting the [Ca^{2+}] in the cell as a whole. Each trace above represents the signal recorded over a single mitochondrion. In the majority of cases the rhod-2 signal plateaued after a rapid rise (e.g. Panel D), although in some cases there was an initial delay followed by an abrupt rise (Panel A). Some mitochondria showed a biphasic calcium uptake, reflecting the calcium change in the whole cell, while in others (Panel C) the signal declined after an initial peak, despite a plateau in the nuclear signal. Occasional flashes of fluorescence were seen that were reminiscent of the TMRE-signalled flickers (arrowed in Panels D,E and F).

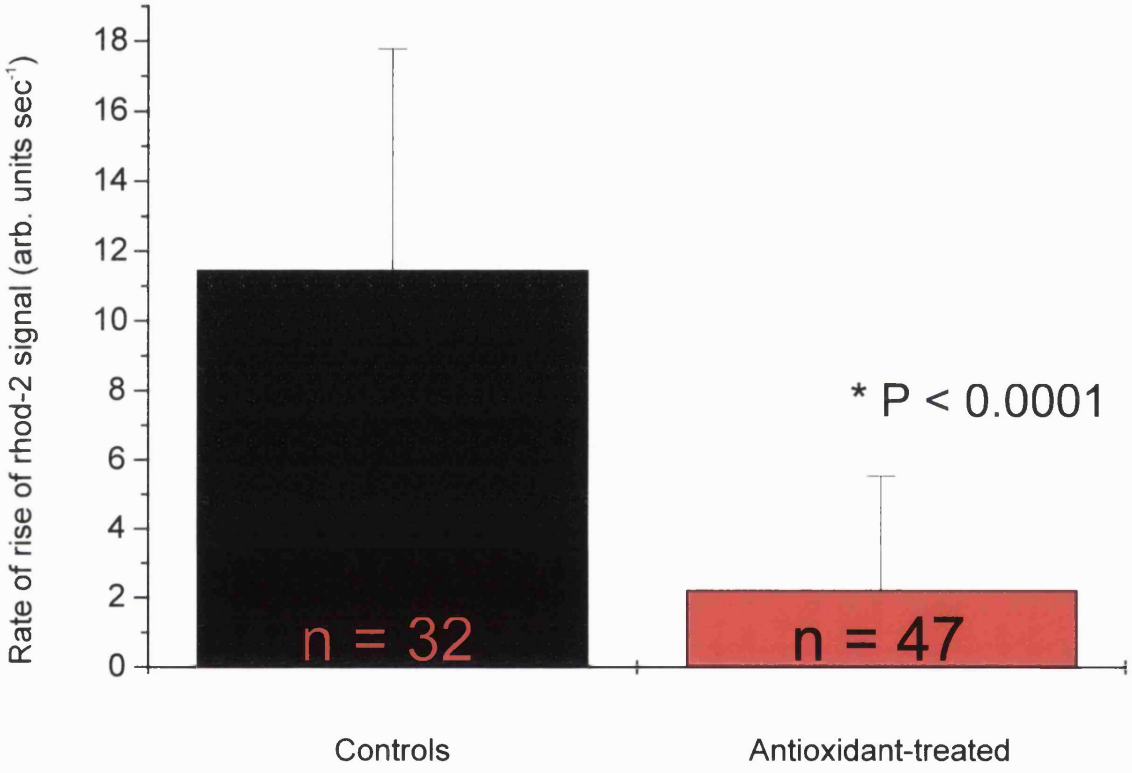

Figure 6.3: free radical scavengers slowed the light-induced rise in rhod-2 fluorescence

reduction in light-induced flickering. The index of variation for the antioxidant-treated cells was 1.11 ± 0.04 (mean ± SD, n = 54). The difference between the medians of the control and antioxidant-treated groups was significant (P value < 0.0001, two-tailed Mann-Whitney test). Additionally, the appearance of flickering was less in the antioxidant-treated cells, as judged subjectively from the images; there were occasional transient events over mitochondria, but these were seen less often than in the controls and some cells appeared completely quiescent. These results are summarised in Figure 6.4 and illustrated by line and surface plots in Figure 6.5.

4. Antioxidants slowed the progression to global mitochondrial depolarisation

Illumination of TMRE-loaded astrocytes using a 30% neutral density filter caused a rapid dequench of TMRE fluorescence in all of the cells imaged. As can be seen from Figure 6.6, most cells had reached maximum fluorescence in 60 seconds and the addition of FCCP by puffer pipette did not increase the signal further, indicating complete dissipation of $\Delta\Psi_m$. However, in the antioxidant-treated group the rate at which the fluorescence increased over the cells in response to the illumination was significantly slower, P < 0.0001, two-tailed Mann Whitney test, (Table 6.1). At 60 seconds, the time at which the controls had maximally depolarised with a rise in signal from baseline of 295%, the fluorescence over the cells which had been treated with antioxidants had only risen by 28%. Indeed, by 125 seconds, when the FCCP was applied, there was only a rise of 84% from baseline in this group. Dissipation of $\Delta\Psi_m$ by FCCP more than doubled this signal.

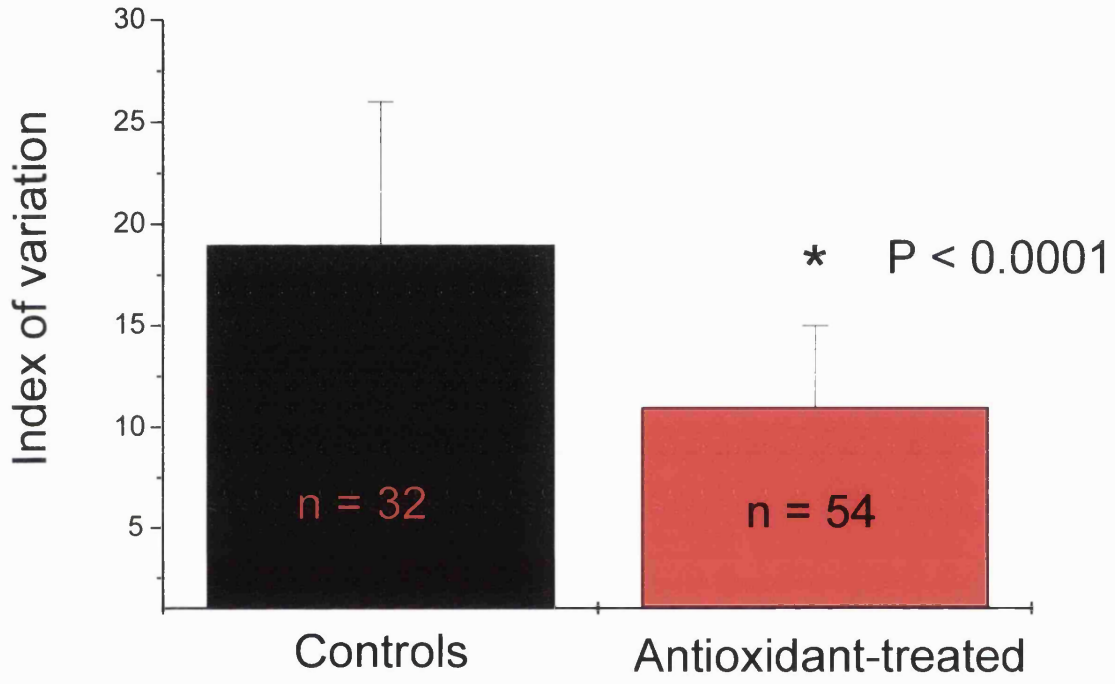

Figure 6.4: antioxidants significantly reduced the index of variation.

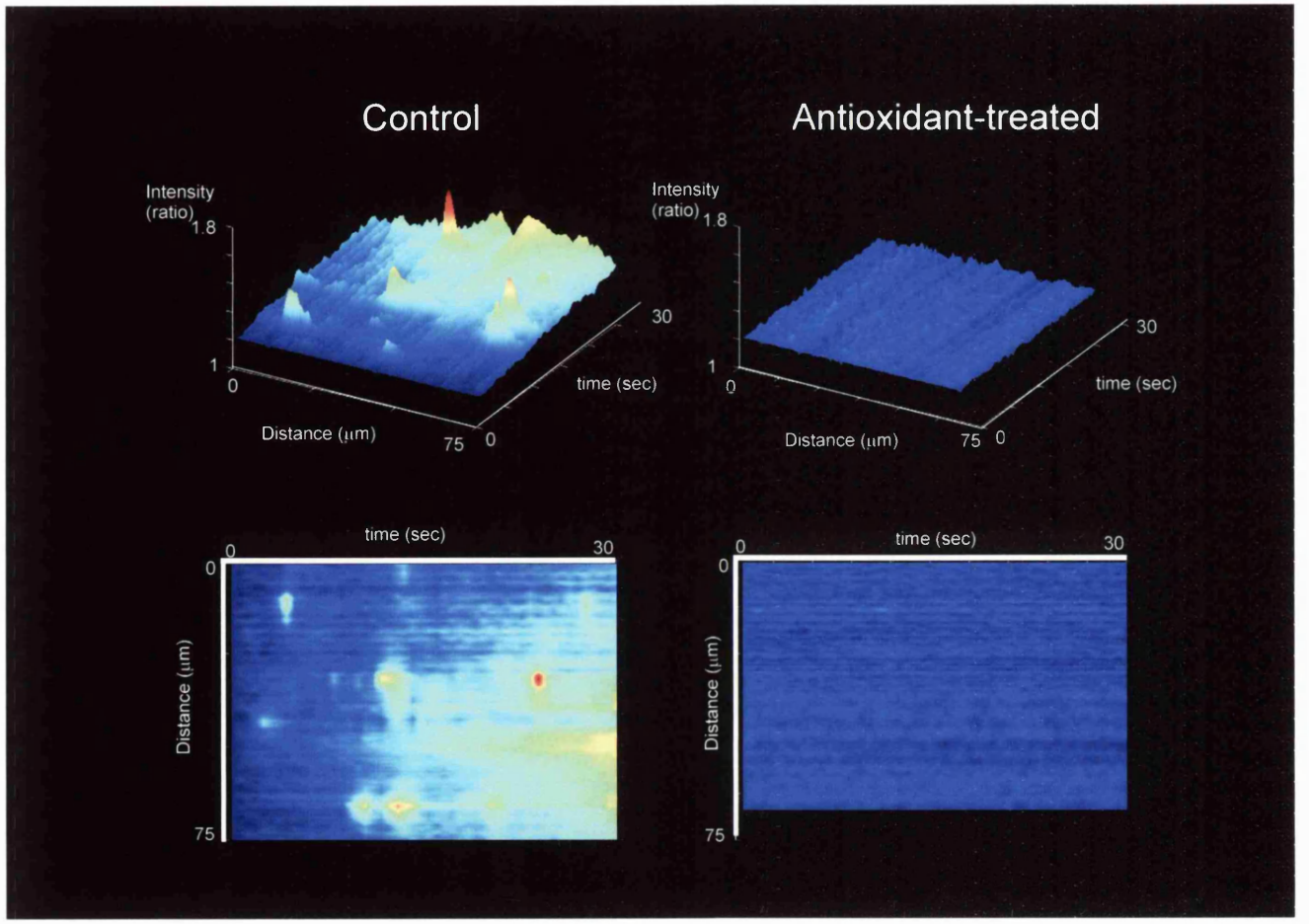

Figure 6.5: treatment with the array of antioxidants greatly attenuated mitochondrial flickering in TMRE-loaded astrocytes. The line and surface plots are taken from single cells before (left), and after (right) cells were treated with the antioxidant solution. The plots illustrate how restricted in time and space the mitochondrial flickers were.

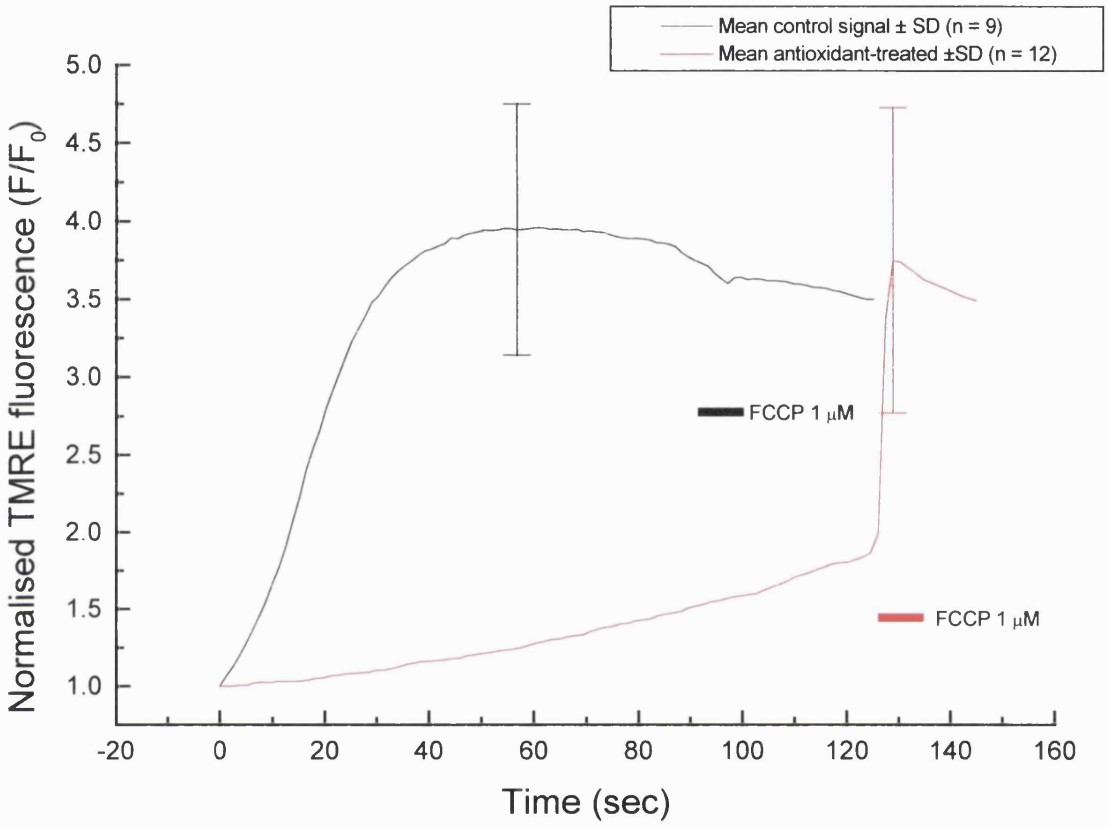

Figure 6.6: Mean TMRE fluorescence from controls (black) and antioxidant-treated cells (red) when illuminated with sufficient light to induce global mitochondrial depolarisation. The error bars at maximum signal are standard deviations.

	Controls	*Antioxidant-treated*	*P value*	*Groups significantly different?*
Slope	0.09388	1.71×10^{-5}	<0.0001	Yes
± SD	± 0.03362	$\pm 3.43 \times 10^{-5}$		
% dequench ±SD	298 ± 81	290 ± 98	0.654	No
n	9	12		

Table 6.1: summary of the data from the global depolarisation experiment. The peak fluorescence reached in both groups was the same, but analysis of the slopes of fluorescence increase confirmed that the rise in fluorescence in the group treated with antioxidants was significantly slower.

(ii) Detection of free radicals using a fluorescent indicator.

Free radical scavengers attenuated both the mitochondrial flickering and the rate of global depolarisation. In view of this, experiments were carried out to try and correlate the appearance of mitochondrial flicker with a quantitative assessment of the rate of ROS production. TMRE-loaded astrocytes were therefore loaded with the fluorescent dye, dihydrofluorescein, which may be used to detect ROS (LeBel, Ischiropoulos & Bondy, 1992) and the dihydrofluorescein signal was used as an assay of ROS production by the TMRE .

Properties of dihydrofluorescein

Chemical reduction of fluorescein to dihydrofluorescein renders the normally strongly fluorescent molecule colourless and non-fluorescent. Oxidation of dihydrofluorescein restores the fluorescence of the dye and so this probe may be used to detect oxidative species. The dye will be oxidised by most oxidative species, including endogenous nitric oxide and atmospheric air, so even control data will tend to show a steady increase in signal as the dihydrofluorescein is oxidised back to the fluorescent parent dye. However, an increase in the rate of oxidation of the dye has been used to signal the generation of reactive oxygen intermediates in a number of models, including dissociated rat cortical neurones (Oyama, Hayashi, Ueha, Chikahisa & Furukawa, 1993), reperfused lung tissue (Kehrer &

Paraidathathu, 1992) and amyloid β protein–mediated increases in H_2O_2 in PC12 cells (Behl, Davis, Lesley & Schubert, 1994). The cell-permeant, anionic version of dihydrofluorescein, 6-carboxy-2',7'-dichlorodihydrofluorescein diacetate, di(acetoxymethyl ester), or H_2DCFDA, forms carboxydichlorofluorescein on oxidation, which has additional negative charges, impeding leakage of the fluorophore from the cell. Carboxydichlorofluorescein when in solution of pH 6 and above, absorbs light at around 495 nm and has a peak emission at 529 nm.

Experimental methods

Experiments were conducted on the microfluorimetry system. Both TMRE and dihydrofluorescein can be excited at 490 nm. Bandpass filters centred at 590 nm (to allow transmission of TMRE fluorescence) and 530 nm (dihydrofluorescein fluorescence) were placed in front of the two PMTs. A dichroic mirror with a 510 nm cut-off was placed in the microscope to minimise transmission of the excitation light and another with a cut-off at 540 nm was placed between the PMTs to separate the two signals.

Astrocytes were loaded with H_2DCFDA by immersion in a 10 μM solution for 15 minutes at room temperature. After washing with saline, the cell dish was mounted on the stage of the microfluorimetry system and illuminated with 490 nm light, the intensity of which was attenuated with a mesh grid. The fluorescence signal was collected from a number of cells to assess the rate of autoxidation of the H_2DCFDA and the same cells were then loaded with TMRE. The fluorescence of the two dyes was then measured and the rate of increase of the dihydrofluorescein signal was compared with controls.

1. Dihydrofluorescein signals varied widely in controls

While the majority of the control dihydrocarboxyfluorescein fluorescence signals showed a negligible increase over 100 seconds, several rose dramatically upon illumination (Figure 6.7a). Photo-activation of the dye has been reported (Haugland, 1996a) and it is likely that the excitation light caused auto-oxidation of the dye in these cells.

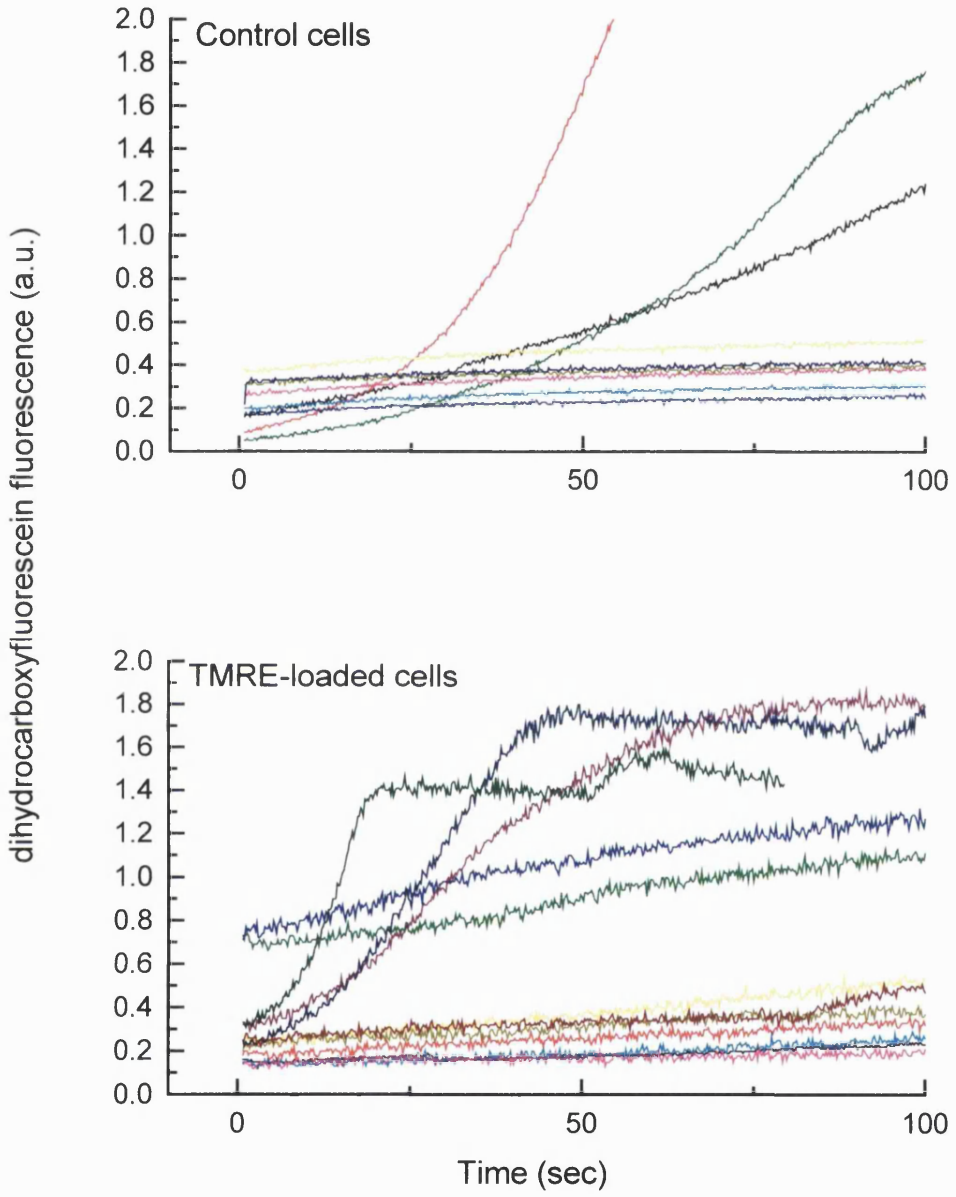

Figure 6.7a (upper panel): dihydrocarboxyfluorescein signal recorded over individual astrocytes. Even in these control cells (i.e. loaded only with H_2DCFDA) the rate of auto-oxidation of H_2DCFDA varies widely.

Figure 6.7b (lower panel): Co-loading these cells with TMRE did not diminish the variation in signal.

The initial fluorescence in the nine cells studied was similar, indeed two of the cells exhibiting a rapid increase in signal had the two lowest initial values, suggesting that a high intracellular H_2DCFDA concentration was unlikely to account for the rapidly changing signal in these cells. It is possible, however, that variations in antioxidant status of individual cells could influence the rate of H_2DCFDA oxidation. Cells with lower endogenous antioxidant defences might show faster rates of dye oxidation.

2. Illumination of TMRE did not change the dihydrofluorescein signal in these cells

In the cells loaded with both H_2DCFDA and TMRE there was a similar variation in rate of onset of fluorescence (Figure 6.7b), however there was no difference in the mean rate of change in signal between the two groups - slope of fluorescence onset in the controls 0.01315 ± 0.02658 (mean ± SD, n = 11), and in the TMRE-loaded group 0.01151 ± 0.01829 (n = 13).

3. In some cells, illumination of TMRE diminished the signal from the H_2DCFDA

The experiment was repeated. In these cells, there was a similar variation in H_2DCFDA signal change in the controls (Figure 6.8a), but the addition of TMRE *diminished* the fluorescence of the free radical detector (Figure 6.8b). The onset of fluorescence in the control cells had a slope of 0.03216 ± 0.02951 (mean ± SD, n = 8), significantly greater than that of the TMRE-loaded cells, 0.001695 ± 0.001633 (n = 8). The P value (two-tailed Mann-Whitney test) was 0.0003.

Further attempts to use H_2DCFDA as an indicator of ROS production by TMRE produced similarly variable results.

4. H_2DCFDA cannot be used to assay ROS in the TMRE-loaded astrocytes

These very mixed data do not confirm the formation of free radicals by illuminated TMRE, yet there was a clear effect of free radical scavengers on both the frequency of mitochondrial flickering and the rate of dye dequench. More puzzling is the fact that in several experiments

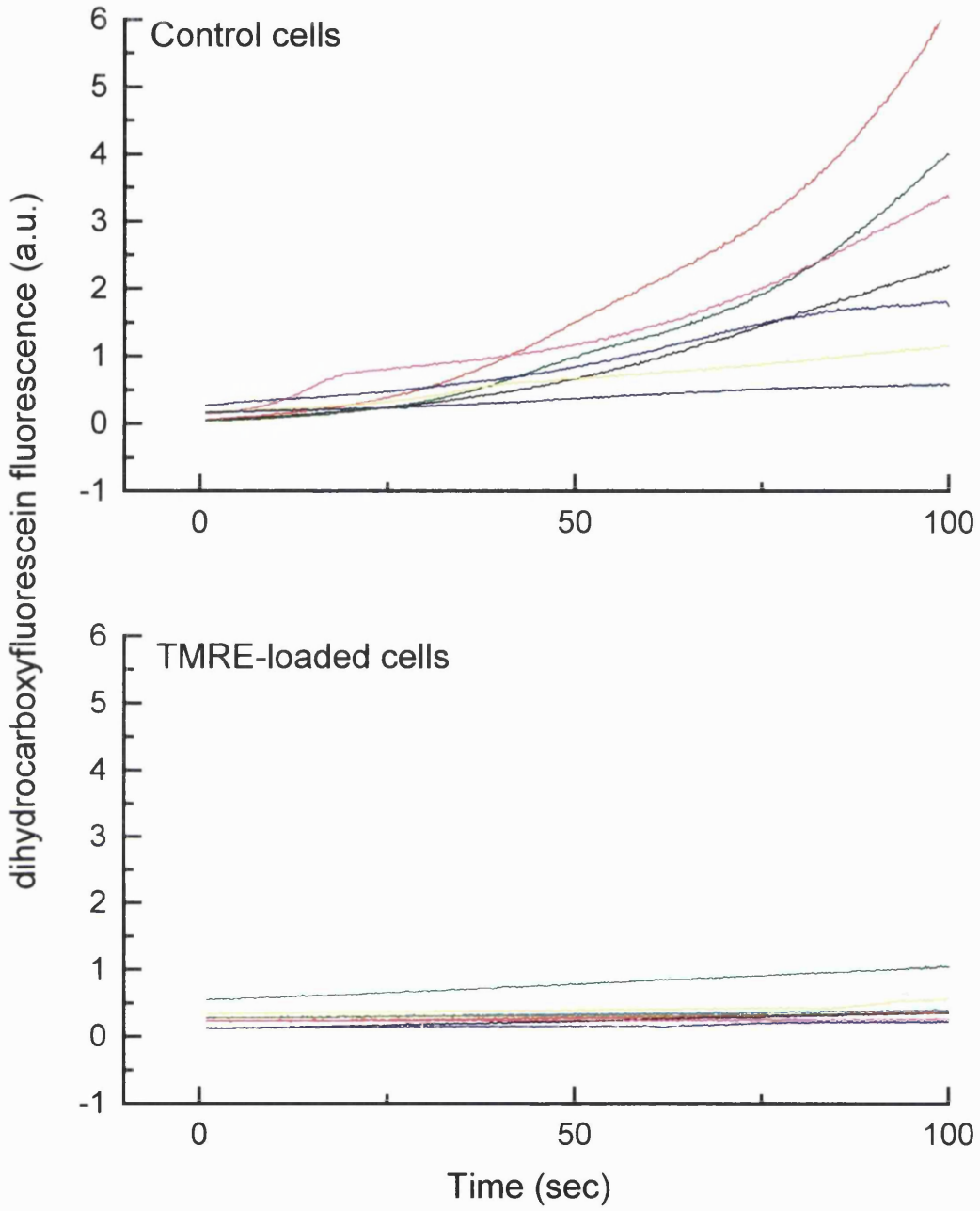

Figure 6.8a (upper panel): rates of H_2DCFDA auto-oxidation in control cells

Figure 6.8b (lower panel): in some experiments, co-loading astrocytes with TMRE and H_2DCFDA diminished the

rate at which the H_2DCFDA was oxidised.

the illumination of TMRE-loaded cells induced a net reduction in dihydrofluorescein signal when one would expect a rise in signal as the dye is oxidised by ROS.

Of note are the spectra of the two dyes. TMRE is excited over a wide range of wavelengths (the data from Section 3 show that TMRE loaded into astrocytes can be excited from 480 to 580 nm, (Figure 3.2), dihydrofluorescein has a peak florescence emission 529 nm (Haugland, 1996a), and the signal from this dye was being measured at 510 – 540 nm. It is possible that concentration of the two dyes into a small space, such as the organelles of a cell, could produce conditions that allow transference of fluorescence energy (i.e. photons) from one dye to another (Ha *et al.*, 1996). Hence, oxidation of H_2DCFDA by free radicals derived from TMRE would cause the fluorescent compound, dihydrocarboxyfluorescein to be formed. Excitation of dihydrocarboxyfluorescein by the 490 nm light would cause the dye to fluoresce at around 530 nm. Photons of this wavelength may be absorbed by nearby TMRE molecules adding to the fluorescence of this dye but reducing the signal measured at 530 nm.

Conclusions

Both the frequency of light-induced mitochondrial flickering and the rate of onset of global fluorescence were strongly attenuated in cells treated with an array of antioxidants. These data suggest that free radicals, known to be produced by TMRE, are involved in both processes, the individual, transient mitochondrial depolarisations, and the overall rise in TMRE signal in illuminated astrocytes.

The action of H_2DCFDA, used as an assay of free radical production in these experiments was complex and the results equivocal. In some cases there was no difference between the control and experimental groups, in others there was a significant drop in fluorescence from the free radical reporter. It is possible that variations in a number of factors confounded the use of this dye in these experiments, and it is noteworthy that the emission spectrum of dihydrocarboxyfluorescein is of a wavelength that might cause energy transfer to co-localised

TMRE. This could explain the quench of carboxydichlorofluorescein seen in several experiments.

Chapter 7: the mitochondrial permeability transition is involved in the depolarisations

Introduction

The data presented in Chapter 5 confirmed that stored intracellular Ca^{2+} is necessary for the mitochondrial depolarisations. The electrophoretic uptake of Ca^{2+} by mitochondria results in a reversible depolarisation of the $\Delta\Psi_m$ in neurones (Duchen, 1992), neuroblastoma cells, (Loew *et al.*, 1994) and in cortical astrocytes stimulated with ATP (Peuchen *et al.*, 1996b; Boitier *et al.*, 1999). Mitochondrial Ca^{2+} uptake has been shown to be significant in shaping calcium waves in the astrocytes (Boitier *et al.*, 1999) and also in Xenopus oocytes (Jouaville, Ichas & Mazat, 1998). However, most of the studies that report mitochondrial depolarisation coincident with mitochondrial Ca^{2+} uptake examined $\Delta\psi_m$ responses to whole-cell Ca^{2+} mobilisation. In contrast, the calcium transients described in Chapter 6 were highly localised, spatially and temporally, suggesting that individual mitochondria may depolarise transiently in response to very local calcium transients.

Moreover, the data presented in Chapter 6 confirm the necessity of ROS for both the transient depolarisations and the progression to global mitochondrial depolarisation. It is possible that the involvement of the free radicals extends only as far as initiating Ca^{2+} release (presumably by oxidation of critical residues on the ER calcium channels), and that the depolarisations are entirely due to the electrogenic uptake of Ca^{2+} by mitochondria. However, the combination of mitochondrial oxidative stress and mitochondrial Ca^{2+} overload may also trigger the opening of a large proteinaceous pore that spans the mitochondrial membranes, the mitochondrial permeability transition (MPT) pore. Pore opening dissipates the $\Delta\Psi$m but the depolarisation may be transient and a membrane potential can be re-established (Hüser *et al.*, 1998).

Thus two models may be evoked to explain the necessity for both stored Ca^{2+} and ROS for the mitochondrial depolarisations:

1. ROS-sensitised release of stored Ca^{2+} and consequent mitochondrial uptake of Ca^{2+}. Electrophoretic uptake of Ca^{2+} causes transient depolarisations.
2. ROS –sensitised Ca^{2+} release and consequent mitochondrial accumulation of Ca^{2+} until a threshold $[Ca^{2+}]_{mit}$ is reached whereupon the MPT pore opens, dissipating the $\Delta\psi_m$.

To distinguish between transient mitochondrial depolarisations caused purely by Ca^{2+} uptake and those caused by flickering of the MPT pore, TMRE-loaded cells were treated with known inhibitors of the MPT, trifluoperazine, cyclosporin A, or n-methyl 4 valine cyclosporin and compared with controls. Additionally, flickering was assessed in neonatal cardiomyocytes transfected with an antisense oligonucletide directed against the mRNA for cyclophilin D in order to suppress expression of this cyclophilin, one of the components of the MPT pore complex. Cyclophilin D-suppression might be expected to inhibit formation of the pore cells and thus should flicker less than controls if the MPT underlies the flickering.

Trifluoperazine

Trifluoperazine is an inhibitor of the Ca^{2+}-calmodulin complex that is used clinically as an anti-psychotic agent. It is also known to inhibit the MPT, and there is evidence that the compound may act synergistically with CsA in this respect (Imberti, Nieminen, Herman & Lemasters, 1992; Broekemeier & Pfeiffer, 1995), however its exact actions on pore formation are unclear. Trifluoperazine is an inhibitor of phospholipase A2 (Broekemeier, Schmid, Schmid & Pfeiffer, 1985) and as products of phospholipid hydrolysis may accumulate in mitochondria under conditions that promote MPT, the inhibition of this enzyme has been assumed to mediate the action of the compound (Nieminen *et al.*, 1995). However, trifluoperazine may be protonated to form an amphipathic cation, thereby making the mitochondrial membrane surface potential more positive upon association. As an increased mitochondrial membrane surface potential gradient may also inhibit MPT pore opening, this action of trifluoperazine may partly account for its synergistic effect with CsA (Broekemeier & Pfeiffer, 1995). Additionally, Periera et al have proposed a model whereby trifluoperazine induces structural changes in membrane proteins, preventing thiol cross-linking under conditions of oxidative stress (Pereira, Bertocchi

& Vercesi, 1992). Thiol cross-linking, and thus conformational and functional changes, may be a result of oxidative damage of proteins.

Cyclosporin A

Nanomolar concentrations of the immunosuppresive drug, cyclosporin A (CsA) inhibit the MPT (Crompton *et al.*, 1988; Halestrap & Davidson, 1990). CsA binds cyclophilins, ubiquitous enzymes capable of catalysing the interconversion of peptidyl-prolyl cis and trans isomers (PPIases) in proteins and peptides. There are several cyclophilin isoforms, Cyp A (cytosol), Cyp B and Cyp C (endoplasmic reticulum) and Cyp D (mitochondria). The cyclophilins are heat- and stress-inducible proteins (Marks, 1996) with a variety of putative functions; they are involved in protein folding and catalyse the folding of some proteins imported into organelles (Matouschek, Rospert, Schmid, Glick & Schatz, 1995). They may have a role in neuronal repair (Sabatini, Lai & Snyder, 1997), and memory formation (Bennett, Singaretnam, Zhao, Lawen & Ng, 1998) however there is also evidence that they can cleave DNA and thus may be involved in the destruction of the genome during apoptosis (Montague, Gaido, Frye & Cidlowski, 1994). Many knockout mutants of single and multiple PPIases are viable with no detectable phenotype (Dolinski, Muir, Cardenas & Heitman, 1997). A mitochondrial cyclophilin, CypD, is associated with the formation of the MPT pore (Halestrap & Davidson, 1990; McGuinness, Yafei, Costi & Crompton, 1990) and binding of Cyp D by CsA inhibits pore formation.

N methyl 4 valine cyclosporin

The cyclophilin-CsA complex also binds calcineurin, a Ca^{2+}- and calmodulin-dependent phosphatase which has several functions, including promotion of transcription of early T cell activation genes (Liu *et al.*, 1991). This is the basis of the immunosuppresive action of cyclosporin. To distinguish between this action of the compound and the inhibition of the MPT, a non-immunosuppresive derivative of CsA, N methyl 4 valine cyclosporin (Me 4-Val-Cs), has been used (Nicolli, Basso, Petronilli, Wenger & Bernardi, 1996). Me 4-Val-Cs binds cyclophilins, but the Me 4-Val-Cs-cyclophilin complex does not bind calcineurin.

Cyp-D –suppressed myocytes

Mitochondrial flicker was assessed in neonatal rat cardiomyocytes in which the expression of mitochondrial cyclophilin, Cyp D, had been very largely suppressed using antisense oligodeoxynucleotides (AS-ODN) directed against Cyp D mRNA. Cells were treated with either a 1 or 3 μM solution of the AS-ODN solution. Suppression of Cyp D expression should inhibit pore formation and thus reduce mitochondrial flicker. The primary cell culture and oligonucleotide transfection were performed by Dr Veronica Doyle working in the laboratory of Dr Martin Crompton (Department of Biochemistry, University College London).

Experimental procedures

Effect of trifluoperazine and cyclosporin A on global mitochondrial depolarisation

Astrocytes were loaded with TMRE and cell dishes were mounted on the stage of the Digital Pixel imaging system. Cells were illuminated with 530 nm light and images of the fluorescence of wavelength greater than 580 nm were collected. In order to study the global depolarisation a 30% neutral density filter was used. All imaging was via a 63x objective lens. Once control images had been taken, the saline medium was removed from the cell dish and replaced with a solution of either 10 μM trifluoperazine or 500 nM cyclosporin A, made up in standard saline. After a 30 minute loading period, the imaging procedure was repeated. The rates of onset of global mitochondrial depolarisation were compared by measuring the slope of the fluorescence change with time.

Effect of N methyl 4 valine cyclosporin on mitochondrial flicker

Dishes of TMRE-loaded cells were mounted on the stage of the fast-scan imaging system and illuminated with 546 nm light. Fluorescence at wavelengths beyond 590 nm was collected and a 63x objective was used. A 1% ND filter was inserted in the light path to image mitochondrial flickering but restrain the progression to a global depolarisation. Series of images of cells showing mitochondrial flickering were acquired, typically lasting around 45 seconds. Towards the end of each imaging sequence, FCCP I μM was applied by puffer

pipette to individual cells in order to establish the maximum TMRE signal on complete mitochondrial depolarisation. Once control images had been collected, the saline in the dish was exchanged for a 200 nM solution of Me 4-Val-Cs, made up in the standard saline. After a 30 minute loading period, the imaging procedure was repeated. The index of variation was calculated for single cells, as described previously. The calculated indices were then statistically compared, as were the maximum TMRE signals seen after FCCP application.

Effect of Cyp D suppression on mitochondrial flicker

Neonatal cardiomyocytes, which had previously been transfected with antisense oligodeoxynucleotides targeted to the mRNA for Cyp D, were loaded with TMRE and imaged with the Hamamatsu imaging system and a 63x objective lens. Using a 1% ND filter, cells were illuminated with sufficient 546 nm light to permit imaging of mitochondrial flickering but suppress a global depolarisation. Once images had been collected, control myocytes which had not been transfected, were loaded with TMRE and imaged in the same fashion. The indices of variation for the mitochondrial flicker were calculated and compared.

Results

1. Trifluoperazine significantly reduced the rate of light-induced global mitochondrial depolarisations.

The rate of light-induced global mitochondrial depolarisation was significantly reduced in cells treated with trifluoperazine 10 μM (Figure 7.1). Trifluoperazine did not reduce the TMRE dequench on application of FCCP 1μM, confirming that these mitochondria were not depolarised compared with controls (Table 7.1)

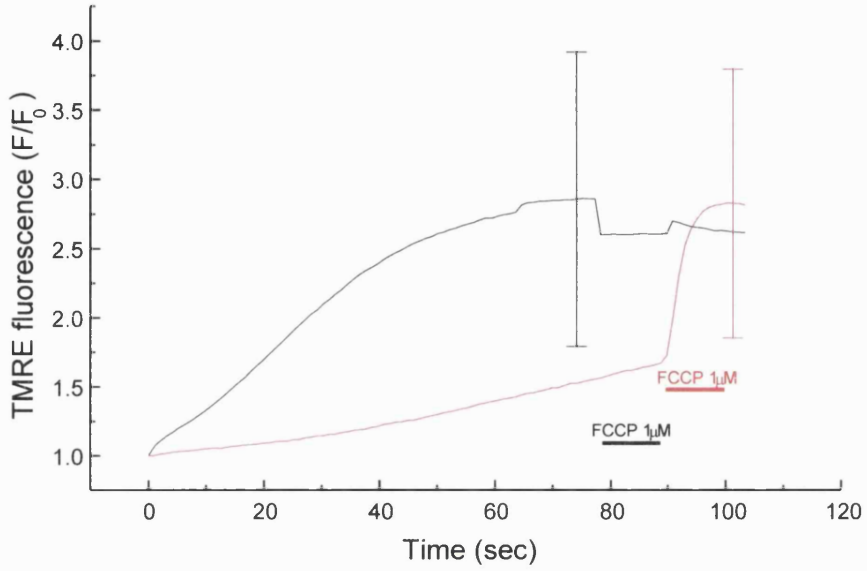

Figure 7.1: treatment with trifluoperizine 10 μM significantly reduced the rate of light-induced TMRE dequench ($P < 0.0001$, unpaired Mann Whitney U test). There was no difference in the peak TMRE signal on application of FCCP 1μM ($P = 0.6375$, unpaired t test). Controls, n = 27; trifluoperazine-treated, n = 60

	Controls	*Trifluoperazine-treated*
Mean rate of change of TMRE fluorescence	0.041	0.008*
Standard deviation	0.018	0.006
% TMRE dequench with FCCP	214	203
Standard deviation	106	92
n	27	60

Table 7.1: the rate of global mitochondrial depolarisation was significantly less in astrocytes treated with trifluoperazine 10 μM (P< 0.0001, unpaired Mann Whitney U test). There was no difference in the peak TMRE signal on application of FCCP 1μM (P = 0.6375, unpaired t test).

2. CsA treatment significantly reduced the rate of global mitochondrial depolarisations.

Treatment with 500 nM CsA significantly slowed the rate of TMRE dequench (Figure 7.2, Table 7.2). However, the peak fluorescence on total dissipation with FCCP 1 μM was also significantly less in the CsA-treated groups. This would suggest that CsA somehow decreases TMRE loading and thus inhibits the dequench on addition of FCCP.

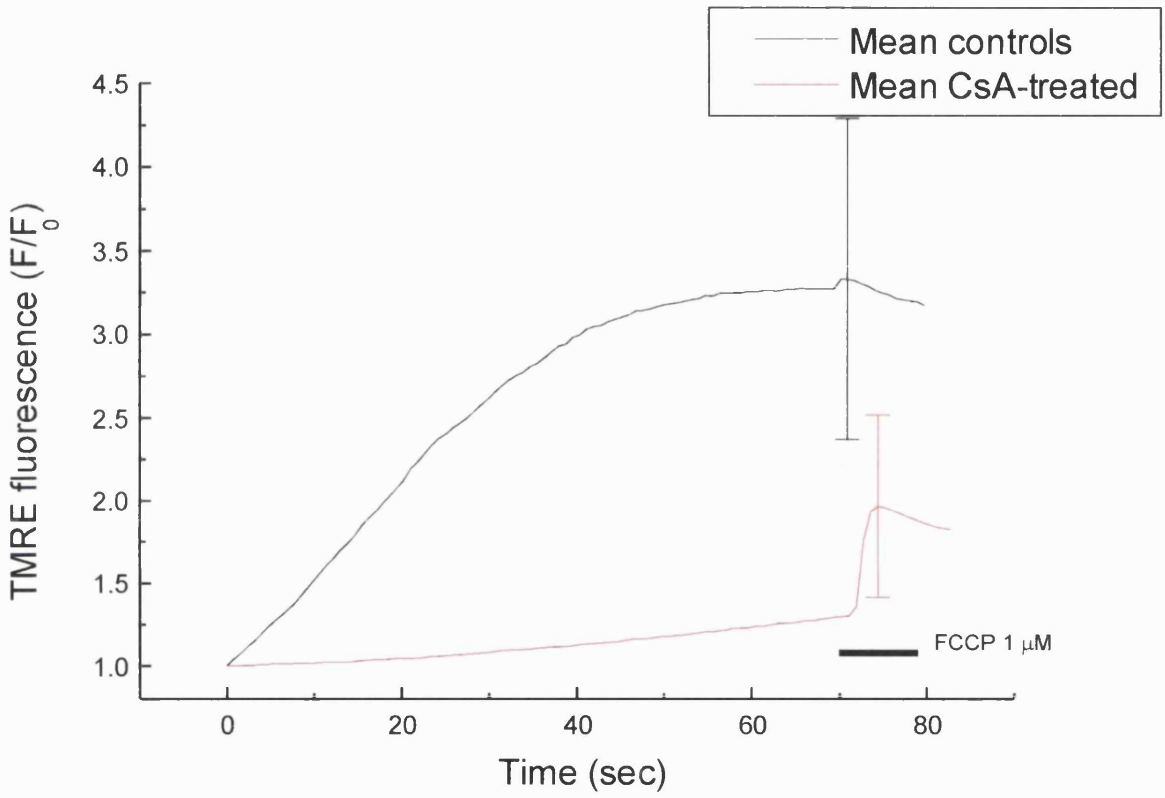

Figure 7.2: treatment of TMRE-loaded astrocytes with 500 nM cyclosporin A significantly slowed the progression to global mitochondrial depolarisation ($P < 0.0001$, Mann Whitney test) but the peak TMRE fluorescence on application of FCCP was also reduced ($P < 0.0001$, Mann-Whitney test). Controls, n = 15; CsA-treated, n = 17

	Controls	CsA-treated
Mean rate of change of TMRE fluorescence	0.058	0.004*
Standard deviation	0.031	0.005
% dequench from baseline on addition of FCCP	233	97*
Standard deviation	96	55
n	15	17

Table 7.2: treatment of TMRE-loaded astrocytes with 500 nM CsA significantly reduced the rate of TMRE dequench ($P < 0.0001$, unpaired Mann Whitney U test). The peak fluorescence attained ion application of FCCP 1 μM was also significantly less ($P < 0.0001$, unpaired Mann Whitney U test).

3. Treatment with Me 4-Val-Cs significantly attenuated the mitochondrial flicker

Treatment with 200 nM Me 4-Val-Cs significantly reduced the index of variation in TMRE-loaded astrocytes, as compared with controls (Table 7.3, Figure 7.3 and 7.5). There was no difference in peak TMRE signal on application of FCCP to these cells.

	Controls	*Me 4-Val-Cs treated*
Index of variation	1.29	1.16*
Standard deviation	0.1	0.05
% dequench from baseline	223	189
Standard deviation	93	101
n	32	55

Table 7.3: treatment of TMRE-loaded cells with Me 4-Val-Cs significantly reduced the flickering, as measured by the index of variation (*$P < 0.0001$, unpaired Mann Whitney U test). No difference in peak fluorescence was seen on application of FCCP ($P = 0.1239$, unpaired t test).

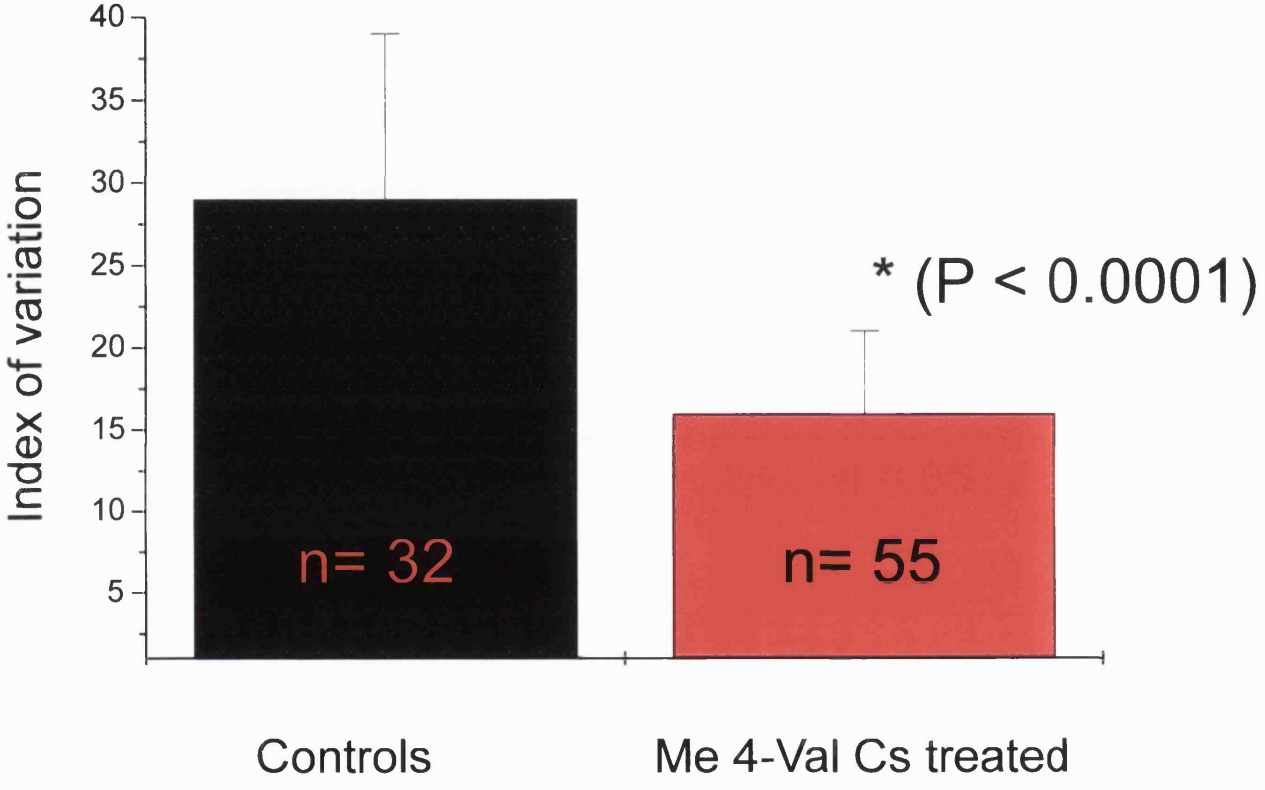

Figure 7.3: treatment with N methyl 4 valine cyclosporin significantly reduced the depolarisations ($P < 0.0001$, unpaired Mann-Witney U test). Error bars denote standard deviations.

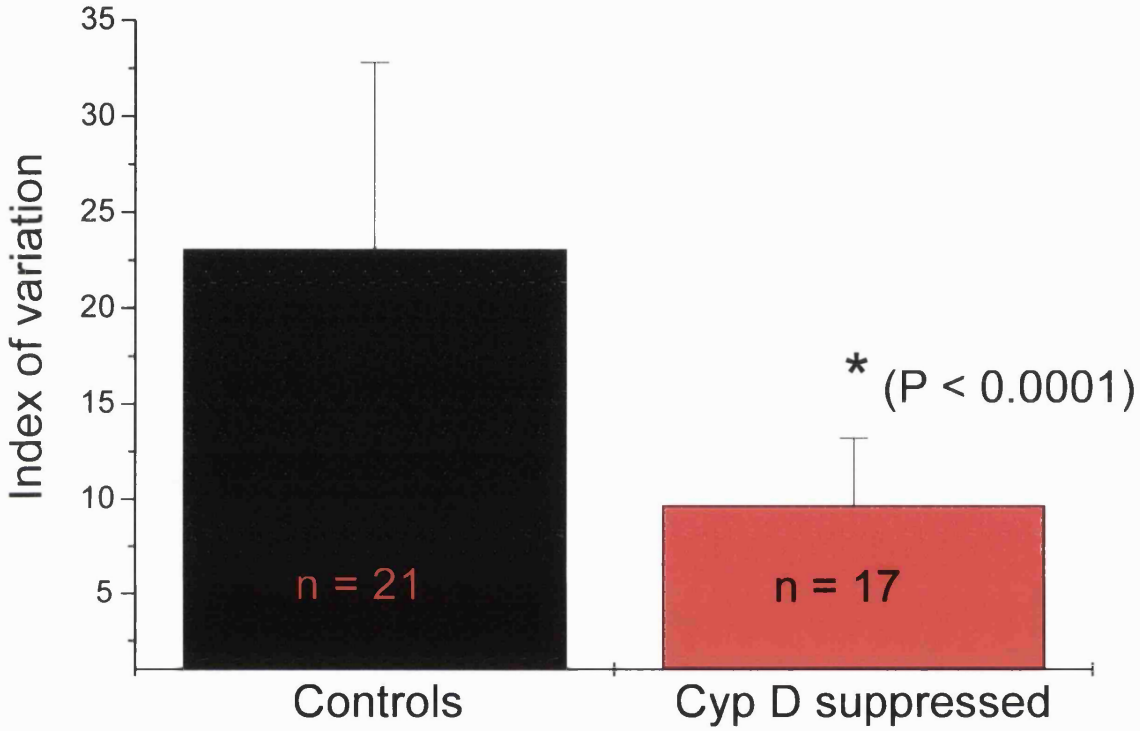

Figure 7.4: suppression of mitochondrial cyclophilin expression significantly reduced the flickering

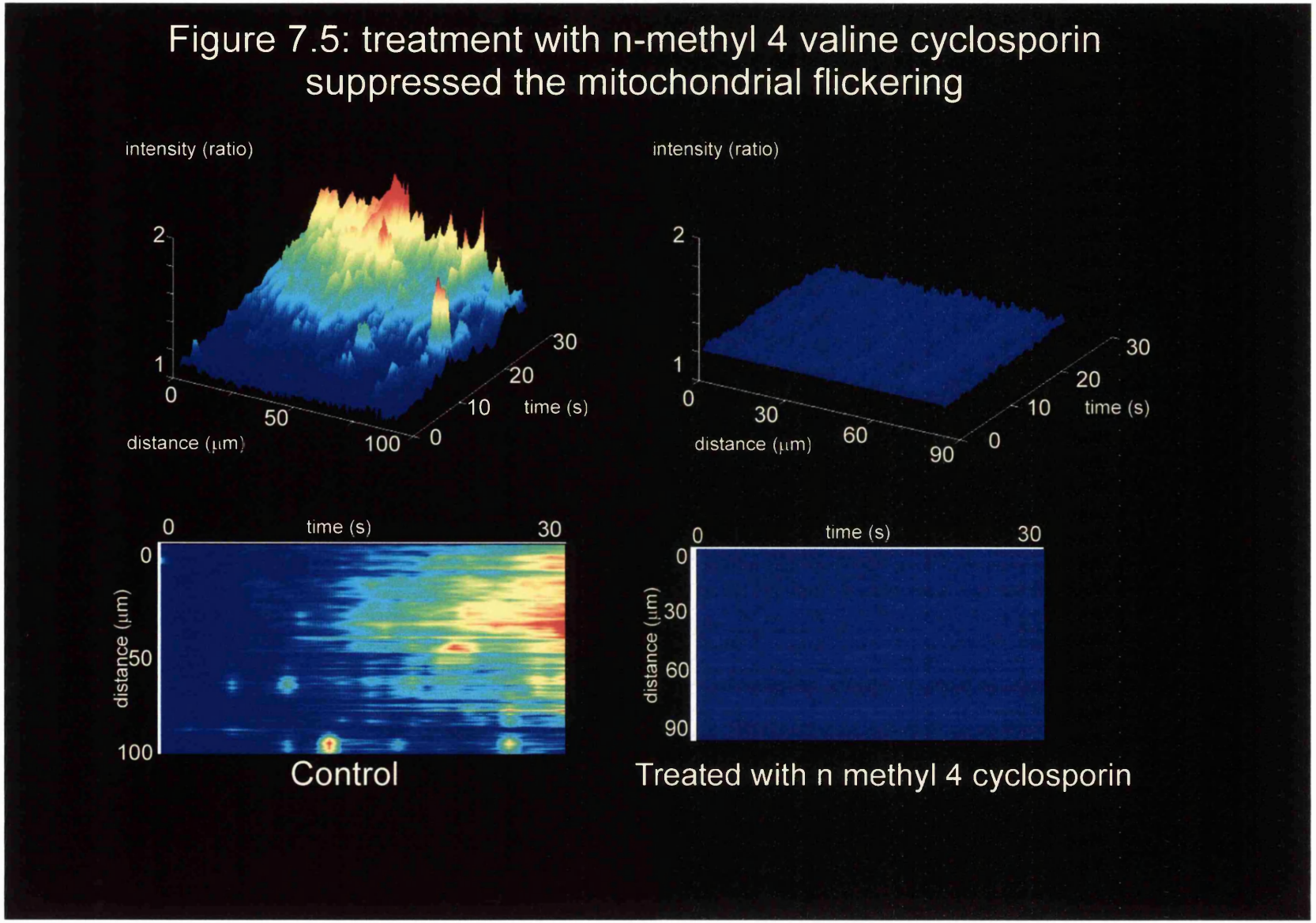
Figure 7.5: treatment with n-methyl 4 valine cyclosporin suppressed the mitochondrial flickering
intensity (ratio)
2
1
0
50
100
distance (μm)
0
10
20
30
time (s)
intensity (ratio)
2
1
0
30
60
90
distance (μm)
0
10
20
30
time (s)
0
time (s)
30
0
50
100
distance (μm)
Control
0
time (s)
30
0
30
60
90
distance (μm)
Treated with n methyl 4 cyclosporin

4. Suppression of Cyp D expression attenuated the mitochondrial flickering

The degree of mitochondrial flickering was significantly less than controls in the cardiomyocytes in which Cyp D expression was suppressed with the AS-ODN (Table 7.4 and Figure 7.4). Treatment with both 1 μM and 3 μM AS-ODN reduced the flickering.

	Controls	*1 μM AS-ODN*	*3 μM AS-ODN*
Index of variation	1.231	1.097*	1.136*
Standard deviation	0.097	0.035	0.089
n	21	17	8

Table 7.4: Both 1 μM and 3 μM solutions of AS-ODN significantly reduced the index of variation ($P < 0.0001$ and $P = 0.007$, respectively; Mann-Whitney U tests).

The peak TMRE fluorescence on application of FCCP 1 mM was also reduced by treatment with AS-ODN (Table 7.5) suggesting that in the Cyp D suppressed cells there was reduced TMRE loading.

	Controls	*1 μM AS-ODN*	*3 μM AS-ODN*
% dequench with FCCP 1 μM	166	77*	40*
Standard deviation	108	33	24
n	21	17	8

Table 7.5: the TMRE dequench seen on application of FCCP was significantly lower in neonatal cardiomyocytes treated with either 1 μM or 3 μM AS-ODN, implying that in these cells the mitochondria were depolarised as compared with controls (*$P = 0.0015$ for 1 μM group, *$P = 0.0032$ for 3 μM group, Mann-Whitney U tests)

Conclusions

Both ROS and mitochondrial Ca^{2+}-loading are involved in the mitochondrial depolarisations seen in TMRE-loaded cells. As both ROS and mitochondrial Ca2+ are initiators of the MPT, direct evidence was sought for the involvement of this phenomenon in the depolarisations. The binding of cyclophilins by either CsA or Me 4-Val-Cs significantly increased the time to global depolarisation, and reduced the flickering. Additionally, flickering was significantly reduced in neonatal cardiomyocytes treated with either 1 μM or 3 μM AS-ODN directed against mitochondrial Cyp D. Trifluoperazine, an inhibitor of the MPT that does not bind Cyp D, also reduced the time to global mitochondrial depolarisation.

Taken, together, these data suggest that the MPT pore is involved in both the flickering and global depolarisations seen in the TMRE-loaded cells.

Chapter 8: mitochondrial flickering does not lead to cell death

Introduction

Prolonged opening of the mitochondrial PTP depletes intracellular [ATP]. Loss of the proton gradient across the inner mitochondrial membrane uncouples electron transport from ATP synthesis by the ATP synthase and ATP production stops. Moreover, in many cell types the loss of the proton gradient may cause the ATP synthase to expel protons, consuming ATP in the process, thus accelerating ATP depletion (Nicholls & Ferguson, 1992). The ATP-depleted cell then dies by a necrotic pathway. However, it is possible that transient PTP openings, such as the flickering described in previous chapters, does not result in complete ATP consumption and that sufficient ATP remains to fuel energy-requiring metabolic processes. Additionally, there is evidence that programmed cell death (apoptosis), itself an ATP-dependent process, may be initiated by signalling pathways that converge on the mitochondrion.

In programmed cell death, cell breakdown is executed by a family of cysteine proteases, the caspases. Caspases act by cleaving proteins at aspartate residues and are constitutively expressed as inactive proenzymes, activated by proteolytic cleavage. Ligand binding of cell-surface receptors such as the Fas receptor may induce such activation, however, there is increasing evidence that mitochondria may initiate, or amplify, caspase activation. Release from mitochondria of the water-soluble component of the respiratory chain, cytochrome c, can induce apoptotic cell death. Liu and colleagues have shown that cytochrome c, on binding of a cytosolic protein, Apaf 1, can cleave procaspase-9, activating caspase-9 and downstream caspases, -3, -6, -7. Additionally, Kroemer's group have cloned a 50 kDa protein, dubbed apoptosis-inducing factor (AIF), that is restricted to the mitochondrial matrix but which translocates to the cytosol and the nucleus on induction of apoptosis. AIF activates endonucleases (it has no caspase activity) and there is also evidence that it can initiate a positive feedback loop involving mitochondria, as addition of the protein to isolated mitochondria has been shown to induce cytochrome c release and procaspase-9 cleavage

(Susin *et al.*, 1999). Interestingly, both cytochrome c and AIF may have parallel dual functions, as both proteins have oxido-reductase activity in addition to their role in activation of apoptotic pathways.

The Bcl-2 family of proteins consists of at least a dozen proteins with pro- or anti-apoptotic regulatory functions. These molecules are distributed in various compartments of the cell (anti-apoptotic Bcl-2 is present in the mitochondrial outer membrane, endoplasmic reticulum and nucleus, pro-apoptotic Bax is predominantly located in the cytosol, as is pro-apoptotic Bid) however, activation of apoptic pathways sees the translocation of these proteins to the outer mitochondrial membrane where the molecules may heterodimerise (Mahajan *et al.*, 1998). As some members of the Bcl-2 inhibit apoptosis and others promote it, it seems likely that release of pro-apoptotic molecules from mitochondria may in some way be regulated by the interaction of these proteins. Bax has been shown to form ion channels when incorporated into lipid bilayers (Antonsson *et al.*, 1997), however Bid has no such properties and yet is effective in inducing cytochrome c release when added to isolated mitochondria (Zou, Henzel, Liu, Lutschg & Wang, 1997).

There is accumulating evidence that the mitochondrial permeability transition may be involved in the transduction of pro-apoptotic signals. Bax has been shown to bind to the voltage-dependent anion channel (VDAC), a constituent of the PTP (Narita *et al.*, 1998) and mitochondria isolated from Bcl-2 transfected cells are more resistant to ROS-induced PTP formation (Susin *et al.*, 1996). Kroemer's group have worked on hexokinase-associated protein complexes extracted from the brain and incorporated into liposomes, the protein complexes approximate the function of the PTP, and pore opening is initiated by inducers off the mitochondrial PTP (Marzo *et al.*, 1998b). Studies using this model have demonstrated that Bax is associated with the protein complex and immunodepletion of Bax resulted in inhibition of pore opening in response to atractyloside (Marzo *et al.*, 1998a).The presence of Bcl-2 or (anti-apoptotic) Bcl-X_L similarly conferred resistance to pore opening by atractyloside, *tert*-butylhydroperoxide, Ca^{2+} and caspases (Marzo *et al.*, 1998b).

In intact cells, application of pro-apoptotic tumour necrosis factor (TNF) induced redistribution of mitochondrially-loaded TMRM and mitochondrial uptake of calcein, indicative of PTP opening. The PTP opening was shown to precede cytochrome c release, caspase activation and the morphological changes associated with apoptosis (Bradham *et al.*, 1998). Treatment with CsA prevented both the fluorescence changes and the cell death. Recently, experiments in HepG2 cells have demonstrated that pro-apoptotic stimuli ceramide and Ca^{2+} can together induce PTP opening which results in cytochrome c release, caspase activation and increased incidence of apoptotic cell death (Szalai *et al.*, 1999). In these experiments, the $\Delta\psi_m$ was seen to re-establish after an initial CsA-sensitive depolarisation. This observation may provide an explanation as to how apoptosis, an ATP-requiring process, may be preceded by PTP opening, an event that would be expected to deplete intracellular [ATP].

In view of the evidence that PTP opening may initiate cell death by either a necrotic or an apoptotic pathway, the fate of the TMRE-loaded cells was investigated.

Experimental methods

Astrocytes were plated out on 25 mm coverslips as usual. Prior to mounting these in the cell chamber, a smaller coverslip etched with grids ('CELLocate', Eppendorf) was glued to the underside of the primary coverslip. The grids consisted of groups of 24 squares, each 55 μm in size, identified by etched lettering. By noting the location of the cells in relation to the grid, the same cells could be re-examined hours later.

The cells were loaded with TMRE as before and the double coverslips were mounted on the stage of the Hamamatsu. A 40x long working distance lens was used in order to focus through both coverslips. Cells were illuminated at 546 nm and a either a 1% or a 30 % neutral density filter was used in order to image either flickering or completely depolarising mitochondria. Each grid of cells was imaged for 130 seconds. Once the imaging had been completed, the saline in the bath was replaced with culture medium and the cells were returned to the incubator. After 4 hours – a sufficient period to detect astrocytic apoptosis in other models (DeGracia *et al.*, 1997; Diaz *et al.*, 1999) – the cells were loaded with the

fluorescent nuclear dyes propidium iodide (PI) and Hoechst 33342 by immersion for 15 minutes in a solution of 10 μM propidium iodide and 15 μM Hoechst. The cell dish was then mounted on the microscope stage and illuminated using 355 nm light and the pattern of staining in the illuminated cells was compared with control areas in the same dish which had not been illuminated.

PI is excluded by healthy cells, while Hoechst is readily taken up whereupon it stains nuclear chromatin producing a faint, diffuse, nuclear signal blue in colour. However, the chromatin condensation seen in apoptotic cell death produces a distinctive, bright blue fluorescence easily distinguishable from that seen in viable cells. Chromatin condensation may also be seen in necrotic cell breakdown but in these cells accompanying plasma membrane disintegration allows entry of PI. Hence, nuclei stained brightly with Hoechst, showing the characteristic chromatin condensation were scored as apoptotic if they also excluded PI. Those nuclei that showed pink PI staining were deemed necrotic (Figure 8.1).

Results

There was no increase in cell death by necrosis in the cells illuminated using the 1% neutral density filter, despite the fact that mitochondria in these cells flickered vigorously (Table 8.1 and Figure 8.2a). Additionally, after 4 hours there was no increase in apoptotic cell death in the illuminated group, as only 3 cells, of 2083 counted, displayed the characteristic nuclear chromatin condensation and bright Hoechst staining.

The incidence of necrotic cell death was significantly increased in the group that had been illuminated via a 30% ND filter (Figure 8.2b). In this group 33 ± 12% of the cells took up PI at 4 hours, compared with 2 ± 2% of the controls ($P = 0.0002$, unpaired t test). No sign of apoptotic cell death was seen in these cells.

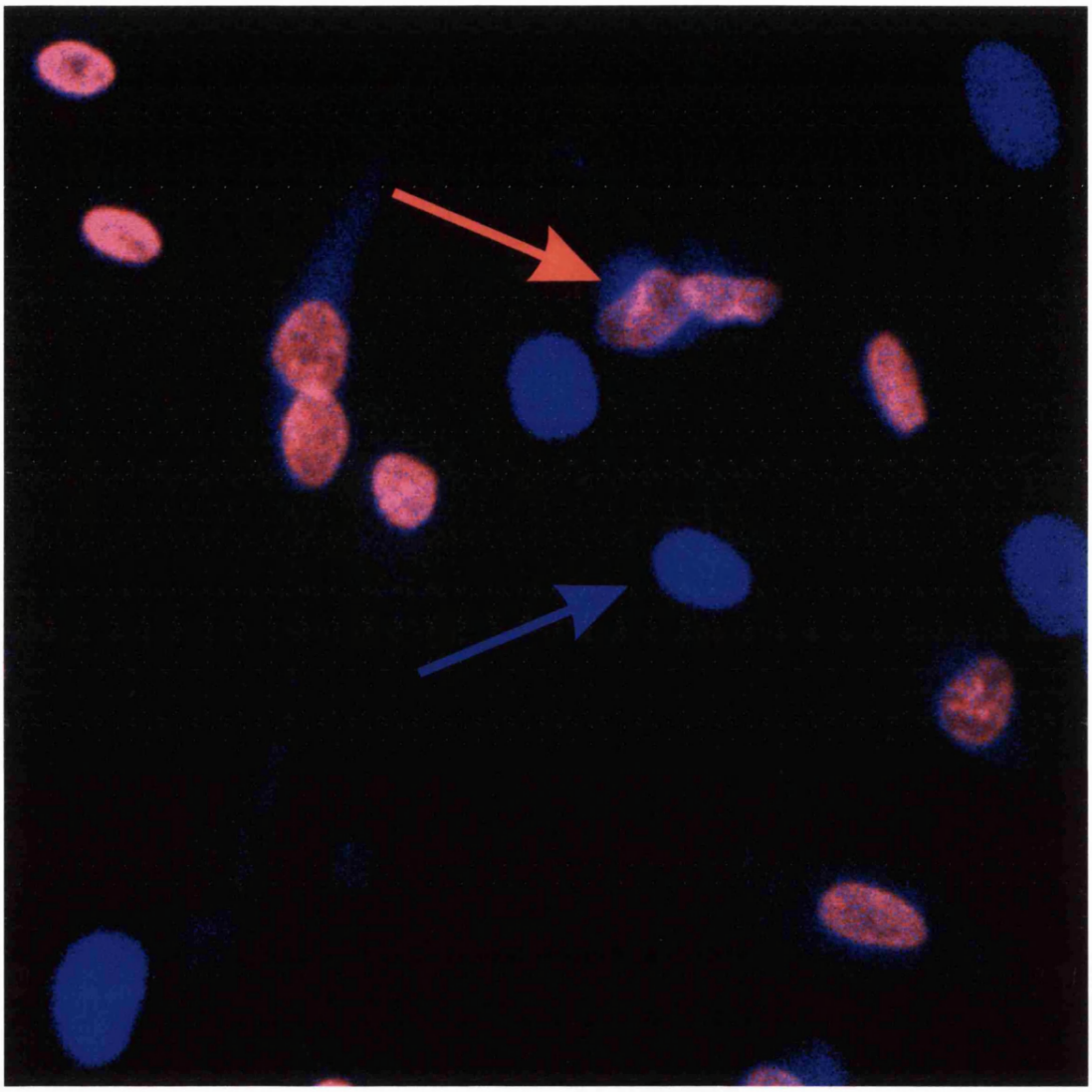

Figure 8.1: dual staining of astrocyte nuclei with propidium iodide and Hoechst 33342. When illuminated with 355 nm light, viable cells show a diffuse, blue staining of the nucleus (blue arrow). Healthy cells exclude propidium iodide, but it enters necrotic cells and stains the nucleus pink (red arrow). Apoptotic cells show a characteristic, bright vermiform staining of condensed chromatin, however very few cells underwent apoptosis in these experiments.

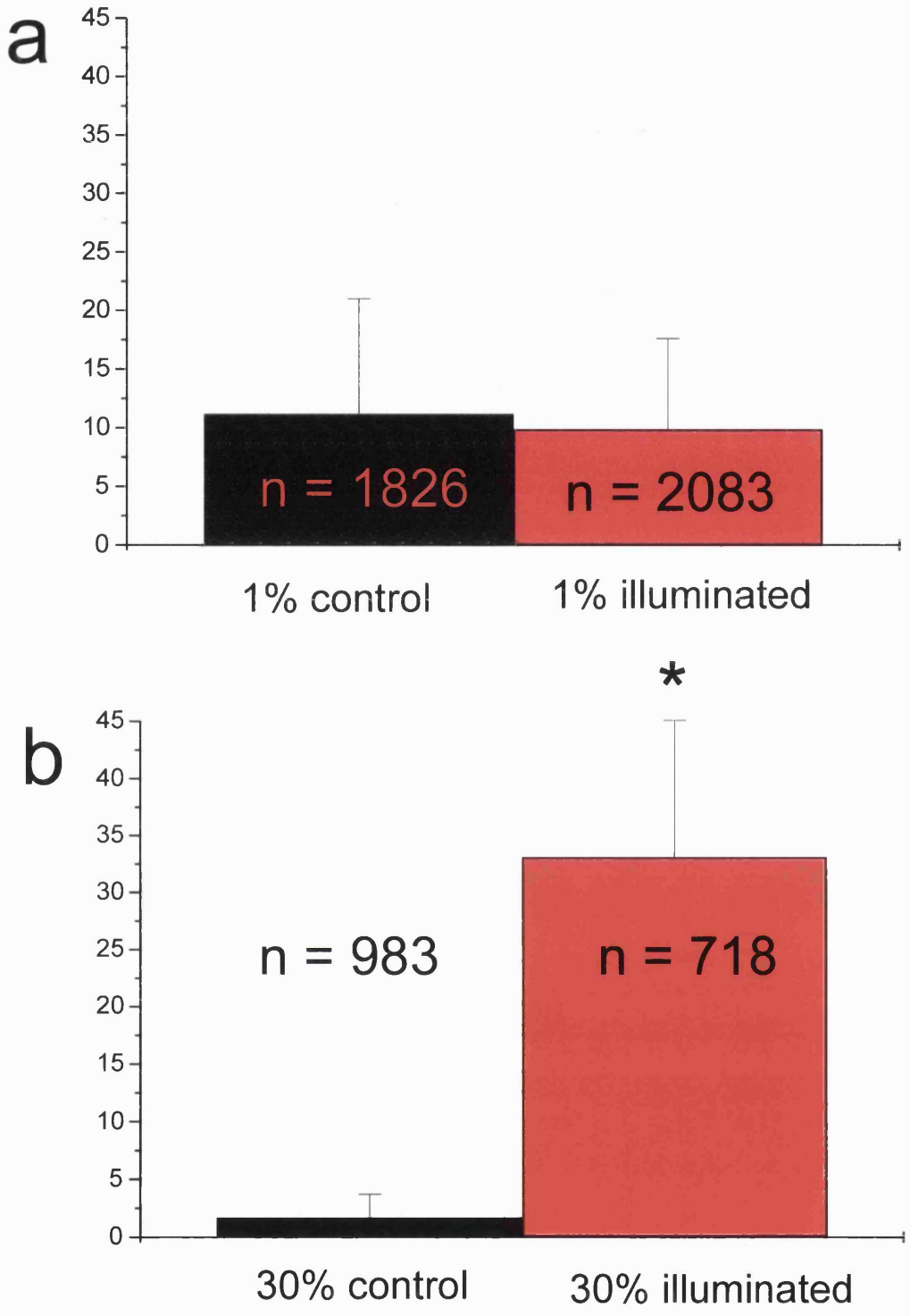

Figure 8.2: the incidence of necrotic death in TMRE-loaded astrocytes after 4 hours, as judged by PI uptake. Those cells that had been illuminated using a 1% ND filter (Panel a, red column) showed the same amount of necrotic death as their controls (Panel a, black column). In the group where a 30% ND filter had been used and global mitochondrial depolarisation occured (Panel b, red column) the incidence of PI uptake was significantly greater (*P = 0.0002, unpaired t test). There was no change in the incidence of apoptotic death in either group.

Group	*Total number of cells examined*	*Number of apoptotic cells*	*Number of necrotic cells*
1% illuminated	2083	4	209
1% controls	1826	3	226
30% illuminated	983	1	13
30% controls	718	0	324

Table 8.1: summary of cell fate experiments. Three different dishes of cells were used in each (1% and 30%) category. There was no increase in necrotic cell death seen at 4 hours in the 1% group, where mitochondrial flicker alone was imaged (P = 0.962, unpaired t test). Global mitochondrial depolarisation induced by illumination using a 30% ND filter caused a rise in necrotic cell death (P = 0.0002) but only one apoptotic cell was identified in this group.

Conclusions

Flickering of the mitochondrial PTP causes no increase in cell death in this model, by either an apoptotic or necrotic pathway. In contrast, those cells that were illuminated using a 30% ND filter, where global mitochondrial depolarisation was induced, there was a significant rise in the incidence of necrotic cell death, as detected by PI uptake.

Chapter 9: general discussion

The experiments presented in this thesis were designed to investigate a model of mitochondrial permeability transition in adult rat cortical astrocytes. Digital imaging of single astrocytes loaded with a fluorescent, potentiometric probe revealed mitochondrial depolarisations, both transient and long-lasting. Pharmacological and molecular biological evidence confirmed that the depolarisations were the result of openings of the MPT pore, and methods for quantifying the occurrence of pore opening are described. Using these assays, the role of ROS in the depolarisations was examined, confirming that excessive mitochondrial ROS production can increase the pore openings. Additionally, the model was used to examine the relationship between $[Ca^{2+}]_i$ and MPT. It is shown that MPT in living cells is Ca^{2+}-dependent, and that stored Ca^{2+} is required for pore opening. Finally, as MPT may presage apoptotic cell death, assays for apoptotic and necrotic death were performed. Accelerating MPT by imposing an oxidative stress on the cells led to increased incidence of necrotic death, however no increase in cell death, by either pathway, was seen in cells where the MPT was transient. Thus, in this model, recurrent flickerings of the MPT pore do not irrevocably lead to cell death.

TMRE faithfully reported mitochondrial depolarisations

The initial experiments for this thesis were designed to validate the use of the potentiometric probe, TMRE, as an indicator of $\Delta\psi_m$. I have shown that the dye loaded well into living astrocytes and that imaging of TMRE-loaded cells revealed selectively stained mitochondria. Under resting conditions minimal fluorescence was detected from mitochondrion-free cytosol and nucleus. Pharmacological manipulation of $\Delta\psi_m$ showed that the changes in signal were invariably consistent with the responses expected from chemiosmotic theory. Dissipation of $\Delta\psi_m$ by two distinct mechanisms, application of the protonophore FCCP and inhibition of Complex I by application of rotenone, induced fluorescence changes that were rapid and repeatable, however the direction of the fluorescence signal change was dependent upon the loading concentration.

If the TMRE was loaded by exposure to a low concentration of dye (50 nM), the dissipation of $\Delta\psi_m$ induced a reduction of fluorescence over the mitochondria and a concomitant rise over nearby cytosol as the dye redistributed within the cell. Loading the dye at higher concentrations, by exposure to a solution of 1.5 μM, revealed that the TMRE fluorescence was quenched by concentration in the mitochondria, and that dissipation of $\Delta\psi_m$ under these conditions led to a *rise* in fluorescence as the dye left the organelles and was diluted in the cytosol. Thus, a dequench of fluorescence signalled a mitochondrial depolarisation. Analysis of the excitation and emission spectra using a monochromator and an imaging spectrograph established that the signal changes were not due to wavelength shifts on depolarisation or by chemical interactions with commonly-used drugs and agonists.

Several fluorescent potentiometric dyes are commercially available and these are widely used as probes of $\Delta\psi_m$ (Salvioli, Ardizzoni, Franceschi & Cossarizza, 1997; Boitier *et al.*, 1999; Dedov & Roufogalis, 1999). Lipophilic cations load rapidly and easily into mitochondria in response to the $\Delta\psi_m$, and fluctuations in membrane polarity may therefore be measured by imaging the redistribution and/or signal change that occurs with depolarisation. However, for some authors doubt remains as to the reliability of these methods of assaying $\Delta\psi_m$ *in vivo* (Nicholls & Budd, 2000). Some commonly used dyes may inhibit mitochondrial respiration; Rotenburg and Wu reported that $DiOC_3(6)$ can result in a 90% inhibition of cell respiration (Rottenberg & Wu, 1998), and Rh 123 used at high concentrations inhibits the F_1F_0-ATPase (Emaus *et al.*, 1986). The potentiometric probe, JC-1 is frequently used (Dubinsky & Levi, 1998; Bedner, Li, Gorczyca, Melamed & Darzynkiewicz, 1999; Dedov & Roufogalis, 1999), and because this dye emits fluorescence at two wavelengths (530 nm and 590 nm), it has been described as 'ratiometric' (White & Reynolds, 1996). However, the exact behaviour of JC-1 is puzzling (Mojet review, in press) and it seems that the local dye environment may determine the wavelength of the fluorescence and thus the resultant ratio (Di Lisa *et al.*, 1995). TMRE may not be entirely innocuous and there is some evidence that micromolar concentrations may inhibit mitochondrial respiration (Scaduto & Grotyohann, 1999), however Farkas et al (Farkas, Wei, Febbroriello, Carson & Loew, 1989) found virtually no toxicity in cells loaded with micromolar TMRE for over 3 hours. Additionally, Farkas assayed $[ATP]_i$ in

TMRE-loaded cells, and found an unchanged $[ATP]_i$, assayed by luciferin-luciferase, after 75 minutes of loading. The experiments described in Chapter 8 confirm that astrocytes may be loaded with TMRE for over 4 hours and yet 90% or more remained viable, suggesting minimal toxicity of the dye under these conditions. The dye has successfully been used in dequench mode to monitor transient mitochondrial depolarisations in cardiomyocytes (Duchen *et al.*, 1998) and waves of mitochondrial depolarisation in cortical astrocytes (Boitier *et al.*, 1999).

As cationic dyes partition according to the Nernst equation, care must be taken to ensure that depolarisation of the plasma membrane does not confound interpretation of mitochondrial signal. Plasmalemmal depolarisation causes dye efflux from the cytosol to the extracellular space, increasing the dye concentration gradient from mitochondrial matrix to cytosol (Nicholls & Budd, 2000), thus initiating a secondary redistribution of dye independent of $\Delta\psi_m$. It is possible that the efflux of fluorophore from the mitochondrion, as the dye equilibrates, may be interpreted as a mitochondrial depolarisation. However, Duchen investigated changes in Rh 123 signal when loaded in quench mode and found little effect of plasma membrane depolarisation (Duchen, 1992). Rh 123 signal was recorded at various plasma membrane voltages by voltage-clamping the cell membrane potential of sensory neurones. These experiments showed that a voltage step from –70 mV to +60 mV caused no significant change in Rh 123 signal. A step to 0 mV caused a small but significant (~20%) increase in signal which was due to the mitochondrial response to a rise in $[Ca^{2+}]_i$ and consequent mitochondrial Ca^{2+} uptake. Although a redistribution of mitochondrial dye might be expected on depolarisation of the plasma membrane, it seems there is little change in fluorescence signal once the dye is quenched, possibly because a substantial reduction in $\Delta\psi_m$ is necessary before a change in fluorescence is seen (see Figure 9.1). Additionally, application of 50 mM K^+ to fura-2 loaded cells evoked no change in fluorescence (data not shown) suggesting, in agreement with other studies (Sontheimer, 1994; Carmignoto, Pasti & Pozzan, 1998), that rat cortical astrocytes in culture are not excitable cells. Although there is evidence of voltage operated Ca^{2+} channels expressed in astrocytes in some culture conditions, (MacVicar, Hochman, Delay & Weiss, 1991) no voltage-gated Ca^{2+} influx was ever seen in

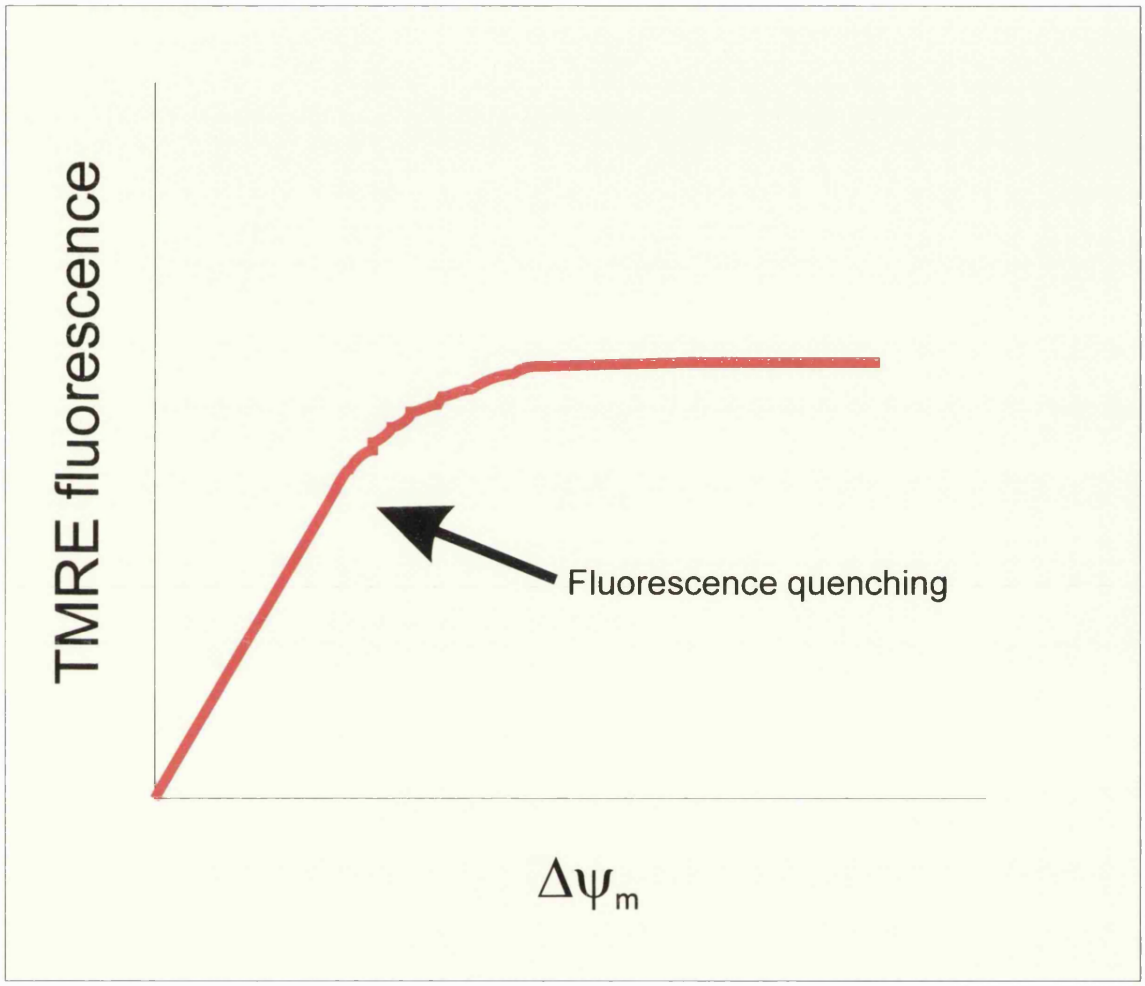

Figure 9.1: TMRE fluorescence is not linearly related to $\Delta\psi_m$. Fluorescence quenching occurs (arrowed) at an unknown $\Delta\psi_m$, thus calibration of the TMRE signal was not performed.

the cells studied for this thesis. Thus the plasma membrane potential was likely to have remained stable under the experimental conditions employed for this thesis.

No attempt has been made to calibrate the TMRE fluorescence against $\Delta\psi_m$ for a number of reasons. Firstly, the majority of experiments were carried out using CCD cameras. The fluorescence from out of focus layers of the cell confounds selective analysis of the signal over tiny organelles such as mitochondria that may comprise only a fraction of the volume of tissue that is imaged, and calibration would require laborious estimation of the signal derived from these out of focus organelles and cytosol (Ubl, Chatton, Chen & Stucki, 1996). Secondly, any non-specific binding of dye to cell structures results in deviations from Nernstian behaviour rendering calibration by the Nernst equation inaccurate. Scaduto and Grotyohann studied the binding of TMRE loaded into isolated mitochondria and found that significant quantities of the probe bound when compared with the non-fluorescent ion, tetraphenylphosphonium (Scaduto & Grotyohann, 1999). Although TMRE fluorescence still sensitively reported changes in $\Delta\psi_m$, calibration by straightforward application of the Nernst equation was not possible. Finally, as knowledge of the precise $\Delta\psi_m$ was not necessary for the detection of transient flickerings of the MPT pore, no calibration was performed.

Importantly, TMRE fluorescence does not vary linearly with $\Delta\psi_m$, as quenching of the fluorescence above a threshold $[TMRE]_{mit}$ implies that with increasing $\Delta\psi_m$ more dye may be electrophoretically accumulated without a proportional rise in fluorescence. That is, once the plateau is reached, where the curve becomes non-linear and quenching begins (see Figure 9.1) a change in $\Delta\psi_m$ may not be signalled by a detectable change in fluorescence. Furthermore, total $[TMRE]_{mit}$ will vary with the concentration gradients from mitochondrion to cytosol, other organelles, and the extracellular space and these in turn may vary due to dye binding and charge distribution across membranes. Nevertheless, qualitative indications of MPT pore opening are readily available, as the data in this thesis attest.

Imaging of TMRE-loaded cells revealed mitochondrial depolarisations

Digital imaging of TMRE-loaded astrocytes revealed spontaneous fluctuations in the TMRE signal measured over individual mitochondria. Confocal imaging of cells established that the fluctuations in TMRE signal were not merely movement of dye-loaded mitochondria out of the plane of focus, as clearly mobile mitochondria were seen, but these did not exhibit the same sudden dequench in TMRE fluorescence and tended to move out of the optical slice during imaging. Mitochondria that remained static within the 1 μm optical slice were frequently seen to flicker. Moreover, differentiation of the digital images revealed that the flickers were associated with marked movement of TMRE into the adjacent cytosol as the cationic dye redistributed on dissipation of $\Delta\psi_m$ (see Figure 4.4). Thus the fluctuations in TMRE signal reflected fluctuations in $\Delta\psi_m$ within living cells.

The amplitude of the flickers was compared with the signal change seen on complete mitochondrial depolarisation with FCCP. The mean flicker amplitude was 39 ± 17% of maximal, and this, in conjunction with the fact that single mitochondria were seen to depolarise and then repolarise several times in sequence suggests that the flickers were not the result of non-specific damage to mitochondrial integrity, but rather were reversible depolarisations of intact organelles. Imaging mitochondrial flickers at around 30 Hz established that the mean time to peak for the transient depolarisations was ~ 260 msec, although a substantial population of transients reached a peak in ~ 150 msec (see Figure 4.7). The high frequency and rapidity of the depolarisations, together with the observation that the global (whole cell) fluorescence tended to rise after several seconds of imaging, meant that quantitation of the events was difficult. Consequently 2 approaches were adopted:

1. The calculation of the 'index of variation' served to compare fluorescence changes from baseline during imaging. The mean fluorescence change from a digital baseline was taken to reflect the relative 'activity' of the TMRE-loaded mitochondria. A quiescent cell, where no transient depolarisations occurred, would therefore have an index of variation of 1. Care had to be taken that there was minimal rise in global fluorescence in cells treated in this way, as any rise in fluorescence, whether over mitochondria or not, would influence

the calculation. For this reason the cell nucleus was excluded from the region of interest, as a rise in fluorescence over the nucleus was nearly always noted due to movement of dye into the nucleus following egress from mitochondria. As the index of variation is a numerical calculation based on average fluorescence rise from a baseline, this approach does not distinguish between cells where there have been many small depolarisations and cells where there have been fewer, but larger, depolarisations. The mean change in signal from baseline in these two cases could well be similar. For this reason, care has been taken not to refer to the 'frequency' of depolarisation, merely to the 'index of variation'. However, using this method of assessing the amount of mitochondrial flicker, the indices of variation strongly reflected the subjective observation of 'active' and 'quiescent' cells.

2. As the data in Chapter 4 established, if imaging was prolonged, the flickering transients progressed until a global fluorescence plateau was reached. As the addition of FCCP at this point elicited no further change in TMRE signal, it was clear that the global mitochondrial depolarisation was complete. The time taken to reach this plateau therefore reflected the rate of progression from transient to complete depolarisation and thus could be viewed as a summation of the distinct events (reminiscent of the 'ensemble behaviour' seen in isolated mitochondria undergoing repeated openings of the MPT pore (Hüser *et al.*, 1998)).

Mitochondrial flickering and Ca^{2+} uptake

As mitochondrial Ca^{2+} uptake is an electrogenic process (Duchen, 1992; Boitier *et al.*, 1999), I looked to see whether the transient depolarisations were simply the result of mitochondrial accumulation of cytosolic Ca^{2+}. The fact that stored Ca^{2+} was necessary for the depolarisations was demonstrated by the combined effect of the SERCA pump inhibitor, thapsigargin, together with BAPTA (see Figure 5.7). The observation that loading the cells with 10 μM BAPTA did not alter the index of variation but did slow the progression to a global dissipation of $\Delta\psi_m$ was intriguing. Evidently, $[Ca^{2+}]_i$ was influencing the rate of the depolarisations, but sufficient Ca^{2+} was available to maintain the transient flickers at a

constitutive frequency. As cytosolic [Ca^{2+}] rarely exceeds 1 μM, the loading of cells in 10 μM BAPTA-AM ought to have been sufficient to chelate $[Ca^{2+}]_{cyt}$, especially as concentration within the cell of the BAPTA free acid may result in a $[BAPTA]_i$ which is in excess of 10 μM (Kao, 1994). However as the concentration of Ca^{2+} within the ER may be even higher, presumably sufficient stored Ca^{2+} was available to maintain a 'constitutive' flicker, even in the presence of BAPTA. A variety of values for $[Ca^{2+}]_{ER}$ have been proposed (for reviews see Meldolesi & Pozzan, 1998 and Bygrave & Benedetti, 1996) and depending upon the techniques used and the cells studied, estimates range from 5 μM (Short, Klein, Schneider & Gill, 1993) to 5 mM (Chen *et al.*, 1996). Recent work using the new generation of 'cameleon' probes targeted to HeLa cell ER suggested that the $[Ca^{2+}]_{ER}$ in these cells is around 400 μM (Miyawaki *et al.*, 1997). BAPTA is a fast Ca^{2+} chelator (Tsien, 1980) and it is likely that local cytosolic Ca^{2+} transients were effectively buffered, indeed the data shown in Figure 5.2 suggests that this was the case, however sufficient stored Ca^{2+} remained to permit MPT.

As chelation of $[Ca^{2+}]_{cyt}$ alone did not prevent the mitochondrial flicker, but a combination of depletion of $[Ca^{2+}]_{ER}$, together with BAPTA, did significantly reduce the depolarisations, it seemed that mitochondria could be loaded with Ca^{2+} from internal stores via a route that avoided the cytosol. This observation is supported by the work of Rizzuto and others, who have seen extremely close apposition of mitochondria and ER in HeLa cells transfected with the Ca^{2+} indicator aequorin (Rizzuto *et al.*, 1993), and have also shown, using mitochondrially-targeted green fluorescent protein targeted to the mitochondrial inner membrane, that mitochondria in these cells are highly responsive to ER Ca^{2+} release (Rizzuto *et al.*, 1998). Additionally, close spatial and functional relationships between mitochondria and ER in astrocytes were observed by Simpson et al (Simpson, Mehotra, Langley, Sheppard & Russell, 1998) who saw a significant correlation between sites of Ca^{2+} wave regeneration and the location of mitochondria in these cells. Immunocytochemical staining revealed a close correlation between location of mitochondria and sites of expression of the ER Ca^{2+}-binding protein, calreticulin. The data presented in Chapter 5 indicate Ca^{2+} release from ER stores may be extremely spatially restricted. In particular, mitochondrial Ca^{2+} transients were identified that occurred in isolation from Ca^{2+} changes in cytosol measured less than 1 μm

distant (Figures 5.13, 5.14 and 5.15). Taken together, these observations suggest that stored Ca^{2+} was necessary for the mitochondrial flicker and that in some cells there may be privileged routes of Ca^{2+} movement between ER and mitochondria.

However, confocal imaging of cells loaded with both TMRE and the Ca^{2+}-indicator, fluo-3 did not reveal a 1:1 relationship between ER Ca^{2+}-release and mitochondrial depolarisation, suggesting that the depolarisations may not be entirely due to electrogenic uptake of the Ca^{2+} ion by mitochondria. Although some images were obtained of depolarisations that were spatially and temporally associated with Ca^{2+} transients (see Figure 5.14), there were many events that could not be associated (Figure 5.16). There are several possible explanations for this lack of correlation between ER Ca^{2+} release and mitochondrial depolarisation. Firstly, as high spatial resolution was required for these experiments, temporal resolution was compromised and the images were acquired at the relatively low rate of ~1 Hz. The data presented in Chapter 4 confirm that the average TMRE flicker reached a peak in ~260 msec and that the mean τ for the decay was ~183 msec, thus mitochondrial flickers could be complete within a second (an example is shown in Figure 4.8) and it is feasible that flickers occurred that were not detected when imaging at this rate. Moreover, Ca^{2+} transients may be extremely rapid indeed, mathematical models of Ca^{2+} spark dynamics modelled in cardiac muscle cells suggest a time to peak of a few hundred microseconds (Soeller & Cannell, 1997), and imaging of fluo-3 loaded cardiomyocytes confirms that some signals last only ~ 40 msec (Gordienko, Bolton & Cannell, 1998). These experiments utilised the much faster line-scan mode of confocal imaging and it may be that to adequately detect such short-lived events most spatial resolution must be exchanged for temporal resolution.

Secondly, the properties of the Ca^{2+} indicator, fluo-3, may not have been ideal for the detection of tiny, highly localised Ca^{2+} transients. Fluo-3 is essentially non-fluorescent until bound to Ca^{2+}, when the probe reportedly undergoes up to a 100-fold enhancement of fluorescence (Molecular Probes website). In practice, however, the signal to noise ratio can be low, and small events may be lost in the background noise. Harkins et al found substantial binding of fluo-3 to intracellular proteins, an observation that may also account for a large shift

in the Ca^{2+} affinity of the dye (Harkins, Kurebayashi & Baylor, 1993). The same group reported that the published K_D for fluo-3 (390 nM; Haugland, 1996) may not be accurate when the dye is loaded into living cells as they found that the K_D could be in excess of 1 μM (2.57 μM in one of their experiments) in frog skeletal muscle fibres. However, other groups have successfully used imaging of fluo-3 loaded cells to study minute Ca^{2+} events (Lipp & Niggli, 1998). A new fluo-3 analogue, fluo-4, has recently been synthesised that may be more suitable for confocal imaging of small Ca^{2+} transients. Fluo-4 has a slightly lower claimed K_D (345 nM in vitro), however the main advantage is likely to be a slight shift in the excitation peak of the dye, resulting in increased fluorescence excitation at 488 nm and consequently higher signal levels for confocal laser scanning microscopy. It is possible that improving the signal to noise ratio in these experiments may reveal Ca^{2+} transients that were invisible using the conditions described in Chapter 5.

Finally, the inability to detect a 1:1 relationship between ER Ca^{2+} release and a change in TMRE fluorescence may simply reflect a lack of such a relationship! While mitochondrial Ca^{2+} uptake is an electrogenic process, it is possible that the consequent depolarisations were so small, or the repolarisation so rapid, that a small drop in $\Delta\psi_m$ was undetectable using the imaging setup as described. Moreover, as TMRE fluorescence is not linear with $\Delta\psi_m$, the TMRE transients may only have signalled substantial depolarisations after accumulation of several aliquots of Ca^{2+}. Certainly, it was possible to image Ca^{2+} transients that were not associated with a dissipation of $\Delta\psi_m$ (see Figure 5.15C and 5.16). In view of the finding that the flickerings signalled MPT, it is likely that a threshold of $[Ca^{2+}]_{mit}$ was required before pore opening. Thus several Ca^{2+} transients may have occurred, loading mitochondria with Ca^{2+}, but no dissipation of $\Delta\psi_m$ occurred until $[Ca^{2+}]_{mit}$ was sufficient to trigger pore opening, reminiscent of similar findings in isolated mitochondria (Vercesi, Ferraz, Macedo & Fiskum, 1988).

The mitochondrial flickerings reflected transient permeability transition

Pharmacological inhibitors of the MPT attenuated the depolarisations. The classical MPT inhibitor, cyclosporin A and its analogue, N methyl 4 valine cyclosporin, which does not bind

calcineurin, significantly reduced the time to global depolarisation and the incidence of mitochondrial flickers, respectively. Moreover, treatment with trifluoperazine, which probably inhibits the MPT by a separate mechanism (Pereira *et al.*, 1992; Broekemeier & Pfeiffer, 1995) slowed the progression to global mitochondrial depolarisation. Involvement of the MPT pore was confirmed by experiments using myocytes in which the expression of the mitochondrial cyclophilin, Cyp D, had been suppressed. Cyp D sensitises pore formation and is associated with other proteins that form the pore (Crompton *et al.*, 1998) particularly during oxidative stress (Halestrap, Woodfield & Connern, 1997). Thus the flickers of TMRE fluorescence reflected transient mitochondrial depolarisations caused by flickering of the MPT pore – flickerings which were sensitised by a combination of mitochondrial oxidative stress (discussed below) and Ca^{2+} overload.

A physiological role for the MPT is elusive. Sustained, full opening of the MPT pore would be expected to be disastrous for the cell. Not only does ATP synthesis stop, but the conversion of the ATP synthase to an ATPase will accelerate ATP depletion in many cells (Leyssens *et al.*, 1996). Additionally, the recently discovered involvement of MPT in apoptotic signalling events seems to suggest a pathophysiological role for the phenomenon. However, there is evidence that subconductance states of the MPT pore may play a role in mitochondrial $[Ca^{2+}]$ homeostasis (Bernardi & Petronilli, 1996), perhaps suggesting that sustained opening of the pore in its full conductance state is required to trigger cell death.

The data presented in this thesis add to the body of evidence that suggests that MPT pore opening may not be an all-or-nothing catastrophic event. Flickering of the MPT pore was first identified in 1979 by Hunter and Haworth who noticed that Ca^{2+}-induced permeability was discontinuous, suggesting a constant switching form the permeable to the impermeable state (Hunter & Haworth, 1979b). Patch clamping of mitoplast membranes revealed that the MPT pore may operate in subconductance states (Kinnally, Campo & Tedeschi, 1989; Zoratti & Szabó, 1994), flickering from fully open to an intermediate subconductance, typically around half of the full 1.3 nS value. Although the dynamics of TMRE dequench are complex, it is noteworthy that the mean time to peak of the flickers was 260 msec with a large

subpopulation which reached a peak at around half this time, ~ 150 msec. Zoratti has postulated that stepwise dissipations of the $\Delta\psi_m$ may move the open probability of the pore away from subconductance states towards a fully open state (Zoratti & Szabó, 1994). Novgorodov has suggested that a subconductance of the pore provides an efflux for protons only, and that oxidation of mitochondrial redox couples converts the closed pore to this subconductance state (Novgorodov & Gudz, 1996). Transition to the fully open state would require mitochondrial Ca^{2+} loading. Low conductance of the pore has been evoked as a Ca^{2+} efflux pathway (Ichas *et al.*, 1997; Ichas & Mazat, 1998) and transient openings of the pore have been observed in living hepatocytes (Petronilli *et al.*, 1999).

Mitochondrial flickering and generation of ROS

The model of MPT described in this thesis makes deliberate use of two properties of the fluorescent, potentiometric dye TMRE. The fluorescence of the dye reflects $\Delta\psi_m$, and thus it may be used to signal mitochondrial depolariations. Additionally, TMRE will generate ROS when illuminated (Bunting, 1992; Hüser *et al.*, 1998). As the MPT has a well-characterised sensitivity to mitochondrial redox state (Zoratti & Szabò, 1995), pro-oxidants have been used to impose oxidative stress and initiate pore opening in several models. Lemasters's group have added *tert*-butylhydroperoxide to hepatocytes loaded with the fluorescent probe calcein (normally excluded from mitochondria), and observed mitochondrial uptake of calcein which was inhibited by the MPT inhibitor, trifluoperazine (Nieminen *et al.*, 1995), Crompton and Costi found that addition of *tert*-butylhydroperoxide to isolated mitochondria, in the presence of Ca^{2+}, opened the pore (Crompton & Costi, 1988), and Bernardi's group have found that oxidation of critical mitochondrial membrane thiol groups by a variety of oxidants led to an increased probability of pore opening (Petronilli *et al.*, 1994). The sensitivity of the MPT to raised $[Ca^{2+}]$ in combination with oxidative stress has prompted the suggestion that the phenomenon may be central to tissue injury after ischaemia/reperfusion, a condition in which both raised $[Ca^{2+}]_{cyt}$ and oxidative stress are manifest (Halestrap, 1999). Halestrap's group have shown in Langendorff-perfused hearts that inducing a reperfusion injury permits mitochondrial loading of [^{3}H]2-deoxyglucose 6-phosphate (DOG 6-phosphate), normally excluded from mitochondria but taken up on pore opening (Griffiths & Halestrap, 1995). Some

protection was provided by cyclosporin A in these experiments, but the effect of the compound was found to be highly concentration-dependent (Halestrap *et al.*, 1998).

Mitochondria are major producers of ROS and are thought to contribute to the oxidative stress associated with neurodegenerative disorders (Schapira, 1998), ageing (Armeni *et al.*, 1997; Lenaz, 1998) and sepsis (Armeni *et al.*, 1997), as well as reperfusion injury (although activation of xanthine oxidase is also important in the latter (Nishino *et al.*, 1997)). However, in experiments modelling mitochondrial generation of ROS, oxidative stress is frequently simulated by addition of exogenous pro-oxidants (Nieminen *et al.*, 1995; Lemasters *et al.*, 1997; Meinicke, Bechara & Vercesi, 1998), and as these highly reactive compounds may have a range of toxic effects throughout the cell (for reviews see (Kourie, 1998) and (Phillis, 1994)) the ensuing reactions may not exactly replicate the cell damage caused by mitochondrial generation of ROS. Additionally, cellular antioxidant defences are not distributed uniformly, mitochondria contain a unique manganese superoxide dismutase, exclude catalase and there are high levels of glutathione transferase, which has peroxidative activity, expressed in astrocyte mitochondrial membranes (Peuchen *et al.*, 1997). Thus responses to ROS may vary in different sub-cellular compartments. In this model, I have specifically induced ROS generation within mitochondria by using TMRE, localised to mitochondria, as the ROS generator.

ROS have been shown to modulate the gating of ion channels, in particular ryanodine sensitive Ca^{2+} channels in the ER (Kaminishi & Kako, 1989; Boraso & Williams, 1994; Eager, Roden & Dulhunty, 1997; Suzuki, Cleemann, Abernethy & Morad, 1998). Data indicating ROS modulation of IP_3-mediated Ca^{2+} channels is less abundant, however oxidised glutathione (Henschke & Elliott, 1995) and ROS derived from xanthine/xanthine oxidase (Wesson & Elliott, 1995) have been shown to induce Ca^{2+}-release from IP_3-mediated stores in endothelial cells and superoxide may stimulate IP_3-mediated Ca^{2+} release in vascular smooth muscle cells (Suzuki & Ford, 1992). Astrocyte Ca^{2+} stores are predominantly IP_3-mediated (Langley & Pearce, 1994; Nadal *et al.*, 1997), however, as ryanodine-sensitive Ca^{2+} stores may be

expressed in these cells, (Figure 5.11), ROS-induced Ca^{2+} release via ryanodine receptors cannot be excluded. Nevertheless, responses to ATP, an agonist of IP_3 mediated Ca^{2+} release, were far more reliable and robust than those to ryanodine (Table 5.1), suggesting that only a sub-population of these astrocytes expressed ryanodine receptors. Mitochondrial flickering was not restricted to a sub-population and this in turn suggests ROS may have modulated both ryanodine- and IP_3- sensitive Ca^{2+} stores in this model.

In this model of MPT formation in cortical astrocytes, both chelation of stored Ca^{2+} and treatment with antioxidants independently attenuated the pore opening, thus it seems clear that an interplay between mitochondrial ROS generation and Ca^{2+} release from intracellular stores is necessary for MPT in these cells. It is possible, therefore, that ROS, generated from within the mitochondria, caused Ca^{2+} release from closely apposed ER, that the released Ca^{2+} was taken up by the mitochondria and the combination of oxidative stress and mitochondrial Ca^{2+} loading was sufficient to trigger MPT (Figure 9.2).

Mitochondrial flickering and cell death

A great deal of work has focussed recently on the relationships between MPT, mitochondrial depolarisation, and the initiation of apoptotic cell death pathways (Liu *et al.*, 1996; Kroemer *et al.*, 1998; Crompton, 1999; Shimizu *et al.*, 1999). In particular, the discovery that mitochondria may release pro-apoptotic signalling factors (cytochrome c and apoptosis inducing factor) has linked the phenomenon of MPT to apoptotic signalling. Cytochrome c, the sole water-soluble cytochrome, shuttles electrons between the Complexes III and IV, and thus is tightly bound to neither. It is held electrostatically on the outer surface of the inner membrane and requires the integrity of the outer mitochondrial membrane to remain within the intermembrane space (Crompton, 1999). The disruption of the outer mitochondrial membrane facilitates the release of cytochrome c and as MPT causes mitochondrial swelling, the two events have been linked. The osmotic shock that mitochondria undergo on permeability transition causes matrix swelling, and due to the large size of the folded inner membrane, the outer membrane ruptures, releasing the intermembrane space contents (Kroemer, 1999). This mechanical disruption may explain how the opening of a pore with a cut-off of ~1500 Da may allow the

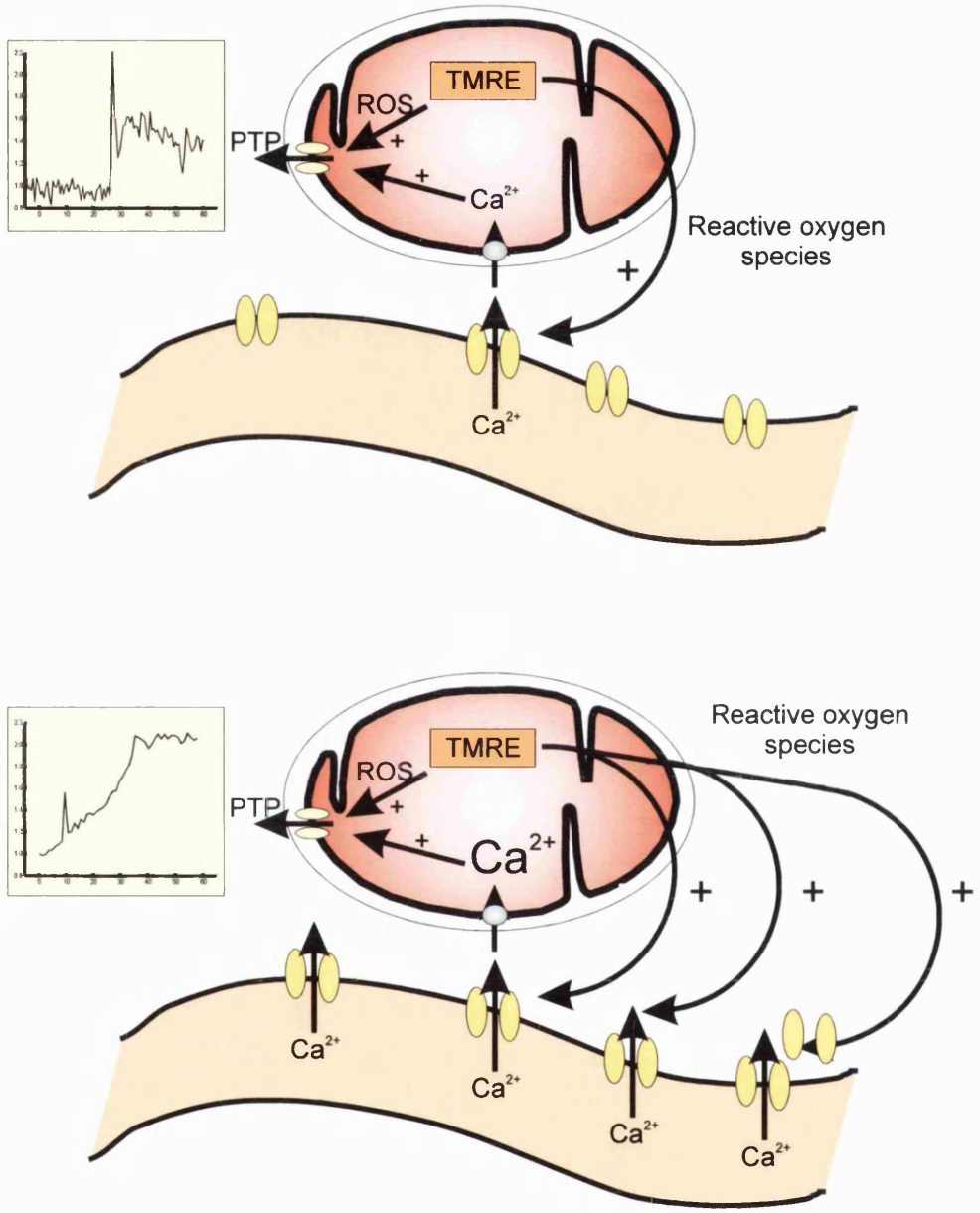

Figure 9.2: model for ROS-induced PTP opening. In the upper panel, the ROS production is minimal, perhaps sufficient to sensitise Ca2+-release from only those ER Ca2+ channels that are directly apposed to the mitochondrion. In this case, there are occasional mitochondrial flickers, and loading the cytosol with BAPTA does not attenuate these pore openings. With more illumination, however, more Ca^{2+} channels are oxidised causing efflux of Ca^{2+} into the cytosol surrounding the mitochondrion and this Ca^{2+} load, together with the large mitochondrial ROS production, results in longer-lived pore openings and a global rise in TMRE signal. In the latter case, cytosolic Ca^{2+}-chelation by BAPTA slowed the onset of global mitochondrial depolarisation.

egress of cytochrome c, a protein weighing ~12,300 Da. Dissipation of $\Delta\psi_m$ is associated with apoptosis in a number of different cell types and appears to be independent of the apoptotic inducer (Kroemer *et al.*, 1998). Collapse of $\Delta\psi_m$ is frequently an early event in apoptosis, and Kroemer's group have found that in cells treated with pro-apoptotic stimuli where mitochondria have depolarised, apoptosis will ensue, even if the apoptotic stimulus is withdrawn (Zamzami *et al.*, 1995). These findings suggest that mitochondrial depolarisation is an early, irreversible event in apoptosis. Furthermore, the anti-apoptotic protein, Bcl-2 has been shown to inhibit cytochrome c release in a cell-free system (Kluck *et al.*, 1997) and some inhibitors of MPT have been shown to inhibit apoptosis (Petit, Susin, Zamzami, Mignotte & Kroemer, 1996).

Nevertheless, it seems paradoxical that apoptosis, an ATP-dependent process (Yasuhara *et al.*, 1997) requires, or is triggered by, an event that ought to result in ATP depletion. Bossy-Wetzel has shown that cytochrome c release may be detected in an apoptotic T lymphoblastoid cell line *before* a dissipation in $\Delta\psi_m$ (Bossy-Wetzel *et al.*, 1998). However, it is noteworthy that the $\Delta\psi_m$ in this case was assayed by fluorescence flow cytometry and therefore it remains possible that a sub-population of the mitochondria did undergo MPT, triggering cytochrome c release sufficient to be detectable by immunoblot analysis. An alternative explanation is that some MPT occurred in these cells, but only temporarily – the pore may have flickered. Asynchronous mitochondrial depolarisation need not be detected by flow cytometry, where thousands of cells are being assayed at once. Recent work where individual cells were examined by confocal microscopy has revealed that Ca^{2+} pulses from IP_3-mediated stores may induce MPT in HepG2 cells when the cells were exposed to pro-apoptotic stimuli (Szalai *et al.*, 1999). The $\Delta\psi_m$ dissipation in this case was transient, and the MPT reversed, however cytochrome c was released into the cytosol and there was an increased incidence of apoptosis after 90 minutes. These data led the authors to conclude that flickering MPT may still induce apoptotic cell death, but that the resealing of the pore might allow continued ATP production. However, although statistically significant, the increase in apoptotic death was remarkably small (8% of the stimulated cells died as compared with

3% controls), which suggests that in excess of 90% of the cells which had received pro-apoptotic/pro-MPT stimuli had survived at 90 minutes.

The data presented in Chapter 8 of this thesis reveal that cells in which flickering MPT had been imaged for 90 seconds did not show an increase in either necrotic or apoptotic death after 4 hours. The excessive oxidative stress imposed on the cells which had progressed to a global mitochondrial depolarisation did lead to cell death, but necrotic, not apoptotic. The prolonged dissipation of $\Delta\psi_m$ in this group is likely to have led to global depletion of [ATP] and thus cell death by a necrotic pathway. However, the survival of the cells where MPT merely flickered suggests that in living cells, transient MPT is not an obligate precursor to cell death, necrotic or apoptotic. This finding, in turn, reprises the question as to the 'purpose' of the MPT pore; is there a physiological role, distinct from the facilitation of cytochrome c release, for the pore?

References

Al-Nasser, I. & Crompton, M. (1986). The reversible Ca2+-induced permeabilization of rat liver mitochondria. *Biochemical Journal,* **239**, 19-29.

Antonsson, B., Conti, F., Ciavatta, A., Montessuit, S., Lewis, S., Martinou, I., Bernasconi, L., Bernard, A., Mermod, J. J., Mazzei, G., Maundrell, K., Gambale, F., Sadoul, R. & Martinou, J. C. (1997). Inhibition of Bax channel-forming activity by Bcl-2. *Science,* **277**, 370-2.

Antunes, F., Salvador, A., Marinho, H. S., Alves, R. & Pinto, R. E. (1996). Lipid peroxidation in mitochondrial inner membranes. I. An integrative kinetic model. *Free Radical Biology And Medicine,* **21**, 917-43.

Armeni, T., Tomasetti, M., Svegliati Baroni, S., Saccucci, F., Marra, M., Pieri, C., Littarru, G. P., Principato, G. & Battino, M. (1997). Dietary restriction affects antioxidant levels in rat liver mitochondria during ageing. *Molecular Aspects Of Medicine,* **18 Suppl**, S247-50.

Babcock, D. F., Herrington, J., Goodwin, P. C., Park, Y. B. & Hille, B. (1997). Mitochondrial participation in the intracellular Ca2+ network. *Journal Of Cell Biology,* **136**, 833-44.

Beal, M. F., Howell, N. & Bodis-Wollner, I. (1997). *Mitochondria and Free Radicals in Neurodegenerative Disease*. New York: Wiley-Liss.

Bedner, E., Li, X., Gorczyca, W., Melamed, M. R. & Darzynkiewicz, Z. (1999). Analysis of apoptosis by laser scanning cytometry. *Cytometry,* **35**, 181-95.

Behl, C., Davis, J. B., Lesley, R. & Schubert, D. (1994). Hydrogen peroxide mediates amyloid beta protein toxicity. *Cell,* **77**, 817-27.

Bennett, P. C., Singaretnam, L. G., Zhao, W. Q., Lawen, A. & Ng, K. T. (1998). Peptidyl-prolyl-cis/trans-isomerase activity may be necessary for memory formation. *Febs Letters,* **431**, 386-90.

Bernardi, P. & Petronilli, V. (1996). The permeability transition pore as a mitochondrial calcium release channel: a critical appraisal. *Journal Of Bioenergetics And Biomembranes,* **28**, 131-8.

Bernardi, P., Scorrano, L., Colonna, R., Petronilli, V. & Di Lisa, F. (1999). Mitochondria and cell death. Mechanistic aspects and methodological issues. *European Journal Of Biochemistry,* **264**, 687-701.

Berridge, M. J. (1997). Elementary and global aspects of calcium signalling. *Journal Of Physiology,* **499 (Pt 2)**, 291-306.

Bezprozvanny, I., Watras, J. & Ehrlich, B. E. (1991). Bell-shaped calcium-response curves of Ins(1,4,5)P3- and calcium-gated channels from endoplasmic reticulum of cerebellum. *Nature,* **351**, 751-4.

Bhatnagar, A., Srivastava, S. K. & Szabo, G. (1990). Oxidative stress alters specific membrane currents in isolated cardiac myocytes. *Circulation Research,* **67**, 535-49.

Boitier, E., Rea, R. & Duchen, M. R. (1999). Mitochondria exert a negative feedback on the propagation of intracellular Ca2+ waves in rat cortical astrocytes. *Journal Of Cell Biology,* **145**, 795-808.

Boraso, A. & Williams, A. J. (1994). Modification of the gating of the cardiac sarcoplasmic reticulum Ca(2+)-release channel by H2O2 and dithiothreitol. *American Journal Of Physiology,* **267**, H1010-6.

Bossy-Wetzel, E., Newmeyer, D. D. & Green, D. R. (1998). Mitochondrial cytochrome c release in apoptosis occurs upstream of DEVD-specific caspase activation and independently of mitochondrial transmembrane depolarization. *Embo Journal,* **17**, 37-49.

Bradham, C. A., Qian, T., Streetz, K., Trautwein, C., Brenner, D. A. & Lemasters, J. J. (1998). The mitochondrial permeability transition is required for tumor necrosis factor alpha-mediated apoptosis and cytochrome c release. *Molecular And Cellular Biology,* **18**, 6353-64.

Brisseau, G. F., Tsai, O., Nordström, T., Marshall, J. C., Grinstein, S. & Rotstein, O. D. (1994). Oxidant stress inhibits pH regulatory mechanisms in murine peritoneal macrophages. *Surgery,* **116**, 268-74; discussion 274-5.

Broekemeier, K. M. & Pfeiffer, D. R. (1995). Inhibition of the mitochondrial permeability transition by cyclosporin A during long time frame experiments: relationship between

pore opening and the activity of mitochondrial phospholipases. *Biochemistry,* **34**, 16440-9.

Broekemeier, K. M., Schmid, P. C., Schmid, H. H. & Pfeiffer, D. R. (1985). Effects of phospholipase A2 inhibitors on ruthenium red-induced Ca2+ release from mitochondria. *Journal Of Biological Chemistry,* **260**, 105-13.

Bunting, J. R. (1992). A test of the singlet oxygen mechanism of cationic dye photosensitization of mitochondrial damage. *Photochemistry And Photobiology,* **55**, 81-7.

Bygrave, F. L. & Benedetti, A. (1996). What is the concentration of calcium ions in the endoplasmic reticulum? *Cell Calcium,* **19**, 547-51.

Carafoli, E. (1987). Intracellular calcium homeostasis. *Annual Review Of Biochemistry,* **56**, 395-433.

Carmignoto, G., Pasti, L. & Pozzan, T. (1998). On the role of voltage-dependent calcium channels in calcium signaling of astrocytes in situ. *Journal Of Neuroscience,* **18**, 4637-45.

Cerbai, E., Ambrosio, G., Porciatti, F., Chiariello, M., Giotti, A. & Mugelli, A. (1991). Cellular electrophysiological basis for oxygen radical-induced arrhythmias. A patch-clamp study in guinea pig ventricular myocytes. *Circulation,* **84**, 1773-82.

Chamberlain, B. K., Volpe, P. & Fleischer, S. (1984). Inhibition of calcium-induced calcium release from purified cardiac sarcoplasmic reticulum vesicles. *Journal Of Biological Chemistry,* **259**, 7547-53.

Chance, B., Sies, H. & Boveris, A. (1979). Hydroperoxide metabolism in mammalian organs. *Physiological Reviews,* **59**, 527-605.

Chen, W., Steenbergen, C., Levy, L. A., Vance, J., London, R. E. & Murphy, E. (1996). Measurement of free Ca2+ in sarcoplasmic reticulum in perfused rabbit heart loaded with 1,2-bis(2-amino-5,6-difluorophenoxy)ethane-N,N,N',N'-tetraacetic acid by 19F NMR. *Journal Of Biological Chemistry,* **271**, 7398-403.

Crompton, M. (1999). The mitochondrial permeability transition pore and its role in cell death. *Biochemical Journal,* **341 (Pt 2)**, 233-49.

Crompton, M. & Costi, A. (1988). Kinetic evidence for a heart mitochondrial pore activated by Ca2+, inorganic phosphate and oxidative stress. A potential mechanism for mitochondrial dysfunction during cellular Ca2+ overload. *European Journal Of Biochemistry,* **178**, 489-501.

Crompton, M., Ellinger, H. & Costi, A. (1988). Inhibition by cyclosporin A of a Ca2+-dependent pore in heart mitochondria activated by inorganic phosphate and oxidative stress. *Biochemical Journal,* **255**, 357-60.

Crompton, M., Virji, S. & Ward, J. M. (1998). Cyclophilin-D binds strongly to complexes of the voltage-dependent anion channel and the adenine nucleotide translocase to form the permeability transition pore. *European Journal Of Biochemistry,* **258**, 729-35.

Dedov, V. N. & Roufogalis, B. D. (1999). Organisation of mitochondria in living sensory neurons. *Febs Letters,* **456**, 171-4.

DeGracia, D. J., Sullivan, J. M., Neumar, R. W., Alousi, S. S., Hikade, K. R., Pittman, J. E., White, B. C., Rafols, J. A. & Krause, G. S. (1997). Effect of brain ischemia and reperfusion on the localization of phosphorylated eukaryotic initiation factor 2 alpha. *Journal Of Cerebral Blood Flow And Metabolism,* **17**, 1291-302.

Denton, R. M., McCormack, J. G., Rutter, G. A., Burnett, P., Edgell, N. J., Moule, S. K. & Diggle, T. A. (1996). The hormonal regulation of pyruvate dehydrogenase complex. *Advances In Enzyme Regulation,* **36**, 183-98.

Di Lisa, F., Blank, P. S., Colonna, R., Gambassi, G., Silverman, H. S., Stern, M. D. & Hansford, R. G. (1995). Mitochondrial membrane potential in single living adult rat cardiac myocytes exposed to anoxia or metabolic inhibition. *J-Physiol-Lond.,* **486**, 1-13.

Diaz, G., Setzu, M. D., Zucca, A., Isola, R., Diana, A., Murru, R., Sogos, V. & Gremo, F. (1999). Subcellular heterogeneity of mitochondrial membrane potential: relationship with organelle distribution and intercellular contacts in normal, hypoxic and apoptotic cells. *Journal Of Cell Science,* **112 (Pt 7)**, 1077-84.

Dolinski, K., Muir, S., Cardenas, M. & Heitman, J. (1997). All cyclophilins and FK506 binding proteins are, individually and collectively, dispensable for viability in Saccharomyces

cerevisiae. *Proceedings Of The National Academy Of Sciences Of The United States Of America,* **94**, 13093-8.

Dubinsky, J. M. & Levi, Y. (1998). Calcium-induced activation of the mitochondrial permeability transition in hippocampal neurons. *Journal Of Neuroscience Research,* **53**, 728-41.

Duchen, M. R. (1992). Ca(2+)-dependent changes in the mitochondrial energetics in single dissociated mouse sensory neurons. *Biochemical Journal,* **283 (Pt 1)**, 41-50.

Duchen, M. R. & Biscoe, T. J. (1992a). Mitochondrial function in type I cells isolated from rabbit arterial chemoreceptors. *Journal Of Physiology,* **450**, 13-31.

Duchen, M. R. & Biscoe, T. J. (1992b). Relative mitochondrial membrane potential and [Ca2+]i in type I cells isolated from the rabbit carotid body. *Journal Of Physiology,* **450**, 33-61.

Duchen, M. R., Leyssens, A. & Crompton, M. (1998). Transient mitochondrial depolarizations reflect focal sarcoplasmic reticular calcium release in single rat cardiomyocytes. *Journal Of Cell Biology,* **142**, 975-88.

Duprat, F., Guillemare, E., Romey, G., Fink, M., Lesage, F., Lazdunski, M. & Honore, E. (1995). Susceptibility of cloned K+ channels to reactive oxygen species. *Proceedings Of The National Academy Of Sciences Of The United States Of America,* **92**, 11796-800.

Eager, K. R., Roden, L. D. & Dulhunty, A. F. (1997). Actions of sulfhydryl reagents on single ryanodine receptor Ca(2+)-release channels from sheep myocardium. *American Journal Of Physiology,* **272**, C1908-18.

Ehrenberg, B., Montana, V., Wei, M. D., Wuskell, J. P. & Loew, L. M. (1988). Membrane potential can be determined in individual cells from the nernstian distribution of cationic dyes. *Biophysical Journal,* **53**, 785-94.

Emaus, R. K., Grunwald, R. & Lemasters, J. J. (1986). Rhodamine 123 as a probe of transmembrane potential in isolated rat-liver mitochondria: spectral and metabolic properties. *Biochimica Et Biophysica Acta,* **850**, 436-48.

Eriksson, O., Pollesello, P. & Geimonen, E. (1999). Regulation of total mitochondrial Ca2+ in perfused liver is independent of the permeability transition pore. *American Journal Of Physiology,* **276**, C1297-302.

Farkas, D. L., Wei, M. D., Febbroriello, P., Carson, J. H. & Loew, L. M. (1989). Simultaneous imaging of cell and mitochondrial membrane potentials [published erratum appears in Biophys J 1990 Mar;57(3):following 684]. *Biophysical Journal,* **56**, 1053-69.

Gallitelli, M. F., Schultz, M., Isenberg, G. & Rudolf, F. (1999). Twitch-potentiation increases calcium in peripheral more than in central mitochondria of guinea-pig ventricular myocytes. *Journal of Physiology,* **518**, 433 - 447.

Gordienko, D. V., Bolton, T. B. & Cannell, M. B. (1998). Variability in spontaneous subcellular calcium release in guinea-pig ileum smooth muscle cells. *Journal Of Physiology,* **507 (Pt 3)**, 707-20.

Griffiths, E. J. & Halestrap, A. P. (1995). Mitochondrial non-specific pores remain closed during cardiac ischaemia, but open upon reperfusion. *Biochemical Journal,* **307 (Pt 1)**, 93-8.

Griffiths-EJ. (1999). Species dependence of mitochondrial calcium transients during excitation-contraction coupling in isolated cardiomyocytes. *Biochem-Biophys-Res-Commun.,* **263**, 554 - 559.

Gunter, K. K. & Gunter, T. E. (1994). Transport of calcium by mitochondria. *Journal Of Bioenergetics And Biomembranes,* **26**, 471-85.

Gupta, M. P., Innes, I. R. & Dhalla, N. S. (1988). Responses of contractile function to ruthenium red in rat heart. *American Journal Of Physiology,* **255**, H1413-20.

Ha, T., Enderle, T., Ogletree, D. F., Chemla, D. S., Selvin, P. R. & Weiss, S. (1996). Probing the interaction between two single molecules: fluorescence resonance energy transfer between a single donor and a single acceptor. *Proceedings Of The National Academy Of Sciences Of The United States Of America,* **93**, 6264-8.

Hajnóczky, G., Hager, R. & Thomas, A. P. (1999). Mitochondria suppress local feedback activation of inositol 1,4, 5-trisphosphate receptors by Ca2+. *Journal Of Biological Chemistry,* **274**, 14157-62.

Hajnóczky, G., Robb-Gaspers, L. D., Seitz, M. B. & Thomas, A. P. (1995). Decoding of cytosolic calcium oscillations in the mitochondria. *Cell,* **82**, 415-24.

Halestrap, A. P. (1999). The mitochondrial permeability transition: its molecular mechanism and role in reperfusion injury. In G. C. Brown, Nicholls, D.G., Cooper, C.E. (Ed.), *Mitochondria and Cell Death* (pp. 181 - 203). London: Portland Press.

Halestrap, A. P. & Davidson, A. M. (1990). Inhibition of Ca2(+)-induced large-amplitude swelling of liver and heart mitochondria by cyclosporin is probably caused by the inhibitor binding to mitochondrial-matrix peptidyl-prolyl cis-trans isomerase and preventing it interacting with the adenine nucleotide translocase. *Biochemical Journal,* **268**, 153-60.

Halestrap, A. P., Kerr, P. M., Javadov, S. & Woodfield, K. Y. (1998). Elucidating the molecular mechanism of the permeability transition pore and its role in reperfusion injury of the heart. *Biochimica Et Biophysica Acta,* **1366**, 79-94.

Halestrap, A. P., Woodfield, K. Y. & Connern, C. P. (1997). Oxidative stress, thiol reagents, and membrane potential modulate the mitochondrial permeability transition by affecting nucleotide binding to the adenine nucleotide translocase. *Journal Of Biological Chemistry,* **272**, 3346-54.

Harkins, A. B., Kurebayashi, N. & Baylor, S. M. (1993). Resting myoplasmic free calcium in frog skeletal muscle fibers estimated with fluo-3 [see comments]. *Biophysical Journal,* **65**, 865-81.

Haugland, R. P. (1996a). Assaying Oxidative Activity in Live Cells and Tissue, *Handbook of Fluorescent Probes and Research Chemicals* (pp. 491 - 497). Leiden: Molecular Probes.

Haugland, R. P. (1996b). Indicators for Ca2+, Mg2+, Zn2+ and Other Metals, *Handbook of Fluorescent Probes and Research Chemicals* (pp. 505). Leiden: Molecular Probes.

Haworth, R. A. & Hunter, D. R. (1979). The Ca2+-induced membrane transition in mitochondria. II. Nature of the Ca2+ trigger site. *Archives Of Biochemistry And Biophysics,* **195**, 460-7.

Henschke, P. N. & Elliott, S. J. (1995). Oxidized glutathione decreases luminal Ca2+ content of the endothelial cell ins(1,4,5)P3-sensitive Ca2+ store. *Biochemical Journal,* **312 (Pt 2)**, 485-9.

Herrero, A. & Barja, G. (1997). ADP-regulation of mitochondrial free radical production is different with complex I- or complex II-linked substrates: implications for the exercise paradox and brain hypermetabolism. *Journal Of Bioenergetics And Biomembranes,* **29**, 241-9.

Hunter, D. R. & Haworth, R. A. (1979a). The Ca2+-induced membrane transition in mitochondria. I. The protective mechanisms. *Archives Of Biochemistry And Biophysics,* **195**, 453-9.

Hunter, D. R. & Haworth, R. A. (1979b). The Ca2+-induced membrane transition in mitochondria. III. Transitional Ca2+ release. *Archives Of Biochemistry And Biophysics,* **195**, 468-77.

Hüser, J., Rechenmacher, C. E. & Blatter, L. A. (1998). Imaging the permeability pore transition in single mitochondria. *Biophysical Journal,* **74**, 2129-37.

Ichas, F., Jouaville, L. S. & Mazat, J. P. (1997). Mitochondria are excitable organelles capable of generating and conveying electrical and calcium signals. *Cell,* **89**, 1145-53.

Ichas, F., Jouaville, L. S., Sidash, S. S., Mazat, J. P. & Holmuhamedov, E. L. (1994). Mitochondrial calcium spiking: a transduction mechanism based on calcium-induced permeability transition involved in cell calcium signalling. *Febs Letters,* **348**, 211-5.

Ichas, F. & Mazat, J. P. (1998). From calcium signaling to cell death: two conformations for the mitochondrial permeability transition pore. Switching from low- to high-conductance state. *Biochimica Et Biophysica Acta,* **1366**, 33-50.

Imberti, R., Nieminen, A. L., Herman, B. & Lemasters, J. J. (1992). Synergism of cyclosporin A and phospholipase inhibitors in protection against lethal injury to rat hepatocytes from oxidant chemicals. *Research Communications In Chemical Pathology And Pharmacology,* **78**, 27-38.

Jornot, L., Maechler, P., Wollheim, C. B. & Junod, A. F. (1999). Reactive oxygen metabolites increase mitochondrial calcium in endothelial cells: implication of the Ca2+/Na+ exchanger. *Journal Of Cell Science,* **112 (Pt 7)**, 1013-22.

Jouaville, L. S., Ichas, F., Holmuhamedov, E. L., Camacho, P. & Lechleiter, J. D. (1995). Synchronization of calcium waves by mitochondrial substrates in Xenopus laevis oocytes. *Nature,* **377**, 438-41.

Jouaville, L. S., Ichas, F. & Mazat, J. P. (1998). Modulation of cell calcium signals by mitochondria. *Molecular And Cellular Biochemistry,* **184**, 371-6.

Kaftan, E. J., Ehrlich, B. E. & Watras, J. (1997). Inositol 1,4,5-trisphosphate (InsP3) and calcium interact to increase the dynamic range of InsP3 receptor-dependent calcium signaling. *Journal Of General Physiology,* **110**, 529-38.

Kalenak, A., McKenzie, R. J. & Conover, T. E. (1991). Response of the electrochromic dye, merocyanine 540, to membrane potential in rat liver mitochondria. *Journal Of Membrane Biology,* **123**, 23-31.

Kaminishi, T. & Kako, K. J. (1989). Sensitivity to oxidants of mitochondrial and sarcoplasmic reticular calcium uptake in saponin-treated cardiac myocytes. *Basic Research In Cardiology,* **84**, 282-90.

Kao, J. P. Y. (1994). Practical Aspects of Measuring [Ca2+] with Fluorescent Indicators. In R. Nuccitelli (Ed.), *A Practical Guide to the Study of Calcium in Living Cells* (pp. 155-180). San Diego: Academic Press.

Kehrer, J. P. & Paraidathathu, T. (1992). The use of fluorescent probes to assess oxidative processes in isolated-perfused rat heart tissue. *Free Radical Research Communications,* **16**, 217-25.

Kinnally, K. W., Campo, M. L. & Tedeschi, H. (1989). Mitochondrial channel activity studied by patch-clamping mitoplasts. *Journal Of Bioenergetics And Biomembranes,* **21**, 497-506.

Kluck, R. M., Martin, S. J., Hoffman, B. M., Zhou, J. S., Green, D. R. & Newmeyer, D. D. (1997). Cytochrome c activation of CPP32-like proteolysis plays a critical role in a Xenopus cell-free apoptosis system. *Embo Journal,* **16**, 4639-49.

Kourie, J. I. (1998). Interaction of reactive oxygen species with ion transport mechanisms. *American Journal Of Physiology,* **275**, C1-24.

Kowaltowski, A. J., Castilho, R. F., Grijalba, M. T., Bechara, E. J. & Vercesi, A. E. (1996). Effect of inorganic phosphate concentration on the nature of inner mitochondrial

membrane alterations mediated by Ca2+ ions. A proposed model for phosphate-stimulated lipid peroxidation. *Journal Of Biological Chemistry,* **271**, 2929-34.

Krishna, M. C., Grahame, D. A., Samuni, A., Mitchell, J. B. & Russo, A. (1992). Oxoammonium cation intermediate in the nitroxide-catalyzed dismutation of superoxide. *Proceedings Of The National Academy Of Sciences Of The United States Of America,* **89**, 5537-41.

Kroemer, G. (1999). Mitochondrial control of apoptosis: an overview. In G. C. Brown, Nicholls, D.G., Cooper, C.E. (Ed.), *Mitochondria and Cell Death* (pp. 1 - 15). London: Portland Press.

Kroemer, G., Dallaporta, B. & Resche-Rigon, M. (1998). The mitochondrial death/life regulator in apoptosis and necrosis. *Annual Review Of Physiology,* **60**, 619-42.

Kroemer, G., Petit, P., Zamzami, N., Vayssière, J. L. & Mignotte, B. (1995). The biochemistry of programmed cell death. *Faseb Journal,* **9**, 1277-87.

Krohn, A. J., Wahlbrink, T. & Prehn, J. H. (1999). Mitochondrial depolarization is not required for neuronal apoptosis. *Journal Of Neuroscience,* **19**, 7394-404.

Kukreja, R. C., Kearns, A. A., Zweier, J. L., Kuppusamy, P. & Hess, M. L. (1991). Singlet oxygen interaction with Ca(2+)-ATPase of cardiac sarcoplasmic reticulum. *Circulation Research,* **69**, 1003-14.

Kunz, W. S., Goussakov, I. V., Beck, H. & Elger, C. E. (1999). Altered mitochondrial oxidative phosphorylation in hippocampal slices of kainate-treated rats. *Brain Research,* **826**, 236-42.

Langley, D. & Pearce, B. (1994). Ryanodine-induced intracellular calcium mobilisation in cultured astrocytes. *Glia,* **12**, 128-34.

Lawrie, A. M., Rizzuto, R., Pozzan, T. & Simpson, A. W. (1996). A role for calcium influx in the regulation of mitochondrial calcium in endothelial cells. *Journal Of Biological Chemistry,* **271**, 10753-9.

LeBel, C. P., Ischiropoulos, H. & Bondy, S. C. (1992). Evaluation of the probe 2',7'-dichlorofluorescin as an indicator of reactive oxygen species formation and oxidative stress. *Chemical Research In Toxicology,* **5**, 227-31.

Lemasters, J. J., Nieminen, A. L., Qian, T., Trost, L. C. & Herman, B. (1997). The mitochondrial permeability transition in toxic, hypoxic and reperfusion injury. *Molecular And Cellular Biochemistry,* **174**, 159-65.

Lenaz, G. (1998). Role of mitochondria in oxidative stress and ageing. *Biochimica Et Biophysica Acta,* **1366**, 53-67.

Leyssens, A., Nowicky, A. V., Patterson, L., Crompton, M. & Duchen, M. R. (1996). The relationship between mitochondrial state, ATP hydrolysis, [Mg2+]i and [Ca2+]i studied in isolated rat cardiomyocytes. *Journal Of Physiology,* **496 (Pt 1)**, 111-28.

Lipp, P. & Niggli, E. (1998). Fundamental calcium release events revealed by two-photon excitation photolysis of caged calcium in Guinea-pig cardiac myocytes. *Journal Of Physiology,* **508 (Pt 3)**, 801-9.

Liu, J., Farmer, J. D. J., Lane, W. S., Friedman, J., Weissman, I. & Schreiber, S. L. (1991). Calcineurin is a common target of cyclophilin-cyclosporin A and FKBP-FK506 complexes. *Cell,* **66**, 807-15.

Liu, X., Kim, C. N., Yang, J., Jemmerson, R. & Wang, X. (1996). Induction of apoptotic program in cell-free extracts: requirement for dATP and cytochrome c. *Cell,* **86**, 147-57.

Loew, L. M., Carrington, W., Tuft, R. A. & Fay, F. S. (1994). Physiological cytosolic Ca2+ transients evoke concurrent mitochondrial depolarizations. *Proceedings Of The National Academy Of Sciences Of The United States Of America,* **91**, 12579-83.

MacVicar, B. A., Hochman, D., Delay, M. J. & Weiss, S. (1991). Modulation of intracellular Ca++ in cultured astrocytes by influx through voltage-activated Ca++ channels. *Glia,* **4**, 448-55.

Mahajan, N. P., Linder, K., Berry, G., Gordon, G. W., Heim, R. & Herman, B. (1998). Bcl-2 and Bax interactions in mitochondria probed with green fluorescent protein and fluorescence resonance energy transfer [see comments]. *Nature Biotechnology,* **16**, 547-52.

Margulis, L. (1975). Symbiotic theory of the origin of eukaryotic organelles; criteria for proof. *Symposia Of The Society For Experimental Biology*, 21-38.

Margulis, L. (1996). Archaeal-eubacterial mergers in the origin of Eukarya: phylogenetic classification of life. *Proceedings Of The National Academy Of Sciences Of The United States Of America,* **93**, 1071-6.

Marks, A. R. (1996). Cellular functions of immunophilins. *Physiological Reviews,* **76**, 631-49.

Marzo, I., Brenner, C., Zamzami, N., Jürgensmeier, J. M., Susin, S. A., Vieira, H. L., Prévost, M. C., Xie, Z., Matsuyama, S., Reed, J. C. & Kroemer, G. (1998a). Bax and adenine nucleotide translocator cooperate in the mitochondrial control of apoptosis. *Science,* **281**, 2027-31.

Marzo, I., Brenner, C., Zamzami, N., Susin, S. A., Beutner, G., Brdiczka, D., Rémy, R., Xie, Z. H., Reed, J. C. & Kroemer, G. (1998b). The permeability transition pore complex: a target for apoptosis regulation by caspases and bcl-2-related proteins. *Journal Of Experimental Medicine,* **187**, 1261-71.

Matlib, M. A., Zhou, Z., Knight, S., Ahmed, S., Choi, K. M., Krause-Bauer, J., Phillips, R., Altschuld, R., Katsube, Y., Sperelakis, N. & Bers, D. M. (1998). Oxygen-bridged dinuclear ruthenium amine complex specifically inhibits Ca2+ uptake into mitochondria in vitro and in situ in single cardiac myocytes. *Journal Of Biological Chemistry,* **273**, 10223-31.

Matouschek, A., Rospert, S., Schmid, K., Glick, B. S. & Schatz, G. (1995). Cyclophilin catalyzes protein folding in yeast mitochondria. *Proceedings Of The National Academy Of Sciences Of The United States Of America,* **92**, 6319-23.

McCormack, J. G. & Denton, R. M. (1993). The role of intramitochondrial Ca2+ in the regulation of oxidative phosphorylation in mammalian tissues. *Biochemical Society Transactions,* **21 (Pt 3)**, 793-9.

McCormack, J. G., Halestrap, A. P. & Denton, R. M. (1990). Role of calcium ions in regulation of mammalian intramitochondrial metabolism. *Physiological Reviews,* **70**, 391-425.

McGuinness, O., Yafei, N., Costi, A. & Crompton, M. (1990). The presence of two classes of high-affinity cyclosporin A binding sites in mitochondria. Evidence that the minor component is involved in the opening of an inner-membrane Ca(2+)-dependent pore [published erratum appears in Eur J Biochem 1991 Feb 14;195(3):871]. *European Journal Of Biochemistry,* **194**, 671-9.

McLeod, L. L. & Sevanian, A. (1997). Lipid peroxidation and modification of lipid composition in an endothelial cell model of ischemia and reperfusion. *Free Radical Biology And Medicine,* **23**, 680-94.

Meinicke, A. R., Bechara, E. J. & Vercesi, A. E. (1998). Ruthenium red-catalyzed degradation of peroxides can prevent mitochondrial oxidative damage induced by either tert-butyl hydroperoxide or inorganic phosphate. *Archives Of Biochemistry And Biophysics,* **349**, 275-80.

Meldolesi, J. & Pozzan, T. (1998). The endoplasmic reticulum Ca2+ store: a view from the lumen. *Trends In Biochemical Sciences,* **23**, 10-4.

Mildazien, V., Baniene, R., Nauciene, Z., Marcinkeviciute, A., Morkuniene, R., Borutaite, V., Kholodenko, B. & Brown, G. C. (1996). Ca2+ stimulates both the respiratory and phosphorylation subsystems in rat heart mitochondria. *Biochemical Journal,* **320 (Pt 1)**, 329-34.

Miyata, H., Silverman, H. S., Sollott, S. J., Lakatta, E. G., Stern, M. D. & Hansford, R. G. (1991). Measurement of mitochondrial free Ca2+ concentration in living single rat cardiac myocytes. *American Journal Of Physiology,* **261**, H1123-34.

Miyawaki, A., Llopis, J., Heim, R., McCaffery, J. M., Adams, J. A., Ikura, M. & Tsien, R. Y. (1997). Fluorescent indicators for Ca2+ based on green fluorescent proteins and calmodulin [see comments]. *Nature,* **388**, 882-7.

Mojet, M. H., Mills, E. & Duchen, M. R. (1997). Hypoxia-induced catecholamine secretion in isolated newborn rat adrenal chromaffin cells is mimicked by inhibition of mitochondrial respiration. *Journal Of Physiology,* **504 (Pt 1)**, 175-89.

Montague, J. W., Gaido, M. L., Frye, C. & Cidlowski, J. A. (1994). A calcium-dependent nuclease from apoptotic rat thymocytes is homologous with cyclophilin. Recombinant cyclophilins A, B, and C have nuclease activity. *Journal Of Biological Chemistry,* **269**, 18877-80.

Moran, O., Sandri, G., Panfili, E., Stühmer, W. & Sorgato, M. C. (1990). Electrophysiological characterization of contact sites in brain mitochondria [published erratum appears in J Biol Chem 1990 Jul 5;265(19):11405]. *Journal Of Biological Chemistry,* **265**, 908-13.

Nadal, A., Fuentes, E., Pastor, J. & McNaughton, P. A. (1997). Plasma albumin induces calcium waves in rat cortical astrocytes. *Glia,* **19**, 343-51.

Narita, M., Shimizu, S., Ito, T., Chittenden, T., Lutz, R. J., Matsuda, H. & Tsujimoto, Y. (1998). Bax interacts with the permeability transition pore to induce permeability transition and cytochrome c release in isolated mitochondria. *Proceedings Of The National Academy Of Sciences Of The United States Of America,* **95**, 14681-6.

Nicholls, D. G. (1978). The regulation of extramitochondrial free calcium ion concentration by rat liver mitochondria. *Biochemical Journal,* **176**, 463-74.

Nicholls, D. G. & Budd, S. L. (2000). Mitochondria and neuronal survival. *PHYSIOLOGICAL REVIEWS,* **80**, 315-360.

Nicholls, D. G. & Ferguson, S. J. (1992). *Bioenergetics 2.* London: Academic Press.

Nicholls, D. G. & Scott, I. D. (1980). The regulation of brain mitochondrial calcium-ion transport. The role of ATP in the discrimination between kinetic and membrane-potential-dependent calcium-ion efflux mechanisms. *Biochemical Journal,* **186**, 833-9.

Nicolli, A., Basso, E., Petronilli, V., Wenger, R. M. & Bernardi, P. (1996). Interactions of cyclophilin with the mitochondrial inner membrane and regulation of the permeability transition pore, and cyclosporin A-sensitive channel. *Journal Of Biological Chemistry,* **271**, 2185-92.

Nieminen, A. L., Petrie, T. G., Lemasters, J. J. & Selman, W. R. (1996). Cyclosporin A delays mitochondrial depolarization induced by N-methyl-D-aspartate in cortical neurons: evidence of the mitochondrial permeability transition. *Neuroscience,* **75**, 993-7.

Nieminen, A. L., Saylor, A. K., Tesfai, S. A., Herman, B. & Lemasters, J. J. (1995). Contribution of the mitochondrial permeability transition to lethal injury after exposure of hepatocytes to t-butylhydroperoxide. *Biochemical Journal,* **307 (Pt 1)**, 99-106.

Nishida, T., Shibata, H., Koseki, M., Nakao, K., Kawashima, Y., Yoshida, Y. & Tagawa, K. (1987). Peroxidative injury of the mitochondrial respiratory chain during reperfusion of hypothermic rat liver. *Biochimica Et Biophysica Acta,* **890**, 82-8.

Nishino, T., Nakanishi, S., Okamoto, K., Mizushima, J., Hori, H., Iwasaki, T., Ichimori, K. & Nakazawa, H. (1997). Conversion of xanthine dehydrogenase into oxidase and its role in reperfusion injury. *Biochemical Society Transactions,* **25**, 783-6.

Novgorodov, S. A. & Gudz, T. I. (1996). Permeability transition pore of the inner mitochondrial membrane can operate in two open states with different selectivities. *Journal Of Bioenergetics And Biomembranes,* **28**, 139-46.

Oyama, Y., Hayashi, A., Ueha, T., Chikahisa, L. & Furukawa, K. (1993). Fluorescent estimation on the effect of Ca2+ antagonists on the oxidative metabolism in dissociated mammalian brain neurons. *Brain Research,* **610**, 172-5.

Pereira, R. S., Bertocchi, A. P. & Vercesi, A. E. (1992). Protective effect of trifluoperazine on the mitochondrial damage induced by Ca2+ plus prooxidants. *Biochemical Pharmacology,* **44**, 1795-801.

Petit, P. X., Goubern, M., Diolez, P., Susin, S. A., Zamzami, N. & Kroemer, G. (1998). Disruption of the outer mitochondrial membrane as a result of large amplitude swelling: the impact of irreversible permeability transition. *Febs Letters,* **426**, 111-6.

Petit, P. X., Susin, S. A., Zamzami, N., Mignotte, B. & Kroemer, G. (1996). Mitochondria and programmed cell death: back to the future. *Febs Letters,* **396**, 7-13.

Petronilli, V., Costantini, P., Scorrano, L., Colonna, R., Passamonti, S. & Bernardi, P. (1994). The voltage sensor of the mitochondrial permeability transition pore is tuned by the oxidation-reduction state of vicinal thiols. Increase of the gating potential by oxidants and its reversal by reducing agents. *Journal Of Biological Chemistry,* **269**, 16638-42.

Petronilli, V., Miotto, G., Canton, M., Brini, M., Colonna, R., Bernardi, P. & Di Lisa, F. (1999). Transient and long-lasting openings of the mitochondrial permeability transition pore can be monitored directly in intact cells by changes in mitochondrial calcein fluorescence. *Biophysical Journal,* **76**, 725-34.

Peuchen, S., Bolaños, J. P., Heales, S. J., Almeida, A., Duchen, M. R. & Clark, J. B. (1997). Interrelationships between astrocyte function, oxidative stress and antioxidant status within the central nervous system. *Progress In Neurobiology,* **52**, 261-81.

Peuchen, S., Clark, J. B. & Duchen, M. R. (1996a). Mechanisms of intracellular calcium regulation in adult astrocytes. *Neuroscience,* **71**, 871-83.

Peuchen, S., Duchen, M. R. & Clark, J. B. (1996b). Energy metabolism of adult astrocytes in vitro. *Neuroscience,* **71**, 855-70.

Peus, D., Vasa, R. A., Meves, A., Pott, M., Beyerle, A., Squillace, K. & Pittelkow, M. R. (1998). H2O2 is an important mediator of UVB-induced EGF-receptor phosphorylation in cultured keratinocytes. *Journal Of Investigative Dermatology,* **110**, 966-71.

Phillis, J. W. (1994). A radical view of cerebral ischemic injury. *Progress In Neurobiology,* **42**, 441-8.

Puskin, J. S., Gunter, T. E., Gunter, K. K. & Russell, P. R. (1976). Evidence for more than one Ca2+ transport mechanism in mitochondria. *Biochemistry,* **15**, 3834-42.

Rizzuto, R., Brini, M., Murgia, M. & Pozzan, T. (1993). Microdomains with high Ca2+ close to IP3-sensitive channels that are sensed by neighboring mitochondria. *Science,* **262**, 744-7.

Rizzuto, R., Pinton, P., Carrington, W., Fay, F. S., Fogarty, K. E., Lifshitz, L. M., Tuft, R. A. & Pozzan, T. (1998). Close contacts with the endoplasmic reticulum as determinants of mitochondrial Ca2+ responses. *Science,* **280**, 1763-6.

Robb-Gaspers, L. D., Rutter, G. A., Burnett, P., Hajnóczky, G., Denton, R. M. & Thomas, A. P. (1998). Coupling between cytosolic and mitochondrial calcium oscillations: role in the regulation of hepatic metabolism. *Biochimica Et Biophysica Acta,* **1366**, 17-32.

Rottenberg, H. & Wu, S. (1998). Quantitative assay by flow cytometry of the mitochondrial membrane potential in intact cells. *Biochimica Et Biophysica Acta,* **1404**, 393-404.

Rouslin, W. & Broge, C. W. (1996). IF1 function in situ in uncoupler-challenged ischemic rabbit, rat, and pigeon hearts. *Journal Of Biological Chemistry,* **271**, 23638-41.

Sabatini, D. M., Lai, M. M. & Snyder, S. H. (1997). Neural roles of immunophilins and their ligands. *Molecular Neurobiology,* **15**, 223-39.

Salvioli, S., Ardizzoni, A., Franceschi, C. & Cossarizza, A. (1997). JC-1, but not DiOC6(3) or rhodamine 123, is a reliable fluorescent probe to assess delta psi changes in intact cells: implications for studies on mitochondrial functionality during apoptosis. *Febs Letters,* **411**, 77-82.

Sandler, V. M. & Barbara, J. G. (1999). Calcium-induced calcium release contributes to action potential-evoked calcium transients in hippocampal CA1 pyramidal neurons. *Journal Of Neuroscience,* **19**, 4325-36.

Scaduto, R. C. J. & Grotyohann, L. W. (1999). Measurement of mitochondrial membrane potential using fluorescent rhodamine derivatives. *Biophysical Journal,* **76**, 469-77.

Schapira, A. H. (1998). Mitochondrial dysfunction in neurodegenerative disorders. *Biochimica Et Biophysica Acta,* **1366**, 225-33.

Shimizu, S., Narita, M. & Tsujimoto, Y. (1999). Bcl-2 family proteins regulate the release of apoptogenic cytochrome c by the mitochondrial channel VDAC [see comments]. *Nature,* **399**, 483-7.

Short, A. D., Klein, M. G., Schneider, M. F. & Gill, D. L. (1993). Inositol 1,4,5-trisphosphate-mediated quantal Ca2+ release measured by high resolution imaging of Ca2+ within organelles. *Journal Of Biological Chemistry,* **268**, 25887-93.

Shoshan-Barmatz, V. & Ashley, R. H. (1998). The structure, function, and cellular regulation of ryanodine-sensitive Ca2+ release channels. *International Review Of Cytology,* **183**, 185-270.

Sies, H. & Cadenas, E. (1985). Oxidative stress: damage to intact cells and organs. *Philosophical Transactions Of The Royal Society Of London. Series B: Biological Sciences,* **311**, 617-31.

Simpson, P. B., Mehotra, S., Langley, D., Sheppard, C. A. & Russell, J. T. (1998). Specialized distributions of mitochondria and endoplasmic reticulum proteins define Ca2+ wave amplification sites in cultured astrocytes. *Journal Of Neuroscience Research,* **52**, 672-83.

Simpson, P. B. & Russell, J. T. (1996). Mitochondria support inositol 1,4,5-trisphosphate-mediated Ca2+ waves in cultured oligodendrocytes. *Journal Of Biological Chemistry,* **271**, 33493-501.

Sitsapesan, R., McGarry, S. J. & Williams, A. J. (1995). Cyclic ADP-ribose, the ryanodine receptor and Ca2+ release. *Trends In Pharmacological Sciences,* **16**, 386-91.

Soeller, C. & Cannell, M. B. (1997). Numerical simulation of local calcium movements during L-type calcium channel gating in the cardiac diad. *Biophysical Journal,* **73**, 97-111.

Song, L., Hennink, E. J., Young, I. T. & Tanke, H. J. (1995). Photobleaching kinetics of fluorescein in quantitative fluorescence microscopy. *Biophysical Journal,* **68**, 2588-600.

Sontheimer, H. (1994). Voltage-dependent ion channels in glial cells. *Glia,* **11**, 156-72.

Stevens, T., Fouty, B., Cornfield, D. & Rodman, D. M. (1994). Reduced PO2 alters the behavior of Fura-2 and Indo-1 in bovine pulmonary artery endothelial cells. *Cell Calcium,* **16**, 404-12.

Stout, A. K., Raphael, H. M., Kanterewicz, B. I., Klann, E. & Reynolds, I. J. (1998). Glutamate-induced neuron death requires mitochondrial calcium uptake. *Nat Neurosci,* **1**, 366-73.

Susin, S. A., Lorenzo, H. K., Zamzami, N., Marzo, I., Snow, B. E., Brothers, G. M., Mangion, J., Jacotot, E., Costantini, P., Loeffler, M., Larochette, N., Goodlett, D. R., Aebersold, R., Siderovski, D. P., Penninger, J. M. & Kroemer, G. (1999). Molecular characterization of mitochondrial apoptosis-inducing factor [see comments]. *Nature,* **397**, 441-6.

Susin, S. A., Zamzami, N., Castedo, M., Hirsch, T., Marchetti, P., Macho, A., Daugas, E., Geuskens, M. & Kroemer, G. (1996). Bcl-2 inhibits the mitochondrial release of an apoptogenic protease. *Journal Of Experimental Medicine,* **184**, 1331-41.

Suzuki, Y. J., Cleemann, L., Abernethy, D. R. & Morad, M. (1998). Glutathione is a cofactor for H2O2-mediated stimulation of Ca2+-induced Ca2+ release in cardiac myocytes. *Free Radical Biology And Medicine,* **24**, 318-25.

Suzuki, Y. J. & Ford, G. D. (1992). Superoxide stimulates IP3-induced Ca2+ release from vascular smooth muscle sarcoplasmic reticulum. *American Journal Of Physiology,* **262**, H114-6.

Szalai, G., Krishnamurthy, R. & Hajnoczky, G. (1999). Apoptosis driven by IP3-linked mitochondrial calcium signals. *EMBO JOURNAL,* **18**, 6349-6361.

Tsien, R. Y. (1980). New calcium indicators and buffers with high selectivity against magnesium and protons: design, synthesis, and properties of prototype structures. *Biochemistry,* **19**, 2396-404.

Turrens, J. F. & Boveris, A. (1980). Generation of superoxide anion by the NADH dehydrogenase of bovine heart mitochondria. *Biochemical Journal,* **191**, 421-7.

Ubl, J. J., Chatton, J. Y., Chen, S. & Stucki, J. W. (1996). A critical evaluation of in situ measurement of mitochondrial electrical potentials in single hepatocytes. *Biochimica Et Biophysica Acta,* **1276**, 124-32.

Vassilev, P. M., Kanazirska, M. P., Charamella, L. J., Dimitrov, N. V. & Tien, H. T. (1987). Changes in calcium channel activity in membranes from cis-diammine-dichloroplatinum(II)-resistant and -sensitive L1210 cells. *Cancer Research,* **47**, 519-22.

Vercesi, A. E., Ferraz, V. L., Macedo, D. V. & Fiskum, G. (1988). Ca2+-dependent NAD(P)+-induced alterations of rat liver and hepatoma mitochondrial membrane permeability. *Biochemical And Biophysical Research Communications,* **154**, 934-41.

Vlessis, A. A. (1990). NADH-linked substrate dependence of peroxide-induced respiratory inhibition and calcium efflux in isolated renal mitochondria. *Journal Of Biological Chemistry,* **265**, 1448-53.

Wesson, D. E. & Elliott, S. J. (1995). The H2O2-generating enzyme, xanthine oxidase, decreases luminal Ca2+ content of the IP3-sensitive Ca2+ store in vascular endothelial cells. *Microcirculation,* **2**, 195-203.

White, R. J. & Reynolds, I. J. (1996). Mitochondrial depolarization in glutamate-stimulated neurons: an early signal specific to excitotoxin exposure. *Journal Of Neuroscience,* **16**, 5688-97.

Yagi, K., Shidoji, Y., Komura, S., Kojima, H. & Ohishi, N. (1998). Dissipation of mitochondrial membrane potential by exogenous phospholipid monohydroperoxide and protection against this effect by transfection of cells with phospholipid hydroperoxide glutathione peroxidase gene. *Biochemical And Biophysical Research Communications,* **245**, 528-33.

Yasuhara, N., Eguchi, Y., Tachibana, T., Imamoto, N., Yoneda, Y. & Tsujimoto, Y. (1997). Essential role of active nuclear transport in apoptosis. *Genes To Cells,* **2**, 55-64.

Ying, W. L., Emerson, J., Clarke, M. J. & Sanadi, D. R. (1991). Inhibition of mitochondrial calcium ion transport by an oxo-bridged dinuclear ruthenium ammine complex. *Biochemistry,* **30**, 4949-52.

Zamzami, N., Marchetti, P., Castedo, M., Zanin, C., Vayssière, J. L., Petit, P. X. & Kroemer, G. (1995). Reduction in mitochondrial potential constitutes an early irreversible step of programmed lymphocyte death in vivo. *Journal Of Experimental Medicine,* **181**, 1661-72.

Zhang, J. J., Williams, A. J. & Sitsapesan, R. (1999). Evidence for novel caffeine and Ca2+ binding sites on the lobster skeletal ryanodine receptor. *British Journal Of Pharmacology,* **126**, 1066-74.

Zoratti, M. & Szabó, I. (1994). Electrophysiology of the inner mitochondrial membrane. *Journal Of Bioenergetics And Biomembranes,* **26**, 543-53.

Zoratti, M. & Szabò, I. (1995). The mitochondrial permeability transition. *Biochimica Et Biophysica Acta,* **1241**, 139-76.

Zou, H., Henzel, W. J., Liu, X., Lutschg, A. & Wang, X. (1997). Apaf-1, a human protein homologous to C. elegans CED-4, participates in cytochrome c-dependent activation of caspase-3 [see comments]. *Cell,* **90**, 405-13.

Missing references:

Le Quoc, K and Le Quoc, D (1989). Involvement of the ADP/ATP carrier in calcium-induced perturbations of the mitochondrial inner membrane permeability: importance of the orientation of the nucleotide binding site. *Arch Biochem Biophys* **265(2)**, 249-257

Mojet, M, Jacobson, J, Keelan, J, Vergun, and Duchen, MR. Monitoring mitochondrial function in single cells. In A. Tepikin (Ed.) *Calcium Signalling: A Practical Approach.* Oxford: Oxford University Press (in press).

Duchen, M. R. (1999). Contributions of mitochondria to animal physiology: from homeostatic sensor to calcium signalling and cell death. *Journal Of Physiology,* **516 (Pt 1)**, 1-17.

Some of the data presented in this thesis have previously been published in abstract form:

Jacobson, D and Duchen, M. R. (1998) Fluorescence imaging of the mitochondrial permeability transition in rat cortical astrocytes in culture. *J Physiol*, **506.P**, 75P.